Diplomarbeit

Experimental and numerical analysis of a latent storage integrated in a heat pump cycle

ausgeführt zum Zwecke der Erlangung des akademischen Grades eines

Diplom-Ingenieurs

eingereicht an der Technischen Universität Wien, Fakultät für Maschinenwesen und Betriebswissenschaft

von

Felix Hochwallner

Matr.Nr.: 01328839

unter der Anleitung von

Privatdoz. Dipl.-Ing. Dr.techn. Christoph Reichl

Institut für Strömungsmechanik und Wärmeübertragung

Wien, am 30.7.2019

TECHNISCHE UNIVERSITÄT WIEN

Ich habe zur Kenntnis genommen, dass ich zur Drucklegung meiner Arbeit unter der Bezeichnung

Diplomarbeit

nur mit Bewilligung der Prüfungskommission berechtigt bin.

Ich erkläre weiters an Eides statt, dass ich meine Diplomarbeit nach den anerkannten Grundsätzen für wissenschaftliche Abhandlungen selbständig ausgeführt habe und alle verwendeten Hilfsmittel, insbesondere die zugrunde gelegte Literatur genannt habe.

Weiters erkläre ich, dass ich dieses Diplomarbeitsthema bisher weder im In- noch Ausland (einer Beurteilerin/einem Beurteiler zur Begutachtung) in irgendeiner Form als Prüfungsarbeit vorgelegt habe und dass diese Arbeit mit der vom Begutachter beurteilten Arbeit übereinstimmt.

Wien, am 30.7.2019 _____

Danksagung

Ich möchte mich an dieser Stelle bei allen bedanken, die mir während des Verfassens meiner Diplomarbeit zur Seite gestanden sind und mich am Weg dahin unterstützt haben.

Mein großer Dank geht an Priv. Doz. Dr. Christoph Reichl, der mich tatkräftig im Verlauf meiner Arbeit betreut hat und mir jederzeit behilflich war, falls es einmal zu Problemen kam. Durch seinen großen Enthusiasmus für das Thema und seine unerschöpfbare Energie getrieben, brachte er mich dazu, über den Tellerrand zu schauen und konnte mir so in meiner Arbeit weiterhelfen und meine Motivation auch in schwierigeren Zeiten hoch halten. Das kritische Hinterfragen und die wertvollen Hinweise im Verlauf der Arbeit besserten Unfeinheiten aus und brachten die Arbeit zu der Form, in der sie jetzt ist.

Ein weiterer Dank geht an das AIT - Austrian Institute of Technology - und dem Center for Thermal Energy Systems. Ganz besonders möchte ich mich hier bei Dr. Johann Emhofer bedanken, der mich nicht nur in die Thematik einführte, sondern mir über den gesamten Weg der Arbeit zur Seite stand. Durch sein immenses Wissen und Erfahrung konnte er mir bei vielen Problemen helfen, gemeinsam Lösungen zu kreieren. Des Weiteren gilt mein Dank Dr. Klemens Marx, Dr. Tilman Barz, Dr. Michael Lauermann und Dr. Thomas Fleckl, die mir unter die Arme griffen und damit den Weg dieser Arbeit ebneten.

Nicht zuletzt gebührt meinen Eltern, meinen Schwestern und meiner Freundin Lisa Dank, welche mich nicht nur während meiner Arbeit, sondern bereits am Weg dahin moralisch unterstützten und ohne die ich dieses Ziel niemals hätte erreichen können.

Kurzfassung

Durch attraktive Preise und hohe Energieeffizienzen werden Kompressions-Wärmepumpen immer häufiger im Gebäudesektor eingesetzt. Wärmepumpen können zum Heizen, zum Kühlen und zur Bereitstellung von Warmwasser für Hausbewohner eingesetzt werden. Die Energieeffizienz von Wärmepumpen ist im Heiz- und Kühlmodus normalerweise höher als bei der Bereitstellung von Warmwasser, da der Temperaturunterschied zwischen Quelle und Senke in diesem Betriebszustand höher ist.

Doch auch im Heiz- und Kühlmodus übertrifft die Temperatur des Kältemittel Heißgases nach dem Verdichter für gewöhnlich die Temperatur des erforderten Warmwassers. Deshalb ist es von Interesse die Wärme dieses Heißgases im Heiz- und Kühlbetrieb zu speichern und anschließend für die Bereitstellung von Warmwasser zu nutzen. Dadurch kann die Effizienz der Warmwasserbereitstellung signifikant erhöht werden. Latente (Phasenumwandlungs-) Wärmespeicher stellen hier eine attraktive Lösung dar, da sie eine hohe Energiedichte aufweisen.

Das neuartige Wärmepumpenkonzept, welches in dieser Arbeit präsentiert wird, integriert einen Kühlmittel/Wasser Wärmetauscher mit einem Phasenumwandlungsmaterial in die überhitzte Heißgas Sektion einer R32 - Luft Wärmepumpe. Der Phasenumwandlungs-Wärmetauscher speichert Energie im Heiz- und Kühlmodus und gibt diese für die energieeffiziente Bereitstellung von Warmwasser wieder ab.

Ein numerisches Modell der Wärmepumpe wurde erstellt und durch durchgeführte Experimente validiert. Zusätzlich wurde die Eisbildung an der Verdampferoberfläche bei Betrieb der Wärmepumpe unter Frierbedingungen analysiert. Mithilfe des validierten numerischen Modells wurde die Leistung des neuartigen Wärmepumpensystems für verschiedene Betriebs- und Umgebungsbedingungen simuliert. Zudem wurde auch die Verwendung unterschiedlicher Phasenumwandlungsmaterialien und Veränderungen in den Betriebsparametern auf ihre Auswirkungen auf die Leistung des Konzepts untersucht. Ein typisches Betriebsszenario des neuartigen Systems, welches einen Betrieb im Heizmodus und Aufladen des Wärmespeichers mit einer anschließenden energieeffizienten Bereitstellung von Warmwasser durch Entladen des Wärmespeicher inkludiert, wurde für eine Umgebungstemperatur von 2 °C simuliert. Die gesamte Wärmeleistung des neuartigen Konzepts ist in diesem Szenario 3.67 mal größer als die erforderte elektrische Leistung. In einer einjährigen Berechnung, bei einem durchschnittlichen mitteleuropäischem Klima, wurde gezeigt, dass das neuartige Wärmepumpensystem, welches ein Phasenumwandlungsmaterial mit einem Schmelzpunkt von 64 °C verwendet, etwa 3.8 % des elektrischen Energieverbrauchs, gegenüber einem konventionellen System, einspart.

Abstract

Today, compression heat pumps gain more and more attention in the buildings sector, due to attractive prices and high energy efficiencies. They can be used for heating, cooling and to provide domestic hot water for the residents. The energy efficiency of a heat pump for heating and cooling of feed water is usually higher than for the domestic hot water generation, because a lower temperature gap between the source and the sink has to be overcome.

However, also in heating and cooling mode the temperature of the hot-gas refrigerant discharging the compressor usually exceeds the temperature of the required domestic hot water. It is therefore of interest to store the high temperature heat of this hot-gas and use the stored heat to increase the efficiency of the domestic hot water generation. Latent (phase change) energy storages are attractive for this approach, due to their high energy density.

The novel heat pump system proposed in this thesis integrates a refrigerant/water heat exchanger with a phase change material in the hot super-heated section of an R32 - air source heat pump. The phase change material stores energy in heating and cooling mode and releases it for energy efficient domestic hot water generation.

A numerical model of the heat pump system is created and validated by experimental testing. Additionally, the frost accumulation on the evaporator coils of the air source heat pump during operation at frosting conditions is analyzed. Using the validated numerical model the performance of the novel heat pump system is simulated for various operation and ambient conditions. Moreover, the use of different phase change materials and changes in the operation parameters of the heat pump are numerically analyzed on their impact on the overall energy efficiency. A typical operation scenario of the novel system, including heating the building and charging the latent storage and afterwards generating domestic hot water by discharging the latent storage, is simulated for an ambient temperature of 2 °C. The total heat output of the novel heat pump system in this scenario is 3.67 times as big as the electrical power demand. In an annual calculation it is shown that the novel heat pump system using a phase change material with a melting point of 64 °C saves about 3.8 % of electrical energy over the year in an average climate, compared to a conventional system.

Nomenclature

Abbreviations

AIT	Austrian Institute Of Technology
CFC	Chlorofluorocarbon
DHW	Domestic Hot Water
GWP	Global Warming Potential
HC	Hydrocarbon
HCFC	Hydrochlorofluorocarbon
HEX	Heat Exchanger
HFC	Hydrofluorocarbon
max	Maximum
min	Minimum
ODP	Ozone Depletion Potential
PCM	Phase Change Material
Q10	10-quantile
Q90	90-quantile
Ref	Reference
Refr	Refrigerant
rpm	Rounds per Minute
RPW-HEX	Refrigerant / Phase Change Material / Water Heat Exchanger
std	Standard Deviation
TES	Thermal Energy Storage

Greek Symbols

η	Efficiency Factor	1
ρ	Density	kg/m^3
Ξ	State of Charge	1
ξ	Phase Fraction	1

Latin Symbols

$\dot{m}$	Mass Flow Rate	kg/s
$\dot{Q}$	Heat Flow Rate	W
$\dot{q}$	Volumetric Flow Rate	m^3/s
$\dot{W}$	Power	W
γ	Angle	rad
θ	Temperature	°C
A	Area	m^2
c	Specific Heat Capacity	J/kgK
COP	Coefficient of Performance	1
d	Diameter	m
EER	Energy Efficiency Ratio	1
f	Fanning Friction Factor	1
h	Specific Enthalpy	J/kg
j	Colburn Factor	1
K	General Factor/Coefficient	1
L	Length	m
m	Mass	kg
N	Rotational Speed	rad/s
Nu	Nusselt Number	1
p	Pressure	Pa or bar
PLR	Part Load Ratio	1
Pr	Prandtl Number	1
Q	Heat	J or Wh
q	Specific Humidity	1
Re	Reynolds Number	1
RH	Relative Humidity	1

$SCOP$	Seasonal Coefficient of Performance	1
SoC	State of Charge	1
T	Temperature	K
U	Heat Transfer Coefficient	W/m^2K
V	Volume	m^3
W	Work	J or Wh

Subscripts

air	Air
b	Isobaric
c	Compression
cell	Cell
comp	Compressor
cond	Condenser
cool	Cooling
cor	Correction
cp	Circulating Pump
db	Dry Bulb Temperature
dc	Collar Diameter
des	Design
dh	Hydraulic Diameter
disc	Discharge
dry	Dry
e	Expansion
eff	Effective
el	Electrical
eva	Evaporator
H	Hot/High
heat	Heating
hyd	Hydraulic
in	Inflow
L	Low
le	Leading Edge
meas	Measurement
nom	Nominal
out	Outflow
port	Port
real	Real
rot	Rotational
s	Isentropic
sat	Saturated
sf	Secondary Fluid
standby	Standby
suct	Suction
th	Thermal
tot	Total
v	Volumetric
vap	Vapor
wall	Wall
water	Water
wb	Wet Bulb Temperature
wet	Wet
wf	Working Fluid

Contents

1 Introduction

Nowadays, close to two-thirds of global greenhouse gas emissions are linked to the production and consumption of energy (Demirel, 2016). This makes the energy sector a promising candidate to mitigate global warming and climate change. The focus should not only be on energy production, but on consumption as well. The buildings and buildings construction sector is one of the major consumers of energy, accounting to approximately 36 % of the world's total energy consumption and nearly 40 % of the total direct and indirect CO_2 emissions. Moreover, the energy demand from buildings continues to rise at nearly 3 % per year. Heating is the largest single end-use within buildings, accounting to approximately 36 % of the total buildings energy consumption. The IEA (2019) suggests, that buildings could be over 40 % more efficient than they are today.

Heat pumps can significantly decrease the the power consumption required for heating and cooling of buildings. Furthermore, they can not only be used to heat and cool a household, but also to provide domestic hot water (DHW) for the residents. Modern households with floor heating can heat a building with water temperatures slightly above the room temperatures. DHW, on the other hand, should be provided with a higher water temperature to maintain thermal comfort of the inhabitants and to decrease the risk of legionella. Therefore, the energy efficiency to generate DHW for the resident is normally significantly lower than for heating or cooling operation. The World Health Organization (2017) proposes that hot water systems should be maintained at temperatures above 55 °C to prevent risk of legionellas. If the temperature of the hot water system is kept at a lower level, greater attention to disinfection and strategies aimed at limiting development of biofilms are required. However, also the size of the water storage is important when classifying the risk of legionellas. While for large water storages for multiple apartments great attention has to be paid to prevent growth of legionellas, the risk of legionellas in small water storages, as for single households, is low.

In order to increase the efficiency of the DHW generation a novel heat pump system setup is proposed in this thesis. The concept integrates a refrigerant/water heat exchanger with a phase change material in the hot super-heated section of an R32 - air source compression heat pump cycle. The phase change material stores energy when the heat pump is operated in heating and cooling mode and releases its energy when DHW is generated. Thereby, the energy efficiency of DHW generation can be increased significantly. Aim of this thesis is to numerically analyze the performance of the proposed novel heat pump system. In addition, the numerical model is validated by experimental data of a reference conventional air source heat pump. Python scripted Modelica simulations are conducted in order to obtain performance maps of both the reference and the novel heat pump system. Furthermore, a typical operation scenario of the novel system, including operation in heating mode and storing energy into the phase change material and a switch to DHW generation and releasing the stored energy, is analyzed regarding its overall performance. Concluding, the annual

performance of the novel system compared to a reference conventional system is calculated and analyzed, using the performance maps calculated for both systems.

In order to calculate the total performance of the novel system over a full year, the performance of the system for various ambient conditions, as the ambient temperature, and operation conditions, as the compressor speed and the required output water temperature of the heat pump, was calculated and listed in performance maps. The obtained performance maps may furthermore be used for other purposes, as enhanced control algorithms for the heat pump system. The total electrical power demand for a full year of operation is used to compare the performance of the novel system to a reference system.

Phase change materials (PCMs) are attractive for storing the energy in this setup, due to their high energy density and the nearly constant temperature during phase change. The melting temperature of the phase change material should be slightly above the desired hot water temperature, to ensure low heat losses, high charging speeds and an appropriate DHW temperature. The proposed refrigerant (R)/water (W) heat exchanger (HEX) with a phase (P) change material is further on referred to as RPW-HEX.

HYBUILD

This thesis has close links to the European H2020 project HYBUILD. In the HYBUILD project two innovative compact hybrid electrical/thermal storage systems are developed. The project aims at developing cost-effective and environmental-friendly solutions for low energy buildings, while ensuring comfort conditions. It is divided into two climates: Mediterranean climate where a stronger focus is put on cooling and Continental climate where the heating demand is of greater importance (HYBUILD, 2019). One thermal storage system solution, part of the project, is the implementation of a latent energy storage in the super-heated section after the compressor of a heat pump cycle, to increase the efficiency of the domestic hot water generation, as mentioned in the previous section. This solution was developed, experimentally tested and numerically analyzed at *AIT*. A detailed analysis regarding this novel system is conducted in this thesis.

Research Questions

The aim of this thesis is to answer the following questions:

1. **Does and how much does the implementation of the RPW-HEX alter the heat pumps characteristics and performance?**

   a) *What are the changes in efficiency and performance for the different heat pump modes (i.e. heating, cooling, hot water generation)?*

   b) *What is the overall change in efficiency over a full year? Can the power demand be decreased significantly by the implementation of the RPW-HEX?*

   c) *Which phase change material should be used? What melting point fits this usage best?*

   d) *Can other operating parameters of the heat pump (e.g. the evaporator fan speed) be adjusted to increase the annual performance?*

   e) *Are there other scenarios (i.e. other climate zones, heating temperatures, DHW consumptions) where the benefit of the novel system is more decisive?*

2. **Is it possible to create an accurate simulation model for the heat pump system?**

   a) *Which components need to be included in the numerical analysis and which parameters need to be set properly to obtain an accurate model of the heat pump?*

   b) *Does the simulation model fit the experimental data well?*

   c) *Which computational speeds are possible?*

3. **How can the icing and deicing of the heat exchanger surface of a heat pump be quantified in experiments?**

   a) *Does putting the heat exchanger on a scale give applicable information about the ice accumulation on the heat exchanger surface?*

   b) *Using pictures of the heat exchanger surface taken by a macro camera, does the amount of pixels which exceed a certain brightness threshold correlate to the amount of ice on the heat exchanger surface?*

2 Theoretical Background

In order to understand the underlying basics of the proposed novel system, concepts and state of the art constructions of used components are described in this chapter. This includes the concept and classification of compression heat pumps and thermal energy storages and the different types of heat exchangers.

2.1 Compression Heat Pump

As Clausius's formulation of the second law of thermodynamics suggests:
It is impossible to construct a system which will operate in a cycle and transfer heat from a cooler to a hotter body without work being done on the system by the surroundings.[1]
it is only possible to transfer heat from a source with a lower temperature to a sink with a higher temperature by introducing work to the system. Exactly this is done by a heat pump. Using this principle, a space can be heated using thermal energy of a source with a lower temperature and it is also possible to cool a space while extracting thermal energy to a sink with a higher temperature (Bundschuh and Chen, 2017). A simple compression heat pump consists of four main components - a compressor, condenser, expansion valve and evaporator in which a working fluid, called refrigerant, circulates, as seen in Figure 1. By externally introducing work to the compressor, the gaseous refrigerant reaches a high temperature and pressure state. In the condenser the refrigerant releases most of its energy by condensing from a gaseous to a liquid state. Afterwards, the refrigerant releases its pressure over a valve while lowering its temperature. In the evaporator thermal energy is transferred from a heat source to the refrigerant and therefore the refrigerant evaporates into the gaseous state again. Thereafter, the gaseous refrigerant flows back into the compressor.

The efficiency of a heat pump is characterized by the so called Coefficient Of Performance (COP). It is the ratio of heat extracted from the refrigerant in the condenser at a high temperature to the total electrical work introduced to the heat pump:

$$COP = \frac{Q_{\mathrm{H}}}{W_{\mathrm{el}}} \tag{1}$$

with Q_{H} denoting the heat flow in the condenser and W_{el} the total electrical work used by the heat pump.

An ideal heat pump works like a reversed Carnot cycle, performing an isentropic compression and expansion and a isothermal heat addition and extraction (evaporation, condensation). The coefficient of performance can therefore directly be calculated by the temperatures of the condenser and evaporator. This gives an estimate of the maximum possible coefficient

[1] as stated in Winterbone and Turan (2015)

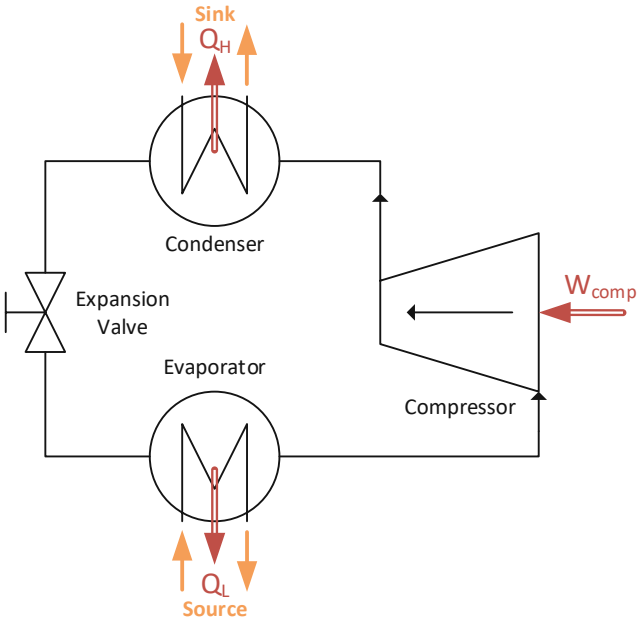

Figure 1: Simplified instrumentation diagram of a simple heat pump showing the main components: compressor, condenser, expansion valve and evaporator.

of performance for a heat pump. Furthermore, the electrical work is equal to the difference of the heat on the high temperature level minus the heat on the low temperature level, as no other energy gets inserted or rejected of the system. This leads to:

$$COP = \frac{Q_{\mathrm{H}}}{W_{\mathrm{el}}} = \frac{Q_{\mathrm{H}}}{Q_{\mathrm{H}} - Q_{\mathrm{L}}} = \frac{T_{\mathrm{H}}}{T_{\mathrm{H}} - T_{\mathrm{L}}} \tag{2}$$

with Q_{L} denoting the heat flow in the evaporator at a low temperature level and T_{H} and T_{L} the high and low temperature level, respectively.

The COP of an actual heat pump is significantly lower than that of an ideal one, as the compressor in a real heat pump has a limited efficiency, frictional and heat losses occur through the cycle and the heat exchangers for the evaporator and condenser need a temperature difference for the heat transfer.

It was previously mentioned that the HYBUILD heat pump can not only be used for heating but also for cooling. For this purpose the flow of the refrigerant is reversed and the condenser becomes the evaporator and vice versa. The coefficient of performance for this operations is calculated by the amount of heat extracted from the evaporator relative to the electrical work introduced to the heat pump:

$$COP_{\mathrm{cooling}} = \frac{Q_{\mathrm{L}}}{W_{\mathrm{el}}} \tag{3}$$

In an ideal heat pump the amount of heat extracted from the evaporator is equal to the amount of heat given to the environment in the condenser minus the total electrical energy consumption of the heat pump. This leads to:

$$COP_{\text{cooling}} = \frac{Q_{\text{L}}}{W_{\text{el}}} = \frac{Q_{\text{H}} - W_{\text{el}}}{W_{\text{el}}} = COP_{\text{heating}} - 1 \tag{4}$$

so the COP for cooling in the evaporator is one less than the COP for heating in the condenser.

The COP is highly dependent on the temperature level in the condenser and evaporator. As these temperatures change over time throughout the operation of the heat pump, it may be appropriate to calculate a long term average COP called the Seasonal Coefficient of Performance ($SCOP$) to compare different heat pump systems.The $SCOP$ of a heat pump is calculated by dividing the total thermal energy output by the total electrical energy consumption, for a full year of operation. There are also definitions of the whole system COP and $SCOP$ where the electrical power of auxiliary pumps and additional backup heaters are considered. When comparing different $COPs$ it should therefore be taken into account which components of the heat pump are included and which have been omitted.

There are many factors which affect the selection of a proper refrigerant. In the last century halogenated refrigerants where widely used due to their good thermodynamic and thermophysical properties. However, halogenated refrigerants have very bad environmental properties with respect to the ozone depletion potential (ODP) and the global warming potential (GWP). Due to these properties the use of halogenated refrigerants was restricted by the international protocols (Montreal any Kyoto). In most nations the use of chlorofluorocarbon (CFCs) was completely stopped, but hydrochlorofluorocarbons (HCFC) refrigerants can still be used until 2030. Halogen free hydrocarbons (HCs) and chlorine free hydrofluorocarbons (HFCs) were developed and due to their relative low environmental impacts, compared to HCFCs, applied in almost all applications. It should be noted that most HC refrigerants are highly flammable, which has to be taken care of (Mohanraj et al., 2011). In Table 1 the properties of some selected refrigerants are listed. A GWP of 1 is based on CO_2. According to the standard DIN EN 378-1 the safety classes are described by two alphanumerical characters. Rarely a third character is used to indicate a subclass. The capital letter in front states the toxicity. Class A signifies no toxicity for concentrations lower than 400 ppm. For class B there is evidence of toxicity above these concentrations. The digit of the safety class categorization corresponds to the flammability. Refrigerants in class 1 do not show any flame propagation in air for ambient conditions (21 °C and 1.01 bar). Class 2 indicates refrigerants with a lower flammability limit of more than 0.1kg/m^3 at ambient conditions and a heat of combustion of less than 19 kJ/kg. Refrigerants in class 3 exceed the limits of class 2. Additionally, there is a subcategory 2L, in which refrigerants of class 2 also have a limited burning velocity of less than 10 cm/s (ANSI/ASHRAE 34-2016, 2016).

Table 1: Properties of selected refrigerants (Hundy et al., 2016).

Refrigerant	Composition	Safety Class	Boiling Point (°C)	GWP
HCFC				
R22	$CHClF_2$	A1	-41	1810
HFCs chlorine free				
R134a	CF_3CH_2F	A1	-26	1430
R125	CF_3CHF_2	A1	-48	3500
R143a	CF_3CHF_3	A2	-48	4470
R32	CH_2F_2	A2L	-52	675
HCs halogen free				
R290	C_3H_8	A3	-42	3
R1270	C_3H_6	A3	-48	3
R600a	C_4H_{10}	A3	-12	3

The evaporator of a heat pump can be heated by different sources. The two most common used heat sources are ambient air and geothermal energy. Using geothermal energy can be advantageous for heating as the temperature of this source does not vary much throughout the year. However, it is cost-intensive as a borehole has to be drilled. The costs of a borehole can differ widely depending on the country, for example because of different soil properties and more competition on the market.

As an alternative to drilling deep into the ground, it is also possible to lay the pipes only slightly underneath the ground, but in a wider area. For this approach a big area is needed and as the whole area needs to be dug up this approach is more interesting for newly built houses and not for a later installation in existing houses.

An air source heat pump, on the other hand, is easier to install and mostly cheaper, as only a compact heat exchanger with a fan is necessary. In general the COP of an air source heat pump is slightly lower for heating operation due to:

- The lower temperature of air compared to ground water during the winter.
- Worse heat transfer from air to refrigerant compared to water to refrigerant.
- The need to power an additional fan.

- The fact that ice may freeze on the heat exchanger surface during the operation, which decreases the heat transfer from air to the refrigerant and leads to an increased air side pressure drop. To ensure continuous operation the frost has to be melted from time to time, which is energy consuming, and therefore reduces the efficiency of the heat pump further.

Also the condenser can heat different media. Nowadays, heat pumps work either with air or water as the heat sink. Heat pumps are named with respect to their heat source and sink media. For example a heat pump with air as its source and water as its sink media is referred to as an air-water heat pump.

Defrosting of an air source heat pump

During operation of an air source heat pump the refrigerant flowing through the outdoor evaporator unit may reach temperatures well below 0 °C. As soon as the temperature of the surface of the heat exchanger is below both water freezing temperature and air dew temperature, frost will start to form. This frost acts as an insulator on the heat exchanger surface and additionally decreases its cross section for the air flow, leading to a larger pressure drop and therefore a higher power demand of the fan, if the volume flow of the air is to be kept constant. As a consequence the COP and capacity of the heat pump decreases and the frost formation may even lead to a shut down of the system, when unconsidered (Amer and Wang, 2017). However, it should be stated that the latent heat transfer of the humidity in the air contributes significantly to the total heat transfer of an air source evaporator.

There are several techniques to slow down, reverse or prevent the frost formation. Most methods which aim on slowing down the frost formation base on coating the surface. In order to prevent frosting the air can be dehumidified in advance, using liquid or solid desiccants. Zhang et al. (2012), for example, describe the use of an additional heat exchanger coated with a solid desiccant in front of the regular outdoor evaporator, to dehumidify the air. The regeneration process of the desiccant can be done very effectively, leading to an increase in the COP of 5-30 %, compared to a regular state-of-the-art air source heat pump.

Active systems which reverse the frost formation by melting are generally based on three types: hot-gas reverse cycling, hot-gas bypassing and thermal resistance heating. In the latter approach a thermal resistance heater is placed at the outdoor heat exchanger unit. Kwak and Bai (2010) studied the benefits of using a thermal resistance heater for small capacity heat pumps, which may have problems with a reverse cycle or a hot-gas bypass defrost mode, due to its complexity. They achieved a stable operation of the heat pump and an increase in the COP under frosting conditions, compared to a reference heat pump without any defrost operation mode. The reference heat pump stopped operation at frosting conditions and used an internal electrical heater instead.

Yaqub et al. (2000) investigated the performance of different hot-gas bypass methods. They concluded that the most efficient method is to inject the hot-gas of the compressor directly into the inlet of the evaporator. Hot-gas reverse cycling means that the whole refrigerant cycle will be reversed, so that the evaporator becomes the condenser and vice versa. This is done by a four way valve which changes the flow direction out of the compressor. The big advantage of this method, compared to thermal resistance heating, is that the heat supplied to the outdoor coil to melt the frost is produced with a higher COP than 1, as the heat pump is transferring heat from the indoor space to the outdoor coil. As now the indoor unit works as the evaporator, heat is removed from the indoor air. For air-air heat pumps the fan of the indoor coil is usually turned off during defrosting, to avoid decreasing the thermal comfort (Minglu et al., 2010). Another advantage of the reverse cycle defrosting method is, that when the heat pump is able to reverse the refrigerant cycle it can also be used for cooling operation during summer, additional to the heating operation during winter.

2.2 Thermal Energy Storage

Thermal energy storage (TES) systems can make thermal energy equipment, as heat pumps, more effective, by offsetting the mismatch between availability and demand of energy. They can be divided into two main groups: Storing thermal energy by rising or lowering the temperature of the storage material is called sensible heat storage. If the energy is stored by changing the phase of the storage material the storage is known as latent heat storage. Both types may also be combined. Energy demands can vary on different time bases, which highly affects the choice of the TES system (Dincer and Rosen, 2011). It should be noted that there are also chemical thermal energy storage systems, but they are still in an earlier research state compared to sensible or latent TES (Alva et al., 2018). Only few commercial applications of chemical TES exist and therefore they are not further analyzed and discussed in this thesis. Sensible TES are of interest in the focus of this thesis as they are used for storing hot water in the buildings sector and a latent TES is implemented in the heat pump cycle for the proposed novel heat pump system.

2.2.1 Sensible Storage

Storage media of almost all sensible TES systems are water, air, oil, rock beds or sands. The amount of energy stored is mainly proportional to the temperature difference between the stored and initial temperature, the mass of the storage media and its heat capacity. They do not undergo any phase change over the temperature range. Each material has its advantages and disadvantages. One of the most used material is water, which has a high heat capacity, density but due to its liquid state at most operation conditions must be contained in a better quality container than a solid media (Dincer and Rosen, 2011). The amount of heat stored can be expressed as:

$$Q = mc_{\mathrm{p}}\Delta T = \rho c_{\mathrm{p}} V \Delta T \tag{5}$$

where Q denotes the stored heat, m the mass, c_p the specific heat capacity, ΔT the temperature difference between the stored and initial temperature, ρ the density and V the volume. It should be noted that as the heat capacity and density change depending on the temperature, averages need to be taken to fulfill this equation.

To store a lot of thermal energy in a small volume a large volumetric thermal capacity ρc_p is desired. In Table 2 the thermal capacities of common sensible TES materials are listed at 20 °C. Additionally the material should be inexpensive and have a large thermal conductance in order to have a large heat transfer to the storage media (Alva et al., 2018).

Table 2: Thermal capacities at 20 °C of some common TES materials (Dincer and Rosen, 2011)

Material	Density (kg/m^3)	Specific heat (J/kg K)	Volumetric thermal capacity ($10^6 J/m^3$ K)
Clay	1458	879	1.28
Brick	1800	837	1.51
Sandstone	2200	712	1.57
Wood	700	2390	1.67
Concrete	2000	880	1.76
Glass	2710	837	2.27
Aluminum	2710	896	2.43
Iron	7900	452	3.57
Steel	7840	465	3.68
Gravelly earth	2050	1840	3.77
Magnetite	5177	752	3.89
Water	988	4182	4.17

2.2.2 Latent Storage

In latent TES the storage material undergoes a phase change. Normally they operate between a liquid and solid state. Therefore they use the enthalpy of fusion/solidification to store energy. This is called the latent heat. Usually, the enthalpy difference between solid and liquid state is much higher than the enthalpy difference for sensible heating for common experienced temperature differences in sensible TES. For example, the latent specific enthalpy difference of water from solid to liquid is in the order of 330 kJ/kg, which is significantly higher than its sensible specific enthalpy difference of about 210 kJ/kg for a temperature increase of ΔT =50 K, which is an already large temperature increase of a sensible water storage. This leads to high TES capacities per unit mass, compared to sensible TES systems. As the phase change occurs at a constant temperature there is only a small temperature range throughout the operation.

Used phase change materials in latent TES are salt compounds, as eutectic salts and salt hydrates, as they are comparably cheap and have a useful phase change temperature. Another frequently used material category is paraffin waxes. They offer a high stability over repeated cycles without degradation of the material, are nontoxic and inexpensive (Dincer and Rosen, 2011).

As an example, the Rubitherm® Technologies GmbH in Germany provides various PCM materials for nearly all temperature ranges. The RT-LINE products are organic materials, which use the phase change from solid to liquid (and vice versa) to store and release heat. The properties of two selected phase change materials used in this work are listed in Table 3.

Table 3: Properties of two selected PCMs from Rubitherm® Technologies.

	Congealing/ Melting Area	Heat Storage Capacity	Density Solid/Liquid	Heat Conductivity
RT54HC	54-53/53-54 °C	200 kJ/kg	0.85/0.8 kg/l	0.2 W/mK
RT64HC	64-61/63-65 °C	250 kJ/kg	0.88/0.78 kg/l	0.2 W/mK

The congealing and melting area of these PCMs are nearly identical and they have a high heat storage capacity in the order of 200 kJ/kg. As their density differs slightly between the solid and liquid state, there is a small volume change during operation. A disadvantage of PCMs is the relative low heat conductivity in the order of 0.2 W/mK, compared to the heat conductivity of water of 0.6 W/mK at 25 °C in liquid state.

2.3 Heat Exchanger

Heat exchangers can be categorized regarding the phases of the media that exchange heat, i.e. solid, liquid or gaseous, and the geometry of the heat exchanger. Heat pumps consist of at least two heat exchangers, the condenser and the evaporator. There are many different kind of heat exchangers and in the present thesis we will focus on plate-heat exchanger for the condenser unit and fin-and-tube heat exchanger for the air cooled evaporator.

2.3.1 Plate Heat Exchanger

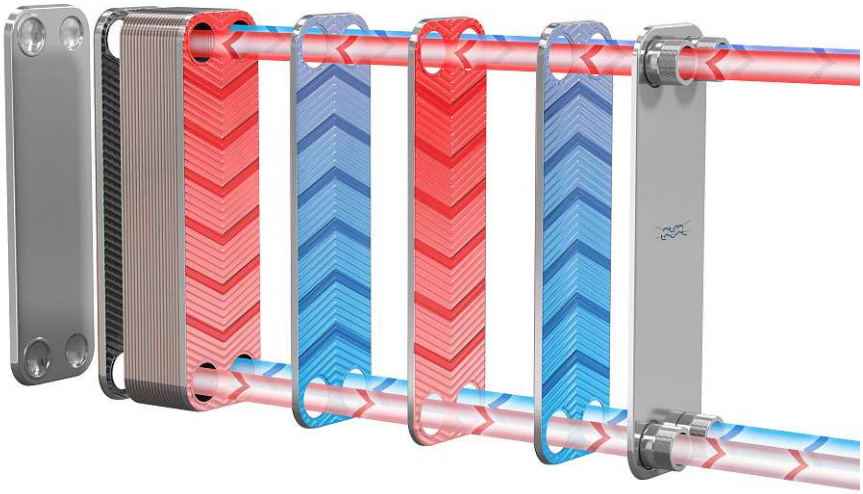

Figure 2: Schematic scheme of a plate heat exchanger (Alfa Laval, 2018). The red stream denotes the hot fluid flow and the blue stream denotes the cold fluid flow.

Plate heat exchangers, as seen in Figure 2, use metal plates in between the flowing fluids to transfer heat between them. The major advantage of plate heat exchangers is the large heat transferring surface, compared to other, mostly tube shaped, heat exchangers. Corrugating the metal plates, to achieve turbulent flow of the liquids, increases the heat transfer coefficient significantly (Zlatković et al., 2017). This leads to small physical sized heat exchangers. The mainly used material for plate heat exchangers is stainless steel and aluminium, due to its ability to withstand high temperatures, high corrosion resistance and strength (Guo et al., 2015). Increasing the heat exchange area of plate heat exchangers, in order to reach lower approach temperatures, may simply be achieved by adding additional plates to the stack. The space between the plates is maintained mostly by rubber sealing gaskets at the edges of the plates or by soldering the plates together. In the rigid frame the plates form parallel channels, in which the hot and cold liquids flow alternatively. By making each chamber fairly thin, the majority of the volume flow of the liquid is in contact with the heat exchange surface, therefore increasing the heat transfer. Additionally, the thin flowing channels lead to turbulent flow, even at low flow speeds, also increasing the heat transfer.

2.3.2 Finned Tube Heat Exchanger

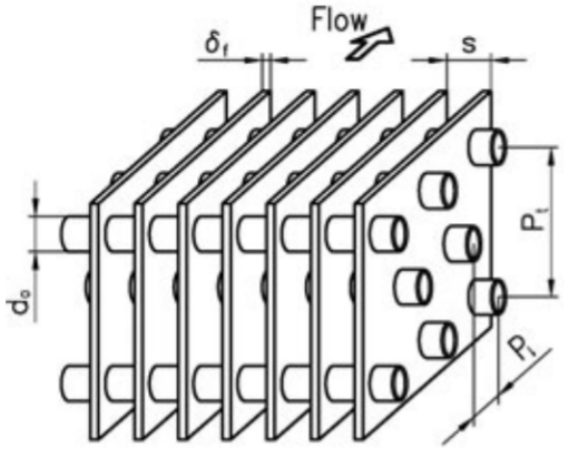

Figure 3: Schematic scheme of a finned tube heat exchanger (Taler, 2019). The geometric measures denoted in the Figure are s for the fin distance, δ_f for the fin thickness, d_o for the outer tube diameter, P_t for the vertical and P_l for the horizontal tube distance.

Finned tube heat exchangers, as sketched in Figure 3, extend the surface of the tubes by attaching metal pieces or whole plates onto the tubes. One fluid, which is mostly pressurized, flows inside these tubes and transfers heat to another gaseous fluid, which passes the finned tube heat exchanger surface in a cross-counter-flow (Taler, 2019). The gaseous fluid is mostly driven by a fan through the heat exchanger, while the fluid inside the pipes is rather driven by a pump or compressor. The tubes should be of a material with a good thermal conductivity, in order to achieve high heat transfer coefficients. The pressure drop of the gaseous fluid increases due to the fins, which has to be compensated by the flow driving fan. The smaller the diameter of the tubes, the better the heat transfer per area due to higher flow speeds, but this also leads to higher pressure drops. Small diameter of the tubes also decrease the amount of fluid in the heat exchanger, which may be of interest when handling flammable or toxic fluids, which should be present in the lowest quantities possible. The fins of a finned tube heat exchanger can be wavy, louver and slit, in order to improve the heat transfer. Still, the most commonly used form is the plain fin, due to its superior reliability under long term operation and lower friction characteristics (Wang et al., 2000).

If the air flows through the heat exchanger from the front to the back it can be referred to as an upright position, as used in car coolers. There are also horizontal finned tube heat exchangers, where the air flows through the heat exchanger from top to bottom, or vice versa. These lying heat exchangers are called table heat exchangers.

3 Experimental Work

The investigated heat pump uses air as heat source and water as sink. Therefore it is called an air-water heat pump. In order to investigate the effect of the implementation of the RPW-HEX, the heat pump is first examined without it and afterwards including it. The RPW-HEX consists of flow-layers of refrigerant and water with phase change material layers between them. In Figure 4 a picture of the RPW-HEX used in this project is shown. It has been manufactured by *AKG Thermal Systems*. In Figure 5 a symbolic sketch of this RPW-HEX can be seen. Each water and refrigerant layer is covered by two PCM layers and therefore the refrigerant and water flow layer never directly contact each other. Still, as each layer includes small fins, a good heat transfer from the refrigerant directly to the water exists. The RPW-HEX is furthermore divided into two levels, c.f. Figure 5a. The refrigerant enters the RPW-HEX on the top level, is redirected at the far end and leaves the RPW-HEX on the lower level. The water is counter-flowing and therefore entering the RPW-HEX on the lower level and leaves it at the top one. When entering the RPW-HEX both fluids are split into equal flows through the channels of the RPW-HEX. At the end these flows are gathered again to form a single output flow.

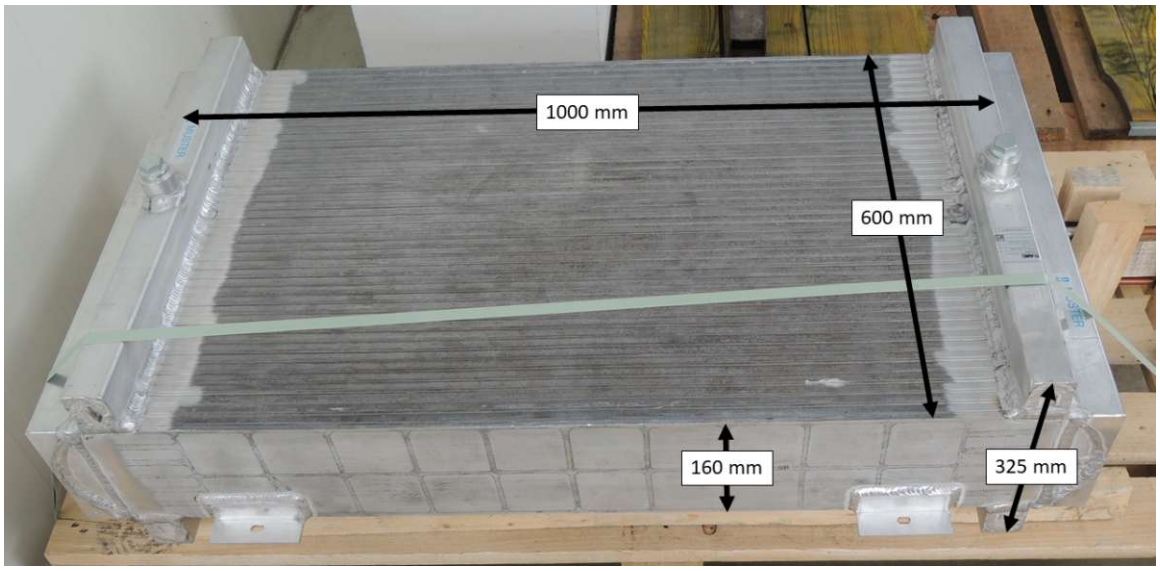

Figure 4: Picture of the RPW-HEX including the main geometric dimensions.

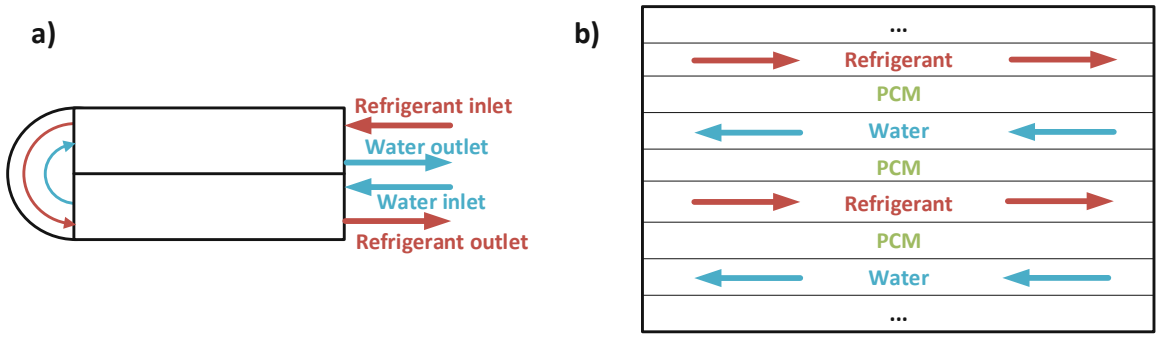

Figure 5: Symbolic scheme of the RPW-HEX. In a) the side view of the RPW-HEX is shown with the two levels and the construction to redirect the flow into the other layer. In b) the top view of the channels in the lower level are shown and the flow directions of the refrigerant and water channel flows are marked.

3.1 Setup

The investigated heat pump is produced by *Ochsner Wärmepumpen*. Not including the RPW-HEX, the setup is shown in Figure 6.

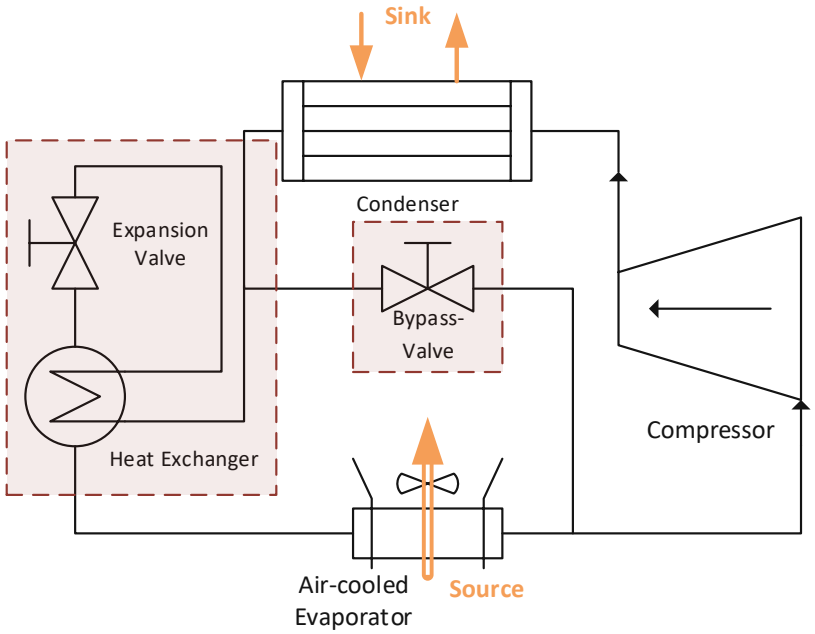

Figure 6: Setup of the heat pump without RPW-HEX. In red frames the new or adjusted components, compared to Figure 1, are highlighted. This includes a bypass valve and a heat exchanger transferring heat from the suction to the discharge stream of the expansion valve.

The heat pump operates with the R32 refrigerant, which is known to have a high temperature after the compressor compared to other refrigerants on the market. As the temperature in the compressor has has to stay below 120 °C, to ensure lubrication of the compressor, a valve is used to bypass some of the liquid refrigerant to the suction point of the compressor. This lowers the enthalpy at the suction point of the compressor and ensure a hot-gas temperature of less than 120 °C after the compressor. Note that by doing this a slight amount of liquid refrigerant is present at the suction point of the compressor, which has to be handled by the compressor. An additional heat exchanger in front of the expansion valve should ensure a liquid state of the refrigerant at the entrance of the valve, by sub-cooling the refrigerant after the condenser with the cold refrigerant at a lower pressure after the expansion valve. The air-cooled evaporator is realized as a horizontal finned tube heat exchanger, with horizontal tubes and vertical fins. The air is blown from the bottom to the top of the evaporator. As the fan can be covered very well, the resulting noise can be kept low. On the other hand, this construction is not as compact as a vertical finned tube heat exchanger. The condenser of the heat pump is realized as a plate heat exchanger, manufactured by *Alfa Laval*.

The setup of the heat pump including the RPW-HEX is shown in Figure 7. The RPW-HEX is located just after the compressor in the heat pump cycle. By using this location the highest temperature level of the refrigerant is used to charge the RPW-HEX.

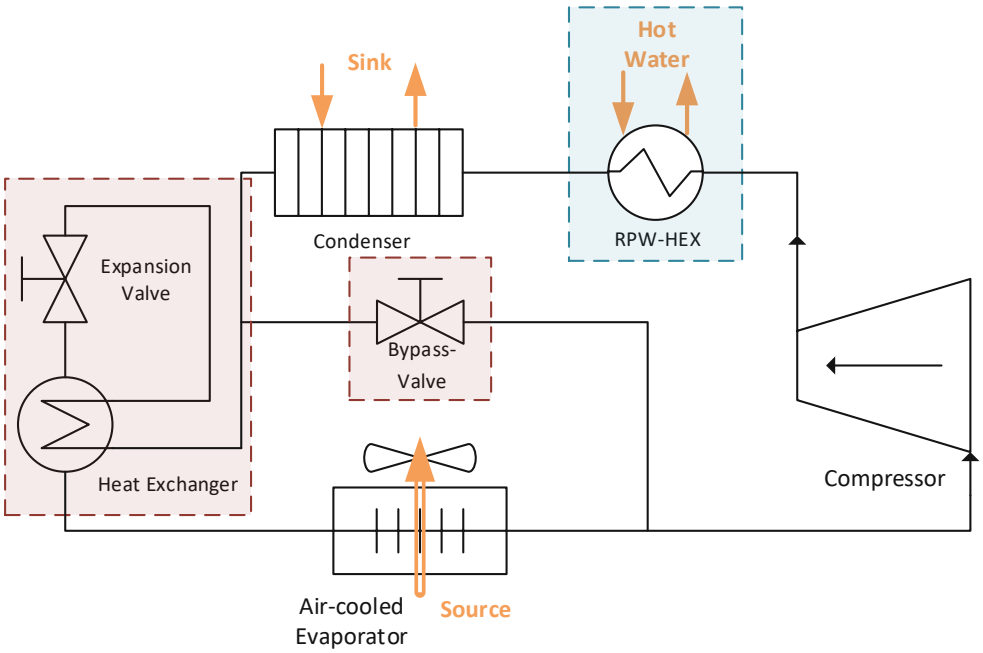

Figure 7: Setup of the heat pump including the RPW-HEX. In a blue frame the newly added RPW-HEX, compared to Figure 6, is highlighted.

RPW-HEX

Different phase-change materials can be used in the RPW-HEX and they are characterised by their melting point, heat capacity, density and thermal conductivity. In this setup the phase change material RT64HC from *Rubitherm* is used. Is has a melting point of around 64 °C. HC stands for a high crystallinity resulting in a high heat capacity. As the condenser, following the RPW-HEX in the refrigerant cycle, usually works on a lower temperature level, which dependents on the desired outlet water temperature of the feed water, only the sensible cooling of the refrigerant is used for charging the RPW-HEX during normal operation, while the whole phase change energy of the refrigerant is still available in the condenser. The RPW-HEX is manufactured by *AKG Thermal Systems*.

3.2 Seasonal Performance

Analyzing the performance of the heat pump was done similar to the standard DIN EN 14825 for air-water heat pumps for intermediate temperature applications. Briefly explained, the heat pump is tested separately in heating, cooling and domestic hot water (DHW) mode for different ambient conditions. The different ambient conditions are weighted accordingly over a regular year of operation and with the knowledge of the performance of the heat pump in the different ambient conditions a seasonal performance factor can be calculated. At first the heat pump is operated at specific nominal conditions with a fixed temperature difference of the feed water inlet and outlet and a fixed mass flow. These nominal conditions depend on the source and sink media of the heat pump and the climate where the heat pump is to be used. The compressor speed (or thermal power outlet) of the heat pump at these nominal conditions is prescribed by the heat pump manufacturer. Either the resulting mass flow or temperature difference is kept constant for the subsequent experiments regarding the part load behaviour. A constant feed water mass flow for all measurement points was chosen for the experiments regarding this thesis.

In the standard DIN EN 14511-3 a correction of the measured thermal power output and electrical power input for heat pumps including a circulating pump is proposed. The circulating pump is used to overcome the pressure drop in the condenser on the secondary, i.e. water, side. Shortly summarizing the correction, the hydraulic power of the circulating pump is calculated by measurement data. Depending on the hydraulic power an efficiency factor is obtained. With this efficiency and the hydraulic power the thermal and electrical power correction is calculated. The hydraulic power of the circulating pump is obtained by:

$$P_{\mathrm{hyd}} = \dot{q}_{\mathrm{water}} \Delta p_{\mathrm{water}} \tag{6}$$

where $\dot{q}$ denotes the volume flow and Δp the pressure drop on the water side.

In Appendix G.3 of the standard DIN EN 14511-3 an equation for the efficiency factor for wet rotor pumps is given:

$$\eta = \frac{0.35644 P_{\text{hyd}}}{1.7 P_{\text{hyd}} + 17\left(1 - e^{-0.3 P_{\text{hyd}}}\right)} \frac{C_{20}}{EEI} \tag{7}$$

with C_{20} a scaling factor of 0.49 and EEI the energy efficiency index of 0.23. The correction of the measured thermal power output and electrical power input of the heat pump due to the circulating pump is then calculated by:

$$\dot{Q}_{\text{th,cor,CP}} = \frac{1-\eta}{\eta} P_{\text{hyd}} \quad , \quad P_{\text{el,cor,CP}} = P_{\text{hyd}}/\eta \tag{8}$$

Regarding the standard, the measured electrical power includes the power demand of the controller and all auxiliary devices of the heat pump. As the following simulations in this thesis only include the power demand of the compressor and fan, the power demand of the auxiliary components of the heat pump should be subtracted from the measured electrical power to ensure comparability. Additionally, as the used heat pump is still in an experimental stage, a laptop and router were connected to the heat pump and therefore the electrical power measurement system. The laptop was necessary to enable changes to the controllers of the heat pump in short time. Via the router changes in the operation parameters of the heat pump can be made remotely and the operation status can be checked in real time. In order to compensate the power demand of all the auxiliary devices, the compressor and fan were turned off for a short time during the experiments and the remaining electrical power demand was measured. The mean of this measurement is then subtracted from the measured electrical power to correct the power demand of the auxiliary devices of the heat pump.

The calculation of the seasonal coefficient of performance of the experimental acquired data is based on the standard DIN EN 14825, without any corrections. It is separately calculated for the heating and cooling mode. The formulae to calculate the $SCOP$ is:

$$SCOP = \frac{\sum_{j=1}^{n} t_{\text{j}} \; P_{\text{H/C}}(\theta_{\text{amb,j}})}{\sum_{j=1}^{n} t_{\text{j}} \; \left(\frac{P_{\text{H/C}}(\theta_{\text{amb,j}})}{COP(\theta_{\text{amb,j}})}\right)} \tag{9}$$

where $\theta_{\text{amb,j}}$ denotes the outdoor temperature level, t_{j} the amount of hours at a specific temperature level $\theta_{\text{amb,j}}$, $P_{\text{H/C}}(\theta_{\text{amb,j}})$ the heating or cooling demand at a specific temperature level $\theta_{\text{amb,j}}$ and $COP(\theta_{\text{amb,j}})$ the coefficient of performance of the heat pump at a specific temperature level $\theta_{\text{amb,j}}$. The outdoor temperature levels and amount of hours at each temperature level are defined in standard DIN EN 14825 for different climates, i.e. hot, average and cold. For the calculation of the season performances in heating and cooling mode of the experimental data an average climate was chosen. The COP in between different outdoor temperature levels is linear interpolated, as suggested in the standard.

3.3 Data Acquisition and Sensor Placement

Temperature and humidity of the climate chamber are recorded in an already available LabView program at AIT. Additionally, the voltage, current, power factor and electrical power are recorded and stored in a csv-file. Internal heat pump parameters are accessed via modbus and are pushed to an OPC UA server hosted by an industrial PC. Additional sensors in the feed water and refrigerant cycle and the measurements of the scale are also stored on this OPC UA server. The data of the OPC UA can be exported as csv-files. The different data sources are read by a python script and stored in pandas data-frames for easy access and further usability.

Figure 8 shows the sensors and their position which are included in the heat pump cycle. The data on the OPC UA server can easily be accessed by the tools of *B&R Industrial Automation GmbH* like APROL DisplayCenter and APROL TrendViewer for quick checks and adjustments to parameters, if necessary.

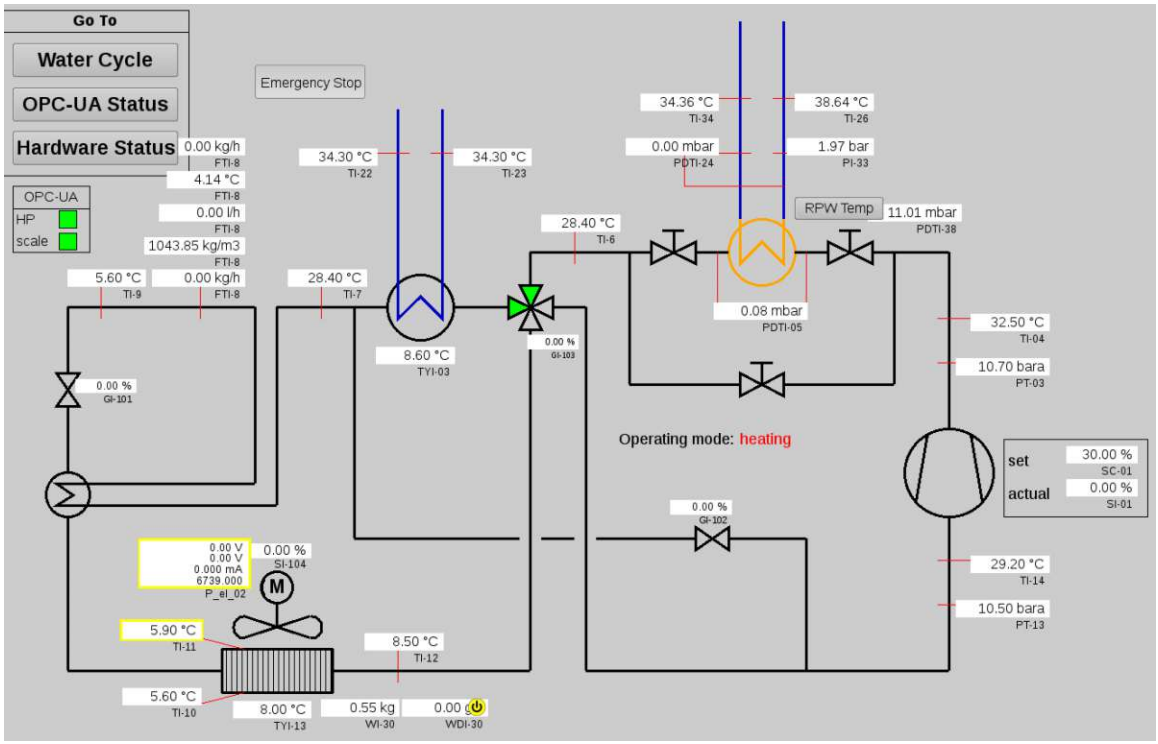

Figure 8: Screenshot of the APROL DisplayCenter of *B&R Industrial Automation GmbH* showing all sensors and their position which are included in the heat pump cycle.

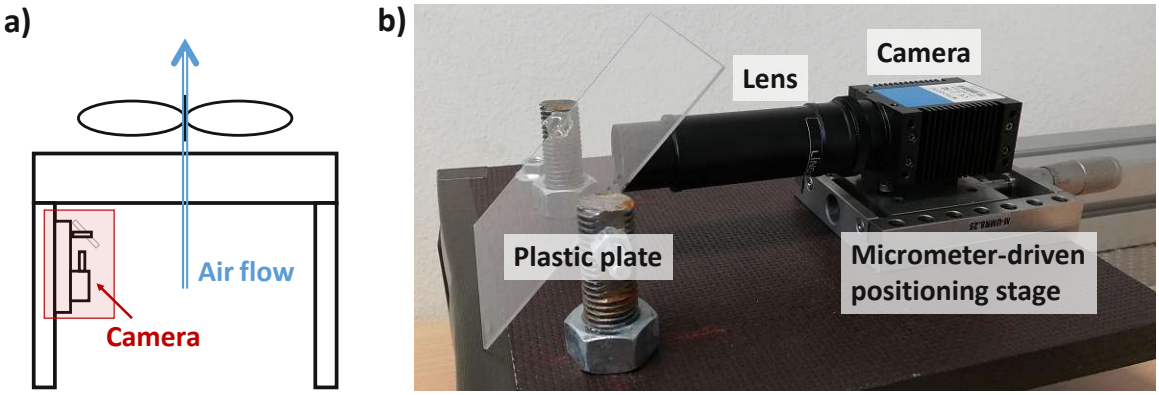

Figure 9: a) Schematic sketch to show where the camera is mounted on the table evaporator. b) Camera with macro lens for observation of frost growth on the heat exchanger surface with construction (plastic plate) to avoid water to fall on the camera.

In order to see the aggregation of frost on the fins of the evaporator during operation at low ambient temperatures, a camera was installed underneath the evaporator. The industrial camera used was a DFK 33GP1300e from *Imaging Source*. As the distance between the fins is very small (a few millimeter) a macro CCD-lens was mounted on top of the camera. The lens is manufactured by *Linos* with a fixed focal length of 50 mm and a camera aperture of 4. In order to focus the camera precisely, the camera was mounted on a micrometer-driven positioning stage. In Figure 9 a schematic sketch is shown to see where the camera is exactly mounted. Additionally, a picture of the camera including a construction to avoid water to fall directly on the camera can be seen. To furthermore quantize the frost formation, the evaporator was put on a scale to measure the weight increase due to condensed water and accumulated frost on its fins. The data of the scale is passed to the OPC UA server, as stated previously.

4 Numerical Setup & Methodology

As a lot of different ambient conditions and feed water temperatures are of interest, experiments alone would not give enough data points in reasonable time. Therefore, a numerical model helps to compare the heat pump including the RPW-HEX to a reference conventional heat pump without it. Furthermore, different phase change materials and changes in the operation parameters can be tested with it. Because the numerical model has to be validated, the experimental measurements are still of great importance.

4.1 Software

For the numerical simulation a DYMOLA/MODELICA model was created using the THERMOCYCLE library (Quoilin et al., 2014) and parts of the AIT MODELICA library, as the RPW-HEX and the outdoor unit (Emhofer et al., 2018; Frazzica et al., 2018). The fluid properties were acquired from the COOLPROP library (Bell et al., 2014). For autonomous starting of simulations with different ambient and operation conditions the Python BUILDINGSPY library was used (Wetter et al., 2014). The plots of the results were created with the MATPLOTLIB library in Python (Hunter, 2007).

4.1.1 Dymola/Modelica

DYMOLA is a commercial modeling and simulation software by the European company *Dassault Systèmes*. The name DYMOLA stands for Dynamic Modeling Language. It is based on the open MODELICA modeling language. MODELICA is developed by the non-profit *Modelica Association*. MODELICA is a object-oriented programming language and its classes mostly consist of set of equations. Contrary to other simulation languages these equations do not necessarily need to be assignments like $x := y+4$, but can have expressions on both the left- and right-hand side, for example $x + 3 = 2y - 2$. These equations do not indicate assignments but equality between the left- and right-hand side. The simulation engine needs to preprocess these equations to determine the order of execution and compute which variables are inputs and which are outputs, c.f. Fritzson (2011).

4.1.2 Thermocycle

THERMOCYCLE is an open-source library for the simulation of thermal systems. It is developed in the MODELICA language. Most MODELICA libraries which are aiming for simulating gas- and steam-cycles do not include the simulation of non-conventional working fluids as refrigerants. The THERMOCYCLE library however does include the simulation of

non-conventional working fluids. This is achieved by a strong coupling with the open-source thermodynamic properties database Coolprop (Quoilin et al., 2014). More information on the THERMOCYCLE library can be found in Quoilin et al. (2013) and on the homepage `http://www.thermocycle.net/`.

4.1.3 CoolProp

COOLPROP is an open-source thermophysical property library. It can handle a large amount of fluids, with more than 110 different fluids included. CoolProp is a C++ library with wrappers for many kinds of software, as for Python, EXCEL and MODELICA (Bell et al., 2014). The underlying methods for the evaluation of fluid properties are described in plenty of works, for example in Bell and Jäger (2016). Additional information on the software can also be obtained on the web page `http://www.coolprop.org/`.

4.1.4 Python

Python is an interpreted, high-level programming language. It supports object oriented programming and is managed by the non-profit Python Software Foundation. Most Python installations come with a wide range of free to use libraries, as NUMPY, PANDAS and the MATPLOTLIB library. NUMPY stands for numerical python and offers a wide range of functions for numerical computation. PANDAS is a library to easily create and access data-structures for data analysis. The MATPLOTLIB library creates good looking 2D plots with very little code needed (Hunter, 2007). For further reading see Donaldson (2008). Moreover, Python can be extended with a variety of extra libraries, as the BUILDINGSPY library. BUILDINGSPY is a python library to run MODELICA simulations using DYMOLA and read the created result files. More information about the BUILDINGSPY library can be taken from Wetter et al. (2014).

4.2 Numerical Model

A DYMOLA model of the reference conventional heat pump and the novel heat pump including the RPW-HEX was created for the 3 different operating modes: heating, cooling and domestic hot water generation. The DYMOLA models consist of various components of the standard MODELICA library and the THERMOCYCLE library. Some components needed adjustments and coding to meet the desired requirements.

4.2.1 Components

The main components needed to model the heat pump are:

- Compressor
- Condenser
- Valve
- Heat Exchanger
- Evaporator
- RPW-HEX

Each component consists of its describing equations, which might be connected to equations of other components. The evaporator and RPW-HEX required self-built models, which where created by modifying and extending existing THERMOCYCLE components.

Compressor

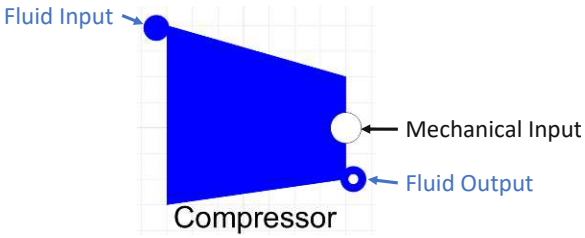

Figure 10: Icon of the THERMOCYCLE compressor component with two fluid ports and one mechanical port.

In Figure 10 the icon of the THERMOCYCLE compressor component is shown. It has two inputs and one output. The blue dots represent the fluid flow input (filled dot) and output (blue dot including a small white dot). The white circle on the right side is a mechanical input, which gives the rotational speed N_{rot} of the shaft. The main equations which describe the component are:

$$h_{\text{out}} = h_{\text{in}} + \frac{h_{\text{out,s}} - h_{\text{in}}}{\eta_{\text{s}}} \quad , \quad \dot{W} = \dot{m}(h_{\text{out}} - h_{\text{in}}) \quad , \quad \dot{m} = \eta_{\text{v}} V_{\text{swept}} N_{\text{rot}} \rho_{\text{in}} \tag{10}$$

where h_{out} and h_{in} state the specific enthalpy at the fluid outlet and inlet port, respectively, $h_{\text{out,s}}$ the specific enthalpy at the fluid outlet port reached when assuming an isentropic compression, η_{s} the isentropic efficiency, $\dot{W}$ the power demand, $\dot{m}$ the fluid mass flow, η_{v} the volumetric efficiency, V_{swept} the swept volume of the compressor, N_{rot} the rotational speed of the compressor and ρ_{in} the density of the fluid at the inlet port.

Heat Exchanger / Condenser

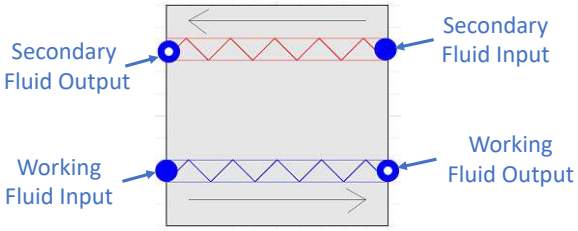

Figure 11: Icon of the THERMOCYCLE heat exchanger component with two fluid input ports and two fluid output ports.

Figure 11 shows the THERMOCYCLE heat exchanger component. It has two inputs and two outputs, representing two fluid flows which exchange heat with each other. In the blue coil flows the working fluid, in the red coil the secondary fluid flows. The condenser component is only a minor modification of the simple heat exchanger component, which allows the working fluid to be compressible and change phase during the heat exchange. The heat exchanger component is discretized into a finite amount of cells. Each cell consists of two 1D-fluid flow components (one for the working and one for the secondary fluid) which exchange heat via a wall component. In each 1D-fluid flow there is one single temperature and pressure, hence one specific fluid state. The energy and mass balance in the 1D-fluid flow component are described as:

$$\begin{aligned} V_{\text{cell}}\rho\dot{h} + \dot{m}_{\text{out}}(h_{\text{out}} - h) - \dot{m}_{\text{in}}(h_{\text{in}} - h) - V_{\text{cell}}\dot{p} &= \dot{Q} \\ \dot{Q} &= A\ U(T_{\text{port}} - T_{\text{cell}}) \\ \dot{m}_{\text{in}} - \dot{m}_{\text{out}} &= V_{\text{cell}}(\frac{d\rho}{dh}\dot{h} + \frac{d\rho}{dp}\dot{p}) \end{aligned} \tag{11}$$

where V_{cell} represents the volume of one cell, ρ the fluid density, h the specific enthalpy of the fluid, $\dot{m}_{\text{out}}$ and $\dot{m}_{\text{in}}$ the fluid mass flow at the outlet and inlet, respectively, h_{out} and h_{in} the specific enthalpy of the fluid at the outlet and inlet, respectively, p the fluid pressure and $\dot{Q}$ the heat flow transferred to the cell. In the second and third equation A denotes the contact area between the cell and the wall, U the coefficient of heat transfer, T_{port} the temperature of the fluid at the heat port, i.e. the wall, and T_{cell} the temperature of the fluid in the cell. The energy balance of the wall component connecting the 2 fluid flow components is described as:

$$m_{\text{wall}}\dot{T}_{\text{wall}}c_{\text{wall}} = \dot{Q}_{\text{in}} - \dot{Q}_{\text{out}} \tag{12}$$

where m_{wall} represents the mass of the wall, T_{wall} the temperature of the wall, c_{wall} the specific heat capacity of the wall and $\dot{Q}_{\text{in}}$ and $\dot{Q}_{\text{out}}$ the heat flow coming in and out of the wall cell, respectively.

The heat transfer coefficient U in the 1D-cell component is dependent on the mass flow and is calculated by:

$$U = U_{\text{nom}} \left(\frac{\dot{m}}{\dot{m}_{\text{nom}}} \right)^{0.8} \tag{13}$$

where U_{nom} and $\dot{m}_{\text{nom}}$ denote the nominal heat transfer coefficient and mass flow, respectively.

Valve

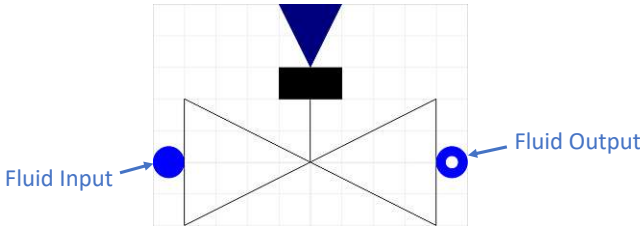

Figure 12: Icon of the THERMOCYCLE valve component with two fluid and one real port, defining the opening position of the valve.

The icon of the THERMOCYCLE valve component is shown in Figure 12. It has two inputs and one output. Besides the fluid flow input and output (blue dots), there is an input for the opening of the valve (blue triangle). The describing equations of the valve are:

$$\dot{m} = A\sqrt{2\rho\Delta p} \quad , \quad A = A_{\text{full}} x_{\text{open}} \tag{14}$$

where A represents the valve cross section, Δp the pressure drop over the valve, A_{full} the valve cross section when fully opened, and x_{open} the opening degree.

Evaporator

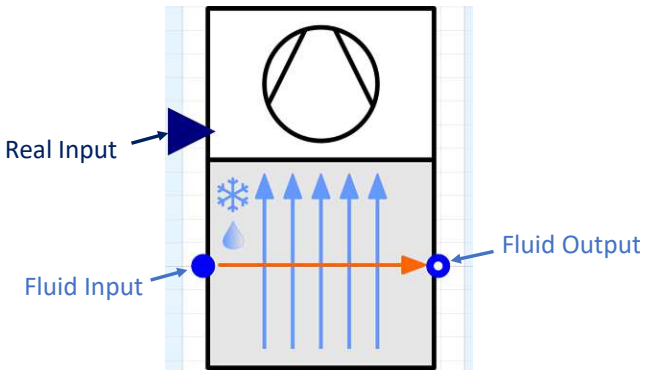

Figure 13: Icon of the THERMOCYCLE evaporator component with two fluid ports and one real port, defining the fan speed.

The evaporator needed to be self-built to meet the desired requirements and to be extendable for future models. The created icon can be seen in Figure 13. Similar to the regular heat exchanger model the evaporator is discretized into a finite amount of cells. Each cell consists out of a THERMOCYCLE 1D-cell component for the refrigerant flow, which is connected to a wall component via a heat port. This wall component is again connected to a self-built air-flow model via the other heat port.

The air-side pressure drop and heat transfer is calculated according to Shah and Sekulic (2007) for corrugated flat fins on a tube array. The describing equations are:

$$\Delta p_{\mathrm{air}} = \rho_{\mathrm{air,in}} \frac{u_{\mathrm{air,m}}^2}{2} 4f \frac{L_{\mathrm{f}}}{d_{\mathrm{h}}} + \rho_{\mathrm{air,in}} \frac{u_{\mathrm{air,le}}^2}{2} (K_{\mathrm{c}} + K_{\mathrm{e}}) \tag{15}$$

$$Nu = jRe_{\mathrm{dh}} Pr^{1/3} \tag{16}$$

where Δp_{air} denotes the pressure drop on the air side, $u_{\mathrm{air,m}}$ the bulk air velocity, $u_{\mathrm{air,le}}$ the leading edge air velocity, L_{f} the length of fins along the air flow, d_{h} the hydraulic diameter, K_{c} the compression and K_{e} the expansion coefficient for the heat exchanger in- and outlet, respectively. The coefficients j and f are the Colburn and fanning friction factor, respectively, and Nu and Re_{dh} denote the Nusselt and Reynolds number based on the hydraulic diameter d_{h}, respectively. Correlations for the coefficients f and j for corrugated flat fins on a tube array are given as:

$$f = 0.01915 Re_{\mathrm{dc}}^{c_5} (\tan\gamma)^{c_6} \left(\frac{d_{\mathrm{fp}}}{d_{\mathrm{l}}}\right)^{c_7} \left(\ln \frac{A_{\mathrm{eff,sc}}}{A_{\mathrm{pt,sc}}}\right)^{-5.35} \left(\frac{d_{\mathrm{h}}}{d_{\mathrm{c}}}\right)^{1.3796} N_{\mathrm{l}}^{-0.0916} \tag{17}$$

$$j = 0.324 Re_{\mathrm{dc}}^{c_1} \left(\frac{d_{\mathrm{fp}}}{d_{\mathrm{l}}}\right)^{c_2} (\tan\gamma)^{c_3} \left(\frac{d_{\mathrm{l}}}{d_{\mathrm{t}}}\right)^{c_4} N_{\mathrm{l}}^{0.428}; \tag{18}$$

where γ denotes the angle of the corrugated fins, d_{fp} the distance between the fins, d_{l} the distance between tubes parallel to the air flow, d_{t} the distance between tubes perpendicular

to the air flow, d_c the collar diameter, $A_{eff,sc}$ the effective heat transfer area for one cell, $A_{pt,sc}$ the tube outside area with no fins and N_l the amount of subsequent rows of tubes. The coefficients c_1-c_7 are calculated by:

$$c_1 = -0.229 + 0.115 \left(\frac{d_{fp}}{d_c}\right)^{0.6} \left(\frac{d_l}{d_h}\right)^{0.54} N_l^{-0.284} \ln(0.5 \tan\gamma) \tag{19a}$$

$$c_2 = -0.251 + \frac{0.232 N_l^{1.37}}{\ln(Re_{dc}) - 2.303} \tag{19b}$$

$$c_3 = -0.439 \left(\frac{d_{fp}}{d_h}\right)^{0.09} \left(\frac{d_l}{d_t}\right)^{-1.75} N_l^{-0.93} \tag{19c}$$

$$c_4 = 0.502 \left(\ln(Re_{dc}) - 2.54\right) \tag{19d}$$

$$c_5 = 0.4604 - 0.01336 \left(\frac{d_{fp}}{d_l}\right)^{0.58} \left(\ln \frac{A_{eff,sc}}{A_{pt,sc}}\right) (\tan\gamma)^{-1.5} \tag{19e}$$

$$c_6 = 3.247 \left(\frac{d_{fp}}{d_t}\right)^{1.4} \ln \frac{A_{eff,sc}}{A_{pt,sc}} \tag{19f}$$

$$c_7 = -\frac{20.113}{\ln Re_{dc}} \tag{19g}$$

RPW-HEX

The RPW-HEX component was modeled using modified versions of the Cell1D, Flow1D and wall components of the ThermoCycle library. It is assumed that all parallel water, refrigerant and PCM passages behave identically. Therefore, the storage can be divided into symmetric cells, consisting of a water cell, a refrigerant cell and a PCM cell. The PCM cell was modelled modifying the wall component, while the water and refrigerant cell are modified Flow1D cells, in order to have two heat ports instead of one. In Figure 14 the RPW-HEX Dymola model consisting of the modified ThermoCycle components is shown.

While the connection of the heat ports between the water or refrigerant layer with the PCM layer is directly related to the contact between those two layer, the connection between the water and refrigerant layer represents the indirect heat transfer via the fins between the channels of the heat exchanger. Actually there would be a PCM layer for every other layer, be it a water or refrigerant layer. Therefore, in one symmetric cell there would be two PCM layers. But there are two RPW-HEX versions in the HYBUILD project, one for the Continental and one for the Mediterranean climate. In the Mediterranean system only one PCM layer is present. In order to use the same RPW-HEX component, it was chosen, that only one PCM layer is modeled and for the Continental system the heat exchange area of the PCM channels is doubled. This leads to the same heat transfer from the refrigerant and water layer and also accounts for the heat capacity of the PCM layer. The advantage of using the existing cell components from the ThermoCycle library is that state-of-the-art

discretization schemes and options for well-established heat transfer correlations, e.g. the first order upwind discretization scheme and Shahs heat transfer correlations, are already implemented. More detailed information about the DYMOLA RPW-HEX model can be seen in Emhofer et al. (2018).

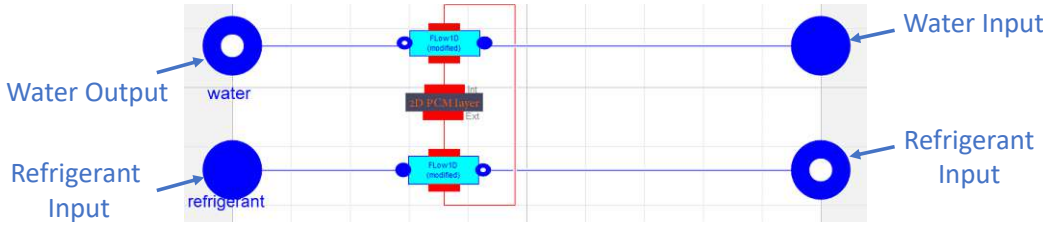

Figure 14: Graphical representation of THERMOCYCLE cells used to define the RPW-HEX model. The Flow1D cells are modified to have two heat ports and the wall component was modified to account for the PCM layer. The red lines denote a heat connection, while the blue lines show the fluid flow.

The State of Charge (SoC) of a latent thermal storage with solid/liquid PCM can be defined in many ways. In this thesis the definition originally proposed by Barz et al. (2018) is used: *The term state of charge (SoC) and the symbol* Ξ *are used to indicate the extent to which a latent thermal storage is charged relative to storable latent heat. The SoC* Ξ *is calculated as the geometric mean of local (liquid mass) phase fraction fields* $\xi(x, y, z)$*, where* x*,* y*,* z *represent spatial coordinates of the PCM contained in the latent thermal storage.*[2]
The local phase fraction values can be directly derived from local temperatures. Therefore, the temperature fields $T(x, y, z)$ can be directly transformed into phase fraction fields $\xi(x, y, z)$. With the assumption that all parallel passages and PCM layers behave identically, the storage internal temperature can be represented by one PCM layer only. It is further assumed that the three-dimensional planar geometry can be reduced to a two dimensional geometry. One coordinate pointing in the water or refrigerant flow direction (x on the domain $0 \leq x \leq L$) and one coordinate pointing into the PCM layer perpendicular to the first coordinate (y on the domain $0 \leq y \leq d$). For this geometry, the state of charge Ξ is calculated by:

$$\Xi = \frac{\int_0^L \int_0^d \xi(x, y) dy dx}{L\ d} \tag{20}$$

with L denoting the length of one cell in flow direction of the refrigerant or water and d the width of the PCM layer perpendicular to the flow direction of the refrigerant or water. The integration of Equation 20 is carried out numerically in the PCM layer cell component, as shown in Figure 14. The Icon of the RPW-HEX component is self constructed and can be seen in Figure 15.

[2] as stated in Emhofer et al. (2018)

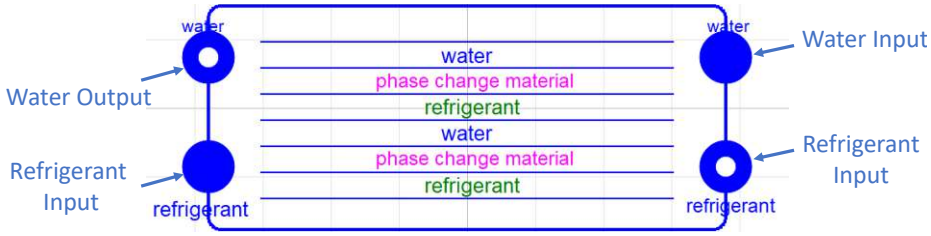

Figure 15: Icon of the self constructed RPW-HEX component with water and refrigerant inlet and outlet ports.

4.2.2 Modes

The heat pump can be operated in heating mode, cooling mode and to generate DHW. For each of these modes two models were created, one for the reference conventional system and one for the proposed novel system, including the RPW-HEX. Performance maps were created for each of these models.

Heating

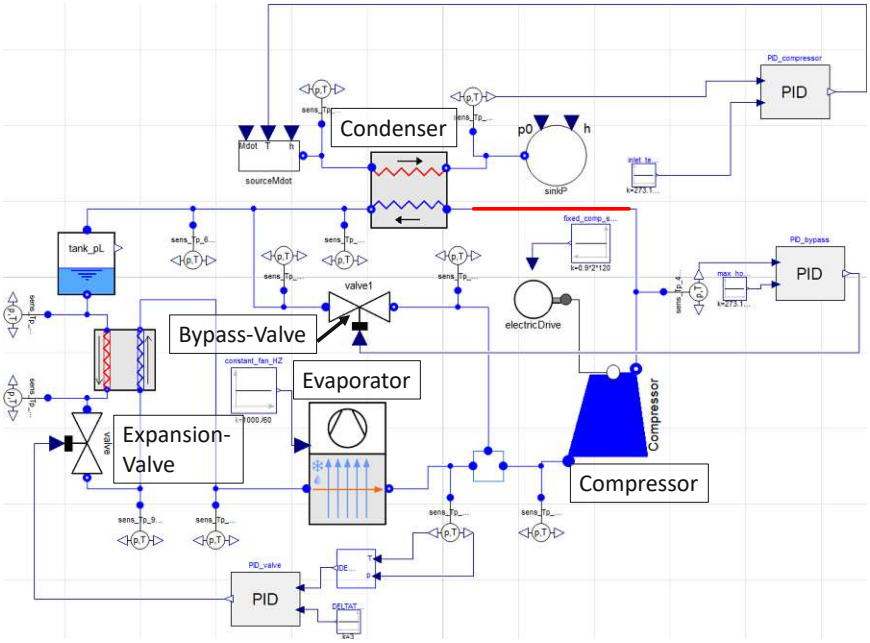

Figure 16: Dymola model of the reference heat pump in heating mode. The red line indicates where the RPW-HEX is going to be included in the novel system model.

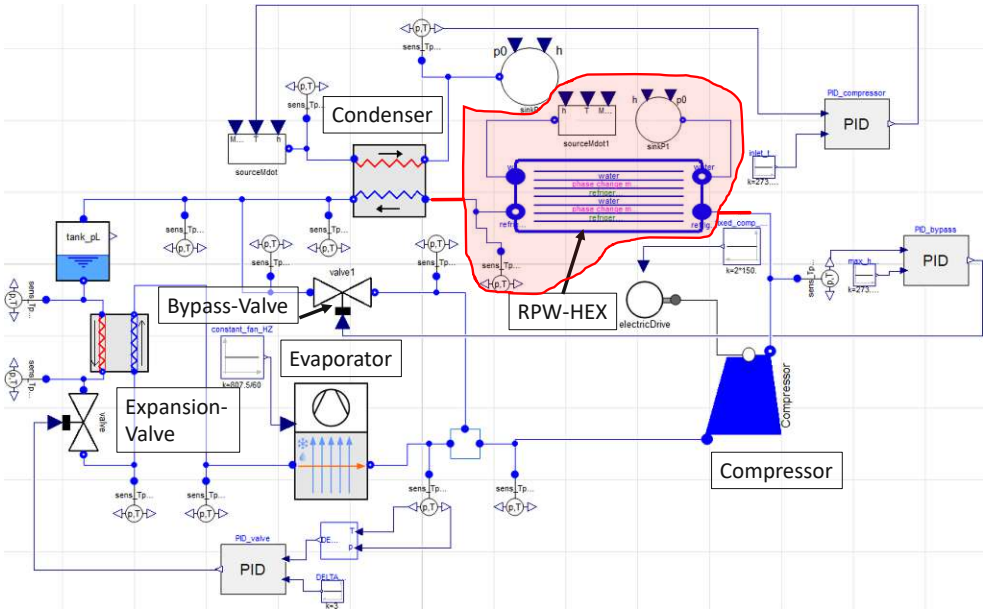

Figure 17: Dymola model of the heat pump including the RPW-HEX in heating mode. The added components, compared to the reference heat pump model as seen in Figure 16, are in the red area. This includes the RPW-HEX, a source, a sink and a sensor.

In Figure 16 the Dymola model of the reference system in heating mode is shown. A PID-Controller is used to adjust the return water temperature in order to reach the desired supply water temperature. Depending on the compressor speed, the fan speed is set. The opening of the expansion valve is adjusted to reach a super-heating of 3 °C after the evaporator. In order to ensure a hot-gas temperature below 115 °C after the compressor, a valve bypasses refrigerant from the outlet of the condenser to the inlet of the compressor. A small fraction of liquid refrigerant at the entrance of the compressor is therefore accepted and has to be handled by the compressor. The tank component after the condenser ensures numerical stability, especially at the initialization and start of the simulation. A small heat exchanger should ensure a liquid state before entering the expansion valve, by cooling the refrigerant at the suction point of the expansion valve with the refrigerant discharging the valve.

The Dymola model of the heat pump including the RPW-HEX in heating mode is displayed in Figure 17. The difference of this model is the inclusion of the RPW-HEX in the super-heated refrigerant section after the compressor, indicated by a red line in the figure. On the secondary side (water side) the RPW-HEX is bypassed, therefore the source in the numerical model is set to zero mass flow. While being in heating mode, the RPW-HEX is charged by the super-heated refrigerant after the compressor.

Cooling

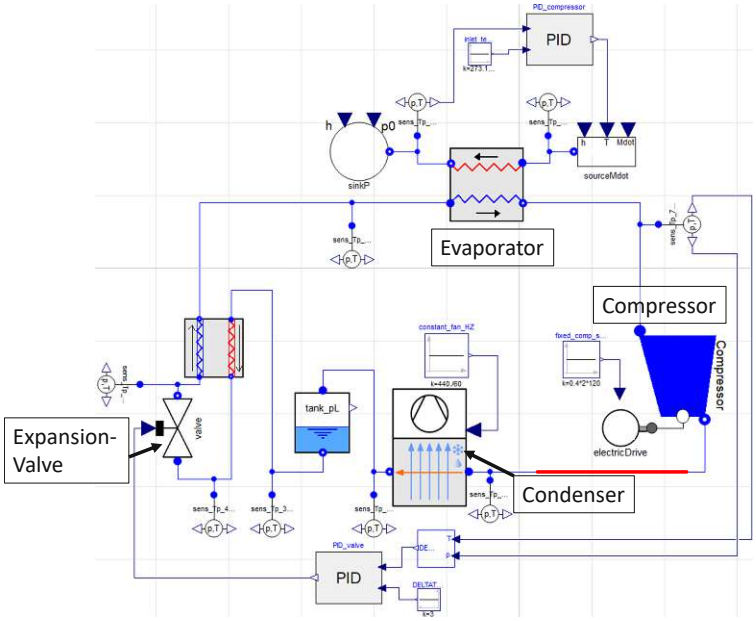

Figure 18: Dymola model of the reference heat pump in cooling mode. The red line indicates where the RPW-HEX is going to be included in the novel system model.

In Figure 18 the Dymola model of the reference system in cooling mode is shown. In this mode the bypass valve is not active, therefore it is not included in the mdoel. The evaporator component now acts as the condenser and transfers heat from the refrigerant to the ambient air. Vice versa, the condenser component now acts as an evaporator and extracts heat from the supply water. As in the heating mode, a small heat exchanger should guarantee liquid refrigerant entering the expansion valve, by cooling the refrigerant at the suction point of the valve with the refrigerant after the valve. The tank component ensures numerical robustness. Regardless of the compressor speed, the evaporator fan works with a fixed revolution speed, as in real operation of the analyzed reference heat pump.

Figure 19 shows the novel system in cooling mode. The RPW-HEX is again located after the compressor to be charged by the super-heated refrigerant, marked with a red edging.

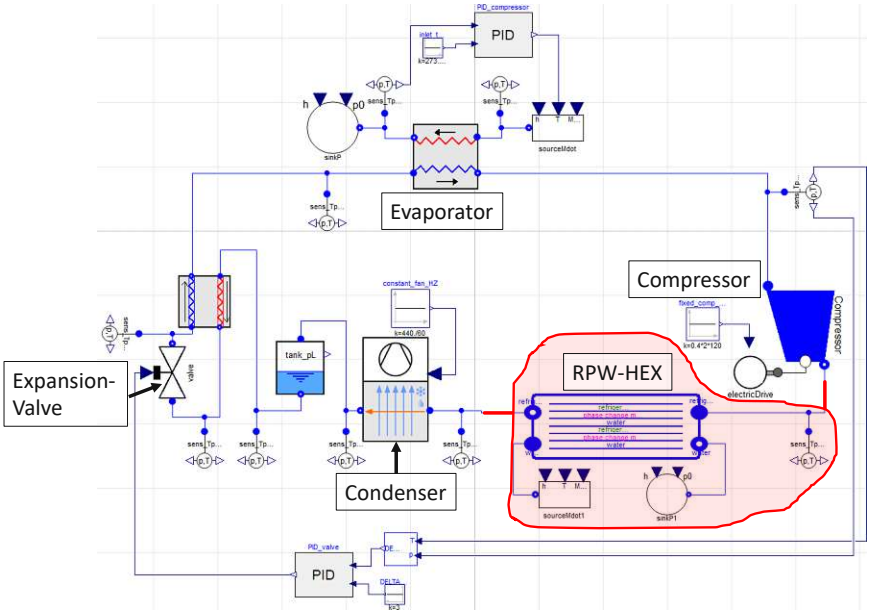

Figure 19: Dymola model of the heat pump including the RPW-HEX in cooling mode. The added components, compared to the reference heat pump model as seen in Figure 18, are in the red area. This includes the RPW-HEX, a source, a sink and a sensor.

Domestic Hot Water

In Figure 20 the Dymola model of the reference system in DHW generation mode is shown. The DHW generation mode for the reference system works identically to the heating mode, but normally with a higher supply water temperature. Due to these high supply water temperatures, high condenser temperatures are necessary and therefore a higher power demand of the compressor compared to the heating mode is required. These high compressor powers lead to high hot-gas temperatures of the refrigerant after the compressor. As in the heating mode, the fan speed of the evaporator is set proportional to the compressor speed.

Figure 21 shows the Dymola model of the novel system in DHW generation mode. As in the heating mode, the super-heated refrigerant flows through the RPW-HEX after the compressor. But in contrast to the heating mode, the RPW-HEX is not bypassed on the water side, but the water is further heated by the refrigerant in the RPW-HEX after the condenser. Therefore, the RPW-HEX simply acts as a heat exchanger in this mode. Even though the refrigerant and the supply water are never in direct contact with each other, as a layer of phase change material exists between them, the heat transfer between the refrigerant and the supply water is rather good, due to the fins inside the layers of the RPW-HEX.

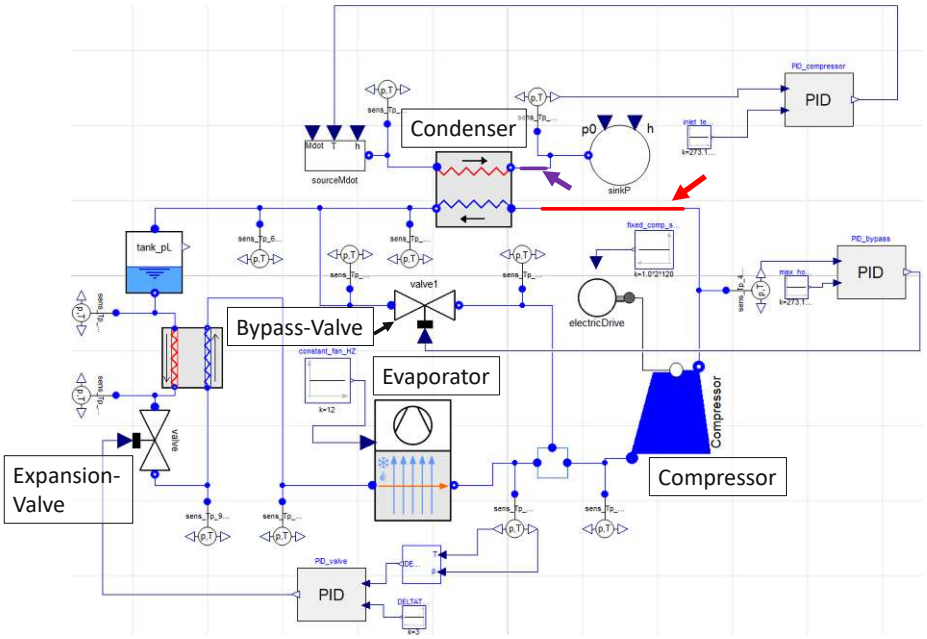

Figure 20: Dymola model of the reference system in DHW generation mode. The red line indicates where the RPW-HEX is going to be included in the refrigerant cycle of the novel system model. The purple line shows where the RPW-HEX will be connected to the water cycle.

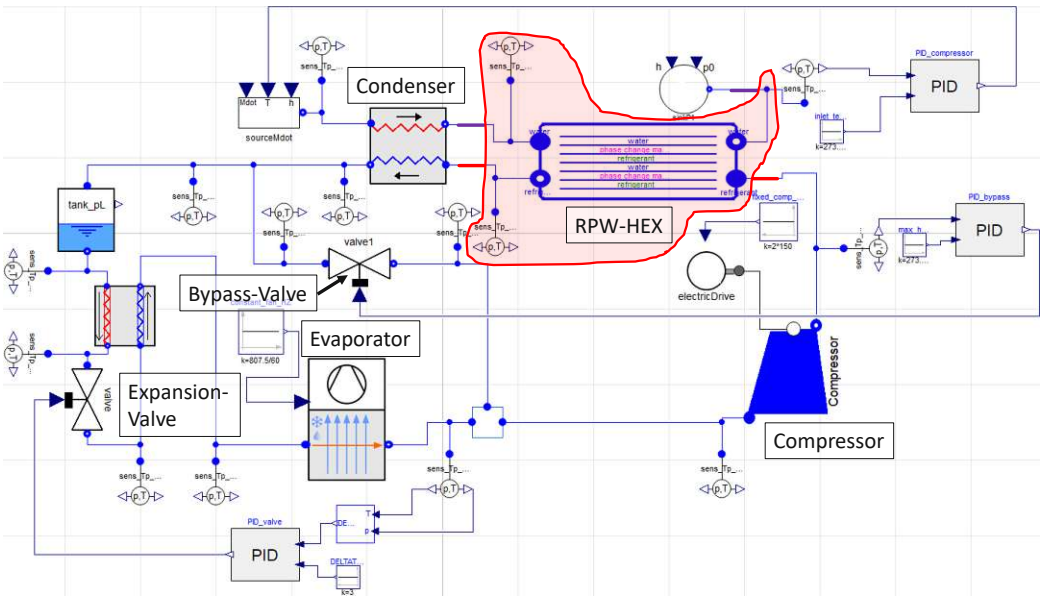

Figure 21: Dymola model of the novel system in DHW generation mode. The added components, compared to the reference heat pump model as seen in Figure 20, are in the red area. This includes the RPW-HEX and two sensors.

4.3 Methods

To analyze the performance of the novel system compared to the reference system for different ambient and operation conditions, performance maps were created for each operation mode. Two different phase change materials were numerically tested, RT64HC and RT54HC, both from *Rubitherm*. The technical datasheets of these materials can be seen in Appendix B.

4.3.1 Performance Maps

The performance maps were created by varying three different parameters, the speed of the compressor, the ambient temperature and the water outlet temperature of the system. With decreasing speed of the compressor, part load conditions of the systems are obtained. Different ambient temperatures state the different ambient conditions for different times and places. The humidity of the ambient air was also considered and set accordingly to the ambient temperature. The relationship between the humidity and temperature of the ambient air can be seen in Appendix A. In heating and cooling mode the water outlet temperature is depended on the heating/cooling system (e.g. floor heating, radiator heating, overhead cooler) and on the ambient conditions. The phase change material used determines the maximum hot water temperature, which can be achieved.

For the performance maps created in this work the parameters are varied according to Table 4. While the heating mode is active at low ambient temperatures below 16 °C, the cooling mode is active at high ambient temperatures above 16 °C. The DHW mode is active throughout the whole year and therefore for the full ambient temperature range.

Table 4: Varying parameters of performance maps.

	$\theta_{\text{water,out}}$ (°C)	θ_{amb} (°C)	N_{rot} (Hz)
Heating	57, 55, 50, 45, 40 35, 30, 25, 22	-22, -20, -15, -10, -5, 0, 5, 10, 15	150, 130, 110, 90, 70, 50, 30, 10
Cooling	18, 16, 12, 8, 6	20, 25, 30, 35, 40	150, 130, 110, 90, 70, 50, 30, 10
DHW	60, 50	-22, -20, -15, -10, -5, 0, 5, 10, 15, 20, 25, 30, 35, 40	150, 130, 110, 90, 70, 50, 30, 10

In heating and cooling mode of the novel system the RPW-HEX gets charged during operation. As the storage has a limited storage capacity the whole process is actually never in steady state but as the storage capacity is fairly high compared to the charging heat flow it can be seen as quasi static. The PCM temperature and therefore the heat transfer between PCM and refrigerant changes only slightly with increasing state of charge of the RPW-HEX. The quasi static steady state at a SoC of 0.5 is taken for the creation of the performance maps.

4.3.2 Annual Performance Calculation

A quasi static approach is used to estimate the annual energy demand of the reference and novel system. Performance parameters at different ambient temperatures were considered on an hourly basis over a full year. The novel system heat pump can be operated in six different modes:

(a) heating mode and charging the RPW-HEX ($0 < SoC \uparrow \leq 1$)

(b) cooling mode and charging the RPW-HEX ($0 < SoC \uparrow \leq 1$)

(c) energy efficient DHW generation by discharging the RPW-HEX ($0 < SoC \downarrow \leq 1$)

(d) conventional (inefficient) direct DHW generation ($SoC = 0$)

(e) heating operation when the RPW-HEX is fully charged ($SoC = 1$)

(f) cooling operation when the RPW-HEX is fully charged ($SoC = 1$)

A conventional system distinguishes between mainly three operating modes, namely heating, cooling and DHW generation, which have similar efficiencies as (d,e,f) in the novel system. Please note, that in operation mode (c) pre-heating of the process water with the condenser is not considered in the following, because this process is highly dynamic and can not be handled with this quasi-static approach. That means, that the entire energy for energy efficient DHW generation is always taken from the RPW-HEX.

The feed water temperature for the heating distribution system (θ_w) was taken from the model, as described in the standard DIN EN 14825 Equation (1), using the intermediate heating and cooling ceiling scenario:

$$\theta_w(\theta_{amb}) = \begin{cases} -0.577\ \theta_{amb} + 39.1\,°C, & \theta_{amb} \leq 2\,°C \\ -1\ \theta_{amb} + 40\,°C, & 2\,°C \leq \theta_{amb} \leq 16\,°C \\ 18\,°C, & \theta_{amb} \geq 20\,°C \end{cases} \tag{21}$$

Note that heating starts below $\theta_{\text{heat,start}}$ =16 °C and cooling starts above $\theta_{\text{cool,start}}$ =20 °C, respectively. The design point of the heat pump is defined by a heating demand of $\dot{Q}_{\text{heat,des}}$ = 2 kW per apartment at $\theta_{\text{amb,des,heat}} = -10\,°\text{C}$. This is a typical heating demand for a low energy building. The heat flow at the condenser is used to describe the heating and cooling demand, as the condenser is directly connected to the heating and cooling distribution system, therefore $\dot{Q}_{\text{heat/cool}} = \dot{Q}_{\text{cond}}$. It should be stated that the condenser unit in heating mode is also called condenser in cooling mode, even though the refrigerant actually evaporates in this unit in cooling mode. The same is true for the naming of the evaporator. The design cooling load $\dot{Q}_{\text{cool,des}}$ is calculated from the definitions for heating by considering solely heat conduction between the apartment and the ambient air, while neglecting solar radiation. This approach underestimates the cooling demand but was used to be able to work without a detailed building mode. The design cooling load is defined at an ambient temperature of $\theta_{\text{amb,des,heat}} = 35\,°\text{C}$:

$$\dot{Q}_{\text{cool,des}} = UA\ (\theta_{\text{amb,des,cool}} - \theta_{\text{cool,start}}) = \underbrace{\left(\frac{\dot{Q}_{\text{heat,des}}}{\theta_{\text{heat,start}} - \theta_{\text{amb,des,heat}}}\right)}_{UA_{\text{heat}}} (\theta_{\text{amb,des,cool}} - \theta_{\text{cool,start}}) \tag{22}$$

which results into a design cooling load of $\dot{Q}_{\text{cool,des}} = 1.15\,\text{kW}$ per apartment at 35 °C. The part load behaviour of $\dot{Q}_{\text{cond}}(\theta_{\text{amb}})$ is obtained assuming a linear dependence between θ_{start} and θ_{design}, for both heating and cooling operation:

$$\dot{Q}_{\text{cond}}(\theta_{\text{amb}}) = \frac{\theta_{\text{amb}} - \theta_{\text{start}}}{\theta_{\text{design}} - \theta_{\text{start}}} \dot{Q}_{\text{design}} \tag{23}$$

The heat transferred on the hot and cold side of the heat pump are given as:

$$\dot{Q}_{\text{hot}}(\theta_{\text{amb}}) = COP_{\text{h}}(\theta_{\text{amb}})\ \dot{W}(\theta_{\text{amb}}) = \begin{cases} \dot{Q}_{\text{cond}} + \dot{Q}_{\text{RPW}}, & \text{heating, DHW generation} \\ \dot{Q}_{\text{eva}} + \dot{Q}_{\text{RPW}}, & \text{cooling} \end{cases} \tag{24}$$

$$\dot{Q}_{\text{cold}}(\theta_{\text{amb}}) = (COP_{\text{h}}(\theta_{\text{amb}}) - 1)\ \dot{W}(\theta_{\text{amb}}) = \begin{cases} \dot{Q}_{\text{eva}}, & \text{heating, DHW generation} \\ \dot{Q}_{\text{cond}}, & \text{cooling} \end{cases} \tag{25}$$

Therefore, the COP_{h} relates not only the heat transferred at the condenser but also the heat flow charging in the RPW-HEX to the electric power demand. The annual Energy Efficiency Ratios (EER) for heating and cooling are defined similar to the basic definitions of the $SCOP$ in the standard DIN EN 14825:

$$EER_{\text{heat}} = \frac{Q_{\text{heat,tot}}}{W_{\text{heat,tot}}} = \frac{\sum_{j=1}^{8760} Q_{\text{cond}}(\theta_{\text{amb}})}{\sum_{j=1}^{8760} \frac{Q_{\text{cond}}(\theta_{\text{amb}})}{COP_{\text{h}}(\theta_{\text{amb}})}} \tag{26}$$

$$EER_{\text{cool}} = \frac{Q_{\text{cool,tot}}}{W_{\text{cool,tot}}} = \frac{\sum_{j=1}^{8760} Q_{\text{cond}}(\theta_{\text{amb}})}{\sum_{j=1}^{8760} \frac{Q_{\text{cond}}(\theta_{\text{amb}})}{COP_{\text{h}}(\theta_{\text{amb}}) - 1}} \tag{27}$$

In the reference as well as in the novel heat pump system in direct DHW generation mode, the COP in DHW mode COP_{DHW} is lower than the COP for heating mode COP_{h}, due to the higher temperature difference between evaporator and condenser in DHW mode. The electric energy consumption in DHW generation mode at a certain hour of the year h_j and at a certain ambient temperature at that hour $\theta_{\mathrm{amb},j}$ for the reference system is given as:

$$W_{\mathrm{DHW}}(\theta_{\mathrm{amb},j}, h_j) = \frac{Q_{\mathrm{DHW}}(h_j)}{COP_{\mathrm{DHW}}(\theta_{\mathrm{amb},j})} \tag{28}$$

With the aid of the RPW-HEX, a certain amount of thermal energy can be generated with a better COP of COP_{h} instead of COP_{DHW} leading to a reduction of the electric energy demand. The situation differs in cooling mode. In the reference system, the total energy transferred in the hot side dissipates in the evaporator and is lost. In the novel system, on the other hand, this heat is used to charge the RPW-HEX and can therefore be seen as free energy, as waste heat is utilized. The electric energy consumption in DHW generation mode for the novel system is therefore given as:

$$W_{\mathrm{DHW,RPW}}(\theta_{\mathrm{amb},j}, h_j) = \begin{cases} \dfrac{Q_{\mathrm{DHW}} - Q_{\mathrm{RPW}}}{COP_{\mathrm{DHW}}} + \dfrac{Q_{\mathrm{RPW}}}{COP_{\mathrm{h}}}, & \text{heating} \\ \dfrac{Q_{\mathrm{DHW}} - Q_{\mathrm{RPW}}}{COP_{\mathrm{DHW}}}, & \text{cooling} \end{cases} \tag{29}$$

In total, the annual efficiency for DHW generation results in:

$$EER_{\mathrm{DHW}} = \frac{Q_{\mathrm{DHW,tot}}}{W_{\mathrm{DHW,tot}}} = \frac{\sum_{j=1}^{8760} Q_{\mathrm{DHW}}(h_j)}{\sum_{j=1}^{8760} W_{\mathrm{DHW,RPW}}(\theta_{\mathrm{amb},j}, h_j)} \tag{30}$$

Further information about the annual calculation can be taken from the Paper submitted to the 25th IIR International Congress of Refrigeration 2019, which is attached in Appendix F.

5 Results & Discussion

The experimental results obtained are presented and analyzed in this chapter. With the use of these results the numerical model of the reference heat pump is validated and discrepancies between the experimental results and the numerical model are analyzed and explained. Graphical representations of the numerical obtained performance maps are shown and discussed. A typical operation scenario of the novel system setup is examined, which included operation in heating mode and charging of the RPW-HEX and a switch to DHW generation and discharging of the RPW-HEX. Using the performance maps an annual performance calculation is conducted in order to compare the performance of the novel system to the reference system.

5.1 Experimental Results

The experimental analysis, as described in Chapter 3, is divided into the three different modes of the heat pump: heating, cooling and DHW. The experiments were conducted following the standards DIN EN 14511-2 and DIN EN 14825 for air-water heat pumps for intermediate ambient temperature applications. In Appendix C the full experimental results are listed in tables. The naming convention of the measurement points is done by defining the ambient and feed water outlet temperature. In front of the ambient temperature is an *A* for **A**mbient and in front of the feed water outlet temperature is a *W* for **W**ater. The temperatures are written in degrees Celsius. For example, a measurement point with an ambient temperature of 7 °C and a feed water outlet temperature of 33 °C is denoted as A7W33.

5.1.1 Heating

The nominal conditions as specified in the standard DIN EN 14511-2 for an air-water heat pump in heating mode and intermediate ambient temperatures are a feed water inlet of $\theta_{\text{water,in}} = 40\,°\text{C}$ and a feed water outlet of $\theta_{\text{water,in}} = 45\,°\text{C}$. The ambient conditions are defined as a dry bulb temperature of $\theta_{\text{air,in,db}} = 7\,°\text{C}$ and a wet bulb temperature of $\theta_{\text{air,in,wb}} = 6\,°\text{C}$ at the air inlet. At these nominal conditions the heat pump manufacturer prescribed a compressor speed of 36 % of the maximum compressor speed ($n_{\text{comp,max}} = 120\text{Hz}$). The evaporator fan speed was regulated according to the compressor speed. At maximum compressor speed the fan was set to 80 % of the maximum speed and at minimum compressor speed (20 %) the fan was set to 40 % speed. The maximum speed of the evaporator fan is $n_{\text{fan,max}} = 720\,\text{rpm}$. The results under these nominal conditions are summarized in Table 5.

Table 5: Experimental results in heating mode under nominal conditions, as defined in DIN EN 14511-2.

	Comp.	Air side		Water side			
	n_{comp}	$\theta_{\text{air,in,db}}$	$RH_{\text{air,in}}$	$\theta_{\text{water,in}}$	$\theta_{\text{water,out}}$	$\dot{m}_{\text{water}}$	P_{th}
A7W45	36 %	7.006 °C	89.134 %	40.001 °C	45.017 °C	0.246 kg/s	5.155 kW

The resulting water mass flow of $\dot{m}_{\text{water}} = 0.246\,\text{kg/s}$ was kept fixed for the following experiments in heating mode. Regarding the standard DIN EN 14825 for part load conditions of air-water heat pumps in the intermediate temperature class 4 points were tested, A-7W43, A2W37, A7W33 and A12W28. The Part Load Ratios (PLR) of these points are calculated according to:

$$PLR = \frac{\theta_{\text{amb}} - 16}{\theta_{\text{heat,des}} - 16} \tag{31}$$

with an design point ambient temperature of $\theta_{\text{heat,des}} = -10\,°\text{C}$.

The design load would have been measured at 100 % compressor speed, an ambient temperature of -10 °C and a feed water outlet temperature of 45 °C. But as the heat pump had problems operating in a stable steady state at these conditions the heat pump manufacturer defined a compressor speed of 90 % of the maximum compressor speed for the first part load point A-7W43. Fixing the water mass flow, the feed water outlet temperature and the compressor speed the thermal power output of the heat pump at this point resulted to $P_{\text{th}} = 9.62\,\text{kW}$. Therefore, the design load can be approximated to be $P_{\text{design}} = P_{\text{th,A-7W43}}/PLR(-7\,°\text{C}) = 10.875\,\text{kW}$. In Table 6 the thermal loads and part load ratios of the heating measurement points are listed and are visualized in Figure 22.

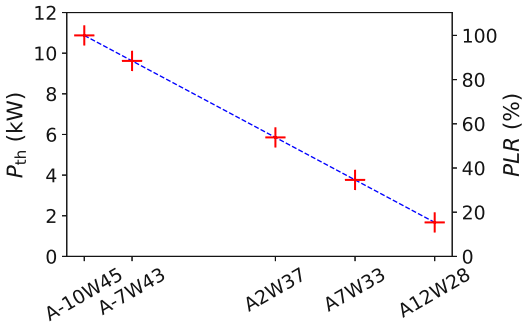

Figure 22: Thermal loads and part load ratios of experimental measurement points in heating mode.

	P_{th}	PLR
A-10W45	10.875 kW	100 %
A-7W43	9.620 kW	88.46 %
A2W37	5.856 kW	53.85 %
A7W33	3.764 kW	34.62 %
A12W28	1.673 kW	15.38 %

Table 6: Thermal loads and part load ratios of experimental measurement points in heating mode.

With knowledge of the feed water mass flow, the desired thermal power output, the feed water outlet temperature and the ambient conditions, the other measurement points for the heating mode were tested. For all measurement points in heating mode, the wet bulb temperature of the ambient air is 1 °C less then the dry bulb temperature. In Table 7 the experimental results are listed and in Figure 23 the thermal and electrical power and the COP are shown.

Table 7: Experimental results and operation conditions for part load measurements of the heat pump in heating mode.

	Air side		Water side			Electrical	
	$\theta_{\text{air,in,db}}$	$RH_{\text{air,in}}$	$\theta_{\text{water,in}}$	$\theta_{\text{water,out}}$	P_{th}	P_{el}	COP
A-7W43	-6.873 °C	70.160 %	33.500 °C	42.966 °C	9.620 kW	3.256 kW	2.954
A2W37	2.119 °C	86.457 %	31.125 °C	36.804 °C	5.814 kW	1.360 kW	4.275
A7W33	7.159 °C	89.152 %	29.255 °C	32.978 °C	3.811 kW	0.719 kW	5.301
A12W28	11.739 °C	90.421 %	25.046 °C	27.985 °C	2.998 kW	0.422 kW	7.100

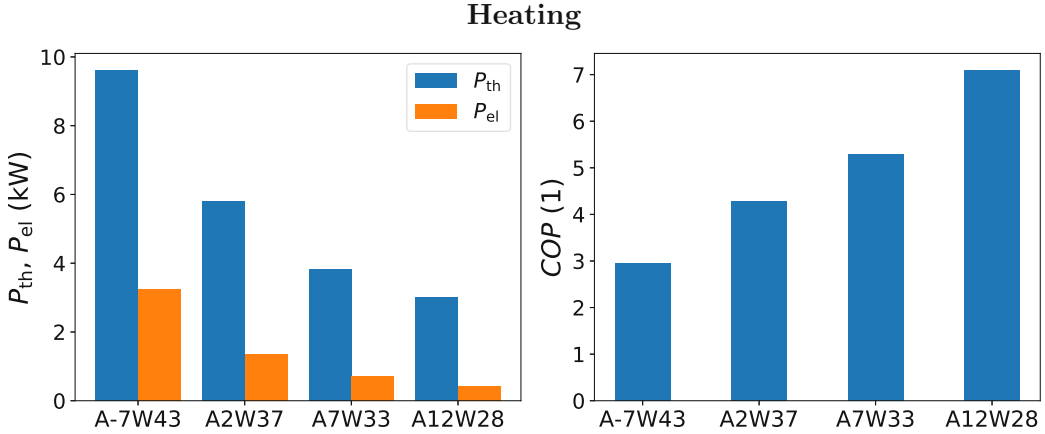

Figure 23: Experimental results of thermal load P_{th}, electrical power demand P_{el} and coefficient of performance COP in heating mode and operation conditions as defined in Table 7.

To reach the desired thermal power output for the point A12W28 a compressor speed below the minimum compressor speed would have been necessary. It was possible to operate the compressor below the minimum compressor speed of 20 %, due to pleasant conditions for the heat pump at this measurement point. The compressor was set to 16.67 %. The COP rises significantly for higher ambient and lower feed water outlet temperatures. This is in agreement with the theoretical ideal thermodynamic cycle, the Carnot cycle, as the absolute temperature of the hot reservoir is lowered and the absolute temperature of the cold reservoir is increased. Practically speaking, the heat pump has a lower pitch for pumping the heat from the cold to the hot reservoir.

The seasonal coefficient of performance for heating mode is calculated according to formulae (9) with the temperature levels and hours as stated in standard DIN EN 14825 A.1.3:

$$SCOP_{\text{heating}} = \frac{\sum_{j=1}^{n} t_{\text{j}} \; P_{\text{H}}(\theta_{\text{amb,j}})}{\sum_{j=1}^{n} t_{\text{j}} \; \left(\frac{P_{\text{H}}(\theta_{\text{amb,j}})}{COP(\theta_{\text{amb,j}})}\right)} = 4.390 \tag{32}$$

5.1.2 Cooling

The experimental tests for the cooling mode were conducted according to the standard DIN EN 14825 for an air-water heat pump with a cooling ceiling. Determination of the feed water mass flow was done at the point A35W18 with a fixed feed water supply temperature of $\theta_{\text{water,in}} = 23\,^{\circ}\text{C}$ and a part load ratio of 100 %. The heat pump manufacturer prescribed a compressor speed of 38.7 % of the maximum compressor speed for this point and an evaporator fan speed of 65 % of the maximum fan speed for all measurements in cooling mode. For the nominal measurement point A35W18 an ambient wet bulb temperature of $\theta_{\text{air,in,wb}} = 24\,^{\circ}\text{C}$ is prescribed in the standard DIN EN 14825. The results of the experiments under these nominal conditions are listed in Table 8.

Table 8: Experimental results and operation conditions for measurements on the heat pump in cooling mode for the nominal point A35W18, as defined in the standard DIN EN 14825.

	Comp.	Air side		Water side			
	n_{comp}	$\theta_{\text{air,in,db}}$	$RH_{\text{air,in}}$	$\theta_{\text{water,in}}$	$\theta_{\text{water,out}}$	$\dot{m}_{\text{water}}$	P_{th}
A35W18	38.7 %	34.841 °C	38.859 %	22.941 °C	17.993 °C	0.297 kg/s	6.174 kW

The thermal power output of this point corresponds to the design load P_{design}, as the part load ratio is 100 %. The formula for the part load percentages in cooling mode is defined in the standard DIN EN 14825 as:

$$PLR = \frac{\theta_{\text{amb}} - 16}{\theta_{\text{cool,des}} - 16} \tag{33}$$

with an design point ambient temperature of $\theta_{\text{cool,des}} = 35\,^{\circ}\text{C}$.

The thermal loads and part load ratios for the cooling measurements are visualized in Figure 24 and listed in Table 9.

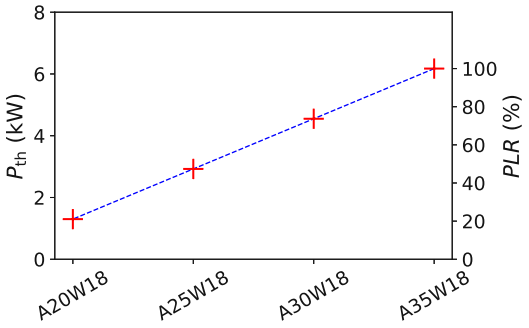

Figure 24: Thermal loads and part load ratios of experimental measurement points in cooling mode.

	PLR	P_{th}
A35W18	100 %	6.174 kW
A30W18	73.68 %	4.549 kW
A25W18	47.37 %	2.925 kW
A20W18	21.05 %	1.300 kW

Table 9: Thermal loads and part load ratios of experimental measurement points in cooling mode.

In cooling mode neither the humidity nor the wet bulb temperature of the ambient air is defined in the standard DIN EN 14825 for the part load measurement points. As a reasonable value, a relative humidity of $RH_{air,in} = 50\,\%$ was chosen. In Table 10 the experimental results for the measurements in cooling mode are listed. The thermal power output, electrical power input and COP are visualized in Figure 25.

Table 10: Experimental results and operation conditions for part load measurements on the heat pump in cooling mode.

	Air side		Water side			Electrical	
	$\theta_{air,in}$	$RH_{air,in}$	$\theta_{water,in}$	$\theta_{water,out}$	P_{th}	P_{el}	COP
A35W18	34.841 °C	38.859 %	22.941 °C	17.993 °C	6.174 kW	1.359 kW	4.545
A30W18	29.931 °C	49.826 %	21.491 °C	17.980 °C	4.388 kW	0.703 kW	6.240
A25W18	25.000 °C	49.352 %	20.599 °C	18.065 °C	3.148 kW	0.408 kW	7.723
A20W18	19.648 °C	49.168 %	20.615 °C	17.934 °C	3.333 kW	0.321 kW	10.378

To reach the desired thermal power output for the points A25W18 and A20W18 a compressor speed below the minimum compressor speed would have been necessary. Therefore, the compressor was set at minimum speed (20 %) for these points. Contrary to the heating mode, the COP rises for lower ambient temperatures. This is still in perfect agreement with the ideal theoretical thermodynamic process, the Carnot process, as the heat is now pumped from the feed water to the ambient air. Therefore, the high temperature reservoir is now the ambient air and the low temperature reservoir corresponds to the feed water. It can also be seen, that very high COP values can be reached in cooling mode. This is due to a relative small gap between the high and low temperature level. Furthermore, the bypass valve is not active in cooling mode, as the hot-gas temperature does not exceed 115 °C during normal operation, therefore no enthalpy is lost due to a lower refrigerant mass flow through the outdoor unit.

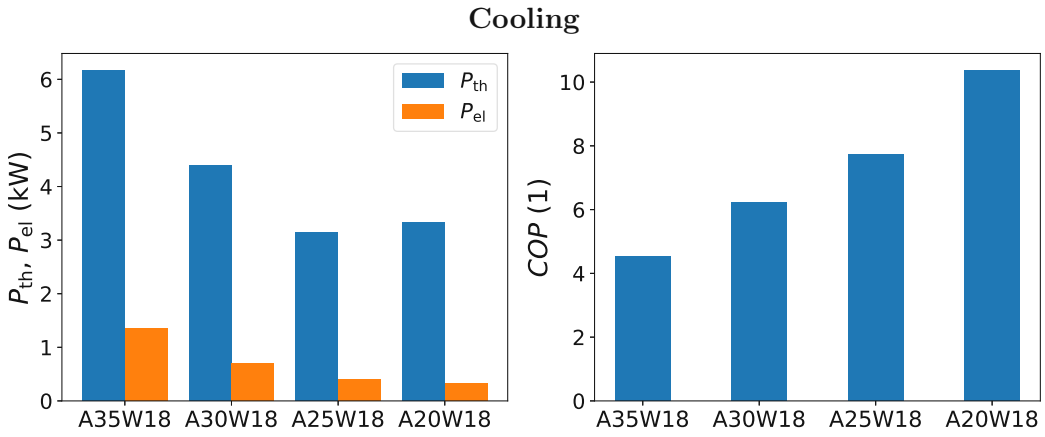

Figure 25: Experimental results of thermal load P_{th}, electrical power demand P_{el} and coefficient of performance COP in cooling mode and operation conditions as defined in Table 10.

The seasonal coefficient of performance for cooling mode is calculated according to formulae (9) with the temperature levels and hours as stated in standard DIN EN 14825 A.1.2:

$$SCOP_{\mathrm{cooling}} = \frac{\sum_{j=1}^{n} t_{\mathrm{j}} \; P_{\mathrm{C}}(\theta_{\mathrm{amb,j}})}{\sum_{j=1}^{n} t_{\mathrm{j}} \; \left(\frac{P_{\mathrm{C}}(\theta_{\mathrm{amb,j}})}{COP(\theta_{\mathrm{amb,j}})}\right)} = 7.454 \tag{34}$$

5.1.3 DHW

In the standards DIN EN 14511-2 and DIN EN 14825 there are no prescribed conditions for experimental testing of the domestic hot water production of heat pumps. Therefore, the following conditions were selected to be able to make meaningful comparison of the reference system to the novel system including the RPW-HEX. A desired hot water temperature of 60 °C was chosen for this sake. As 3 sensible hot water tanks should be charged with 200 l/min each, the water mass flow was chosen as:

$$\dot{m}_{\mathrm{water}} = \dot{V}_{\mathrm{water}} / \rho_{\mathrm{water}} \approx 0.167\,\mathrm{kg/s} \tag{35}$$

Three different ambient temperatures were experimentally tested: -10 °C, -7 °C and 2 °C. As in heating mode, the wet bulb temperature of the ambient air was set 1 °C less than the dry bulb temperature. The compressor speed was set to reach approximately the same thermal power output of $P_{\mathrm{th}} = 9\,\mathrm{kW}$ for all points and the evaporator fan speed was set to a constant value of $n_{\mathrm{fan}} = 80\,\%$ of the maximum fan speed. The experimental results are listed in Table 11 and the thermal and electrical power and the COP are visualized in Figure 26.

Table 11: Experimental results and operation conditions for measurements on the heat pump in DHW generation mode.

	Air side		Water side			Electrical	
	$\theta_{\text{air,in}}$	$RH_{\text{air,in}}$	$\theta_{\text{water,in}}$	$\theta_{\text{water,out}}$	P_{th}	P_{el}	COP
A-10W60	-10.138 °C	77.054 %	47.128 °C	60.000 °C	8.846 kW	4.947 kW	1.788
A-7W60	-6.890 °C	77.623 %	46.731 °C	59.818 °C	9.000 kW	4.613 kW	1.951
A2W60	1.971 °C	85.599 %	54.936 °C	59.822 °C	8.599 kW	3.967 kW	2.168

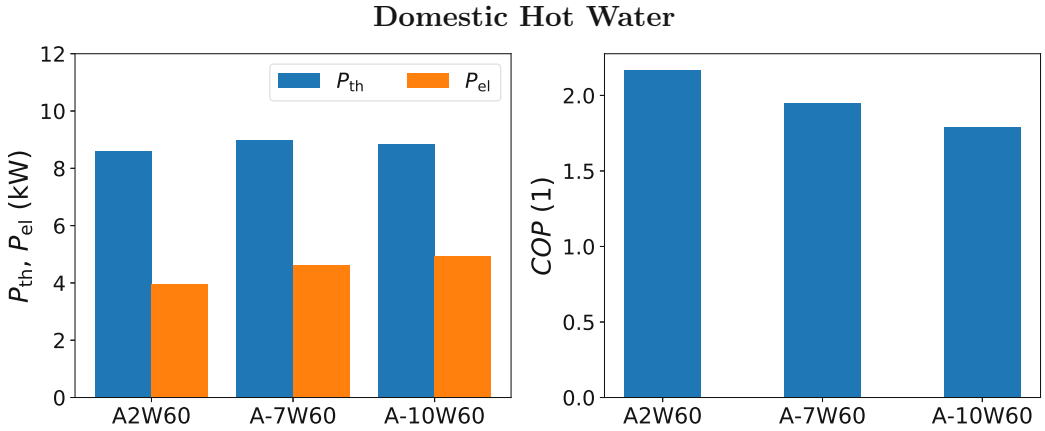

Figure 26: Experimental results of thermal load P_{th}, electrical power demand P_{el} and coefficient of performance COP in DHW generation mode and operation conditions as defined in Table 11.

As expected, the COP is slightly lower for lower ambient temperatures. Therefore, the electrical power input is slightly higher, as the thermal power output is approximately the same for all points. As in heating mode, this can be explained by the theoretical ideal thermodynamic cycle, the Carnot cycle. The hot water outlet corresponds to the high temperature reservoir, which is approximately the same for all points. The ambient temperature correlates to the low temperature reservoir. If the low temperature reservoir has a lower temperature, a greater pitch has to be overcome by the heat pump, when pumping heat from the low to the high temperature reservoir.

5.1.4 Frosting Behaviour

Additionally to performance testing of the heat pump, the frosting behaviour of the outdoor fan unit was examined. It was visualized by a camera and furthermore quantified by putting the heat exchanger on a scale. The camera was used to give a detailed view of the frost accumulation and dissipation on one or two fins of the heat exchanger. By mounting the heat exchanger on a scale, the weight increase of the heat exchanger, due to the water

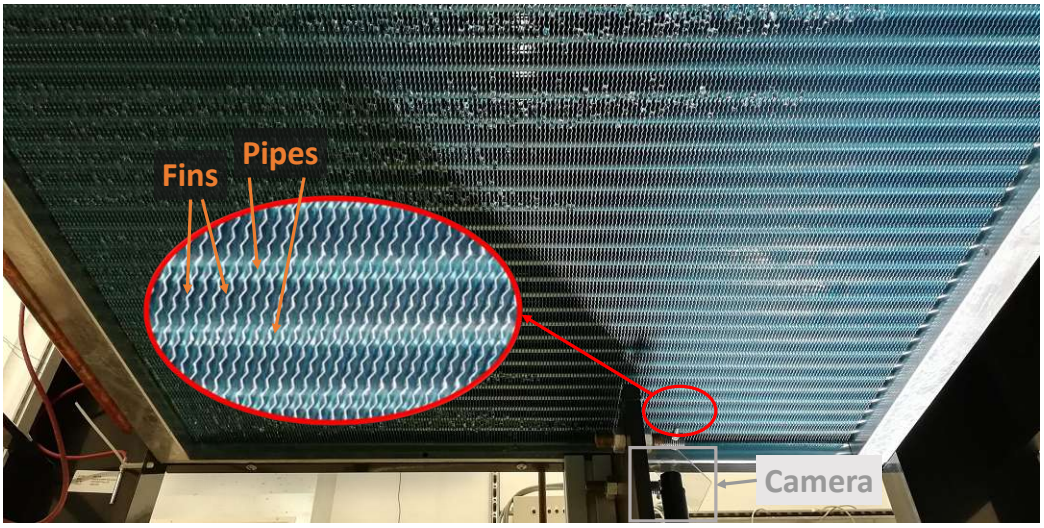

Figure 27: Surface of the HYBUILD outdoor heat exchanger and macro camera used to visualize the frost accumulation on the heat exchanger fins.

and frost accumulation, can be quantified. It should be stated, that the heat exchanger and the rest of the heat pump are in different physical places in the laboratory, as in real applications. The heat exchanger, where the frost is accumulating, is located outdoors, in contact with ambient air, while the rest of the heat pump can either be located outdoors or indoors. Therefore, not only the frost accumulation but also shifting of the refrigerant from the outdoor heat exchanger and the rest of the heat pump is measured by the scale signal. The calibration of the scale can be seen in Appendix D.1. In Figure 27 the surface of the heat exchanger and the macro camera used to visualize the frost accumulation on the heat exchanger fins is shown.

Frost formation is occurring fastest if the ambient air, which heats the refrigerant, is a few degrees Celsius above 0 °C. At these conditions the ambient air still contains high absolute amounts of water, compared to lower ambient temperatures, and the heat exchanger surface is below water freezing temperatures to provide a sufficient temperature difference for heat transfer. The operational conditions for the experiments on the frosting behaviour of the experimentally analyzed heat pump are listed in Table 12, where A_{eff} states the effective heat exchange area of the evaporator. As the heat pump is part of the HYBUILD project it is from now on referred to as the HYBUILD heat pump.

Table 12: Operation and ambient conditions for the analysis on the frosting behaviour of the HYBUILD heat pump.

θ_{amb}	RH_{amb}	n_{comp}	n_{fan}	Refr.	Fin type/Coating	A_{eff}
1.7 °C	89.35 %	52.8 Hz	6.45 Hz	R32	Corrugated flat fins/None	46.1 m^2

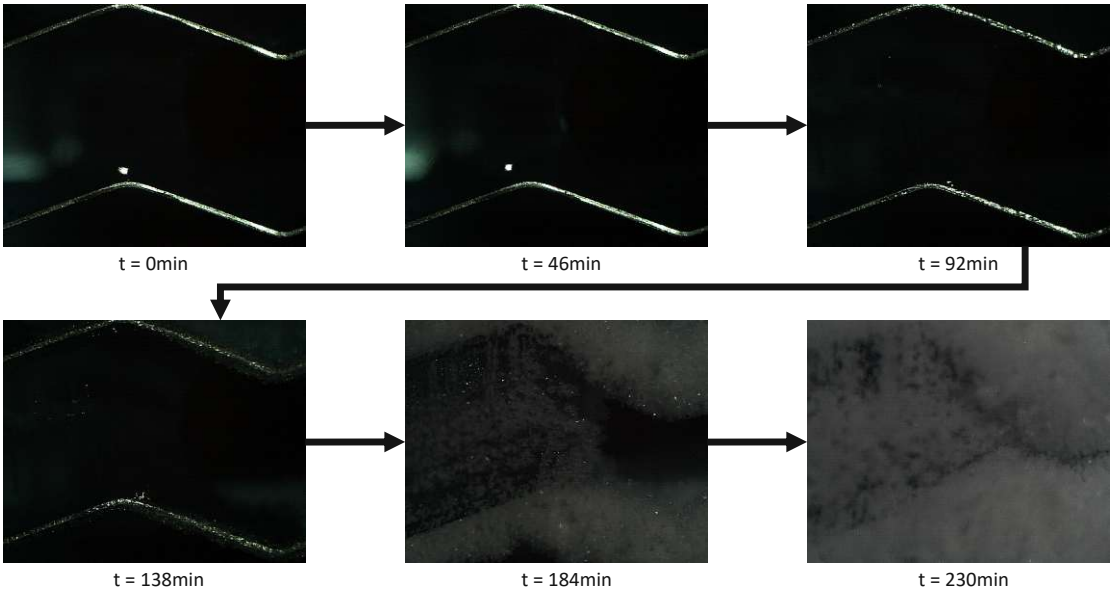

Figure 28: Frost accumulation on two evaporator fins of the HYBUILD heat pump for the operation and ambient conditions as stated in Table 12.

The heat pump was operated until the frost nearly blocked the full air flow cross section of the heat exchanger. Normally defrosting of the evaporator would have been done earlier. In Figure 28 the frost accumulation between two fins can be seen.

As described earlier the used heat exchanger is a table heat exchanger with a horizontal alignment of the fins and a vertical flow direction of the air. The camera is located at the bottom end of the heat exchanger. In order to avoid water to fall on the camera a small transparent plastic plate is used to deflect the water. To increase the contrast between the fin and the background a LED lamp was used. As seen in the the pictures of Figure 28, this sometimes leads to reflections, especially when no frost is present. Also the metallic surface of the fins reflected the LED light better than the ice, therefore the pictures look dimmer as soon as the first ice appears.

The built frost acts as an insulation of the evaporator on the air side and therefore the refrigerant temperature needs to be lowered to still be able to transfer the desired heat between the ambient air and the refrigerant. As a result of that, the condenser pressure gets lower during operation at frosting conditions. The suction point of the compressor is hence moved to a lower temperature and pressure level. As the compressor is operated at a fixed speed the discharged refrigerant also lowers its pressure level during operation. The suction and discharge pressure of the compressor can be seen in Figure 29. Neglecting the pressure drop in the heat exchangers, the suction pressure corresponds to the refrigerant pressure in the evaporator and the discharge pressure corresponds to the refrigerant pressure in the condenser. Due to a lower mean pressure level and a constant compressor speed, the

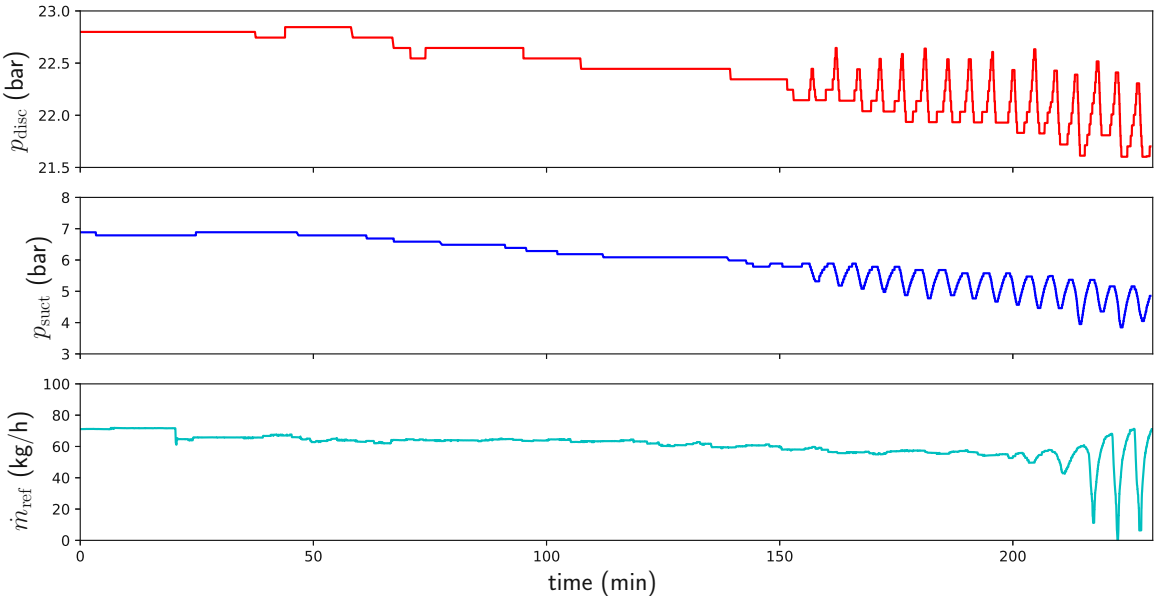

Figure 29: Development of the suction and discharge pressure and refrigerant mass flow over time during operation of the HYBUILD heat pump at frosting conditions.

refrigerant mass flow is decreasing as well. The development of the refrigerant mass flow can also be seen in Figure 29.

The refrigerant and air temperatures in the heat pump cycle are shown in Figure 30. While the air inlet temperature stays approximately the same throughout the whole operation, the outlet air temperature decreases with increasing frost accumulation. Also the evaporator suction temperature and the compressor suction temperature (which is equal to the evaporator discharge temperature, without operation of the bypass valve) decrease during the operation. The compressor discharge temperature actually increases slightly during operation, which points to a decreasing isentropic efficiency of the compressor with lower suction temperatures and pressures. The condenser discharge and valve suction temperatures stay approximately constant for a long time of operation at frosting conditions.

The development of thermal power output $\dot{Q}_{\mathrm{H}}$, electrical power input P_{el} and the COP during operation of the HYBUILD heat pump at frosting conditions is shown in Figure 31. Following the decrease in the refrigerant mass flow, the thermal power output of the heat pump at the condenser decreases as well. Additionally, the compressor power consumption decreases slightly as the refrigerant mass flow and the mean pressure level are decreasing. Still, in total the COP decreases during operation of the heat pump at frosting conditions.

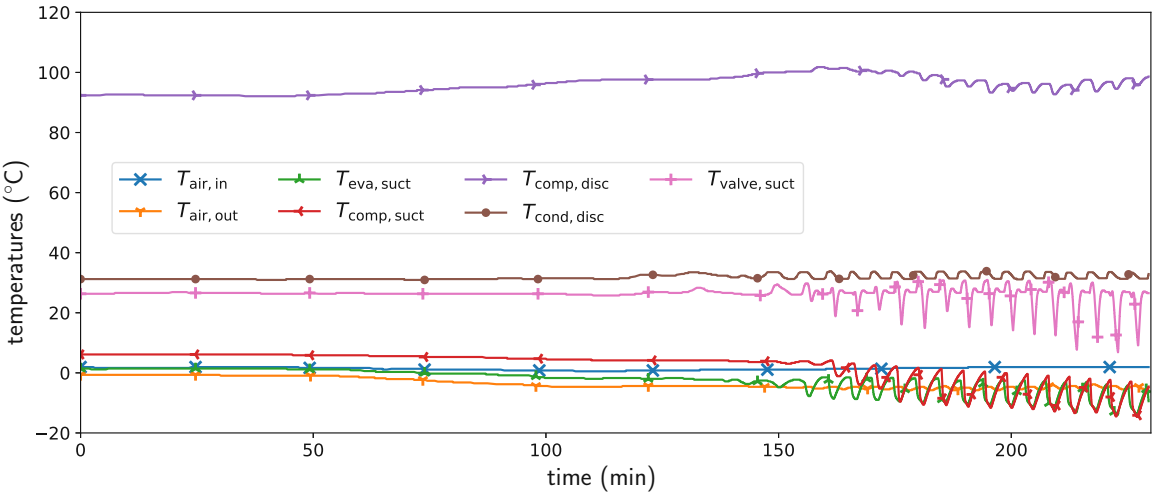

Figure 30: Development of the refrigerant and air temperatures over time during operation of the HYBUILD heat pump at frosting conditions.

The compressor suction and discharge pressure, the thermal power output, the electrical power consumption and most of the refrigerant temperatures are fluctuating a lot after 150min. It can therefore be said that the heat pump is not operating very stable in this period of time and should be defrosted earlier than 150 min of operational time at these climate and operation conditions.

In order to quantify the frost accumulation the scale signal and the amount of pixel exceeding a certain brightness threshold in the pictures may be used. A pixel exceeds the brightness threshold if the mean of the red, green and blue value is higher than 200. At the beginning only the pixels displaying the metallic surface of the fins and possibly the pixels showing the reflection of the plastic plate will exceed this brightness threshold. But as soon as frost is accumulating, additional pixel will exceed this threshold. Pixels exceeding the stated threshold are from now on denoted as highlight events. In Figure 32 the scale measurements and the amount of highlight events is shown over time.

The scale signal shows only a slight increase of mass during the first 50 min. Afterwards the increase is going at a faster rate until around 200 min, when the scale signal starts to fluctuate heavily. These oscillations are caused by the unstable operation of the heat pump at these conditions, i.e. fluctuation in the refrigerant mass flow, as seen in Figure 29. The amount of highlight events is not changing for the first 150 minutes. Afterwards a sharp increase in highlight events is visible. This suggests, that condensing water on the fins is not seen as a highlight event, but only accumulated frost. Therefore, the scale signal is increasing earlier, as condensed water on the fins already increases the weight of the heat exchanger on the scale.

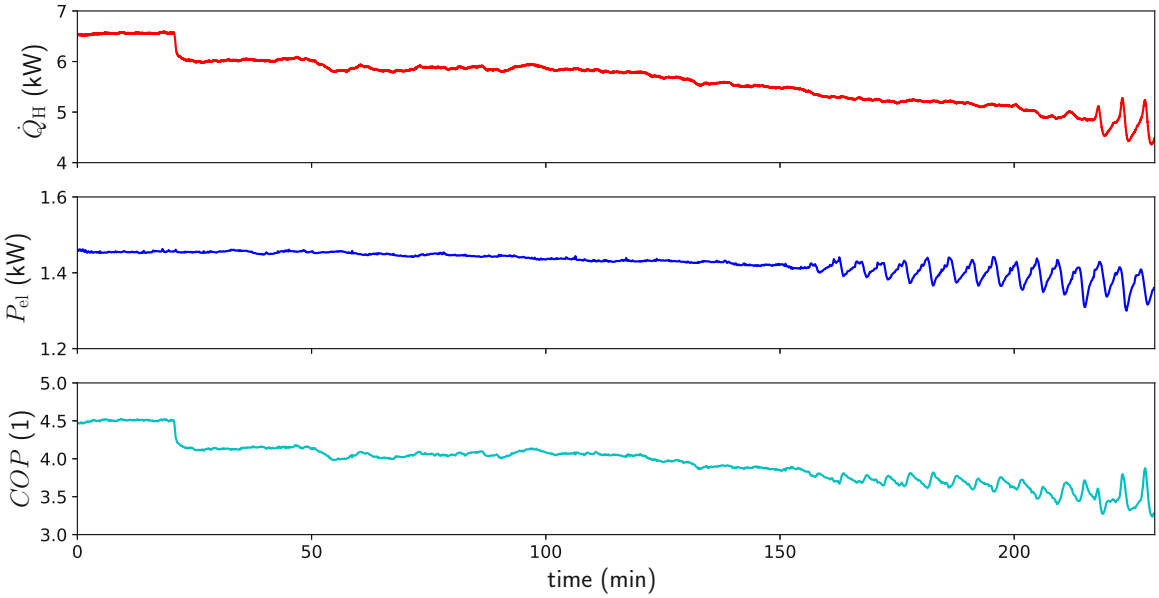

Figure 31: Development of the thermal power output, electrical power input and COP over time during operation of the HYBUILD heat pump at frosting conditions.

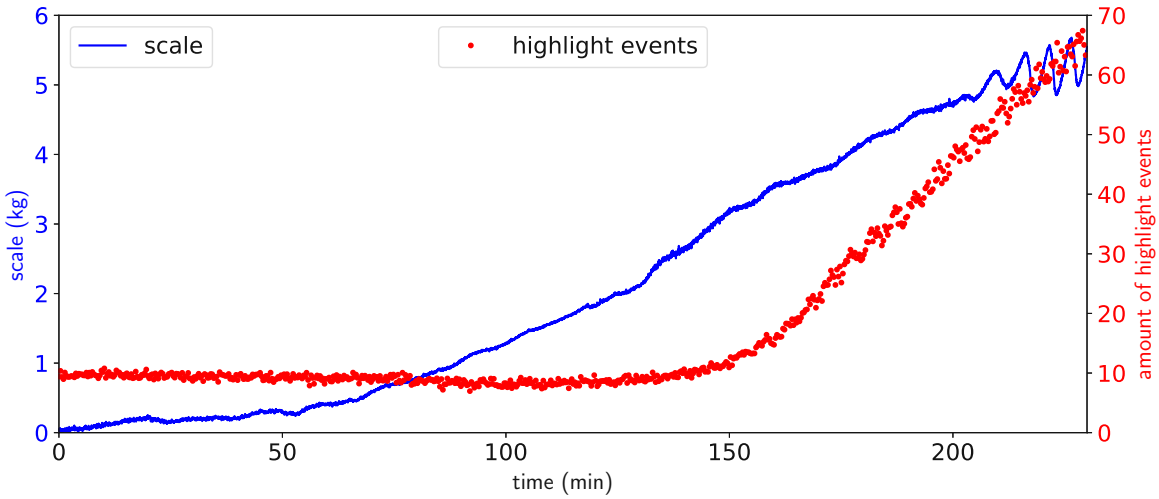

Figure 32: Scale measurement and amount of highlight events in pictures of the HYBUILD heat pump at frosting conditions.

As the use of a table heat exchanger limits the results of the frosting behaviour analysis, as a coverage is necessary to avoid water to fall on the camera and the camera positioning at the bottom of the heat exchanger comes with constructional challenges, a similar analysis was conducted on another heat pump. Said heat pump is part of the SilentAirHP project (Reichl, 2018). Thanks to a vertical heat exchanger surface, the camera can be placed in front of the heat exchanger, without having to worry about water falling onto the camera. Additionally, the heat pump is not divided into an outdoor and an indoor part, therefore the full heat pump can be placed on the scale and the scale signal can be completely correlated to the condensation and frosting phenomenon. In Figure 33 the surface of the SilentAirHP heat exchanger and the macro camera used to visulaize the frost accumulation on the heat exchanger fins is shown. The calibration of the scale can be seen in Appendix D.2. The boundary conditions for the frosting behaviour analysis of the SilentAirHP are listed in Table 13. The pictures of the frost accumulation between two fins can be seen in Figure 34.

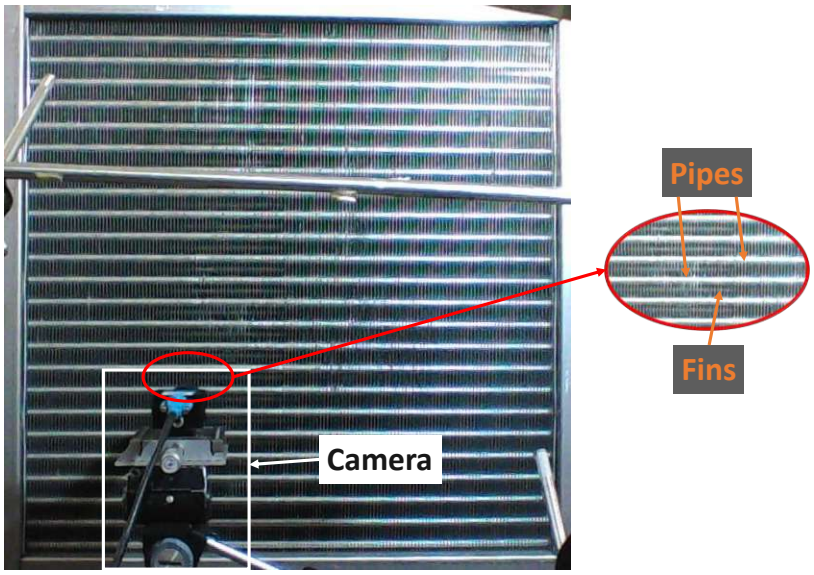

Figure 33: Surface of the SilentAirHP heat exchanger and macro camera used to visualize the frost accumulation on the heat exchanger fins.

Table 13: Operation and ambient conditions for the analysis of the frosting behaviour of the SilentAirHP.

θ_{amb}	RH_{amb}	n_{comp}	n_{fan}	Refr.	Fin type/Coating	A_{eff}
4.6 °C	71.75 %	94 Hz	9.9 Hz	R410A	Straight flat fins/ Clearcoat U-Sil 120 GL	11.44 m^2

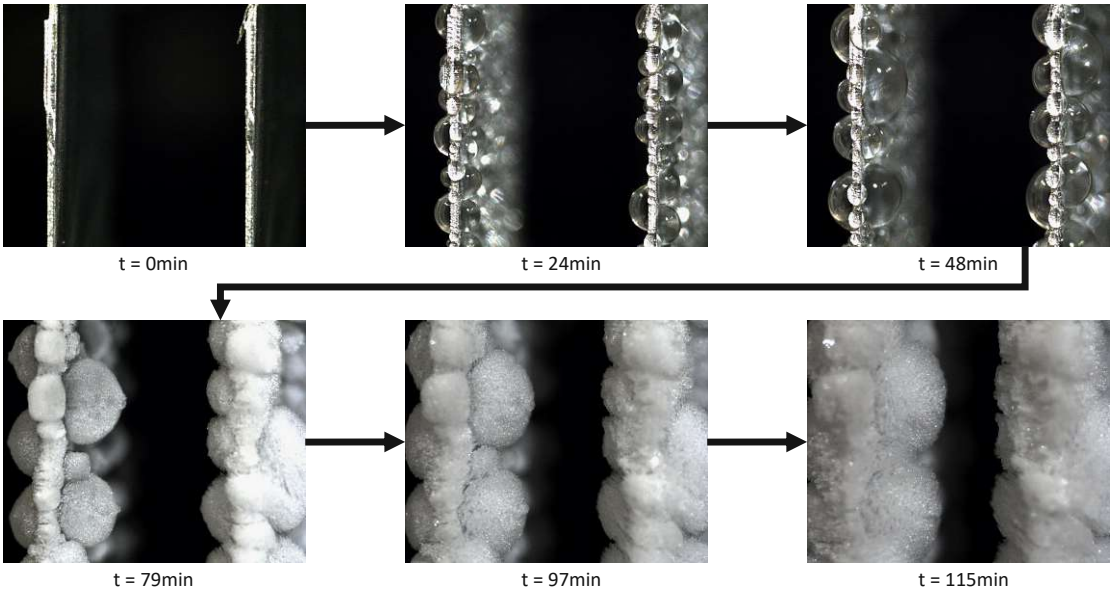

Figure 34: Frost accumulation on two fins of the SilentAirHP for operation and ambient conditions as defined in Table 13.

Frosting of the SilentAirHP starts with small water drops condensing on the surface of the vertical fins. The water drops start fusing together forming bigger water drops. These bigger water drops start to freeze, building frost globes on the fins of the heat exchanger. Advancing in time, the frost globes start fusing together and the frost continues to densify. When the frost layer is too thick, the SilentAirHP starts to defrost, in order to assure continues stable operation. This defrosting is done by reversing the cycle via a four way valve. After reversing the cycle the frosted heat exchanger, which acted as the evaporator for the refrigerant, afterwards works as the condenser for the refrigerant, transferring heat to the outlet air and to the frost on its fins. Defrosting of the heat exchanger is done in a very short period of time. The defrosting of the SilentAirHP can be seen in Figure 35.

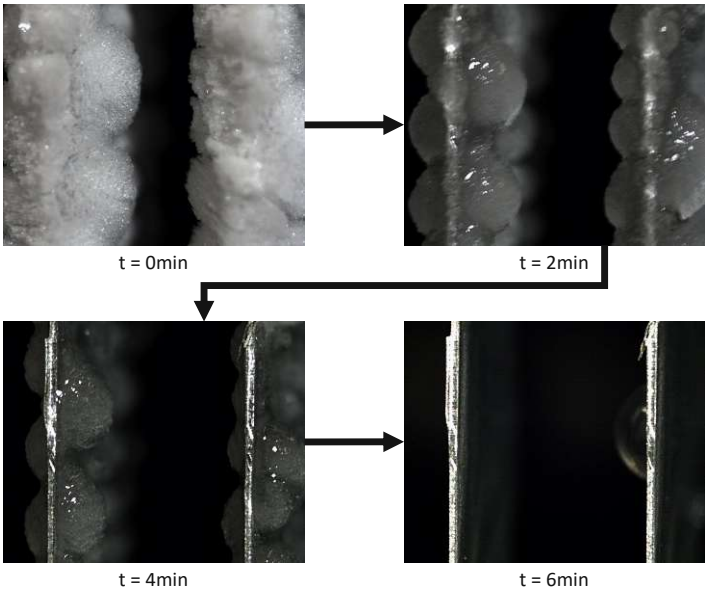

Figure 35: Defrosting of the SilentAirHP for operation and ambient conditions as defined in Table 13.

Defrosting of the SilentAirHP takes only 6 min, while the operation at frosting conditions was able to be operated in a stable manner for 115 min. Therefore, the heat pump can be operated in regular heating mode for approximately 95 % of the time at these conditions. During the remaining 5 % of the time it has to be defrosted. When defrosting is started the fins rapidly take the hot temperature of the refrigerant. Therefore, the frost is melted from its surface, forming liquid water which flows down the vertical fins. This water flows down the heat exchanger until it reaches the ground it stands on. In Figure 36 the scale measurements and the amount of highlight events in the pictures during frosting and defrosting operation of the SilentAirHP is shown.

The mass on the heat exchanger is constantly rising, due to condensing water on the heat exchanger fins and afterwards frosting of the water drops and densifying of the frost. During the first 70min nearly no change in highlight events is visible, as the condensed water drops do not count as highlight events, but only frost does. After 70min the amount of highlight events is increasing. Just after beginning of defrost operation, which is marked with a dotted line in the plot, the amount of highlight events and the mass on the scale is decreasing rapidly, as the frost is melting and the water drains off.

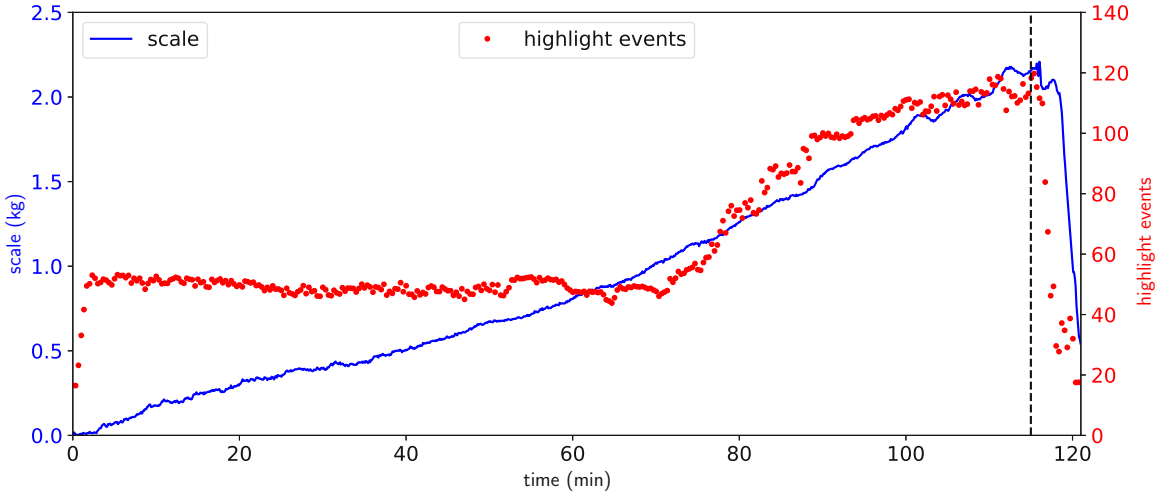

Figure 36: Scale measurement and amount of highlight events in pictures of the SilentAirHP during frosting conditions and defrosting operation. The time when defrosting is initiated is marked with a dotted line.

It should be stated that the frost is not forming uniformly on the whole heat exchanger surface, but rather patchy. A common webcam was used to visualize the nonuniform frost accumulation on the heat exchanger surface. The images can be seen in Figure 37. The camera with the macro lenses to visualize the frost growth between two fins is located at a representative area, where the frost growth is clearly visible. The rod looming over the pictures is a humidity sensor. On the first and last picture, where the close up camera suggests complete termination of the defrosting operation, falling water drops are sill visible on the webcam pictures.

The refrigerant temperatures during operation are shown in Figure 38. During operation of the heat pump at frosting conditions most refrigerant temperatures fluctuate but the mean of most temperatures stay approximately constant. However, about thirty minutes before defrosting the mean of some refrigerant temperatures, as the compressor suction and discharge temperatures, decrease slightly. When defrosting is initiated the compressor discharge temperature, the valve suction temperature, the condenser suction temperature and the condenser discharge temperature fall. Meanwhile, the compressor suction and the valve discharge temperature rise. This operation mode is maintained only for a very short time and the temperatures are fluctuating heavily during this mode.

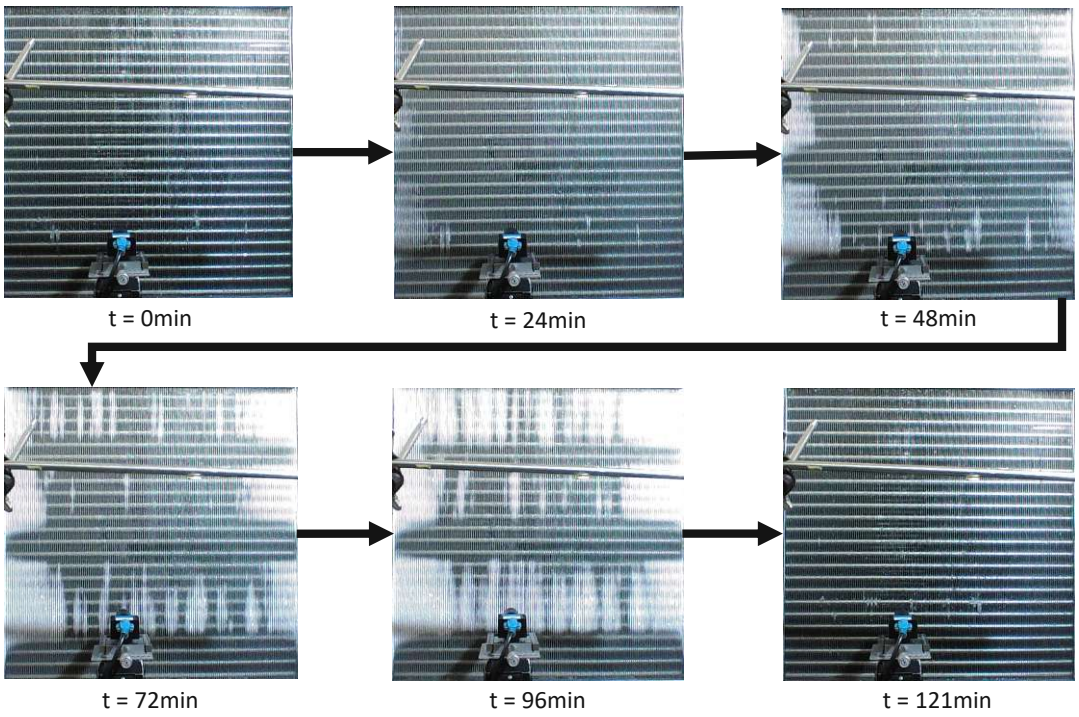

Figure 37: Nonuniform frost formation on the heat exchanger surface of the SilentAirHP.

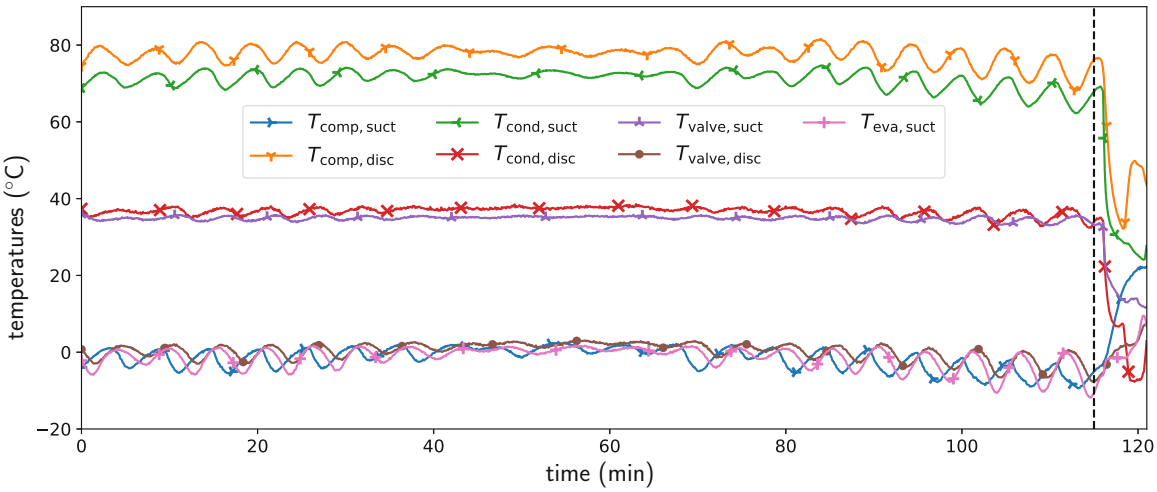

Figure 38: Development of the refrigerant temperatures over time during operation of the SilentAirHP at frosting conditions. The time when defrosting is initiated is marked with a black dotted line.

5.2 Validation of the Numerical Model

In order to validate the numerical model described in Chapter 4, the experimental measurement points were simulated with the existing numerical model. Several parameters were adjusted in a reasonable range, to achieve a good fit to the experimental results. The parameters which were adjusted are the isentropic and volumetric efficiency of the compressor η_s and η_v, respectively, the heat transfer coefficient of the condenser at the secondary fluid and working fluid side $U_{cond,sf}$ and $U_{cond,wf}$, respectively, the heat transfer coefficient of the evaporator on the working fluid side $U_{eva,wf}$ and the nominal refrigerant mass flow $\dot{m}_{nom}$. Even though each change in a parameter affects nearly all parts of the system, some parts are affected more and some less. The isentropic efficiency of the compressor mainly determines the electrical power consumption of the compressor and the hot-gas temperature of the refrigerant after the compressor. The volumetric efficiency has very little impact on the rest of the system, but determines the compressor speed. How much heat is transferred at the condenser, and therefore the temperature level of the refrigerant in the condenser, is defined by the heat transfer coefficients of the condenser. The heat transfer coefficient of the evaporator on the working fluid side has only very little impact, as the important figure is the heat transfer coefficient on the secondary (air) side. As defined in Section 4.2.1 the heat transfer coefficient on the refrigerant side in the condenser and evaporator is dependent on the refrigerant mass flow. This dependence is nonlinear and therefore the nominal refrigerant mass flow has an impact on the mass flow dependent change of the heat transfer coefficient, especially for low and high refrigerant mass flows. The determined parameters of the numerical model validation are listed in Table 14.

Table 14: Determined parameters of the validation of the numerical model.

Compressor		Condenser		Evaporator	Refr. Mass Flow
η_s	η_v	$U_{cond,sf}$	$U_{cond,wf}$	$U_{eva,wf}$	$\dot{m}_{nom}$
0.55	0.78	2500 W/m^{2}K	800 W/m^{2}K	100 W/m^{2}K	80 kg/h

In Figure 39 four selected variables of the heat pump cycle are compared between the experimental measurements and the simulation results. The data is listed in Table 15.

The simulation results for the rotational speed of the compressor slightly exceeds the experimental measurements for points with a high absolute compressor speed, as for heating and domestic hot water production mode with low ambient temperatures. For the other points the simulation results undercut the experimental measurements a bit. This suggests, that the volumetric efficiency of the compressor varies slightly for different boundary conditions. But as the fit, assuming a constant volumetric efficiency, is in a reasonable range and a different volumetric efficiency does not effect the rest of the simulation results, it was left constant for all points.

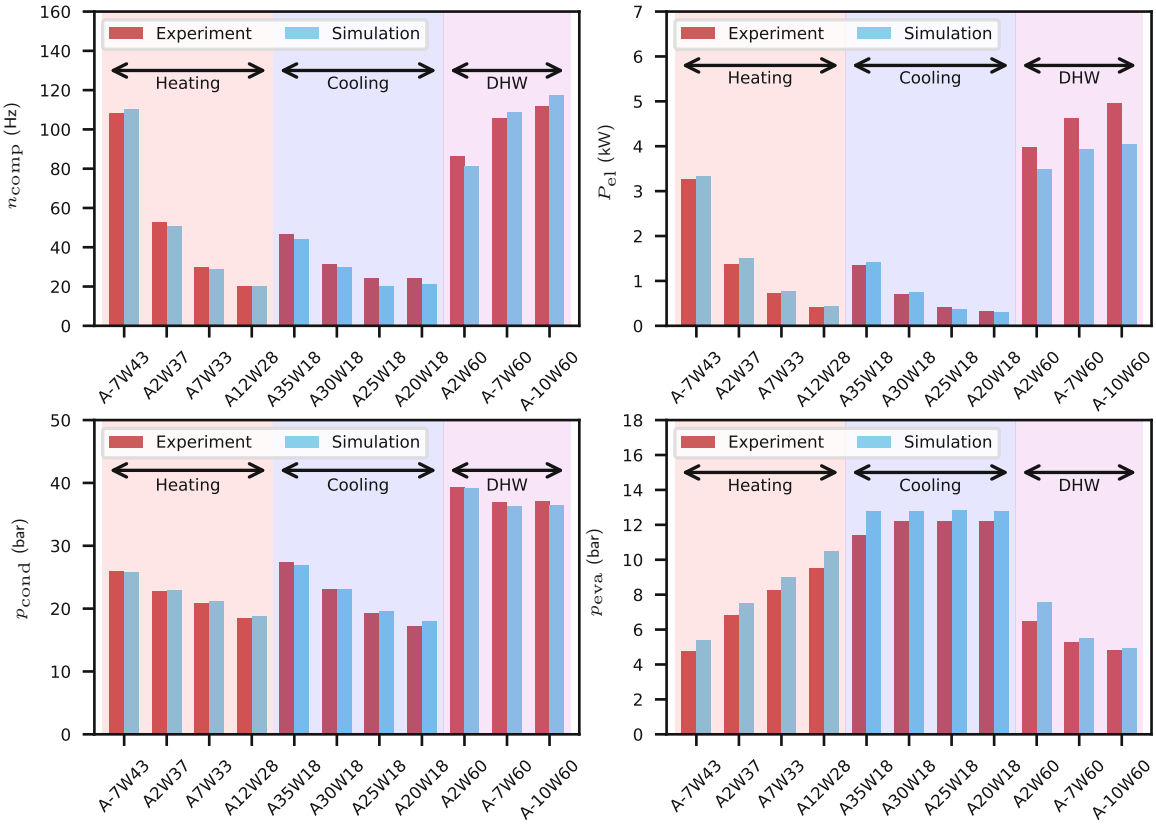

Figure 39: Comparison of selected variables between experimental measurements and simulation results, data listed in Table 15.

Comparing the electrical power consumption of the heat pump between the experimental measurements and the simulation, a good match for the heating and cooling mode is observed. For the domestic hot water production the experimental measurements overshoot the simulation results significantly. Especially for low ambient temperatures the increase in electrical power consumption is larger for the experimental measurements than for the simulation results. This is an indication that the compressor has a variant isentropic efficiency, which is dependent on the suction and discharge refrigerant state. Unfortunately, no reliable information on the isentropic efficiency of the used compressor could be obtained and was therefore left constant for all simulations. It should be stated however, that the acquired constant isentropic efficiency of the compressor is fairly low. This efficiency should rather be seen as the isentropic efficiency of the full heat pump cycle and not as the isentropic efficiency of the compressor alone, as no additional heat losses are implemented in the numerical model.

Table 15: Simulation and experimental results of selected variables for the validation of the numerical model, visualized in Figure 39.

		N_{comp} (Hz)	p_{cond} (bar)	p_{eva} (bar)	P_{el} (kW)
A-7W43	Simulation	110.38	25.75	5.38	3.34
	Experiment	108.00	25.92	4.75	3.26
A2W37	Simulation	50.79	22.91	7.54	1.50
	Experiment	52.80	22.79	6.80	1.36
A7W33	Simulation	28.85	21.16	9.00	0.77
	Experiment	29.88	20.90	8.25	0.72
A12W28	Simulation	20.15	18.77	10.49	0.43
	Experiment	20.00	18.50	9.52	0.42
A35W18	Simulation	44.13	26.84	12.81	1.41
	Experiment	46.44	27.45	11.40	1.36
A30W18	Simulation	29.74	23.03	12.80	0.75
	Experiment	31.20	23.10	12.20	0.70
A25W18	Simulation	20.27	19.62	12.83	0.38
	Experiment	24.00	19.20	12.20	0.41
A20W18	Simulation	21.05	18.05	12.78	0.31
	Experiment	24.00	17.20	12.20	0.32
A2W60	Simulation	81.19	39.11	7.59	3.49
	Experiment	86.40	39.25	6.50	3.97
A-7W60	Simulation	108.70	36.30	5.53	3.94
	Experiment	105.60	37.00	5.30	4.61
A-10W60	Simulation	117.58	36.50	4.95	4.04
	Experiment	111.60	37.10	4.80	4.95

The refrigerant pressure inside the condenser is directly related to the temperature level in the condenser, as the refrigerant is in a two phase state inside the condenser. Therefore, the pressure is linked to the heat transfer between the refrigerant and the water in the condenser. Comparing the refrigerant pressure in the condenser between the experimental and simulation results, a good match can be observed. It should be stated that the condenser pressure in cooling mode is measured in the same component as in heating and DHW generation mode, which actually acts as the evaporator in cooling mode.

Comparing the evaporator pressure between the experimental measurements and the simulation results, the simulation results slightly exceed the experimental measurements. This points to a higher temperature level in the evaporator unit in the simulations. In heating and DHW generation mode this means that the heat transfer in the simulation is slightly better, as the evaporator works with a lower temperature gap between the refrigerant and the ambient air. In cooling mode the opposite is true. As the pressure level, and therefore the temperature level, in the evaporator (outdoor) unit is higher, the evaporator requires a

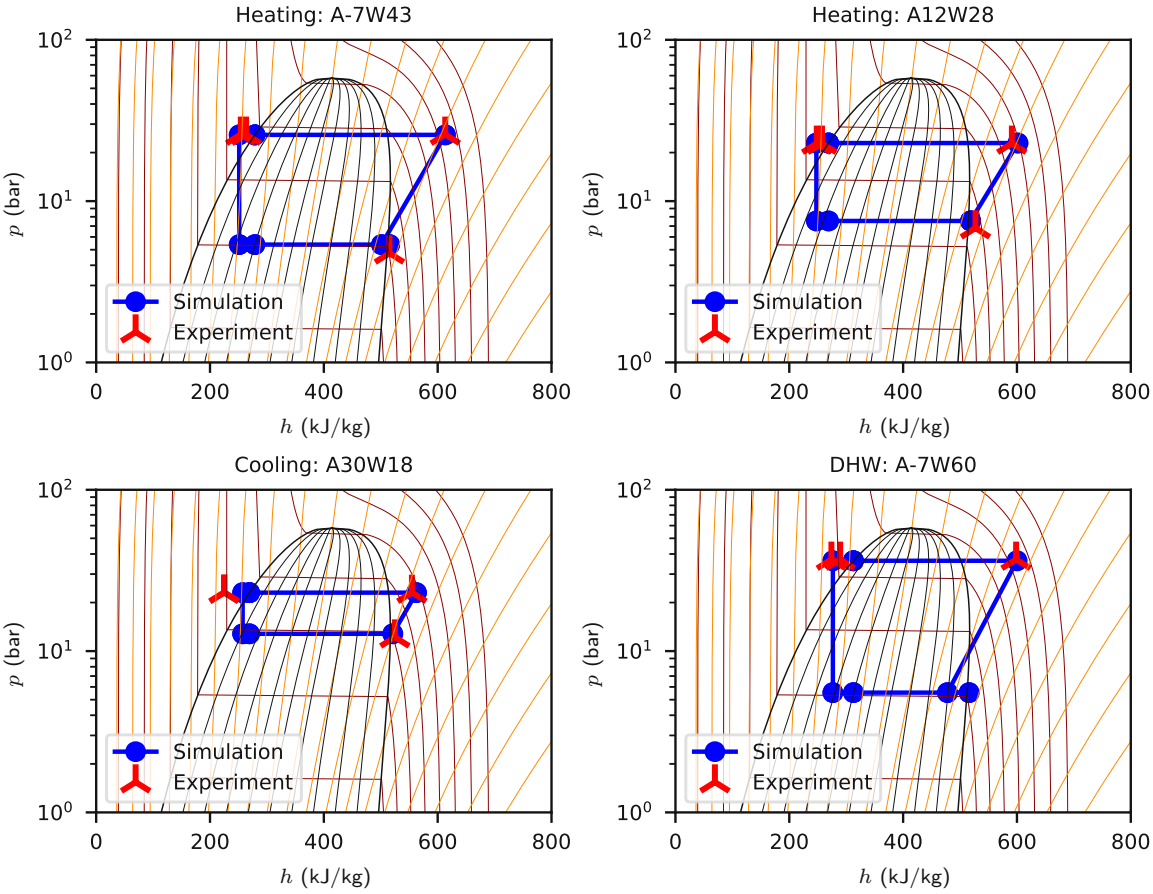

Figure 40: Comparison of log p-h diagrams for selected points of the validation simulations.

higher temperature gap between the refrigerant and the ambient air in order to be able to transfer the required heat. It should be stated again, that the evaporator unit in cooling mode actually acts as the condenser for the refrigerant cycle.

In Figure 40 the log p-h diagrams of selected validation simulations are shown and compared to the experimental measurements. The log p-h diagrams of the heating mode show a very good match of the experimental points to the simulation results. One discrepancy can be seen at the suction point of the compressor. The measured pressure slightly undercuts the simulation result. This may be due to the fact that no pressure drop on the refrigerant side in the heat exchangers are implemented in the numerical code. Another discrepancy visible is at the outlet of the condenser and inlet to the additional heat exchanger, which sub-cools the refrigerant before entering the expansion valve. This discrepancy is caused by the tank component in the simulation, which is actually not present in the experimental setup, but is necessary to ensure numerical stability and assist the initialization process. As only temperatures and pressures are measured, no measurements on points in the two-phase region are reliable. In cooling mode two discrepancies can be observed. First the discharge

hot-gas temperature after the compressor is slightly higher in the simulation than in the experimental measurements. This is due to the fact that the isentropic efficiency is rather low in the experiments to compensate all heat losses of the cycle. The second discrepancy can be spotted at the outlet of the condenser. In the experimental measurements the outlet of the condenser is actually still slightly located in the two-phase region. That is the reason why no point is indicated in the figure. In the numerical model the tank component forces the outlet to be exactly on the boiling curve. Furthermore, the additional heat exchanger sub-cools the refrigerant more than the numerical model suggests. In DHW generation mode the simulation results match the experimental results very well. The only discrepancy at the outlet of the condenser is caused by the tank component, as it fixes the condenser outlet to the boiling curve. The suction point of the compressor now lies inside the two-phase region, as the bypass valve is active in order to avoid hot-gas temperatures discharging the compressor of more than 115 °C. As the suction point now lies in the two phase region it is not shown in the figure, as the measurements on temperature and pressure alone do not suffice to give a reliable information about the thermodynamic state.

5.3 Performance Maps

With use of the validated numerical model performance maps were created for different system setups. These setups include:

(A) Reference system

(B) Novel system including the RPW-HEX, filled with RT64HC PCM

(C) Novel system including the RPW-HEX, filled with RT54HC PCM

(D) Novel system including the RPW-HEX, filled with RT54HC PCM and a reduced fan speed in cooling mode of 360 rpm

In the following sections the different setups are analyzed and compared. The simulation results of these setups, which are used for the plots in the next sections, are listed in Appendix E. For a fair comparison between the reference and novel heat pump system the COP_{h} was calculated according to Equation (24), as stated in Section 4.3.2.

5.3.1 Reference System (A) vs. Novel System with RT64HC PCM (B)

Comparing the simulation results of the reference system (A) with the novel system including the RPW-HEX filled with RT64HC PCM (B) it is expected to achieve a slightly lower COP_{h} for the novel system in heating mode and a slightly higher COP_{h} in cooling and DHW

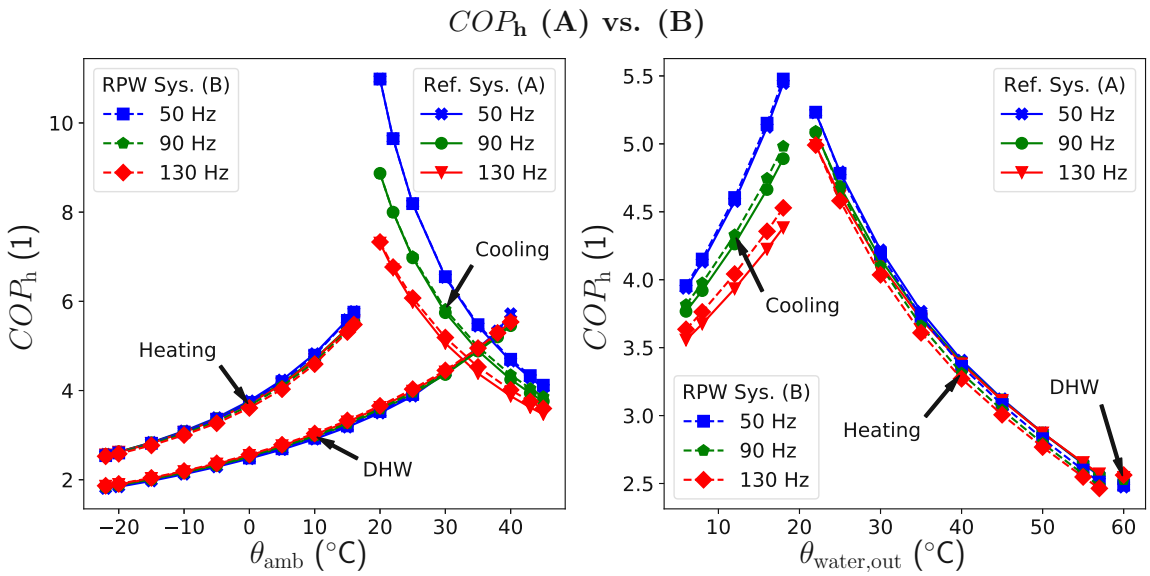

Figure 41: Comparison of the COP_h between the reference system (A) and the novel system including the RPW-HEX filled with RT64HC (B). For plot (a) the feed water outlet temperature is left constant with $\theta_{water,out} = 35\,°C$ for heating, $\theta_{water,out} = 18\,°C$ for cooling and $\theta_{water,out} = 60\,°C$ for DHW generation mode. For plot (b) the ambient temperature is left constant with $\theta_{amb} = 0\,°C$ for heating and DHW generation and $\theta_{amb} = 35\,°C$ for cooling mode.

generation mode. This is due to the fact that in heating mode the RPW-HEX takes some of the high temperature heat of the hot-gas, which is then unavailable in the condenser. In cooling mode, the RPW-HEX relieves the evaporator, by already pre-cooling the hot-gas before it enters the evaporator unit. During operation in DHW generation mode, without discharging the RPW-HEX, the RPW-HEX only acts as a heat exchanger between the refrigerant and water, leading to an increased heat transfer and therefore increasing the efficiency of the heat pump cycle.

In Figure 41 the COP_h of the reference and novel system including the RPW-HEX filled with RT64HC PCM are compared for all modes. In heating mode the COP_h of the reference system slightly exceeds the COP_h of the novel system. As already discussed, this is due to the fact that part of the high temperature heat of the refrigerant after the compressor is already used to charge the RPW-HEX and is therefore not available in the condenser to heat the feed water. For a constant feed water outlet temperature and feed water mass flow this means that the condenser temperature level and therefore the condenser pressure needs to be slightly higher, as the refrigerant at the inlet is not as super-heated in the novel system, as in the reference system. In cooling mode the COP_h of the novel system is slightly larger than for the reference system. In this mode the RPW-HEX actually helps the outdoor unit by removing enthalpy from the refrigerant before entering the outdoor unit. As the compressor

speed and the ambient temperature increases, the discrepancy between the reference and novel system increases. The increase in compressor speed leads to a larger heat flow at the hot side of the heat pump, therefore the system benefits more from the heat removal of the RPW-HEX. For higher ambient temperatures the heat transfer in the evaporator gets worse, due to a lower temperature difference. The benefit from removing some heat of the hot-gas before it enters the evaporator is therefore more significant in this operation scenario. In DHW generation mode the RPW-HEX acts as an additional heat exchanger between the refrigerant and the feed water for the novel system. Therefore, the COP_{h} for the novel system is slightly higher than for the reference system under all conditions. As this difference is only very little, it can not really be identified in this figure.

5.3.2 Novel System with RT64HC PCM (B) vs. Novel System with RT54HC PCM (C)

Using a PCM with a lower melting point temperature is expected to raise the heat flow charging the RPW-HEX, as the temperature difference between the refrigerant and the PCM gets larger. This will also lead to a slightly lower COP_{h} in heating mode, as the heat flow charging the RPW-HEX is now unavailable in the condenser. Due to a lower reachable DHW temperature, the COP_{h} is expected to be larger for the system using the PCM with a lower melting point temperature. In cooling mode the COP_{h} will be slightly higher for the system using RT54HC PCM, as the heat flow charging the RPW-HEX is larger and therefore less heat has to be removed from the refrigerant in the evaporator.

In Figure 42 the COP_{h} is compared between the novel system using RT64HC (B) and RT54HC (C) as PCM. In heating mode the COP_{h} of system (B) is slightly higher, due to the fact that as the PCM has a higher melting temperature the refrigerant temperature discharging the RPW-HEX is higher than for system (C). Therefore more high temperature heat is available in the condenser. In cooling mode nearly no difference in the COP_{h} is visible. However, as the RPW-HEX actually relieves the outdoor unit, because some enthalpy is already removed from the refrigerant before entering the outdoor unit, the (C) system using RT54HC PCM results in a slightly better COP_{h}, as a larger heat flow is charging the RPW-HEX. This might be seen as free energy charging the RPW-HEX for DHW generation. The increase in the COP_{h} for the DHW generation mode is due to the reason that the hot water for the RT64HC (B) system is provided at a higher temperature level of $\theta_{\mathrm{water,out}} = 60\,^{\circ}\mathrm{C}$, compared to the hot water temperature of $\theta_{\mathrm{water,out}} = 50\,^{\circ}\mathrm{C}$ for the RT54HC (C) system. Therefore, the heat pump has a smaller pitch to pump the heat from the cold side to the hot side.

The heat flow charging the RPW-HEX for the systems using RT64HC (B) and RT54HC (C) is visualized in Figure 43. For all conditions the heat flow charging the RPW-HEX is larger for the system using RT54HC PCM (C). This is due to the fact that the PCM temperature of system (C) is lower, therefore leading to a higher temperature gap between

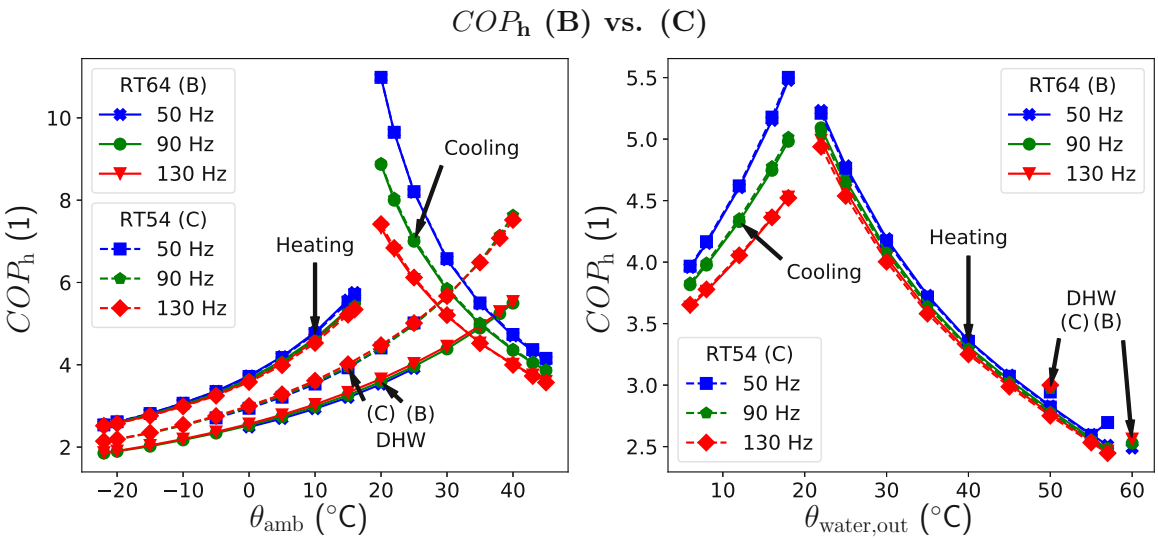

Figure 42: Comparison of the COP_h between the novel systems using RT64HC (B) and RT54HC PCM (C). For plot (a) the feed water outlet temperature is left constant with $\theta_{water,out} = 35\,°C$ for heating and $\theta_{water,out} = 18\,°C$ for cooling mode. For the DHW generation mode the feed water outlet temperature is $\theta_{water,out} = 60\,°C$ for the system using RT64HC PCM (B) and $\theta_{water,out} = 50\,°C$ for the system using RT54HC PCM (C). For plot (b) the ambient temperature is left constant with $\theta_{amb} = 0\,°C$ for heating and DHW generation and $\theta_{amb} = 35\,°C$ for cooling mode.

the refrigerant and the PCM. For a constant feed water temperature of $\theta_{water,out} = 18\,°C$ in cooling mode the heat flow charging the RPW-HEX becomes 0W for a compressor speed of less than 50Hz and ambient temperatures lower than 22 °C for both systems. At these conditions the hot-gas temperature discharging the compressor become less than the PCM melting temperature, actually leading to a sensible discharge of the RPW-HEX. For an ambient temperature of $\theta_{amb} = 0\,°C$, operation in heating mode and a feed water outlet temperature of more than 40 °C the bypass valve is needed to inject liquid refrigerant into the suction point of the compressor, to avoid hot-gas temperatures of more than 115 °C. This can be seen in Figure 43(b), as the gradient of the heat flow charging the RPW-HEX is decreasing for increasing feed water outlet temperatures, as the hot-gas temperature stays constant and the increase in heat flow now only depends on the increase in refrigerant mass flow.

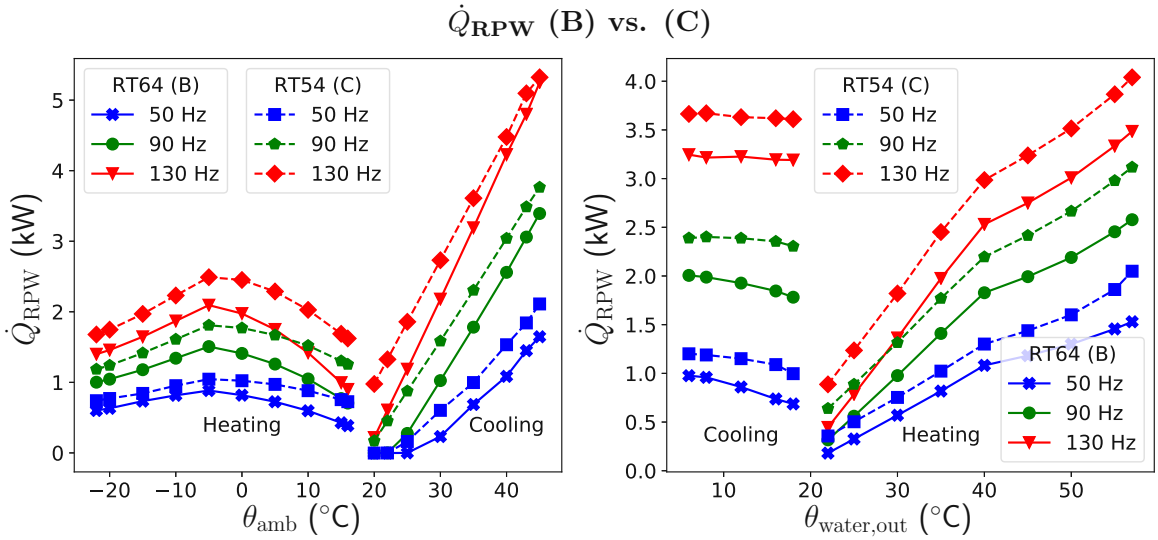

Figure 43: Comparison of the heat flow charging the RPW-HEX $\dot{Q}_{\mathrm{RPW}}$ between the novel system including the RPW-HEX, using RT64HC and RT54HC PCM. For plot (a) the feed water outlet temperature is left constant with $\theta_{\mathrm{water,out}} = 35\,°\mathrm{C}$ for heating and $\theta_{\mathrm{water,out}} = 18\,°\mathrm{C}$ for cooling mode. For the DHW mode the feed water outlet temperature is $\theta_{\mathrm{water,out}} = 60\,°\mathrm{C}$ for the RT64HC PCM and $\theta_{\mathrm{water,out}} = 50\,°\mathrm{C}$ for the RT54HC PCM. For plot (b) the ambient temperature is left constant with $\theta_{\mathrm{amb}} = 0\,°\mathrm{C}$ for heating and DHW and $\theta_{\mathrm{amb}} = 35\,°\mathrm{C}$ for cooling mode.

5.3.3 Novel System with RT54HC PCM (C) vs. Novel System with RT54HC PCM and a reduced fan speed in cooling mode (D)

As the heat flow charging the RPW-HEX in cooling mode may be seen as free energy, as the system utilizes waste heat, it is desired to get as much heat as possible into the RPW-HEX in this mode. Reducing the evaporator fan speed leads to a reduction of the heat transfer in the evaporator, therefore increasing the the heat available to charge the RPW-HEX. Additionally, it will decrease the electrical power input slightly. However, it will also lead to a decrease in the COP_{h} of the system, as the heat transfer in the evaporator is reduced.

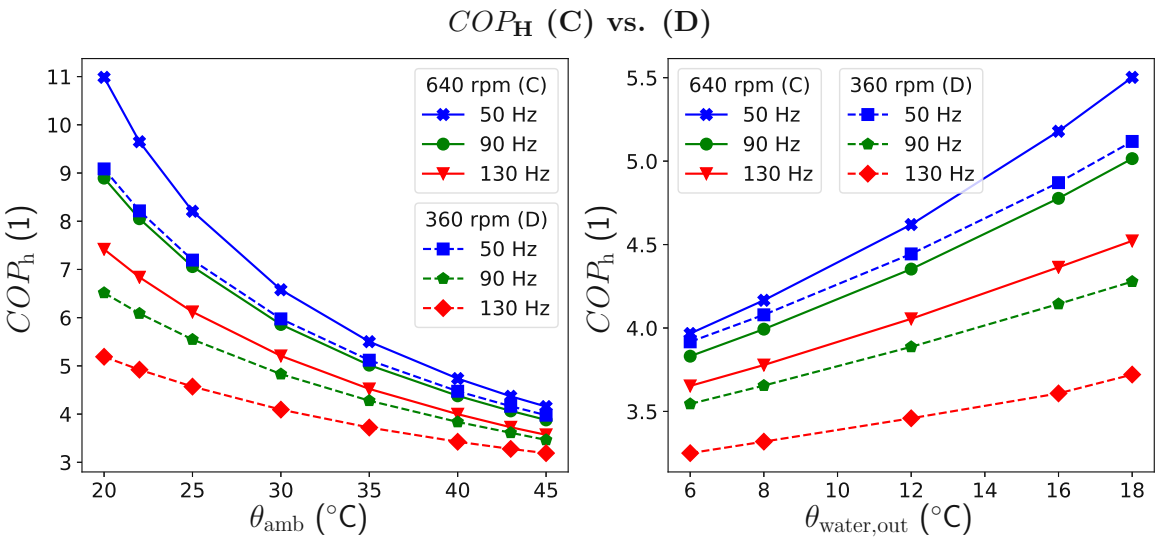

Figure 44: COP_h of the novel system in cooling mode using RT54HC PCM with different evaporator fan speeds. For plot (a) the feed water outlet temperature is left constant with $\theta_{water,out} = 18\,°C$ and for plot (b) the ambient temperature is left constant with $\theta_{amb} = 35\,°C$.

In Figure 44 the COP_h of the novel system in cooling mode using RT54HC PCM with different fan speeds is shown. As expected, the COP_h for the system with reduced fan speed (D) is lower than for the system with a higher fan speed (C). This difference is getting more significant for higher compressor speeds, lower ambient temperatures and higher feed water outlet temperatures. For high compressor speeds the heat flow at the hot side of the heat pump is larger, therefore the decrease of the evaporator fan speed and consequently the heat transfer in the evaporator reduces the efficiency of the system in this operational scenario more significant than in other scenarios. As the ambient temperature decreases, a lower refrigerant temperature in the evaporator suffices for the heat transfer. Reducing the evaporator fan speed at these ambient conditions reduces the efficiency of the heat pump more significantly, than for higher ambient temperatures.

The heat flow charging the RPW-HEX is shown in Figure 46. As the fan speed is decreased, the heat transfer of the outdoor unit is decreased as well, leading to a higher heat flow charging the RPW-HEX. This is true for all operation conditions. This discrepancy slightly increases for higher feed water outlet temperatures. But as the fan speed decreases, the refrigerant hot-gas temperature after the compressor increases as well. As the bypass valve is not active in cooling mode, the refrigerant might exceed temperatures above 120 °C. This needs to be avoided as it causes lubrication problems in the compressor. Therefore, operation conditions where the hot-gas temperature exceeds 120 °C can not be used in real applications.

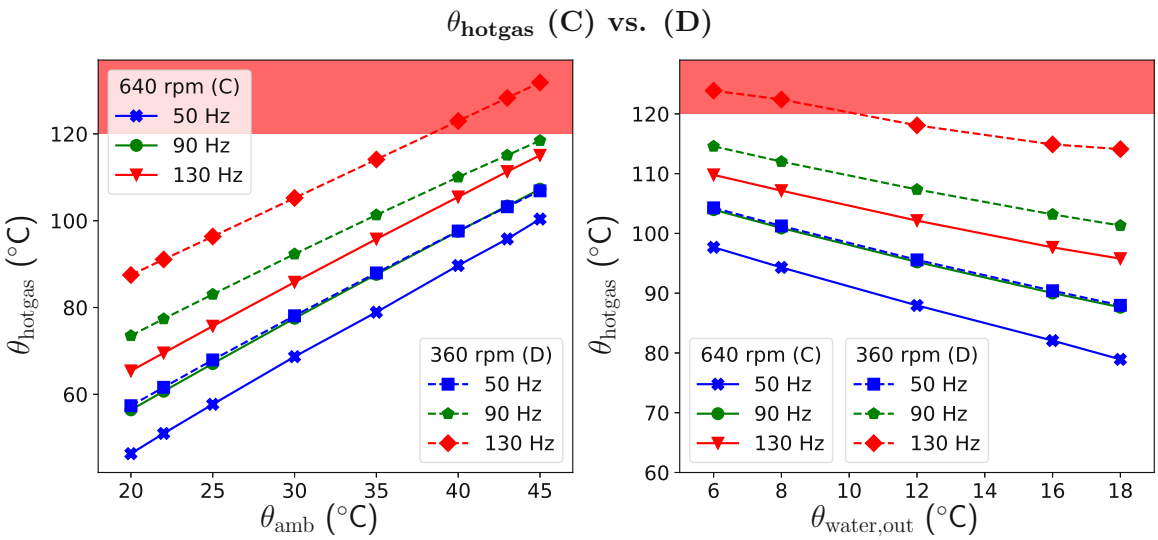

Figure 45: Refrigerant hot-gas temperature discharging the compressor of the novel system in cooling mode using RT54HC PCM with different evaporator fan speeds. For plot (a) the feed water outlet temperature is left constant with $\theta_{\text{water,out}} = 18\,°\text{C}$ and for plot (b) the ambient temperature is left constant with $\theta_{\text{amb}} = 35\,°\text{C}$.

Figure 45 shows the refrigerant hot-gas temperatures after the compressor for both cases, with regular (C) and decreased fan speed (D). The highlighted red area is where the refrigerant hot-gas temperature exceeds 120 °C. It can be seen, that for a compressor speed of $n_{\text{comp}} = 130\,\text{Hz}$, a feed water outlet temperature of $\theta_{\text{water,out}} = 18\,°\text{C}$ and ambient temperatures above 40 °C the system with reduced fan speed (D) exceeds refrigerant hot-gas temperatures of 120 °C. The same is true for a compressor speed of $n_{\text{comp}} = 130\,\text{Hz}$, an ambient temperature of $\theta_{\text{amb}} = 35\,°\text{C}$ and feed water outlet temperatures of less than 10 °C. At these conditions the system can not be operated with a reduced evaporator fan speed.

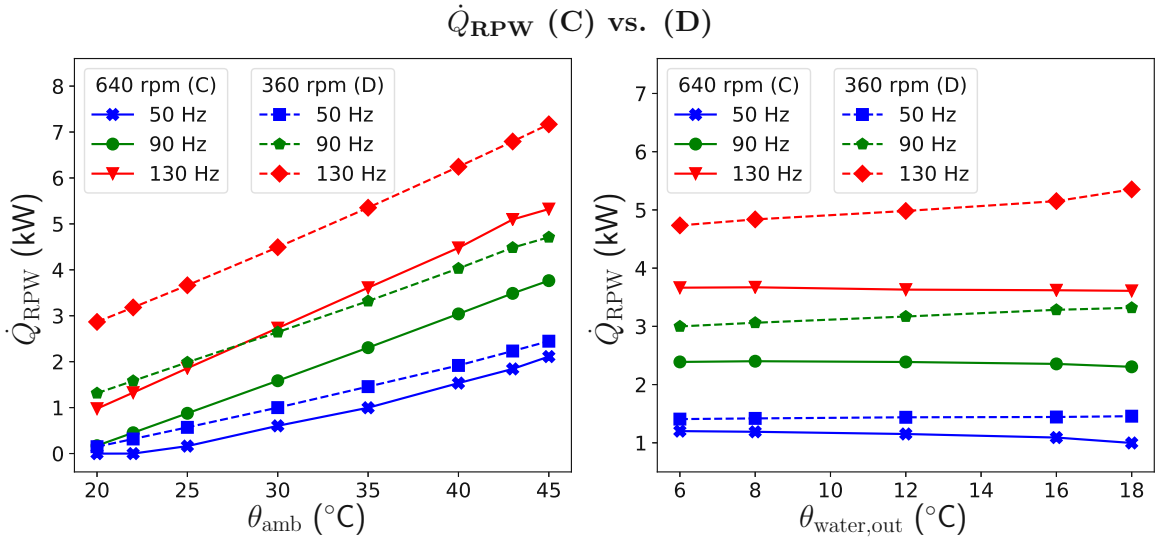

Figure 46: Heat flow charging the RPW-HEX of the novel system in cooling mode using RT54HC PCM with different evaporator fan speeds. For plot (a) the feed water outlet temperature is left constant with $\theta_{water,out} = 18\,°C$ and for plot (b) the ambient temperature is left constant with $\theta_{amb} = 35\,°C$.

5.4 Typical Operation Scenario of Novel System

In the following a typical operation scenario of the novel system is examined. This includes operation in heating mode and charging of the RPW-HEX and a switch to DHW generation and discharging of the RPW-HEX. The simulation model of the heat pump as discussed in the previous sections was used. Typical operation conditions in winter were chosen, with an outdoor temperature of 2 °C and a constant return water temperature of 32 °C. The compressor speed was set so 52.8 Hz and the fan speed was set to 6.45 Hz. The RPW-HEX is filled with a RT64HC PCM material.

In the beginning the *SoC* of the RPW-HEX is 5 %, so nearly no latent heat is stored yet. The heat pump is operated in heating mode for 3760 s (≈ 63 min), in which the RPW-HEX is charged to approximately 40 %. Afterwards, DHW is produced and the RPW-HEX is discharged back to the initial 5 %. This DHW production operation takes about 290 s (≈ 5 min). In Figure 47(a) the *SoC* development is shown. Due to numerical problems with the local integration to obtain the *SoC* there is two abrupt unforeseen changes in the *SoC*, once after approximately 15 min in heating mode, where the *SoC* drops for about 1 % and once just after the switch between heating and DHW generation mode, where the *SoC* spikes for about 2 %. In Figure 47(b) the development of the water temperatures during operation is shown. In heating mode the water outlet temperature is equal to the condenser outlet temperature, as the RPW-HEX is bypassed. In DHW generation mode, on the other hand, the RPW-HEX additionally heats the water discharging the condenser, which leads

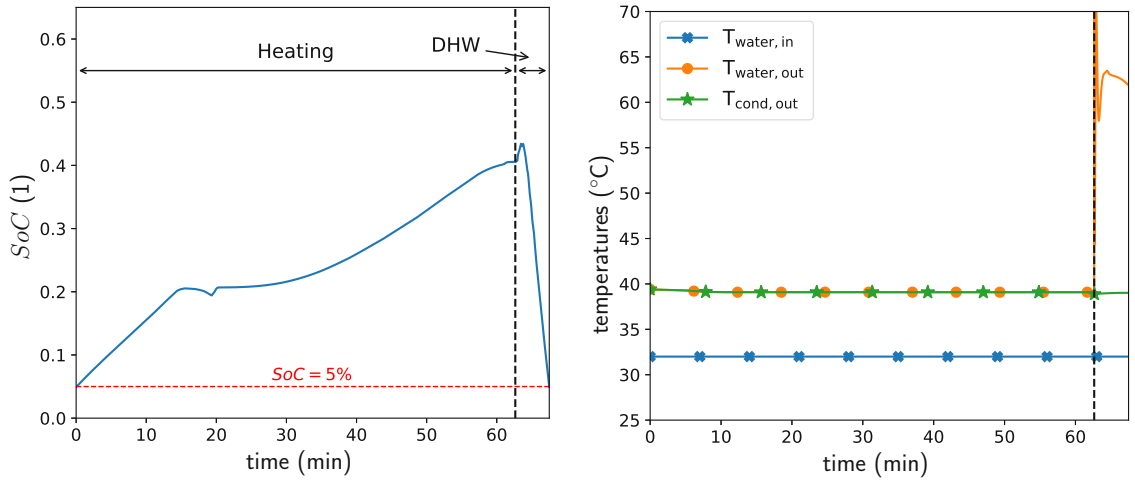

Figure 47: *SoC* and water temperature development in a typical operation scenario of the novel system. In heating mode the RPW-HEX is charged and the *SoC* is therefore increasing, while in DHW generation mode the RPW-HEX is discharged and the *SoC* decreases. The water outlet temperature is equal to the condenser outlet temperature in heating mode, while in DHW generation mode the RPW-HEX additionally heats the water discharging the condenser.

to a higher water outlet temperature. By this, hot water temperatures of more than 60 °C can be reached without increasing the compressor speed.

In Figure 48 the heat flows charging and discharging the RPW-HEX and the heat flow which heats the water in the condenser are shown. Additionally, the power demand of the compressor and fan are marked. During heating mode all heat flows and power demands stay nearly constant. The power demand of the compressor is significantly larger than the power demand of the fan and therefore dominates the total power consumption. After switching to DHW generation the RPW-HEX is discharged. The heat flow discharging the RPW-HEX is unsteady, spiking in the beginning followed by an abrupt low. Afterwards the heat flow is rising again. The total heat transferred to the water in both heat exchangers, namely the condenser and RPW-HEX, is displayed in the left-hand box and the total energy demand of the compressor and fan is displayed in the right-hand box.

The overall *COP* for the heat pump over one full cycle of heating and DHW generation can be calculated by:

$$COP = \frac{Q_{\text{cond}} + Q_{\text{RPW}}}{W_{\text{comp}} + W_{\text{fan}}} \tag{36}$$

This results into a *COP* of 3.67 for the combination of heating and DHW generation.

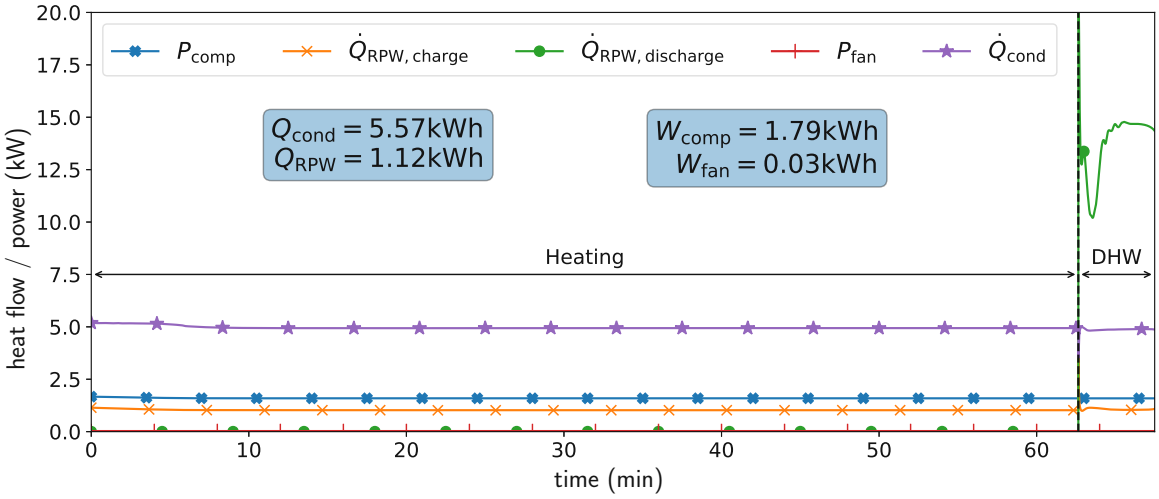

Figure 48: Heat flow and power demand development during a typical operation scenario of the novel system, including operation in heating mode, followed by a switch to DHW generation. The total heat transferred to the water in both heat exchangers, namely the condenser and RPW-HEX, and the total energy demand of the compressor and the fan are displayed in the blue boxes.

5.5 Annual Performance

With aid of the RPW-HEX, the novel heat pump system can generate DHW with a better COP of COP_{h} than COP_{DHW}. Additionally, as seen in Section 5.3, the COP in cooling mode is also slightly increased, as the RPW-HEX removes enthalpy from the refrigerant, relieving the evaporator. However, the COP in heating mode is slightly decreased in the novel system, as the refrigerant at the condenser inlet has a lower temperature, as enthalpy of the super-heated refrigerant is stored in the RPW-HEX. In this section the results of an annual calculation, as described in Section 5.5 and in the Paper submitted to the 25th IIR International Congress of Refrigeration 2019, as attached in Appendix F, are shown and compared to the annual performance of the reference system. The performance map data from Section 5.3 was used for this calculation. The assumed scenario is defined by ambient temperatures from Strasbourg in an hourly resolution, obtained from Meteonorm (2016). Three apartments located in a low energy building are provided with heating, cooling and DHW. This results into an annual heating and cooling demand of $Q_{\mathrm{heat,tot}} = 12\ 847\,\mathrm{kWh}$ and $Q_{\mathrm{cool,tot}} = 1\ 093\,\mathrm{kWh}$, respectively. Furthermore, the annual heating demand for DHW is $Q_{\mathrm{DHW,tot}} = 6\ 400\,\mathrm{kWh}$. The calculation is done for the 4 different setups, as stated and discussed in Section 5.3:

(A) Reference system

(B) Novel system including the RPW-HEX, filled with RT64HC PCM

(C) Novel system including the RPW-HEX, filled with RT54HC PCM

(D) Novel system including the RPW-HEX, filled with RT54HC PCM and a reduced fan speed in cooling mode of 360 rpm

The reference system had to be split, as two different domestic hot water temperatures are used for the novel systems with the different PCMs. For the system using RT64HC PCM, (B), a domestic hot water temperature of 60 °C is used and for the systems using RT54HC PCM, (C) and (D), a domestic hot water temperature of 50 °C is used. The reference system with a domestic hot water temperature of 60 °C is called (A1) and the reference system with a domestic hot water temperature of 50 °C is called (A2).

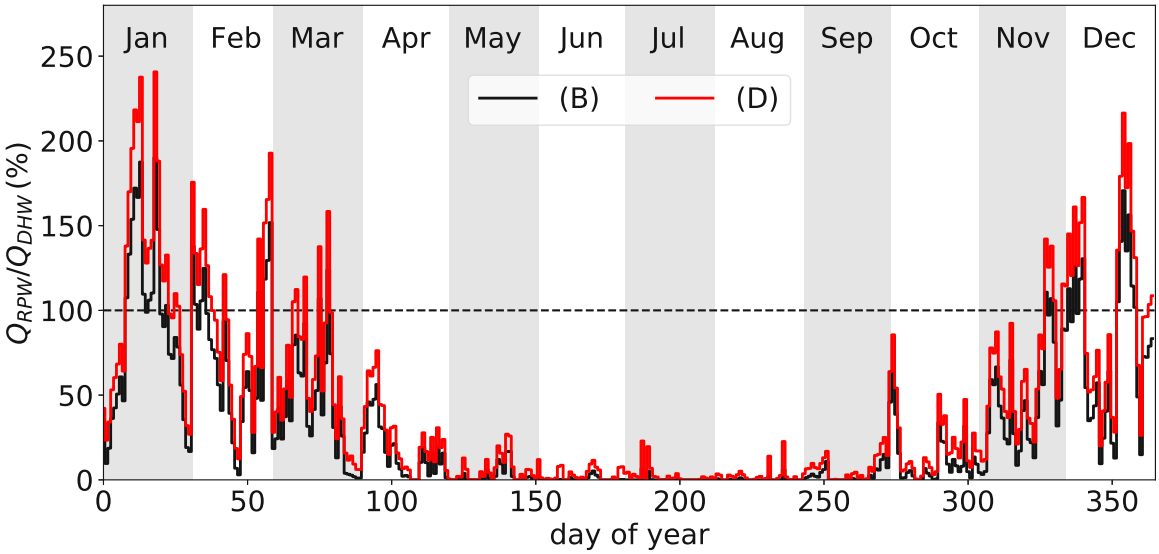

Figure 49: Coverage ratio of energy for DHW generation provided by the RPW-HEX for system setup (B) and (D).

Figure 49 shows how much thermal energy can be provided by the RPW-HEX for DHW generation on a daily basis for the setup (B) and (D). It was assumed that when the system generates more DHW than necessary it can be stored in decentralized DHW storages and the surplus of thermal energy can be shifted to the following days. During the colder months where significant heating is necessary, i.e. October to March, both setups can cover most of the energy needed for DHW generation by the RPW-HEX. In the months where a mild climate is present, i.e. April and May, the heat pump is operated in a low part load ratio and therefore not enough energy is provided by the super-heated hot-gas to fully cover the energy needed for DHW generation. During the months with high ambient temperatures where cooling is needed, i.E. June to September, the energy stored in the RPW-HEX is significantly less than the energy needed for DHW generation for both setups. This is due to a mild climate in Strasbourg, where heating of buildings dominates over cooling and therefore only very low part load ratios of the heat pump are present while being in cooling

mode. However, as the energy stored in cooling operation is for free and does not reduce the heat pump efficiency, but actually increases it slightly, this small energy reduction for the DHW generation still pays of in total electric energy usage of the heat pump system. Using a PCM with a lower melting point, as done in setup (D) compared to setup (B), the coverage ratio can be increased significantly during the whole year of operation. Especially for the operation in cooling mode, setup (D) can still utilize some of the energy, while setup (B) can not, because of low hot-gas temperatures at these low part load ratios. Table 16 summarizes the calculated annual energy efficiencies and the electric power demand for the different setups.

Table 16: Calculated annual energy efficiencies and electric power demands for the different heat pump setups.

	$Q_{\mathrm{RPW,tot}}$(kWh)	W_{tot}(kWh)	W_{DHW}(kWh)	EER_{h}	EER_{c}	EER_{DHW}
(A1)	0	5373	2090	4.04	6.35	3.06
(A2)	0	5033	1750	4.04	6.35	3.66
(B)	1919	5167	1869	4.01	6.68	3.42
(C)	2652	4903	1597	4.00	6.68	4.01
(D)	2681	4846	1591	4.00	8.19	4.02

Reference setup (A1) and (A2) have a different domestic hot water temperature of 60 °C and 50 °C, respectively. This leads to a significant increase in the energy efficiency ratio of the DHW generation EER_{DHW} of setup (A2) and hence a lower electrical energy demand for the DHW generation W_{DHW}. Setup (B) utilizes some of the super-heated hot-gas enthalpy in order to generate DHW. By this, the energy efficiency ratio in heating mode is slightly decreased from 4.04 of the reference setup (A1) to 4.01 for the novel system setup (B), while the energy efficiency for the DHW generation is increased from 3.06 to 3.42. This is because some of the energy required for domestic hot water generation can be generated with the higher energy efficiency in heating operation, or is even free as it is obtained during cooling operation. The energy efficiency in cooling operation is increased for the novel setup (B) compared to the reference setup (A1), as the charging of the RPW-HEX relives the evaporator, as less heat is needed to be transferred to the ambient air. However, as the cooling operation only contributes very slightly to the total electrical power consumption over a full year in the analyzed climate, this increase in efficiency is only of minor importance. Concluding, the novel setup (B) decreases the electrical energy demand of the heat pump over a full year by 206 kWh, which is about 3.8 % of the total electrical energy consumption of the reference setup (A1). Using a PCM with a lower melting point temperature, as done in setup (C) compared to (B), the total energy stored in the RPW-HEX can be increased significantly from 1919 kWh for setup (B) to 2652 kWh for setup (C). The energy efficiency ratio in heating decreases slightly, while the energy efficiency ratio in cooling stays approximately the same for setup (C) compared to setup (B). However, the energy efficiency in DHW generation is increased significantly from 3.42 to 4.01. Attention should be paid as this increase in energy efficiency is more related to the decrease in DHW temperature from 60 °C to 50 °C. Comparing the energy efficiency for DHW generation of setup (C) to

the reference setup (A2), an increase from 3.66 to 4.01 is achieved. This results in saving 130 kWh of electrical energy for a full year of operation, which is about 2.6 % of the total electrical energy demand of the reference setup (A2). In setup (D) the fan speed in cooling mode is reduced, compared to setup (C). Surprisingly, this actually leads to a significant increase in the energy efficiency ratio in cooling mode of 8.19 for setup (D) compared to 6.68 of setup (C). This is due to the fact that the heat pump is operating at a very low part load ratio in cooling operation for the analyzed climate conditions. Therefore, the electrical power demand of the fan contributes significantly to the total electrical power demand of the heat pump. However, as the heat pump is operated only seldom in cooling mode the decrease in fan speed does not contribute to a major increase in heat stored in the RPW-HEX. Over a full year 26 kWh are additionally stored in the RPW-HEX and used for DHW generation for setup (D) compared to setup (C). This leads to a reduction of about 6 kWh of electrical energy demand for DHW generation. However, the increase in electrical energy efficiency in cooling mode for setup (D) contributes more significantly to the total electrical energy saving compared to setup (C). Concluding, setup (D) saves 185 kWh of electrical energy compared to the reference setup (A2), which is about 3.7 % of the total energy demand of the reference setup.

6 Conclusion & Future Research

Technical details for a novel heat pump system were presented and a numerical simulation model was generated. In the novel system a Refrigerant/Phase Change Material (PCM)/Water Heat EXchanger (RPW-HEX) is integrated in the hot-gas section of an air-source heat pump, for energy efficient domestic hot water (DHW) generation. In order to validate the numerical model, experiments on a reference air-source heat pump were conducted. The experimental measurements were carried out for three different heat pump operation modes, namely heating, cooling and domestic hot water generation mode. In progress of the experimental trials the behaviour of the heat pump during operation at frosting conditions was analyzed. It was shown that the frost formation is occurring fastest if the temperature of the ambient air is a few degrees Celsius above 0 °C. At these conditions the ambient air still contains high absolute amounts of water, compared to lower ambient temperatures, and the heat exchanger surface is below water freezing temperatures. When operating the heat pump at a fixed compressor speed, the suction and discharge pressure of the compressor and the refrigerant mass flow are constantly falling, while frost is building on the surface of the evaporator coils. The frost accumulation also leads to a reduced heat transfer at the condenser. In total, the coefficient of performance of the heat pump is decreasing during operation of the heat pump at frosting conditions and the evaporator needs to be defrosted from time to time to ensure stable operation. The frost accumulation was measured by putting the heat pump on a scale. Furthermore, a camera was installed in front of the evaporator coils and the amount of pixels in the pictures exceeding a certain brightness threshold also correlate to the amount of frost present. However, the frost is not forming uniformly on the full evaporator surface and therefore the camera either has to be put at an appropriate position or multiple cameras have to be used.

The established numerical model of the heat pump was validated using the data obtained by the experimental measurements. A good match, with most values being equal to a precision of ±10 % between the simulation and experimental results, was achieved. With use of the validated numerical simulation model the performance and internal heat flows of the heat pump were calculated for several ambient and operation conditions. This was done for four different heat pump setups: the reference system, the novel system using the RT64HC PCM, the novel system using the RT54HC PCM and the novel system using the RT54HC PCM and having a reduced fan speed in cooling mode of 360 rpm. Discrepancies in the heat pump performances and heat flows were analyzed and explained.

A typical operation scenario of the novel system is presented. This includes operation in heating mode and charging of the RPW-HEX and a switch to domestic hot water production and discharging of the RPW-HEX. At typical operation conditions as present during winter times, with an ambient temperature of 2 °C, it was shown that the novel system can be operated in heating mode, providing a constant heat flow of 5 kW, while charging the RPW-HEX with a constant heat flow of 1.03 kW. After 63 min of operation in heating mode the heat pump was switched to DHW generation, releasing the energy stored in the RPW-HEX. After 5 min 1.12 kWh of heat is transferred from the PCM to the DHW. Additionally, the condenser still provides 5 kW to the water during operation in DHW generation mode. Concluding, the COP for the combination of heating and DHW generation is 3.67.

Annual calculations for average climatic conditions, intermediate heating temperatures and medium DHW consumptions indicate estimated savings of about 3.8 % of electric energy with the novel system using RT64HC PCM and about 3.7 % for the novel system using RT54HC PCM and a reduced fan speed in cooling mode. These energy savings result from a 12 % and 10 % higher energy efficiency for DHW generation, respectively, an increase in the energy efficiency for cooling mode and only a slight decrease in energy efficiency in heating mode. Considering three apartments in a low energy building, each with a heat demand of 2 kW at -10°C and a DHW demand of 5.825 kWh per day, the absolute energy savings amount to 206 kWh for the novel system using RT64HC PCM and 185 kWh for the novel system using RT54HC PCM and having a reduced fan speed in cooling mode. Hence it was shown, that the novel system saves electrical energy on a yearly basis and that the energy saving potential depends both on the PCM used and the operation parameters of the heat pump, as the fan speed in cooling mode.

Next steps will include the assessment of the annual performances for other climatic conditions, heating demands and building conditions, as the yearly performance strongly depend on these constraints. It was also shown that the energy efficiency in cooling mode of the analyzed heat pump varies greatly with the fan speed. It is therefore of interest to optimize the fan speed in respect to the energy efficiency in cooling mode. In addition to that, experimental measurements on the novel system heat pump, including the RPW-HEX will be carried out to confirm the simulation results. Including an appropriate frosting model to the numerical analysis will improve the results at operation conditions, where frost accumulation on the evaporator coils is present.

6.1 Research Questions

In this section the research questions as defined in Section 1 are answered in the order mentioned:

1. **Does and how much does the implementation of the RPW-HEX alter the heat pumps characteristics and performance?**

   a) *What are the changes in efficiency and performance for the different heat pump modes (i.e. heating, cooling, hot water generation)?*
   In heating and cooling mode the novel system heat pump either charges the RPW-HEX or the RPW-HEX is already fully charged. In DHW generation mode the RPW-HEX is either discharged or it is already fully discharged. In order to ensure a fair comparison between the reference and the novel system the DHW generation mode an already fully discharged RPW-HEX is considered for the novel system setup. In heating mode the super-heated hot-gas refrigerant charges the RPW-HEX before entering the condenser. Therefore, refrigerant with a lower temperature level, as in the reference setup, is provided to the condenser. This leads to a slight decrease in efficiency of the novel system in heating mode. Moreover, as the RPW-HEX is charged the heat pump provides less thermal power to the water in the condenser at the same compressor speed and electrical power input. In total, the energy efficiency ratio in heating mode for operation in average climatic conditions is 4.04 for the reference conventional system, compared to 4.01 for the novel system setup using RT64HC PCM. In cooling and DHW generation mode the novel system outperforms the reference system. The RPW-HEX extracts enthalpy from the hot-gas refrigerant in cooling mode, therefore reliving the evaporator. This may be seen as free energy for DHW generation and leads to an increased efficiency in this operation mode. Concluding, the energy efficiency in cooling mode at average climatic conditions is 6.35 for the reference conventional heat pump system setup compared to 6.68 for the novel system using RT64HC PCM. In DHW generation mode with a fully discharged RPW-HEX, the RPW-HEX still acts as an additional heat exchanger between the hot water and the refrigerant, therefore reliving the condenser. This also leads to a slight increase in efficiency of the novel system compared to the reference system.

   b) *What is the overall change in efficiency over a full year? Can the power demand be decreased significantly by the implementation of the RPW-HEX?*
   The energy efficiency ratio in heating mode for average climatic conditions and intermediate heating temperatures is 4.01 for the novel system using RT64HC PCM and 4.04 for the reference system. For cooling mode the energy efficiency ratio results in 6.68 for the novel system and 6.35 for the reference system. The most significant difference is in the energy efficiency ratio of DHW generation,

which is 3.42 for the novel system and 3.06 for the reference system, assuming a medium DHW consumption. Concluding, annual calculations indicate estimated savings of about 3.8 % of electrical energy with the novel system using RT64HC PCM, which is mainly caused by the 12 % larger energy efficiency for the DHW generation.

c) *Which phase change material should be used? What melting point fits this usage best?*
Looking at the total electrical energy consumption it is better to use a phase change material with a lower melting temperature, in order to load the RPW-HEX with more energy from the hot-gas refrigerant and in general generate DHW with a higher energy efficiency. However, the maximum DHW temperature, which can be provided by the system, is always less than the melting temperature of the PCM, as a finite temperature difference needs to be present for heat transfer. Therefore, the selection of the used PCM material also depends on the desired sensible DHW storage temperature.

d) *Can other operating parameters of the heat pump (e.g. the evaporator fan speed) be adjusted to increase the annual performance?*
By decreasing the evaporator fan speed from 640 rpm to 360 rpm in the novel system setup using RT54HC PCM, the savings in electrical energy for a full year of operation is increased from 2.6 % to 3.7 %, compared to the reference conventional heat pump system.

e) *Are there other scenarios (i.e. other climate zones, heating temperatures, DHW consumptions) where the benefit of the novel system is more decisive?*
The annual performance benefit of the novel system strongly depends on several factors, which include the climate zone, the heating temperature level and the DHW consumption. In climate zones where the cooling demand is more critical, the RPW-HEX can be charged more often with waste heat in cooling mode, which leads to an increased annual performance. A higher heating temperature level, due to a worse heat transfer system in the building, increases the temperature and refrigerant pressure level in the condenser. Assuming a constant pressure level in the evaporator, this leads to an increased refrigerant hot-gas temperature after the compressor and therefore more energy available to charge the RPW-HEX, which in total leads to an increased annual performance benefit of the novel system. If in any case more energy would be provided by discharging the RPW-HEX, than necessary for heating DHW, this energy would simply be lost. An increased DHW consumption would lead to an increased benefit of the novel system in this case.

2. **Is it possible to create an accurate simulation model for the heat pump system?**

   a) *Which components need to be included in the numerical analysis and which parameters need to be set properly to obtain an accurate model of the heat pump?*
   The main components defining the performance of the heat pump are the compressor, the condenser, the expansion valve and the evaporator. Additionally, another heat exchanger and a bypass valve were present in the heat pump examined in this thesis. All of these need accurate models with real geometric data and several parameters need to be set accordingly. For the compressor this includes the isentropic and volumetric efficiency, which significantly impact the electrical power demand and the rotational speed of the compressor, respectively. For the condenser the heat exchange coefficient on both the refrigerant and water side needs to be set accordingly, as these are relevant for the present condenser pressure and temperature level. In the evaporator the same is true for the refrigerant and air side heat exchange coefficients. For the air side heat exchange well established correlations were used from available literature. A volumetric (tank) component ensures numerical stability, especially at initialization and startup of the dynamic simulation. The nominal refrigerant mass flow needs to be set properly, as it significantly impacts the heat transfer in the condenser and evaporator, especially for high and low part load ratios.

   b) *Does the simulation model fit the experimental data well?*
   Most results from the simulation match the experimental measurements to a precision of $\pm 10\,\%$, which is a good fit for the highly dynamic model of a heat pump system.

   c) *Which computational speeds are possible?*
   The computational speed of the present model is very dependent on the internal dynamics of the states of the heat pump. If fast changes are occurring the integration step size is decreased by the Dymola integrator, leading to slower computational speeds, and vice versa. Therefore, it is not possible to give a general answer for the computational speed of the model. However, typical values are stated to estimate the usability of the model for further investigations, including preliminary simulations for dimensioning or control theory related tasks. The simulation of a steady state operational point for predefined compressor speed, feed water mass flow and outlet temperature and ambient conditions takes time in the scale of one minute. When performing simulations with high dynamics, as simulations including a change in the operation mode, the solver slows down significantly. These simulations may take a couple of minutes, depending on the simulation time and the amount of events.

3. **How can the icing and deicing of the heat exchanger surface of a heat pump be quantified in experiments?**

   a) *Does putting the heat exchanger on a scale give applicable information about the ice accumulation on the heat exchanger surface?*
   By putting the heat exchanger on a scale the weight increase due to condensed water and frost accumulated on the heat exchanger fins can be measured. It should be stated however, that the heat exchanger and the rest of the heat pump may be in different physical places. While the heat exchanger is located outdoors in contact with ambient air, the rest of the heat pump can either be located outdoors or indoors. Therefore, shifting of the refrigerant between the outdoor and indoor unit affects the scale measurement if only the outdoor heat exchanger is put on the scale. Hence, this shifting of the refrigerant has to be measured and the scale measurements have to be corrected, in order to quantify the frost and water accumulation on the heat exchanger surface solely by measuring the weight of the heat exchanger.

   b) *Using pictures of the heat exchanger surface taken by a macro camera, does the amount of pixels which exceed a certain brightness threshold correlate to the amount of ice on the heat exchanger surface?*
   If a pixel of the pictures taken by a macro camera of the heat exchanger surface displays frost accumulated on the heat exchanger surface it has a significantly high brightness value. Therefore, the amount of pixels exceeding a certain brightness threshold correlate to the amount of ice present on the heat exchanger surface. However, attention should be paid as the frost accumulation on the heat exchanger surface may not form uniformly on the full surface. Therefore, the camera either has to be put at an appropriate position or multiple cameras have to be used. Additionally, it should be stated that the brightness of pixels displaying the condensed water drops on the heat exchanger surface is rather low and may not exceed the chosen threshold, therefore only frost accumulated on the heat exchanger surface may be quantified by this approach. Moreover, the frost layer is not only growing in thickness but also in density. This increase in density does not necessarily lead to a significant increase in brightness. Using the scale measurement as well as the camera measurement, both phenomena, the growing thickness of the frost layer and its increase in density, can be quantified.

6.2 Acknowledgement

Parts of this work have received funding from the European Union's Horizon 2020 research and innovation program under grant agreement No 768824 (HYBUILD).

List of Figures

List of Tables

References

Alfa Laval (2018). Plate heat exchanger (image online). [Online]. Available: `https://www.alfalaval.com/products/heat-transfer/plate-heat-exchangers/brazed-plate-heat-exchangers/cbaq/` (accessed 23.06.2019).

Alva, G., Lin, Y., and Fang, G. (2018). An overview of thermal energy storage systems. *Energy*, 144:341–378.

Amer, M. and Wang, C.-C. (2017). Review of defrosting methods. *Renewable and Sustainable Energy Reviews*, 73:53–74.

ANSI/ASHRAE 34-2016 (2016). Designation and safety classification of refrigerants.

Barz, T., Seliger, D., Marx, K., Sommer, A., Walter, S. F., Bock, H. G., and Körkel, S. (2018). State and state of charge estimation for a latent heat storage. *Control Engineering Practice*, 72:151 – 166.

Bell, I. and Jäger, A. (2016). Helmholtz energy transformations of common cubic equations of state for use with pure fluids and mixtures. *Journal of Research of the National Institute of Standards and Technology*, 121:238.

Bell, I. H., Wronski, J., Quoilin, S., and Lemort, V. (2014). Pure and pseudo-pure fluid thermophysical property evaluation and the open-source thermophysical property library coolprop. *Industrial & Engineering Chemistry Research*, 53(6):2498–2508. PMID: 24623957.

Bundschuh, J. and Chen, G. (2017). *Sustainable energy solutions in agriculture*. CRC Press. OCLC: 1038435777.

Demirel, Y. (2016). *Energy; Production, Conversion, Storage, Conservation, and Coupling*. Green Energy and Technology. Springer International Publishing, Cham, Cham. Understanding the sustainable use of energy in various processes is an integral part of engineering and scientific studies, which rely on a sound knowledge of energy...

DIN EN 14511-2:2018-5 (2018). Luftkonditionierer, Flüssigkeitskühlsätze und Wärmepumpen für die Raumbeheizung und -kühlung und Prozess-Kühler mit elektrisch angetriebenen Verdichtern – Teil 2: Prüfbedingungen.

DIN EN 14511-3:2018-5 (2018). Luftkonditionierer, Flüssigkeitskühlsätze und Wärmepumpen für die Raumbeheizung und -kühlung und Prozess-Kühler mit elektrisch angetriebenen Verdichtern – Teil 3: Prüfverfahren.

DIN EN 14825:2016-10 (2016). Luftkonditionierer, Flüssigkeitskühlsätze und Wärmepumpen mit elektrisch angetriebenen Verdichtern zur Raumbeheizung und -kühlung – Prüfung und Leistungsbemessung unter Teillastbedingungen und Berechnung der saisonalen Arbeitszahl.

DIN EN 378-1:2018-04 (2018). Refrigerating systems and heat pumps – safety and environmental requirements – part 1: Basic requirements, definitions, classification and selection criteria.

Dincer, I. and Rosen, M. A. (2011). *Thermal energy storage: systems and applications*. Wiley, Chichester, 2. ed edition. OCLC: 706985660.

Donaldson, T. (2008). *Python*. Visual quickstart guide. Peachpit Press, 2nd ed. edition.

Emhofer, J., Barz, T., Palomba, V., Frazzica, A., Sergi, F., Varvagiannis, S., Karellas, S., Oró, E., Zsembinszki, G., and Cabeza, L. (2018). Deliverable D3.1 of the HYBUILD-project: Modular flow sheet simulation of the hybrid (sub-)system. [Online]. Available: `http://www.hybuild.eu/publications/deliverables/` (accessed 25.06.2019).

Frazzica, A., Palomba, V., Sergi, F., Ferraro, M., Cabeza, L., Zsembinszki, G., E., O., Karellas, S., Varvagiannis, S., Emhofer, J., and Barz, T. (2018). Dynamic modelling of a hybrid solar thermal/electric energy storage system for application in residential buildings. In *Proceedings of the 12th International Conference on Solar Energy for Buildings and Industry, Raperswil, Switzerland*.

Fritzson, P. A. (2011). *Introduction to modeling and simulation of technical and physical systems with Modelica*. Wiley-IEEE Press.

Guo, K., Zhang, N., and Smith, R. (2015). Optimisation of fin selection and thermal design of counter-current plate-fin heat exchangers. *Applied Thermal Engineering*, 78:491 – 499.

Hans, H. (2008). *Meteorologie*. E. Ulmer, 6 edition.

Hundy, G., Trott, A., and Welch, T. (2016). Chapter 3 - Refrigerants. In Hundy, G., Trott, A., and Welch, T., editors, *Refrigeration, Air Conditioning and Heat Pumps (Fifth Edition)*, pages 41–58. Butterworth-Heinemann.

Hunter, J. D. (2007). Matplotlib: A 2d graphics environment. *Computing in Science & Engineering*, 9(3):90–95.

HYBUILD (2019). HYBUILD Innovative compact hybrid storage systems for low energy buildings. [Online]. Available: `http://www.hybuild.eu/` (accessed 24.06.2019).

IEA (2019). Energy efficiency: Buildings. [Online]. Available: https://www.iea.org/topics/energyefficiency/buildings/ (accessed 11.07.2019).

Kwak, K. and Bai, C. (2010). A study on the performance enhancement of heat pump using electric heater under the frosting condition: Heat pump under frosting condition. *Applied Thermal Engineering*, 30(6):539–543.

Meteonorm (2016). Irradiaton data for every place on Earth. [Online]. Available: https://meteonorm.com/en/ (accessed 24.06.2019).

Minglu, Q., Liang, X., Deng, S., and Yiqiang, J. (2010). Improved indoor thermal comfort during defrost with a novel reverse-cycle defrosting method for air source heat pumps. *Building and Environment*, 45(11):2354–2361.

Mohanraj, M., Muraleedharan, C., and Jayaraj, S. (2011). A review on recent developments in new refrigerant mixtures for vapour compression-based refrigeration, air-conditioning and heat pump units. *International Journal of Energy Research*, 35(8):647–669.

Monteith, J. L. and Unsworth, M. H. (2013). Chapter 2 - properties of gases and liquids. In Monteith, J. L. and Unsworth, M. H., editors, *Principles of Environmental Physics (Fourth Edition)*, pages 5 – 23. Academic Press, Boston, fourth edition edition.

Munn, R. (1966). 6 - air temperature and humidity near the earth's surface. In Munn, R., editor, *Descriptive Micrometeorology*, pages 42 – 52. Academic Press.

Murray, F. W. (1967). On the computation of saturation vapor pressure. *Journal of Applied Meteorology*, 6(1):203–204.

Quoilin, S., Desideri, A., Wronski, J., and Bell, I. (2013). Robust and computationally efficient dynamic simulation of orc systems: The thermocycle modelica library. In *Paper presented at 2nd International Seminar on ORC Power Systems*.

Quoilin, S., Desideri, A., Wronski, J., Bell, I., and Lemort, V. (2014). Thermocycle: A modelica library for the simulation of thermodynamic systems. In *Proceedings of the 10th International Modelica Conference 2014*.

Reichl, C. (2018). SilentAirHP Fortschrittliche Methoden zur Bewertung und Entwicklung von Schallreduktionsmaßnahmen für Luftwärmepumpensysteme. [Online]. Available: https://www.energieforschung.at/projekte/282/fortschrittliche-methoden-zur-bewertung-und-entwicklung-von-schallreduktionsmassnahmen-fuer-luftwaermepumpensysteme (accessed 24.06.2019).

Shah, R. K. and Sekulic, D. P. (2007). *Surface Basic Heat Transfer and Flow Friction Characteristics*, pages 425–562. Wiley.

Taler, D. (2019). *Numerical modelling and experimental testing of heat exchangers*. Springer, Cham, Switzerland. OCLC: 1081418357.

Wang, C.-C., Chi, K.-Y., and Chang, C.-J. (2000). Heat transfer and friction characteristics of plain fin-and-tube heat exchangers, part ii: Correlation. *International Journal of Heat and Mass Transfer*, 43(15):2693 – 2700.

Wetter, M., Zuo, W., Nouidui, T. S., and Pang, X. (2014). Modelica buildings library. *Journal of Building Performance Simulation*, 7(4):253–270.

Winterbone, D. E. and Turan, A. (2015). Chapter 2 - The Second Law and Equilibrium. In Winterbone, D. E. and Turan, A., editors, *Advanced Thermodynamics for Engineers (Second Edition)*, pages 13–33. Butterworth-Heinemann, Boston.

World Health Organization (2017). *Guidelines for drinking-water quality*. World Health Organization, 4 edition. OCLC: 975491910.

Yaqub, M., M. Zubair, S., and Khan, J.-u.-R. (2000). Performance evaluation of hot-gas by-pass capacity control schemes for refrigeration and air-conditioning systems. *Energy*, 25(6):543–561.

Zhang, L., Fujinawa, T., and Saikawa, M. (2012). A new method for preventing air-source heat pump water heaters from frosting. *International Journal of Refrigeration*, 35(5):1327–1334.

Zlatković, N., Majstorović, D., Kijevčanin, M., and Živković, E. (2017). Plate heat exchanger design software for industrial and educational applications. *HEMIJSKA INDUSTRIJA*, 71(5):439–449.

Appendix

A Humidity calculation

The air humidity for experimental testing of air-source heat pumps in heating mode is defined in the standard DIN EN 14511-2 using the dry and wet bulb temperature of the ambient air. The following steps are used in this work to calculate other humidity defining properties as the relative humidity RH and the specific humidity q from the dry and wet bulb temperatures. The Tetens equation provides a formula to calculate the saturation vapor pressure of water over liquid and ice, with use of the temperature. Monteith and Unsworth (2013) give Tetens formula for temperatures above 0 °C:

$$p_{\mathrm{vap,sat}} = 0.61078 \exp\left(\frac{17.27\,\theta_{\mathrm{amb,db}}}{\theta_{\mathrm{amb,db}} + 237.3}\right) \tag{37}$$

Murray (1967) give Tetens equation for temperatures below 0°C:

$$p_{\mathrm{vap,sat}} = 0.61078 \exp\left(\frac{21.875\,\theta_{\mathrm{amb,db}}}{\theta_{\mathrm{amb,db}} + 265.5}\right) \tag{38}$$

where the ambient dry bulb temperature $\theta_{\mathrm{amb,db}}$ is in degrees Celsius (°C) and the saturation pressure $p_{\mathrm{vap,sat}}$ in kilopascals (kPa). With use of the psychrometric formulae, as described by Hans (2008), the partial pressure of water vapor in the air is obtained:

$$p_{\mathrm{vap}} = p_{\mathrm{vap,sat,wet}} - 0.00066(1 + 0.00115\,\theta_{\mathrm{wb}})(\theta_{\mathrm{amb}} - \theta_{\mathrm{wb}})p_{\mathrm{amb}} \tag{39}$$

where $p_{\mathrm{vap,sat,wet}}$ is the saturation vapor pressure with respect to the wet bulb temperature θ_{wb} (in degrees Celsius) and p_{amb} is the pressure of the ambient air.

The relative humidity RH is defined as the ratio of the partial pressure of water vapor to the equilibrium vapor pressure of water at a given temperature:

$$RH = \frac{p_{\mathrm{vap}}}{p_{\mathrm{vap,sat,dry}}} \tag{40}$$

The specific humidity q is defined as the ratio of the mass of water vapor to the total mass of air. It can be calculated by (Munn, 1966):

$$q = \frac{0.622\,p_{\mathrm{vap}}}{p_{\mathrm{amb}} - 0.378\,p_{\mathrm{vap}}} \tag{41}$$

In the standard DIN EN 14511-2 it is defined that the wet bulb temperature is always 1 °C less than the dry bulb temperature for heating mode. For cooling mode the humidity is not defined for the part load measurements, but only for the nominal point A35W18 the wet

bulb temperature is defined to be $\theta_{\text{air,in,wb}} = 24\,°\text{C}$. This results in a relative humidity of approximately $RH = 39.5\,\%$. For the part load measurements in cooling mode a relative humidity of 50 % was assumed.

The humidity in the ambient air has an important effect on the heat properties of ambient air (Munn, 1966). In order to get a steady humidity correlation for all ambient air temperatures throughout the year (-22 °C to 40 °C) a second order polynomial was least-squares fitted to the specific humidity points from heating and cooling mode. As in the standard, the wet bulb temperature was assumed to be 1 °C less than the dry bulb temperature in heating mode and in cooling mode the relative humidity was assumed to be 50 %. This resulted into a second order polynomial with the coefficients:

$$q = 2.3437 \cdot 10^{-3} + 1.9772 \cdot 10^{-4}\ \theta_{\text{amb}} + 6.0722 \cdot 10^{-6}\ (\theta_{\text{amb}})^2 \tag{42}$$

where the ambient temperature θ_{amb} is in degrees Celsius (°C) and the specific humidity q is in $\text{g}_{\text{water}}/\text{kg}_{\text{dry air}}$. The fitted curve can be seen in Figure 50.

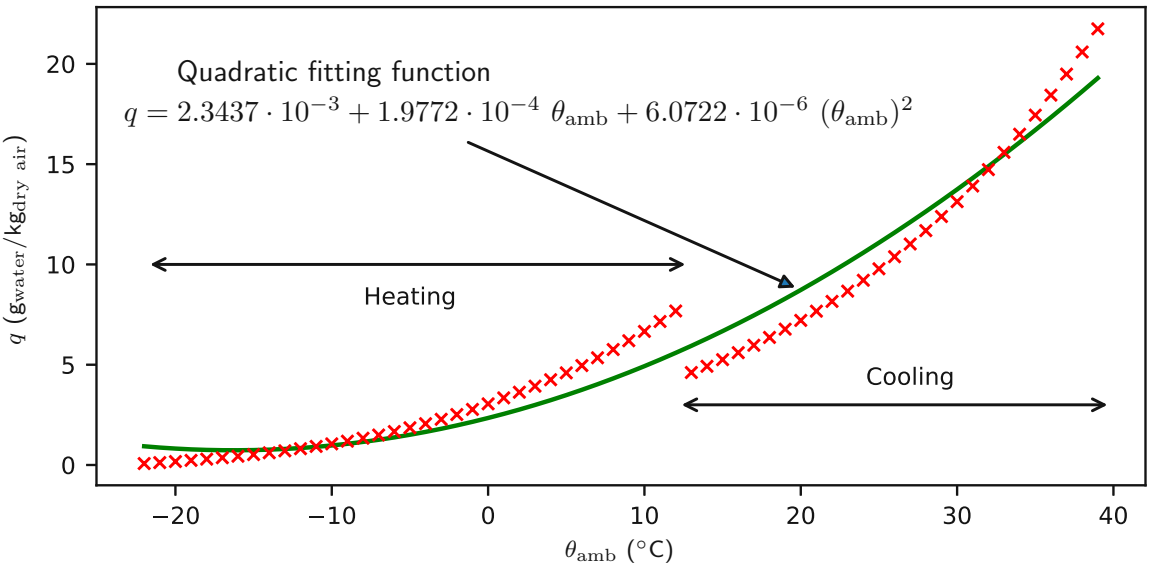

Figure 50: Specific humidity as a function of the ambient temperature.

B PCM-Materials

Technisches Datenblatt

RUBITHERM

RT64HC

RUBITHERM® RT ist ein ungebundenes Wärmespeichermaterial und nutzt den Schmelzvorgang fest/flüssig, um bei nahezu konstanter Temperatur große Wärmemengen zu speichern und bei Bedarf wieder abzugeben.
So kann man Wärme und sogar Kälte sehr viel effektiver speichern, als mit allgemein verbreiteten Speichermaterialien.
Alle unsere reinen RT Produkte weisen eine hohe Kristalllinität auf, besonders die RTHC Materialien. Hierdurch erreicht man gegenüber herkömmlichen Speichermaterialien eine bis zu 30% höhere Speicherkapazität.
Damit sind für verschiedene Anwendungen selbst bei wenig Raum und kleinen Temperaturdifferenzen große Wärmemengen effektiv nutzbar.

Wir freuen uns Ihre Fragen und Bedürfnisse mit Ihnen zu besprechen.
Merkmale:
- hohe Wärmespeicherkapazität, keine Unterkühlung, praktisch chemisch iner
- ein– und ausspeichern der Wärme erfolgen bei nahezu konstanter Temperatur
- hohe Kristalllinität, langlebig, zyklenstabil
- für sehr viele Temperaturen stehen die optimalen Speichermaterialien zur Verfügung (von –4°C bis 100°C).
- durch verschiedene Zusätze kann eine höhere Viskosität und eine höhere Dichte erreicht werden, dies verhindert das Zerfließen beim Aufschmelzen.

Daten im Überlick:	**Typische Werte**	
Schmelzbereich	**63-65** Maximum: 64	**[°C]**
Erstarrungsbereich	**64-61** Maximum: 64	**[°C]**
Wärmespeicherkapazität ± 7,5%	**250**	**[kJ/kg]***
Kombination aus latenter und sensibler Wärme im Temperaturbereich von 57 °C bis 72 °C.	**70**	**[Wh/kg]***
Spezifische Wärmekapazität	**2**	**[kJ/kg·K]**
Dichte fest bei 20 °C	**0,88**	**[kg/l]**
Dichte flüssig bei 80 °C	**0,78**	**[kg/l]**
Wärmeleitfähigkeit	**0,2**	**[W/(m·K)]**
Volumenausdehnung	**11**	**[%]**
Flammpunkt	**>190**	**[°C]**
Max. Arbeitstemperatur	**95**	**[°C]**

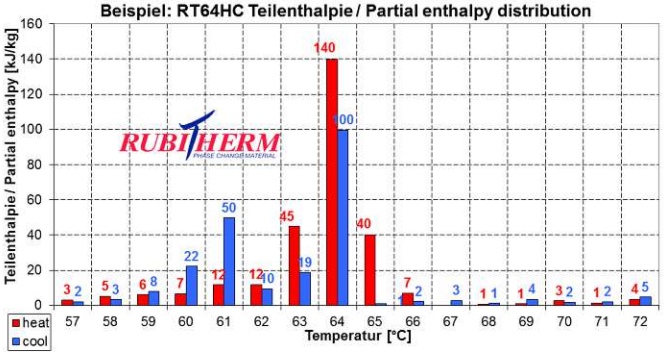

** Ermittelt mittels 3-Schicht-Kalorimeter.*

Rubitherm Technologies GmbH
Sperenberger Str. 5a
D-12277 Berlin
Tel: (030) 720004-62
Fax: (030) 720004-99
E-Mail: info@rubitherm.com
Internet: www.rubitherm.com

Die Datenblätter sind unverbindliche Planungshilfen, technische Änderungen vorbehalten. Stand:
Dienstag, 31. Mai 2016

Technisches Datenblatt

RT54HC

RUBITHERM RT ist ein ungebundenes Wärmespeichermaterial und nutzt den Schmelzvorgang fest/flüssig, um bei nahezu konstanter Temperatur große Wärmemengen zu speichern und bei Bedarf wieder abzugeben.
So kann man Wärme und sogar Kälte sehr viel effektiver speichern, als mit herkömmlichen Speichermaterialien.
Alle unsere reinen RT Produkte weisen eine hohe Kristalllinität auf, besonders die RTHC Materialien. Hierdurch erreicht man gegenüber herkömmlichen Speichermaterialien eine bis zu 30% höhere Speicherkapazität.
Damit sind für verschiedene Anwendungen selbst bei wenig Raum und kleinen Temperaturdifferenzen große Wärmemengen effektiv nutzbar.

Merkmale RT-Serie:
- hohe Wärmespeicherkapazität
- Ein– und Ausspeichern der Wärme erfolgen bei nahezu konstanter Temperatur
- keine Unterkühlung
- Für sehr viele Temperaturen stehen die optimalen Speichermaterialien zur Verfügung (von –9°C bis 100°C).

Daten im Überlick:

	Typische Werte	
Schmelzbereich	**53-54** Maximum: 54	**[°C]**
Erstarrungsbereich	**54-53** Maximum: 54	**[°C]**
Wärmespeicherkapazität ± 7,5% Kombination aus latenter und sensibler Wärme im Temperaturbereich von 46 °C bis 61 °C.	**200**	**[kJ/kg]***
	56	**[Wh/kg]***
Spezifische Wärmekapazität	**2**	**[kJ/kg·K]**
Dichte fest bei 25 °C	**0,85**	**[kg/l]**
Dichte flüssig bei 60 °C	**0,8**	**[kg/l]**
Wärmeleitfähigkeit	**0,2**	**[W/(m·K)]**
max. Arbeitstemperatur	**85**	**[°C]**
Korrosivität	**korrosiv gegenüber Metallen**	

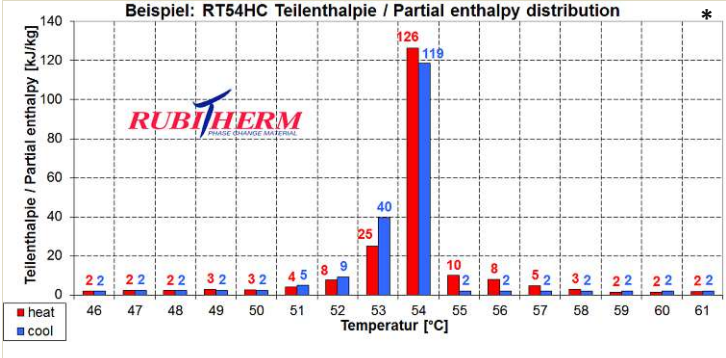

* Ermittelt mittels 3-Schicht-Kalorimeter.

Rubitherm Technologies GmbH
Sperenberger Str. 5a
D-12277 Berlin
Tel: (030) 720004-62
Fax: (030) 720004-99
E-Mail: info@rubitherm.com
Internet: www.rubitherm.com

Die Datenblätter sind unverbindliche Planungshilfen, Technische Änderungen vorbehalten Stand:
Dienstag, 5. Februar 2019

C Experimental-Results

The experimental results, as described in Section 5.1 and used to validate the simulation model in Section 5.2, are listed in tables in the following sections. For all recorded data and data calculated by the recorded data a mean value, a maximum and minimum value, the standard deviation and the 10- and 90-quantiles are given. In the last column the mean value is given until its last significant digit and the standard deviation, which signals the uncertainty, is marked in brackets. This columns is marked with value*.

C.1 Heating

Table 17: Measurement data of experimental point A-7W43.

Variable (Unit)	mean	max	min	std	Q90	Q10	value*
$\theta_{\text{air,in}}$ (°C)	-6.873	-6.332	-7.631	0.279	-6.496	-7.167	-6.9(3)
$RH_{\text{air,in}}$ (%)	70.164	72.38	68.7	0.927	71.66	69.002	-70.2(9)
$\theta_{\text{water,in}}$ (°C)	33.508	33.887	33.137	0.205	33.777	33.239	-33.5(2)
$\theta_{\text{water,out}}$ (°C)	42.966	43.437	42.577	0.214	43.255	42.673	43.0(2)
$p_{\text{water,in}}$ (bar)	2.401	2.413	2.379	0.008	2.409	2.388	2.4(1)
Δp_{water} (mbar)	97.138	97.819	90.778	0.188	97.333	96.946	97.1(2)
$\dot{m}_{\text{water}}$ (kg/s)	0.2438	0.245	0.243	$2.4 \cdot 10^{-4}$	0.244	0.243	0.2438(2)
$P_{\text{th,CP}}$ (W)	14.303	14.393	13.556	0.024	14.329	14.277	14.30(2)
$\dot{Q}_{\text{H}}$ (kW)	9.620	9.916	9.272	0.102	9.755	9.495	9.6(1)
$P_{\text{el,meas}}$ (kW)	3.353	3.437	3.304	0.023	3.384	3.324	3.35(2)
$P_{\text{el,standby}}$ (W)	96.237	108.700	91.670	4.842	102.150	91.805	96(5)
$P_{\text{el,HP}}$ (kW)	3.256	3.341	3.208	0.023	3.288	3.228	3.26(2)
COP (1)	2.954	3.045	2.841	0.039	3.006	2.900	2.95(4)

Table 18: Measurement data of experimental point A2W37.

Variable (Unit)	mean	max	min	std	Q90	Q10	value*
$\theta_{\text{air,in}}$ (°C)	2.119	2.647	1.506	0.224	2.355	1.778	2.1(2)
$RH_{\text{air,in}}$ (%)	86.457	92.179	76.227	3.735	90.615	81.19	86(4)
$\theta_{\text{water,in}}$ (°C)	31.125	31.281	30.907	0.083	31.22	31.006	31.1(1)
$\theta_{\text{water,out}}$ (°C)	36.804	37.042	36.447	0.117	36.942	36.628	36.8(1)
$p_{\text{water,in}}$ (bar)	2.938	2.949	2.922	0.006	2.945	2.928	2.94(1)
Δp_{water} (mbar)	96.229	96.773	95.45	0.155	96.424	96.035	96.2(2)
$\dot{m}_{\text{water}}$ (kg/s)	0.2457	0.247	0.245	$2.2 \cdot 10^{-4}$	0.246	0.245	0.2457(2)
$P_{\text{th,CP}}$ (W)	14.268	14.345	14.18	0.02	14.294	14.242	14.27(2)
$\dot{Q}_{\text{H}}$ (kW)	5.814	5.945	5.619	0.066	5.888	5.698	5.8(1)
$P_{\text{el,meas}}$ (kW)	1.454	1.463	1.444	0.003	1.458	1.449	1.454(3)
$P_{\text{el,standby}}$ (W)	93.763	96.300	93.130	0.556	94.140	93.350	93.8(6)
$P_{\text{el,HP}}$ (kW)	1.36	1.369	1.35	0.003	1.364	1.355	1.360(3)
COP (1)	4.275	4.364	4.167	0.043	4.326	4.203	4.28(4)

Table 19: Measurement data of experimental point A7W33.

Variable (Unit)	mean	max	min	std	Q90	Q10	value*
$\theta_{\text{air,in}}$ (°C)	7.159	7.258	7.089	0.037	7.21	7.115	7.16(4)
$RH_{\text{air,in}}$ (%)	89.152	90.872	86.522	0.959	90.136	87.607	89(1)
$\theta_{\text{water,in}}$ (°C)	29.255	29.368	29.172	0.048	29.328	29.185	29.26(5)
$\theta_{\text{water,out}}$ (°C)	32.978	33.096	32.861	0.052	33.042	32.914	32.98(5)
$p_{\text{water,in}}$ (bar)	2.009	2.019	2.000	0.004	2.015	2.004	2.009(4)
Δp_{water} (mbar)	97.134	98.035	96.087	0.186	97.356	96.913	97.1(2)
$\dot{m}_{\text{water}}$ (kg/s)	0.2460	0.247	0.245	$2.2 \cdot 10^{-4}$	0.246	0.246	0.2460(2)
$P_{\text{th,CP}}$ (W)	14.373	14.488	14.231	0.024	14.403	14.345	14.37(2)
$\dot{Q}_{\text{H}}$ (kW)	3.811	3.858	3.747	0.021	3.835	3.778	3.81(2)
$P_{\text{el,meas}}$ (kW)	1.454	1.463	1.444	0.003	1.458	1.449	1.454(3)
$P_{\text{el,standby}}$ (W)	63.412	65.490	62.580	0.740	64.415	62.653	63.4(7)
$P_{\text{el,HP}}$ (kW)	0.719	0.730	0.715	0.002	0.721	0.717	0.719(2)
COP (1)	5.301	5.372	5.204	0.033	5.341	5.251	5.30(3)

Table 20: Measurement data of experimental point A12W28.

Variable (Unit)	mean	max	min	std	Q90	Q10	value*
$\theta_{\text{air,in}}$ (°C)	11.739	11.868	11.568	0.074	11.821	11.626	11.74(7)
$RH_{\text{air,in}}$ (%)	90.421	91.086	89.633	0.213	90.727	90.18	90.4(2)
$\theta_{\text{water,in}}$ (°C)	25.046	25.103	24.985	0.031	25.086	25.006	25.05(3)
$\theta_{\text{water,out}}$ (°C)	27.985	28.049	27.917	0.034	28.031	27.937	27.99(3)
$p_{\text{water,in}}$ (bar)	2.416	2.429	2.405	0.005	2.424	2.409	2.416(5)
Δp_{water} (mbar)	95.736	96.245	95.145	0.15	95.927	95.551	95.7(2)
$\dot{m}_{\text{water}}$ (kg/s)	0.2453	0.246	0.245	$2 \cdot 10^{-4}$	0.246	0.245	0.2453(2)
$P_{\text{th,CP}}$ (W)	14.172	14.237	14.101	0.019	14.196	14.148	14.17(2)
$\dot{Q}_{\text{H}}$ (kW)	2.998	3.029	2.952	0.016	3.016	2.972	3.00(2)
$P_{\text{el,meas}}$ (kW)	0.495	0.504	0.492	0.002	0.497	0.493	0.495(2)
$P_{\text{el,standby}}$ (W)	72.919	76.660	72.010	0.710	73.292	72.470	72.9(7)
$P_{\text{el,HP}}$ (kW)	0.422	0.431	0.419	0.002	0.424	0.42	0.422(2)
COP (1)	7.100	7.199	6.866	0.055	7.159	7.028	7.10(6)

C.2 Cooling

Table 21: Measurement data of experimental point A35W18.

Variable (Unit)	mean	max	min	std	Q90	Q10	value*
$\theta_{\text{air,in}}$ (°C)	34.841	35.070	34.645	0.102	34.990	34.726	34.8(1)
$RH_{\text{air,in}}$ (%)	38.859	39.545	38.263	0.310	39.300	38.484	38.9(3)
$\theta_{\text{water,in}}$ (°C)	22.941	23.155	22.784	0.098	23.103	22.828	22.9(1)
$\theta_{\text{water,out}}$ (°C)	17.993	18.217	17.816	0.099	18.158	17.885	18.0(1)
$p_{\text{water,in}}$ (bar)	1.663	1.671	1.656	0.003	1.666	1.659	1.663(3)
Δp_{water} (mbar)	96.557	97.269	95.824	0.177	96.780	96.332	96.6(2)
$\dot{m}_{\text{water}}$ (kg/s)	0.2973	0.298	0.296	$2.2 \cdot 10^{-4}$	0.298	0.297	0.2973(2)
$P_{\text{th,CP}}$ (W)	16.395	16.483	16.302	0.023	16.425	16.366	16.40(2)
$\dot{Q}_{\text{H}}$ (kW)	6.174	6.272	6.063	0.040	6.225	6.117	6.17(4)
$P_{\text{el,meas}}$ (kW)	1.434	1.451	1.418	0.006	1.442	1.427	1.434(6)
$P_{\text{el,standby}}$ (W)	75.802	78.310	75.170	0.483	76.360	75.360	75.8(5)
$P_{\text{el,HP}}$ (kW)	1.359	1.375	1.342	0.006	1.366	1.351	1.359(6)
COP (1)	4.545	4.642	4.466	0.030	4.587	4.507	4.55(3)

Table 22: Measurement data of experimental point A30W18.

Variable (Unit)	mean	max	min	std	Q90	Q10	value*
$\theta_{\text{air,in}}$ (°C)	29.931	30.075	29.808	0.067	30.020	29.845	29.93(7)
$RH_{\text{air,in}}$ (%)	49.826	50.504	49.008	0.316	50.192	49.410	49.8(3)
$\theta_{\text{water,in}}$ (°C)	21.491	21.636	21.369	0.088	21.613	21.393	21.5(1)
$\theta_{\text{water,out}}$ (°C)	17.980	18.140	17.849	0.078	18.090	17.895	18.0 (1)
$p_{\text{water,in}}$ (bar)	1.959	1.969	1.951	0.004	1.964	1.955	1.959(4)
Δp_{water} (mbar)	96.665	97.473	95.864	0.181	96.890	96.434	96.7(2)
$\dot{m}_{\text{water}}$ (kg/s)	0.2974	0.298	0.296	$2.2 \cdot 10^{-4}$	0.298	0.297	0.2974(2)
$P_{\text{th,CP}}$ (W)	16.409	16.508	16.311	0.024	16.439	16.379	16.41(2)
$\dot{Q}_{\text{H}}$ (kW)	4.388	4.448	4.323	0.026	4.422	4.353	4.39(3)
$P_{\text{el,meas}}$ (kW)	0.779	0.785	0.772	0.003	0.782	0.776	0.779(3)
$P_{\text{el,standby}}$ (W)	75.802	78.310	75.170	0.483	76.360	75.360	75.8(5)
$P_{\text{el,HP}}$ (kW)	0.703	0.709	0.696	0.003	0.707	0.700	0.703(3)
COP (1)	6.240	6.363	6.120	0.045	6.303	6.186	6.24(5)

Table 23: Measurement data of experimental point A25W18.

Variable (Unit)	mean	max	min	std	Q90	Q10	value*
$\theta_{\text{air,in}}$ (°C)	25.000	25.136	24.865	0.078	25.099	24.890	25.0(1)
$RH_{\text{air,in}}$ (%)	49.352	50.166	48.713	0.353	49.848	48.922	49.4(4)
$\theta_{\text{water,in}}$ (°C)	20.599	20.649	20.547	0.025	20.634	20.566	20.60(3)
$\theta_{\text{water,out}}$ (°C)	18.065	18.145	17.996	0.031	18.108	18.025	18.07(3)
$p_{\text{water,in}}$ (bar)	2.143	2.153	2.134	0.004	2.149	2.138	2.143(4)
Δp_{water} (mbar)	97.336	98.083	96.625	0.210	97.600	97.062	97.3(2)
$\dot{m}_{\text{water}}$ (kg/s)	0.2951	0.296	0.294	$2.2 \cdot 10^{-4}$	0.295	0.295	0.2951(2)
$P_{\text{th,CP}}$ (W)	16.400	16.505	16.287	0.027	16.434	16.365	16.40(3)
$\dot{Q}_{\text{H}}$ (kW)	3.148	3.200	3.089	0.019	3.172	3.124	3.15(2)
$P_{\text{el,meas}}$ (kW)	0.483	0.489	0.476	0.002	0.486	0.480	0.483(2)
$P_{\text{el,standby}}$ (W)	75.802	78.310	75.170	0.483	76.360	75.360	75.8(5)
$P_{\text{el,HP}}$ (kW)	0.408	0.413	0.401	0.002	0.411	0.405	0.408(2)
COP (1)	7.723	7.944	7.530	0.069	7.815	7.640	7.72(7)

Table 24: Measurement data of experimental point A20W18.

Variable (Unit)	mean	max	min	std	Q90	Q10	value*
$\theta_{\text{air,in}}$ (°C)	19.648	19.933	19.321	0.158	19.856	19.402	19.6(2)
$RH_{\text{air,in}}$ (%)	49.168	50.061	48.478	0.347	49.597	48.706	49.2(3)
$\theta_{\text{water,in}}$ (°C)	20.615	20.673	20.550	0.034	20.652	20.563	20.62(3)
$\theta_{\text{water,out}}$ (°C)	17.934	18.039	17.731	0.054	17.990	17.865	17.93(5)
$p_{\text{water,in}}$ (bar)	2.065	2.074	2.057	0.003	2.069	2.061	2.065(3)
Δp_{water} (mbar)	97.326	98.024	96.596	0.211	97.596	97.057	97.3(2)
$\dot{m}_{\text{water}}$ (kg/s)	0.2954	0.296	0.295	$2.2 \cdot 10^{-4}$	0.296	0.295	0.2954(2)
$P_{\text{th,CP}}$ (W)	16.411	16.500	16.320	0.027	16.446	16.375	16.41(3)
$\dot{Q}_{\text{H}}$ (kW)	3.333	3.510	3.206	0.039	3.373	3.289	3.33(4)
$P_{\text{el,meas}}$ (kW)	0.397	0.407	0.388	0.003	0.401	0.393	0.397(3)
$P_{\text{el,standby}}$ (W)	75.802	78.310	75.170	0.483	76.360	75.360	75.8(5)
$P_{\text{el,HP}}$ (kW)	0.321	0.331	0.312	0.003	0.326	0.317	0.321(3)
COP (1)	10.378	11.042	10.003	0.166	10.573	10.183	10.4(2)

C.3 DHW

Table 25: Measurement data of experimental point A2W60.

Variable (Unit)	mean	max	min	std	Q90	Q10	value*
$\theta_{\text{air,in}}$ (°C)	1.971	2.860	1.491	0.448	2.787	1.527	2.0(4)
$RH_{\text{air,in}}$ (%)	85.599	87.811	82.512	1.404	87.174	83.669	86(1)
$\theta_{\text{water,in}}$ (°C)	54.936	55.086	54.771	0.064	55.020	54.855	54.94(6)
$\theta_{\text{water,out}}$ (°C)	59.822	60.228	59.533	0.157	60.090	59.644	59.8(2)
$p_{\text{water,in}}$ (bar)	2.372	2.394	2.352	0.008	2.383	2.362	2.372(8)
Δp_{water} (mbar)	95.969	100.437	91.940	1.378	96.862	93.630	96(1)
$\dot{m}_{\text{water}}$ (kg/s)	0.422	0.429	0.415	0.003	0.426	0.421	0.422(3)
$P_{\text{th,CP}}$ (W)	20.819	21.204	20.444	0.113	20.928	20.643	20.8(1)
$\dot{Q}_{\text{H}}$ (kW)	8.599	9.245	8.165	0.248	8.995	8.321	8.6(2)
$P_{\text{el,meas}}$ (kW)	4.041	4.098	3.996	0.024	4.079	4.015	4.04(2)
$P_{\text{el,standby}}$ (W)	73.978	76.880	71.860	1.266	76.135	72.540	74(1)
$P_{\text{el,HP}}$ (kW)	3.967	4.024	3.922	0.024	4.005	3.941	3.97(2)
COP (1)	2.168	2.292	2.066	0.051	2.247	2.112	2.17(5)

Table 26: Measurement data of experimental point A-7W60.

Variable (Unit)	mean	max	min	std	Q90	Q10	value*
$\theta_{\text{air,in}}$ (°C)	-6.890	-6.537	-7.162	0.151	-6.683	-7.100	-6.9(2)
$RH_{\text{air,in}}$ (%)	77.623	83.813	74.228	2.531	81.503	74.788	78(3)
$\theta_{\text{water,in}}$ (°C)	46.731	46.885	46.540	0.067	46.816	46.644	46.73(7)
$\theta_{\text{water,out}}$ (°C)	59.818	60.037	59.515	0.098	59.944	59.704	59.8(1)
$p_{\text{water,in}}$ (bar)	2.620	2.645	2.586	0.015	2.638	2.600	2.62(2)
Δp_{water} (mbar)	98.430	99.011	97.949	0.139	98.602	98.251	98.4(1)
$\dot{m}_{\text{water}}$ (kg/s)	0.1647	0.165	0.164	$2.1 \cdot 10^{-4}$	0.165	0.164	0.1647(2)
$P_{\text{th,CP}}$ (W)	10.676	10.735	10.624	0.017	10.698	10.655	10.68(2)
$\dot{Q}_{\text{H}}$ (kW)	9.000	9.211	8.815	0.072	9.090	8.899	9.00(7)
$P_{\text{el,meas}}$ (kW)	4.680	4.718	4.631	0.016	4.699	4.657	4.68(2)
$P_{\text{el,standby}}$ (W)	66.471	67.280	66.000	0.471	67.016	66.040	66.5(5)
$P_{\text{el,HP}}$ (kW)	4.613	4.652	4.565	0.016	4.633	4.591	4.61(2)
COP (1)	1.951	1.987	1.917	0.015	1.971	1.931	1.95(2)

Table 27: Measurement data of experimental point A-10W60.

Variable (Unit)	mean	max	min	std	Q90	Q10	value*
$\theta_{\text{air,in}}$ (°C)	-10.138	-9.826	-10.510	0.177	-9.888	-10.390	-10.1(2)
$RH_{\text{air,in}}$ (%)	77.054	82.021	68.584	3.384	80.908	71.489	77(3)
$\theta_{\text{water,in}}$ (°C)	47.128	47.289	46.930	0.070	47.213	47.031	47.13(7)
$\theta_{\text{water,out}}$ (°C)	60.000	60.257	59.594	0.124	60.174	59.838	60.0(1)
$p_{\text{water,in}}$ (bar)	2.454	2.515	2.403	0.035	2.504	2.410	2.45(4)
Δp_{water} (mbar)	98.397	98.902	93.774	0.163	98.579	98.219	98.4(2)
$\dot{m}_{\text{water}}$ (kg/s)	0.1645	0.166	0.163	$2.2 \cdot 10^{-4}$	0.165	0.164	0.1645(2)
$P_{\text{th,CP}}$ (W)	10.669	10.729	10.255	0.018	10.691	10.648	10.67(2)
$\dot{Q}_{\text{H}}$ (kW)	8.846	9.069	8.518	0.097	8.964	8.715	8.8(1)
$P_{\text{el,meas}}$ (kW)	5.013	5.056	4.965	0.018	5.038	4.992	5.01(2)
$P_{\text{el,standby}}$ (W)	66.471	67.280	66.000	0.471	67.016	66.040	66.5(5)
$P_{\text{el,HP}}$ (kW)	4.947	4.990	4.899	0.018	4.972	4.926	4.95(2)
COP (1)	1.788	1.831	1.734	0.018	1.809	1.765	1.79(2)

D Scale calibration

The calibration of the scale for the HYBUILD and SilentAirHP project are described in the next two sections.

D.1 HYBUILD heat pump

As the weight of the heat exchanger to be put on the scale overshoots the maximum weight the scale can measure, and also the dimensions of the heat exchanger overshoot the foundation plate of the scale, a lever construction was used. The weight measured is therefore not identical to the weight of the heat exchanger but is proportional to it. To find the proportionality factor precision weights are put on the center of the heat exchanger and the scale signal is documented. In Table 28 the used precision weights and the corresponding scale measurements are listed. In Figure 51 the measurements are visualized and a linear fit is shown.

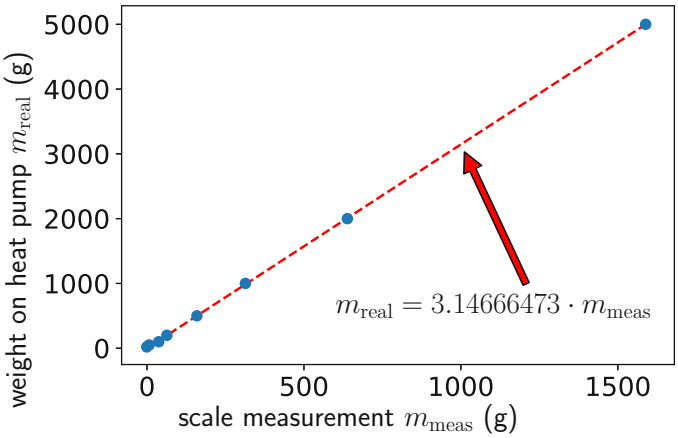

Figure 51: Calibration of the scale for the HYBUILD heat pump setup using the precision weights as listed in Table 28.

m_{real}	m_{meas}
20 g	-0.864 g
50 g	6.699 g
100 g	37.319 g
200 g	63.397 g
500 g	159.051 g
1000 g	313.393 g
2000 g	638.377 g
5000 g	1588.630 g

Table 28: Used precision weights and scale measurement for the HYBUILD heat pump.

The calibration of the scale for the HYBUILD heat pump measurements resulted in:

$$m_{\text{real}} = 3.14666473 \cdot m_{\text{meas}} \tag{43}$$

D.2 SilentAirHP

The same procedure was done to calibrate the scale for the SilentAirHP measurements. The used precision weights and their corresponding scale measurements are listed in Table 29 and are visualized in Figure 52.

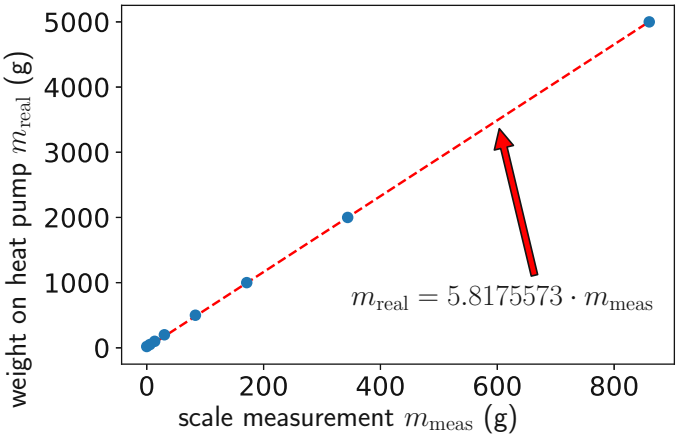

Figure 52: Calibration of the scale for the SilentAirHP setup using the precision weights as listed in Table 29.

m_{real}	m_{meas}
20 g	0 g
50 g	5.35 g
100 g	13.60 g
200 g	30.20 g
500 g	83.30 g
1000 g	171.15 g
2000 g	343.90 g
5000 g	860.05 g

Table 29: Used precision weights and scale measurement for the SilentAirHP.

The calibration of the scale for the SilentAirHP measurements resulted in:

$$m_{\text{real}} = 5.8175573 \cdot m_{\text{meas}} \tag{44}$$

E Performance-Maps

The data, which is used in Section 5.3 to plot the change in performance for different ambient and operational conditions, is listed in tables in the next sections. For every operational mode (heating, cooling, DHW generation) and for each heat pump setup an individual performance map is available. This data is furthermore used for the annual calculation in Section 5.5.

E.1 Heating - Reference Setup

		dot_Q_cond [kW]								P_el [kW]							
		N_rot [Hz]								N_rot [Hz]							
T_water [°C]	T_ambient [°C]	150	130	110	90	70	50	30	10	150	130	110	90	70	50	30	10
22	16	20.997	18.382	15.682	12.957	10.252	7.532	4.698	1.711	2.389	2.024	1.705	1.388	1.065	0.74	0.426	0.17
	15	20.653	18.025	15.378	12.706	10.053	7.382	4.601	1.674	2.417	2.08	1.754	1.43	1.099	0.766	0.446	0.179
	10	18.638	16.27	13.882	11.471	9.088	6.658	4.135	1.495	2.677	2.323	1.966	1.608	1.244	0.881	0.524	0.216
	5	16.707	14.584	12.447	10.331	8.18	5.979	3.701	1.329	2.884	2.505	2.125	1.738	1.351	0.966	0.582	0.244
	0	14.942	13.07	11.181	9.268	7.327	5.344	3.305	1.173	3.016	2.62	2.223	1.823	1.423	1.022	0.621	0.258
	-5	13.373	11.689	9.99	8.272	6.529	4.753	2.995	1.032	3.082	2.679	2.276	1.869	1.461	1.053	0.656	0.265
	-10	11.901	10.395	8.877	7.342	5.787	4.204	2.649	0.912	3.096	2.691	2.286	1.879	1.471	1.061	0.679	0.274
	-15	10.527	9.189	7.84	6.478	5.099	3.706	2.322	0.79	3.061	2.66	2.258	1.856	1.454	1.05	0.683	0.261
	-20	9.388	8.185	6.973	5.751	4.51	3.327	2.022	#NV	2.993	2.599	2.205	1.811	1.417	1.042	0.664	#NV
	-22	9.048	7.89	6.722	5.543	4.343	3.196	1.932	0.648	2.965	2.574	2.183	1.792	1.403	1.031	0.654	0.244
25	16	21.127	18.438	15.728	12.993	10.29	7.556	4.71	1.71	2.69	2.334	1.977	1.616	1.246	0.874	0.512	0.199
	15	20.718	18.081	15.425	12.742	10.09	7.406	4.613	1.673	2.746	2.383	2.021	1.653	1.276	0.899	0.529	0.207
	10	18.707	16.328	13.93	11.509	9.124	6.681	4.147	#NV	2.99	2.599	2.207	1.811	1.405	1	0.6	#NV
	5	16.775	14.642	12.505	10.377	8.213	6.001	3.712	1.325	3.167	2.755	2.341	1.921	1.497	1.074	0.65	0.263
	0	15.017	13.135	11.234	9.311	7.359	5.365	3.312	1.171	3.271	2.845	2.418	1.987	1.554	1.119	0.681	0.276
	-5	13.443	11.749	10.04	8.312	6.559	4.773	2.993	1.032	3.313	2.882	2.451	2.017	1.579	1.139	0.706	0.281
	-10	11.966	10.45	8.923	7.379	5.815	4.223	2.654	0.921	3.302	2.873	2.443	2.01	1.575	1.137	0.723	0.293
	-15	10.586	9.239	7.882	6.511	5.124	3.72	2.33	0.786	3.244	2.821	2.398	1.972	1.545	1.117	0.718	0.27
	-20	9.46	8.244	7.02	5.789	4.535	3.326	2.008	0.676	3.152	2.736	2.322	1.907	1.492	1.086	0.687	0.258
	-22	9.065	7.898	6.725	5.544	4.336	3.178	1.92	0.647	3.1	2.69	2.282	1.874	1.465	1.07	0.674	0.255
30	16	21.224	18.519	15.793	13.043	10.345	7.59	4.725	1.703	3.27	2.846	2.42	1.991	1.546	1.098	0.653	0.245
	15	20.817	18.164	15.491	12.793	10.145	7.44	4.628	1.663	3.316	2.887	2.456	2.022	1.571	1.118	0.668	0.252
	10	18.81	16.414	14	11.581	9.177	6.714	4.162	1.487	3.51	3.058	2.603	2.143	1.673	1.199	0.725	0.279
	5	16.879	14.729	12.592	10.446	8.264	6.033	3.728	1.321	3.637	3.169	2.697	2.222	1.74	1.253	0.762	0.296
	0	15.135	13.234	11.316	9.376	7.406	5.396	3.325	1.17	3.695	3.219	2.741	2.259	1.772	1.279	0.781	0.306
	-5	13.552	11.841	10.116	8.372	6.604	4.802	2.981	1.03	3.695	3.219	2.741	2.26	1.773	1.282	0.788	0.307
	-10	12.066	10.535	8.993	7.435	5.856	4.251	2.654	0.903	3.644	3.174	2.701	2.227	1.748	1.264	0.79	0.301
	-15	10.684	9.319	7.945	6.561	5.162	3.738	2.312	0.776	3.539	3.077	2.616	2.154	1.689	1.22	0.765	0.285
	-20	9.423	8.208	6.987	5.758	4.502	3.284	1.984	#NV	3.371	2.927	2.484	2.041	1.595	1.153	0.724	#NV
	-22	9.027	7.862	6.692	5.507	4.304	3.137	1.894	0.636	3.31	2.873	2.438	2	1.564	1.132	0.709	0.264
35	16	21.303	18.583	15.843	13.094	10.39	7.616	4.734	1.691	3.846	3.355	2.86	2.358	1.844	1.32	0.794	0.289
	15	20.897	18.229	15.542	12.846	10.19	7.466	4.638	1.657	3.882	3.387	2.888	2.382	1.863	1.336	0.806	0.295
	10	18.896	16.485	14.056	11.637	9.22	6.74	4.173	1.475	4.026	3.513	2.996	2.471	1.938	1.397	0.849	0.316
	5	16.968	14.808	12.669	10.504	8.306	6.059	3.74	1.314	4.105	3.581	3.052	2.52	1.98	1.431	0.873	0.329
	0	15.24	13.323	11.388	9.432	7.446	5.421	3.337	1.164	4.117	3.591	3.062	2.528	1.988	1.439	0.88	0.333
	-5	13.65	11.924	10.184	8.425	6.642	4.827	2.962	1.028	4.076	3.554	3.03	2.501	1.966	1.424	0.872	0.33
	-10	12.159	10.609	9.049	7.477	5.886	4.272	2.641	0.888	3.976	3.462	2.946	2.429	1.909	1.381	0.85	0.317
	-15	10.632	9.269	7.899	6.519	5.126	3.702	2.279	#NV	3.786	3.292	2.798	2.304	1.807	1.305	0.807	#NV
	-20	9.364	8.154	6.938	5.704	4.457	3.199	1.953	0.654	3.588	3.115	2.644	2.171	1.696	1.221	0.758	0.279
	-22	8.968	7.808	6.641	5.453	4.26	3.068	1.862	0.625	3.517	3.053	2.59	2.125	1.661	1.194	0.742	0.273
40	16	21.362	18.628	15.876	13.145	10.423	7.633	4.738	1.678	4.419	3.861	3.297	2.722	2.137	1.541	0.934	0.334
	15	20.958	18.276	15.576	12.897	10.223	7.483	4.641	1.639	4.446	3.884	3.317	2.74	2.151	1.553	0.943	0.337
	10	18.964	16.539	14.098	11.692	9.253	6.758	4.179	1.465	4.54	3.966	3.386	2.798	2.2	1.593	0.972	0.353
	5	17.041	14.889	12.733	10.553	8.339	6.078	3.747	1.308	4.57	3.99	3.407	2.816	2.217	1.608	0.983	0.363
	0	15.333	13.4	11.449	9.478	7.479	5.441	3.344	1.161	4.539	3.963	3.383	2.796	2.201	1.597	0.978	0.362
	-5	13.73	11.983	10.226	8.453	6.659	4.837	2.957	1.011	4.445	3.875	3.303	2.726	2.144	1.555	0.952	0.348
	-10	12.081	10.536	8.982	7.416	5.834	4.229	2.579	0.874	4.256	3.706	3.154	2.6	2.043	1.479	0.904	0.334
	-15	10.552	9.196	7.833	6.46	5.075	3.656	2.234	0.751	4.031	3.505	2.979	2.453	1.925	1.388	0.849	0.313
	-20	9.28	8.077	6.862	5.633	4.398	3.143	1.915	0.644	3.802	3.301	2.801	2.298	1.796	1.29	0.794	0.293
	-22	8.885	7.732	6.56	5.384	4.2	3	1.833	0.613	3.722	3.231	2.738	2.246	1.755	1.259	0.777	0.285
45	16	21.397	18.653	15.89	13.182	10.443	7.639	4.734	1.666	4.989	4.364	3.731	3.085	2.429	1.759	1.073	0.38
	15	20.996	18.303	15.593	12.933	10.243	7.489	4.638	1.632	5.006	4.378	3.744	3.097	2.438	1.766	1.079	0.383
	10	19.013	16.576	14.145	11.729	9.275	6.768	4.179	1.463	5.051	4.417	3.775	3.124	2.462	1.786	1.095	0.399
	5	17.106	14.955	12.784	10.589	8.362	6.089	3.749	1.3	5.033	4.399	3.76	3.112	2.453	1.782	1.093	0.395
	0	15.387	13.433	11.466	9.483	7.475	5.434	3.334	1.141	4.947	4.317	3.684	3.044	2.397	1.74	1.068	0.384
	-5	13.619	11.879	10.13	8.367	6.586	4.778	2.912	0.99	4.761	4.151	3.538	2.92	2.295	1.664	1.019	0.367
	-10	11.97	10.433	8.888	7.333	5.764	4.166	2.521	0.857	4.534	3.948	3.36	2.769	2.176	1.574	0.96	0.352
	-15	10.442	9.095	7.742	6.381	5.001	3.597	2.192	0.733	4.273	3.715	3.158	2.6	2.038	1.469	0.895	0.322
	-20	9.167	7.966	6.756	5.543	4.318	3.082	1.876	0.628	4.013	3.482	2.952	2.422	1.891	1.358	0.83	0.302
	-22	8.771	7.615	6.457	5.297	4.121	2.94	1.794	#NV	3.923	3.402	2.883	2.364	1.845	1.323	0.81	#NV
50	16	21.407	18.654	15.908	13.2	10.448	7.634	4.722	1.65	5.554	4.865	4.162	3.448	2.72	1.975	1.21	0.428
	15	21.008	18.307	15.613	12.952	10.249	7.485	4.627	1.62	5.562	4.87	4.168	3.453	2.724	1.978	1.214	0.43
	10	19.039	16.593	14.185	11.757	9.29	6.771	4.173	1.45	5.56	4.865	4.164	3.45	2.723	1.979	1.216	0.434
	5	17.118	14.947	12.762	10.557	8.326	6.057	3.725	1.278	5.481	4.788	4.09	3.384	2.667	1.938	1.191	0.424
	0	15.231	13.288	11.333	9.364	7.373	5.352	3.271	1.115	5.301	4.626	3.947	3.261	2.567	1.863	1.143	0.407
	-5	13.463	11.736	10	8.252	6.488	4.701	2.853	0.967	5.075	4.424	3.77	3.111	2.445	1.772	1.083	0.387
	-10	11.817	10.293	8.763	7.223	5.672	4.086	2.464	0.836	4.809	4.187	3.563	2.936	2.306	1.666	1.014	0.368
	-15	10.295	8.962	7.623	6.277	4.905	3.519	2.131	0.718	4.512	3.923	3.334	2.744	2.148	1.547	0.94	0.342
	-20	9.006	7.816	6.625	5.429	4.218	3.008	1.832	0.611	4.216	3.657	3.1	2.542	1.982	1.422	0.868	0.313
	-22	8.607	7.468	6.329	5.18	4.024	2.869	1.751	0.584	4.115	3.568	3.023	2.477	1.931	1.385	0.846	0.306
55	16	21.388	18.629	15.921	13.203	10.441	7.617	4.702	1.634	6.106	5.357	4.594	3.811	3.012	2.191	1.346	0.475
	15	20.995	18.296	15.638	12.965	10.249	7.474	4.611	1.606	6.106	5.359	4.596	3.813	3.012	2.191	1.348	0.478
	10	18.945	16.51	14.097	11.664	9.201	6.696	4.122	1.42	6.043	5.288	4.521	3.744	2.954	2.148	1.321	0.467
	5	16.905	14.747	12.578	10.393	8.185	5.944	3.641	1.244	5.875	5.132	4.383	3.625	2.857	2.075	1.274	0.451
	0	15.018	13.091	11.155	9.205	7.239	5.246	3.193	1.082	5.653	4.932	4.207	3.475	2.735	1.984	1.215	0.43
	-5	13.255	11.545	9.828	8.101	6.362	4.593	2.776	0.94	5.386	4.694	3.999	3.299	2.592	1.877	1.145	0.406
	-10	11.617	10.111	8.599	7.082	5.546	3.985	2.392	0.815	5.081	4.423	3.763	3.1	2.432	1.755	1.066	0.389
	-15	10.105	8.789	7.47	6.129	4.784	3.42	2.064	0.696	4.747	4.127	3.507	2.882	2.254	1.621	0.984	0.355
	-20	8.796	7.628	6.46	5.276	4.096	2.918	1.782	#NV	4.412	3.825	3.242	2.654	2.068	1.484	0.905	#NV
	-22	8.402	7.286	6.16	5.032	3.905	2.783	1.694	0.564	4.301	3.728	3.156	2.583	2.013	1.443	0.879	0.315
57	16	21.394	18.637	15.941	13.21	10.437	7.61	4.696	1.628	6.339	5.564	4.773	3.961	3.13	2.278	1.401	0.493
	15	21.015	18.281	15.616	12.931	10.212	7.443	4.592	1.588	6.341	5.556	4.761	3.948	3.117	2.269	1.397	0.492
	10	18.813	16.412	14.005	11.581	9.13	6.639	4.083	1.402	6.214	5.438	4.652	3.852	3.038	2.209	1.359	0.481
	5	16.8	14.648	12.489	10.314	8.118	5.89	3.602	1.228	6.03	5.27	4.5	3.722	2.932	2.13	1.307	0.463
	0	14.914	12.995	11.068	9.129	7.174	5.195	3.157	1.068	5.793	5.054	4.311	3.56	2.802	2.032	1.244	0.439
	-5	13.154	11.453	9.745	8.029	6.301	4.542	2.74	0.927	5.509	4.801	4.09	3.373	2.65	1.917	1.169	0.413
	-10	11.52	10.023	8.522	7.014	5.485	3.939	2.362	0.802	5.189	4.516	3.842	3.165	2.481	1.79	1.087	0.398
	-15	10.014	8.707	7.389	6.061	4.728	3.374	2.033	0.686	4.84	4.207	3.572	2.935	2.296	1.649	1	0.361
	-20	8.698	7.541	6.376	5.206	4.039	2.878	1.757	#NV	4.488	3.891	3.295	2.697	2.101	1.507	0.919	#NV
	-22	8.307	7.198	6.079	4.964	3.851	2.744	1.671	#NV	4.373	3.79	3.206	2.623	2.044	1.465	0.892	#NV

E.2 Heating - Novel System using RT64 PCM

		dot_Q_cond [kW]								dot_Q_RPW [kW]								P_el [kW]							
		N_rot [Hz]								N_rot [Hz]								N_rot [Hz]							
T_water [°C]	T_ambient [°C]	150	130	110	90	70	50	30	10	150	130	110	90	70	50	30	10	150	130	110	90	70	50	30	10
22	16	21.677	19.576	16.233	13.17	10.334	7.692	4.977	#NV	0.01	0.01	0.01	0.01	0.01	-0.088	-0.165	-0.283	#NV	2.293	2.016	1.687	1.366	1.044	0.723	0.415	#NV
	15	21.16	19.077	15.847	12.761	10.137	7.541	4.864	#NV	0.01	0.01	0.01	-0.061	-0.091	-0.165	-0.267	#NV	2.355	2.068	1.732	1.4	1.077	0.75	0.435	#NV
	10	18.649	16.71	13.916	11.52	9.167	6.789	4.281	#NV	-0.023	0.01	-0.042	-0.055	-0.085	-0.136	-0.147	#NV	2.625	2.298	1.93	1.581	1.224	0.867	0.517	#NV
	5	16.425	14.537	12.391	10.286	8.152	5.969	3.709	#NV	0.292	0.039	0.049	0.04	0.025	0.008	-0.009	#NV	2.847	2.472	2.099	1.719	1.339	0.953	0.579	#NV
	0	14.444	12.626	10.799	8.951	7.077	5.162	3.197	#NV	0.499	0.445	0.382	0.317	0.25	0.181	0.1	#NV	3.018	2.619	2.22	1.82	1.421	1.021	0.62	#NV
	-5	12.522	10.938	9.339	7.73	6.099	4.429	2.745	#NV	0.861	0.758	0.655	0.545	0.432	0.325	0.179	#NV	3.111	2.699	2.288	1.878	1.467	1.056	0.643	#NV
	-10	10.782	9.407	8.025	6.631	5.212	3.776	#NV	#NV	1.135	0.999	0.859	0.715	0.578	0.429	#NV	#NV	3.14	2.723	2.307	1.894	1.481	1.067	#NV	#NV
	-15	9.215	8.034	6.847	5.646	4.428	3.209	#NV	#NV	1.33	1.167	1.002	0.837	0.674	0.491	#NV	#NV	3.112	2.697	2.285	1.875	1.465	1.055	#NV	#NV
	-20	8.002	6.966	5.92	4.87	3.802	2.754	#NV	#NV	1.414	1.24	1.069	0.892	0.715	0.494	#NV	#NV	3.044	2.636	2.232	1.83	1.429	1.028	#NV	#NV
	-22	7.71	6.711	5.702	4.689	3.657	2.502	#NV	#NV	1.365	1.198	1.034	0.865	0.692	0.572	#NV	#NV	3.011	2.607	2.208	1.81	1.414	1.002	#NV	#NV
25	16	21.14	19.239	15.756	13.034	10.345	7.667	4.899	1.753	-0.025	0.01	-0.035	-0.046	-0.06	-0.115	-0.192	-0.099	2.63	2.279	1.935	1.585	1.225	0.859	0.502	0.172
	15	20.737	18.74	15.452	12.776	10.146	7.516	4.784	1.704	0.01	0.01	-0.034	-0.039	-0.061	-0.114	-0.174	-0.086	2.694	2.332	1.98	1.623	1.255	0.884	0.521	0.179
	10	18.333	16.369	13.949	11.512	9.136	6.706	4.18	1.466	0.334	0.051	-0.025	-0.007	-0.016	-0.027	-0.034	-0.028	2.957	2.533	2.172	1.786	1.388	0.99	0.595	0.209
	5	16.334	14.229	12.139	10.076	7.978	5.835	3.621	1.263	0.44	0.412	0.365	0.3	0.235	0.166	0.092	0.028	3.163	2.751	2.335	1.915	1.493	1.071	0.648	0.231
	0	14.143	12.359	10.563	8.754	6.918	5.04	3.115	#NV	0.885	0.784	0.676	0.56	0.442	0.326	0.194	#NV	3.304	2.869	2.432	1.996	1.559	1.122	0.682	#NV
	-5	12.259	10.7	9.136	7.559	5.959	4.32	2.674	#NV	1.202	1.061	0.912	0.758	0.603	0.453	0.261	#NV	3.367	2.921	2.477	2.034	1.589	1.145	0.697	#NV
	-10	10.55	9.201	7.848	6.483	5.094	3.685	2.28	#NV	1.437	1.264	1.084	0.902	0.724	0.54	0.301	#NV	3.366	2.918	2.475	2.031	1.589	1.145	0.698	#NV
	-15	9.013	7.857	6.694	5.517	4.33	3.124	1.932	#NV	1.594	1.398	1.198	1.001	0.798	0.592	0.321	#NV	3.311	2.87	2.432	1.996	1.56	1.124	0.685	#NV
	-20	7.886	6.951	5.908	4.856	3.786	2.723	1.659	#NV	1.47	1.289	1.108	0.929	0.746	0.551	0.297	#NV	3.195	2.768	2.344	1.923	1.501	1.08	0.656	#NV
	-22	7.649	6.657	5.656	4.648	3.618	2.617	1.584	#NV	1.411	1.237	1.065	0.893	0.715	0.496	0.284	#NV	3.14	2.719	2.302	1.888	1.474	1.059	0.644	#NV
30	16	21.325	18.462	15.712	12.949	10.279	7.562	4.73	1.679	0.01	0.051	0.077	0.091	0.063	0.027	-0.005	-0.028	3.266	2.804	2.388	1.968	1.53	1.087	0.648	0.224
	15	20.762	18.01	15.325	12.629	10.021	7.366	4.602	1.631	0.029	0.15	0.162	0.162	0.122	0.072	0.025	-0.013	3.318	2.855	2.432	2.004	1.558	1.109	0.664	0.23
	10	18.11	15.763	13.413	11.082	8.789	6.441	4.001	1.401	0.704	0.654	0.589	0.5	0.388	0.273	0.161	0.039	3.529	3.073	2.613	2.148	1.674	1.199	0.724	0.254
	5	15.704	13.669	11.675	9.68	7.66	5.595	3.456	1.195	1.189	1.07	0.927	0.77	0.606	0.439	0.274	0.085	3.699	3.216	2.731	2.241	1.75	1.258	0.764	0.27
	0	13.614	11.89	10.154	8.406	6.639	4.827	2.975	1.017	1.545	1.364	1.174	0.977	0.771	0.57	0.352	0.127	3.781	3.284	2.786	2.288	1.789	1.288	0.784	0.28
	-5	11.791	10.287	8.778	7.256	5.718	4.134	2.548	0.853	1.79	1.575	1.353	1.125	0.891	0.67	0.399	0.156	3.792	3.291	2.792	2.293	1.793	1.293	0.788	0.284
	-10	10.141	8.842	7.535	6.222	4.889	3.53	2.172	0.718	1.954	1.715	1.472	1.221	0.972	0.723	0.422	0.166	3.742	3.247	2.753	2.26	1.769	1.275	0.777	0.282
	-15	8.919	7.769	6.615	5.449	4.267	3.055	1.879	#NV	1.756	1.543	1.325	1.108	0.891	0.68	0.383	#NV	3.601	3.123	2.648	2.175	1.702	1.227	0.747	#NV
	-20	7.855	6.834	5.809	4.77	3.704	2.646	1.616	#NV	1.558	1.367	1.173	0.982	0.793	0.581	0.321	#NV	3.418	2.961	2.508	2.057	1.605	1.154	0.7	#NV
	-22	7.522	6.543	5.593	4.554	3.54	2.536	1.544	#NV	1.496	1.312	1.127	0.947	0.76	0.546	0.306	#NV	3.353	2.904	2.459	2.015	1.573	1.129	0.686	#NV
35	16	20.345	17.689	15.031	12.392	9.842	7.231	4.507	1.593	0.966	0.9	0.816	0.706	0.55	0.386	0.228	0.059	3.892	3.393	2.889	2.378	1.852	1.323	0.794	0.275
	15	19.831	17.241	14.651	12.081	9.596	7.04	4.384	1.547	1.075	0.996	0.895	0.77	0.595	0.427	0.254	0.068	3.939	3.433	2.923	2.406	1.874	1.34	0.807	0.28
	10	17.343	15.078	12.814	10.602	8.4	6.145	3.802	1.328	1.571	1.42	1.25	1.048	0.824	0.597	0.372	0.11	4.127	3.593	3.055	2.51	1.959	1.407	0.853	0.298
	5	15.029	13.081	11.171	9.256	7.317	5.337	3.273	1.13	1.964	1.75	1.513	1.259	0.995	0.725	0.467	0.147	4.233	3.68	3.125	2.567	2.007	1.444	0.878	0.309
	0	13.041	11.373	9.713	8.033	6.338	4.606	2.808	0.963	2.235	1.975	1.695	1.41	1.114	0.818	0.529	0.178	4.257	3.699	3.14	2.579	2.017	1.454	0.886	0.313
	-5	11.307	9.862	8.401	6.93	5.456	3.945	2.404	0.802	2.384	2.094	1.804	1.507	1.192	0.884	0.552	0.202	4.216	3.66	3.106	2.552	1.996	1.439	0.877	0.311
	-10	10.016	8.724	7.428	6.126	4.807	3.452	2.112	0.695	2.125	1.87	1.61	1.342	1.074	0.816	0.488	0.183	4.066	3.529	2.994	2.46	1.927	1.391	0.848	0.301
	-15	8.742	7.61	6.475	5.333	4.171	2.964	1.819	#NV	1.874	1.646	1.415	1.178	0.940	0.734	0.416	#NV	3.854	3.342	2.834	2.327	1.821	1.313	0.798	#NV
	-20	7.686	6.683	5.679	4.651	3.606	2.556	1.563	#NV	1.662	1.458	1.25	1.045	0.845	0.632	0.35	#NV	3.639	3.153	2.671	2.188	1.707	1.226	0.743	#NV
	-22	7.358	6.398	5.43	4.444	3.428	2.442	1.495	#NV	1.596	1.399	1.2	1.002	0.826	0.601	0.331	#NV	3.564	3.087	2.614	2.14	1.671	1.198	0.726	#NV
40	16	19.392	16.829	14.282	11.794	9.353	6.857	4.262	1.497	1.388	1.811	1.602	1.361	1.077	0.778	0.476	0.15	4.571	3.983	3.389	2.786	2.174	1.558	0.94	0.328
	15	18.871	16.406	13.919	11.494	9.112	6.674	4.145	1.455	2.103	1.884	1.666	1.413	1.117	0.81	0.497	0.155	4.606	4.011	3.413	2.806	2.19	1.57	0.949	0.33
	10	16.515	14.334	12.168	10.075	7.975	5.824	3.587	1.254	2.476	2.225	1.944	1.629	1.286	0.937	0.593	0.18	4.725	4.112	3.496	2.873	2.245	1.614	0.98	0.342
	5	14.298	12.454	10.62	8.794	6.939	5.056	3.088	1.072	2.775	2.467	2.133	1.774	1.407	1.025	0.66	0.202	4.766	4.144	3.52	2.893	2.263	1.63	0.992	0.347
	0	12.535	10.919	9.296	7.674	6.032	4.362	2.633	0.905	2.861	2.53	2.188	1.828	1.459	1.082	0.711	0.226	4.731	4.112	3.492	2.869	2.245	1.619	0.987	0.346
	-5	11.122	9.689	8.253	6.803	5.345	3.856	2.314	0.788	2.573	2.267	1.953	1.634	1.304	0.975	0.64	0.216	4.572	3.972	3.372	2.772	2.171	1.568	0.957	0.338
	-10	9.76	8.504	7.233	5.959	4.674	3.35	2.02	#NV	2.288	2.009	1.731	1.444	1.152	0.873	0.543	#NV	4.354	3.779	3.206	2.635	2.063	1.489	0.907	#NV
	-15	8.514	7.406	6.297	5.182	4.047	2.878	1.748	#NV	2.013	1.769	1.52	1.267	1.021	0.773	0.453	#NV	4.105	3.56	3.018	2.479	1.94	1.396	0.847	#NV
	-20	7.472	6.494	5.505	4.506	3.488	2.46	#NV	#NV	1.785	1.565	1.341	1.116	0.903	0.678	#NV	#NV	3.858	3.342	2.829	2.317	1.807	1.296	#NV	#NV
	-22	7.151	6.21	5.259	4.299	3.324	2.341	#NV	#NV	1.712	1.502	1.286	1.075	0.869	0.654	#NV	#NV	3.773	3.268	2.764	2.263	1.765	1.264	#NV	#NV
45	16	18.31	15.887	13.463	11.135	8.803	6.443	3.996	1.382	3.067	2.779	2.434	2.059	1.645	1.196	0.739	0.258	5.249	4.573	3.888	3.186	2.498	1.793	1.084	0.376
	15	17.889	15.497	13.116	10.849	8.583	6.274	3.885	1.34	3.128	2.821	2.485	2.097	1.668	1.218	0.754	0.262	5.268	4.587	3.903	3.208	2.507	1.8	1.091	0.378
	10	15.608	13.524	11.491	9.5	7.505	5.468	3.362	1.157	3.429	3.071	2.677	2.243	1.78	1.302	0.817	0.271	5.322	4.631	3.936	3.236	2.53	1.821	1.107	0.386
	5	13.787	11.974	10.181	8.402	6.602	4.78	2.894	0.999	3.404	3.048	2.652	2.223	1.781	1.318	0.856	0.271	5.282	4.604	3.912	3.217	2.517	1.814	1.105	0.385
	0	12.225	10.63	9.046	7.463	5.862	4.241	2.552	0.877	3.097	2.75	2.381	1.993	1.595	1.182	0.777	0.242	5.119	4.451	3.782	3.11	2.437	1.76	1.075	0.375
	-5	10.775	9.376	7.978	6.571	5.155	3.715	2.215	#NV	2.787	2.458	2.12	1.773	1.416	1.054	0.692	#NV	4.889	4.256	3.613	2.97	2.326	1.68	1.024	#NV
	-10	9.439	8.207	6.984	5.746	4.502	3.217	1.908	#NV	2.481	2.186	1.877	1.567	1.249	0.941	0.608	#NV	4.641	4.029	3.417	2.808	2.198	1.585	0.963	#NV
	-15	8.225	7.151	6.07	4.991	3.89	2.759	#NV	#NV	2.18	1.916	1.649	1.374	1.099	0.831	#NV	#NV	4.354	3.776	3.201	2.628	2.054	1.477	#NV	#NV
	-20	7.203	6.245	5.284	4.322	3.336	2.341	#NV	#NV	1.931	1.691	1.45	1.206	0.971	0.735	#NV	#NV	4.074	3.526	2.983	2.442	1.903	1.363	#NV	#NV
	-22	6.881	5.964	5.048	4.125	3.17	2.242	#NV	#NV	1.852	1.623	1.389	1.157	0.94	0.609	#NV	#NV	3.977	3.442	2.911	2.383	1.855	1.287	#NV	#NV
50	16	17.231	14.874	12.612	10.398	8.189	5.981	3.696	1.258	4.163	3.772	3.316	2.812	2.262	1.655	1.026	0.37	5.91	5.156	4.386	3.607	2.822	2.028	1.229	0.426
	15	16.849	14.464	12.283	10.126	7.98	5.821	3.593	1.222	4.173	3.829	3.349	2.837	2.272	1.666	1.034	0.369	5.917	5.162	4.391	3.611	2.825	2.031	1.232	0.427
	10	15.021	12.977	11.002	9.053	7.124	5.154	3.137	1.053	4.009	3.626	3.203	2.719	2.187	1.627	1.039	0.368	5.877	5.12	4.359	3.59	2.813	2.026	1.233	0.428
	5	13.302	11.531	9.786	8.049	6.33	4.58	2.774	0.93	3.701	3.329	2.905	2.454	1.964	1.458	0.943	0.324	5.709	4.969	4.225	3.477	2.724	1.967	1.201	0.418
	0	11.742	10.201	8.656	7.133	5.592	4.037	2.418	#NV	3.364	3.009	2.616	2.19	1.754	1.3	0.847	#NV	5.47	4.772	4.054	3.334	2.612	1.886	1.15	#NV
	-5	10.336	8.969	7.621	6.273	4.91	3.534	2.091	#NV	3.045	2.699	2.328	1.945	1.556	1.154	0.756	#NV	5.225	4.539	3.853	3.167	2.479	1.789	1.089	#NV
	-10	9.03	7.838	6.664	5.475	4.282	3.053	#NV	#NV	2.715	2.398	2.058	1.721	1.372	1.022	#NV	#NV	4.927	4.276	3.627	2.979	2.332	1.678	#NV	#NV
	-15	7.848	6.808	5.786	4.743	3.688	2.654	#NV	#NV	2.389	2.105	1.806	1.508	1.2	0.81	#NV	#NV	4.601	3.99	3.382	2.775	2.166	1.523	#NV	#NV
	-20	6.843	5.925	5.007	4.089	3.179	2.292	#NV	#NV	2.109	1.85	1.586	1.316	0.953	0.598	#NV	#NV	4.28	3.705	3.133	2.564	1.945	1.348	#NV	#NV
	-22	6.535	5.656	4.779	3.805	2.988	2.161	#NV	#NV	2.021	1.773	1.52	1.262	0.861	0.508	#NV	#NV	4.174	3.611	3.054	2.496	1.852	1.271	#NV	#NV
55	16	16.587	14.16	11.958	9.823	7.676	5.559	3.386	1.112	4.681	4.4	3.924	3.368	2.762	2.068	1.317	0.5	6.516	5.695	4.855	4.001	3.138	2.262	1.373	0.475
	15	16.178	13.83	11.711	9.604	7.506	5.44	3.319	1.093	4.653	4.339	3.854	3.308	2.709	2.027	1.294	0.485	6.495	5.672	4.835	3.984	3.134	2.254	1.372	0.475
	10	14.309	12.327	10.443	8.554	6.686	4.84	2.949	#NV	4.411	4.022	3.534	3.022	2.455	1.825	1.18	#NV	6.345	5.529	4.703	3.873	3.035	2.19	1.337	#NV
	5	12.644	10.911	9.255	7.582	5.924	4.284	2.591	#NV	4.104	3.699	3.22	2.733	2.207	1.634	1.039	#NV	6.132	5.334	4.532	3.729	2.923	2.109	1.286	#NV
	0	11.149	9.645	8.159	6.685	5.228	3.768	2.257	#NV	3.738	3.335	2.905	2.454	1.967	1.456	0.928	#NV	5.862	5.094	4.326	3.557	2.785	2.01	1.224	#NV
	-5	9.772	8.453	7.15	5.875	4.591	3.289	#NV	#NV	3.367	2.994	2.601	2.175	1.74	1.284	#NV	#NV	5.552	4.821	4.092	3.362	2.631	1.896	#NV	#NV
	-10	8.505	7.361	6.23	5.122	3.986	2.851	#NV	#NV	3.012	2.666	2.307	1.921	1.532	1.125	#NV	#NV	5.21	4.571	3.834	3.148	2.46	1.763	#NV	#NV
	-15	7.355	6.368	5.398	4.42	3.426	2.452	#NV	#NV	2.664	2.354	2.016	1.676	1.335	0.976	#NV	#NV	4.845	4.2	3.558	2.916	2.275	1.612	#NV	#NV
	-20	6.361	5.503	4.654	3.821	2.942	2.093	#NV	#NV	2.353	2.06	1.76	1.429	1.145	0.837	#NV	#NV	4.481	3.878	3.277	2.647	2.061	1.445	#NV	#NV
	-22	6.068	5.264	4.432	3.597	2.76	1.96	#NV	#NV	2.258	1.968	1.686	1.334	1.073	0.785	#NV	#NV	4.364	3.775	3.188	2.594	1.972	1.373	#NV	#NV
57	16	16.113	13.845	11.705	9.566	7.453	5.37	3.286	#NV	5.027	4.574	4.073	3.521	2.899	2.188	1.393	#NV	6.781	5.879	5.011	4.13	3.24	2.337	1.423	#NV
	15	15.786	13.591	11.395	9.349	7.284	5.258	3.211	1.063	4.889	4.475	4.043	3.463	2.846	2.137	1.363	0.503	6.712	5.854	4.99	4.111	3.223	2.326	1.418	0.492
	10	13.906	12.047	10.166	8.313	6.479	4.681	2.847	#NV	4.673	4.193	3.706	3.165	2.579	1.921	1.221	#NV	6.54	5.694	4.843	3.986	3.123	2.254	1.375	#NV
	5	12.331	10.654	9.002	7.356	5.736	4.14	2.501	#NV	4.3	3.85	3.369	2.868	2.322	1.72	1.088	#NV	6.304	5.48	4.655	3.83	3	2.165	1.319	#NV
	0	10.849	9.383	7.919	6.476	5.045	3.64	2.188	#NV	3.92	3.485	3.043	2.578	2.078	1.53	0.959	#NV	6.014	5.222	4.435	3.645	2.854	2.059	1.253	#NV
	-5	9.5	8.21	6.929	5.67	4.437	3.17	#NV	#NV	3.524	3.132	2.728	2.297	1.83	1.35	#NV	#NV	5.683	4.933	4.186	3.439	2.691	1.937	#NV	#NV
	-10	8.257	7.133	6.025	4.943	3.842	2.737	#NV	#NV	3.148	2.795	2.424	2.022	1.611	1.187	#NV	#NV	5.323	4.618	3.916	3.215	2.511	1.797	#NV	#NV
	-15	7.126	6.159	5.214	4.258	3.334	2.339	#NV	#NV	2.788	2.469	2.116	1.764	1.39	1.036	#NV	#NV	4.942	4.283	3.626	2.971	2.306	1.64	#NV	#NV
	-20	6.143	5.297	4.46	3.676	2.877	1.976	#NV	#NV	2.463	2.167	1.855	1.503	1.181	0.898	#NV	#NV	4.56	3.945	3.331	2.692	2.081	1.467	#NV	#NV
	-22	5.857	5.043	4.265	3.461	2.71	1.841	#NV	#NV	2.364	2.079	1.768	1.401	1.1	0.846	#NV	#NV	4.439	3.836	3.239	2.576	1.986	1.393	#NV	#NV

E.3 Heating - Novel System using RT54 PCM

		dot_Q_cond [kW]								dot_Q_RPW [kW]								P_el [kW]							
		N_rot [Hz]								N_rot [Hz]								N_rot [Hz]							
T_water [°C]	T_ambient [°C]	150	130	110	90	70	50	30	10	150	130	110	90	70	50	30	10	150	130	110	90	70	50	30	10
22	16	22.783	18.966	16.049	12.975	10.382	7.552	4.735	#NV	0.01	0.01	0.01	-0.023	0.01	-0.022	-0.043	#NV	2.593	2.131	1.668	1.36	1.054	0.729	0.421	#NV
	15	22.153	18.481	15.649	12.72	10.065	7.401	4.643	#NV	0.01	0.01	0.01	-0.019	-0.017	-0.021	-0.045	#NV	2.637	2.177	1.719	1.403	1.081	0.756	0.44	#NV
	10	19.187	16.179	13.766	11.23	9.008	6.616	#NV	#NV	0.01	0.107	0.111	0.244	0.077	0.04	#NV	#NV	2.83	2.38	1.941	1.586	1.232	0.874	#NV	#NV
	5	16.526	14.088	11.965	9.93	7.87	5.732	3.575	#NV	0.499	0.536	0.484	0.401	0.31	0.246	0.126	#NV	2.978	2.538	2.126	1.739	1.351	0.958	0.581	#NV
	0	14.169	12.194	10.42	8.634	6.83	4.988	3.072	#NV	0.948	0.887	0.767	0.639	0.5	0.357	0.227	#NV	3.083	2.649	2.242	1.836	1.431	1.026	0.622	#NV
	-5	12.096	10.563	9.016	7.462	5.904	4.283	#NV	#NV	1.296	1.141	0.984	0.817	0.621	0.472	#NV	#NV	3.141	2.722	2.306	1.89	1.474	1.06	#NV	#NV
	-10	10.419	9.085	7.726	6.407	5.049	3.614	2.187	#NV	1.507	1.327	1.148	0.943	0.744	0.594	0.386	#NV	3.163	2.741	2.328	1.903	1.486	1.07	0.652	#NV
	-15	8.901	7.835	6.612	5.551	4.278	3.073	1.828	#NV	1.65	1.431	1.24	0.992	0.826	0.627	0.419	#NV	3.13	2.718	2.295	1.897	1.47	1.058	0.645	#NV
	-20	7.744	6.74	5.671	4.719	3.656	2.598	#NV	#NV	1.682	1.474	1.261	1.048	0.863	0.651	#NV	#NV	3.058	2.642	2.206	1.835	1.432	1.03	#NV	#NV
	-22	7.455	6.491	5.336	4.526	3.533	2.379	#NV	#NV	1.621	1.417	1.251	1.027	0.817	0.696	#NV	#NV	3.021	2.615	2.156	1.814	1.416	1.004	#NV	#NV
25	16	21.384	18.615	15.714	12.97	10.279	7.574	4.747	1.671	0.01	0.01	0.008	0.019	0.007	-0.02	-0.038	-0.016	2.757	2.39	1.938	1.589	1.228	0.863	0.506	0.172
	15	20.823	18.128	15.328	12.655	10.026	7.383	4.621	1.621	0.01	0.01	0.085	0.064	0.061	0.022	-0.009	-0.003	2.811	2.437	1.996	1.631	1.262	0.888	0.525	0.18
	10	18.172	15.826	13.451	11.096	8.806	6.456	4.024	#NV	0.506	0.479	0.48	0.413	0.318	0.223	0.123	#NV	3.045	2.641	2.208	1.811	1.404	0.99	0.598	#NV
	5	15.756	13.714	11.698	9.701	7.682	5.61	3.48	1.183	1.034	0.937	0.815	0.681	0.533	0.388	0.233	0.095	3.216	2.791	2.364	1.935	1.506	1.068	0.651	0.23
	0	13.649	11.915	10.182	8.432	6.663	4.864	2.985	#NV	1.391	1.236	1.064	0.887	0.7	0.503	0.325	#NV	3.344	2.898	2.455	2.011	1.569	1.127	0.683	#NV
	-5	11.836	10.321	8.804	7.283	5.75	4.157	2.533	#NV	1.637	1.449	1.25	1.038	0.814	0.618	0.402	#NV	3.397	2.945	2.495	2.046	1.597	1.149	0.699	#NV
	-10	10.181	8.851	7.564	6.249	4.953	3.546	2.126	#NV	1.815	1.608	1.373	1.139	0.884	0.68	0.454	#NV	3.389	2.94	2.488	2.041	1.604	1.148	0.699	#NV
	-15	8.694	7.572	6.574	5.33	4.258	3.04	#NV	#NV	1.921	1.688	1.369	1.192	0.905	0.693	#NV	#NV	3.329	2.884	2.452	2.003	1.572	1.131	#NV	#NV
	-20	7.708	6.707	5.702	4.692	3.649	2.6	#NV	#NV	1.747	1.533	1.315	1.109	0.884	0.68	#NV	#NV	3.207	2.776	2.35	1.927	1.503	1.084	#NV	#NV
	-22	7.382	6.42	5.468	4.493	3.484	2.452	#NV	#NV	1.678	1.473	1.256	1.049	0.85	0.661	#NV	#NV	3.15	2.727	2.308	1.891	1.476	1.061	#NV	#NV
30	16	20.547	17.747	15.093	12.432	9.866	7.256	4.536	1.581	0.674	0.777	0.705	0.614	0.481	0.335	0.189	0.075	3.349	2.872	2.44	2.003	1.551	1.1	0.653	0.224
	15	20.003	17.305	14.715	12.122	9.616	7.066	4.414	1.532	0.803	0.866	0.782	0.675	0.532	0.374	0.214	0.087	3.398	2.921	2.482	2.037	1.579	1.121	0.669	0.23
	10	17.44	15.157	12.881	10.641	8.428	6.174	3.841	1.304	1.388	1.27	1.127	0.949	0.753	0.542	0.323	0.136	3.594	3.125	2.652	2.174	1.691	1.208	0.728	0.255
	5	15.129	13.149	11.226	9.295	7.349	5.374	3.322	1.112	1.776	1.6	1.384	1.163	0.921	0.663	0.408	0.165	3.75	3.257	2.759	2.262	1.764	1.265	0.766	0.27
	0	13.112	11.445	9.758	8.072	6.358	4.646	2.84	#NV	2.06	1.82	1.577	1.316	1.054	0.753	0.487	#NV	3.821	3.314	2.809	2.304	1.799	1.294	0.786	#NV
	-5	11.344	9.893	8.432	6.968	5.493	3.961	2.406	0.825	2.245	1.978	1.704	1.415	1.116	0.846	0.542	0.18	3.822	3.315	2.81	2.306	1.804	1.297	0.789	0.282
	-10	9.751	8.498	7.235	5.971	4.708	3.378	#NV	0.694	2.351	2.067	1.777	1.476	1.159	0.878	#NV	0.19	3.766	3.266	2.767	2.27	1.775	1.278	#NV	0.282
	-15	8.586	7.476	6.357	5.243	4.116	2.934	1.732	#NV	2.089	1.833	1.582	1.337	1.044	0.8	0.529	#NV	3.616	3.134	2.656	2.191	1.705	1.229	0.748	#NV
	-20	7.556	6.572	5.587	4.598	3.561	2.51	#NV	#NV	1.856	1.681	1.396	1.157	0.936	0.718	#NV	#NV	3.43	2.982	2.535	2.061	1.607	1.155	#NV	#NV
	-22	7.234	6.288	5.352	4.393	3.388	2.391	#NV	#NV	1.783	1.565	1.337	1.109	0.914	0.692	#NV	#NV	3.363	2.912	2.465	2.019	1.575	1.131	#NV	#NV
35	16	19.587	16.97	14.399	11.849	9.401	6.893	4.302	1.483	1.739	1.622	1.455	1.255	0.995	0.726	0.433	0.17	3.974	3.48	2.941	2.413	1.875	1.336	0.799	0.276
	15	19.097	16.558	14.035	11.555	9.16	6.713	4.186	1.436	1.825	1.688	1.519	1.303	1.038	0.755	0.452	0.18	4.017	3.497	2.973	2.44	1.896	1.352	0.812	0.281
	10	16.708	14.481	12.288	10.136	8.019	5.862	3.637	1.223	2.221	2.027	1.787	1.521	1.211	0.882	0.537	0.216	4.189	3.644	3.094	2.537	1.972	1.417	0.856	0.299
	5	14.46	12.554	10.714	8.853	6.987	5.092	3.136	1.043	2.545	2.288	1.983	1.67	1.328	0.971	0.604	0.237	4.283	3.721	3.155	2.589	2.021	1.452	0.88	0.309
	0	12.532	10.907	9.302	7.681	6.049	4.402	2.702	0.876	2.755	2.451	2.115	1.77	1.407	1.023	0.637	0.254	4.298	3.73	3.163	2.586	2.018	1.46	0.887	0.312
	-5	10.896	9.482	8.062	6.637	5.259	3.789	2.285	#NV	2.814	2.49	2.156	1.809	1.366	1.045	0.674	#NV	4.247	3.685	3.125	2.565	1.995	1.443	0.879	#NV
	-10	9.614	8.364	7.11	5.858	4.557	3.316	1.969	#NV	2.525	2.231	1.926	1.61	1.302	0.953	0.63	#NV	4.086	3.545	3.006	2.468	1.935	1.393	0.849	#NV
	-15	8.383	7.287	6.192	5.095	4.003	2.856	1.676	#NV	2.234	1.97	1.697	1.416	1.12	0.843	0.558	#NV	3.87	3.354	2.843	2.334	1.825	1.314	0.799	#NV
	-20	7.361	6.393	5.427	4.454	3.47	2.456	#NV	#NV	1.988	1.747	1.5	1.241	0.983	0.771	#NV	#NV	3.651	3.162	2.678	2.193	1.709	1.234	#NV	#NV
	-22	7.043	6.117	5.188	4.26	3.303	2.304	#NV	#NV	1.909	1.678	1.44	1.186	0.953	0.74	#NV	#NV	3.575	3.096	2.62	2.144	1.672	1.199	#NV	#NV
40	16	18.721	16.185	13.659	11.24	8.887	6.496	4.044	1.375	2.677	2.471	2.233	1.923	1.548	1.141	0.696	0.272	4.644	4.044	3.439	2.823	2.199	1.572	0.945	0.327
	15	18.243	15.772	13.309	10.96	8.653	6.327	3.932	1.329	2.755	2.532	2.284	1.955	1.579	1.16	0.711	0.281	4.675	4.07	3.462	2.841	2.213	1.583	0.954	0.33
	10	15.931	13.76	11.625	9.61	7.576	5.517	3.417	1.137	3.074	2.808	2.498	2.104	1.69	1.246	0.766	0.303	4.782	4.161	3.535	2.9	2.263	1.624	0.983	0.343
	5	13.751	11.923	10.14	8.369	6.589	4.791	2.949	0.968	3.33	3.006	2.623	2.204	1.764	1.292	0.801	0.312	4.814	4.184	3.551	2.915	2.278	1.638	0.994	0.348
	0	12.104	10.476	8.899	7.319	5.736	4.152	2.517	0.822	3.315	2.985	2.603	2.196	1.762	1.301	0.83	0.311	4.769	4.142	3.516	2.887	2.257	1.625	0.988	0.346
	-5	10.663	9.252	7.774	6.467	5.077	3.679	2.167	#NV	3.017	2.697	2.402	1.969	1.572	1.152	0.784	#NV	4.595	3.992	3.392	2.783	2.178	1.571	0.959	#NV
	-10	9.325	8.108	6.886	5.657	4.433	3.201	1.881	#NV	2.72	2.404	2.079	1.744	1.391	1.024	0.682	#NV	4.375	3.796	3.219	2.644	2.069	1.491	0.908	#NV
	-15	8.12	7.05	5.982	4.918	3.86	2.758	#NV	#NV	2.408	2.124	1.833	1.53	1.211	0.894	#NV	#NV	4.122	3.573	3.028	2.486	1.943	1.397	#NV	#NV
	-20	7.116	6.178	5.223	4.276	3.331	2.488	#NV	#NV	2.14	1.879	1.62	1.343	1.058	0.631	#NV	#NV	3.871	3.353	2.837	2.321	1.809	1.259	#NV	#NV
	-22	6.808	5.899	4.996	4.096	3.176	2.391	#NV	#NV	2.056	1.808	1.548	1.279	1.017	0.521	#NV	#NV	3.786	3.277	2.771	2.267	1.767	1.197	#NV	#NV
45	16	17.802	15.315	12.877	10.568	8.305	6.053	3.744	1.257	3.636	3.365	3.029	2.632	2.149	1.58	0.991	0.381	5.31	4.627	3.935	3.233	2.523	1.807	1.09	0.377
	15	17.342	14.915	12.539	10.292	8.064	5.893	3.643	1.222	3.691	3.409	3.075	2.662	2.207	1.604	0.996	0.38	5.326	4.645	3.949	3.243	2.541	1.815	1.096	0.378
	10	15.085	12.978	10.95	8.986	7.076	5.131	3.169	1.045	3.948	3.618	3.228	2.761	2.218	1.64	1.012	0.388	5.366	4.675	3.975	3.264	2.55	1.832	1.111	0.386
	5	13.348	11.498	9.707	7.95	6.234	4.493	2.725	0.889	3.827	3.504	3.131	2.681	2.159	1.669	1.025	0.384	5.318	4.629	3.94	3.24	2.533	1.823	1.107	0.385
	0	11.747	10.132	8.592	7.035	5.518	3.984	2.392	#NV	3.557	3.238	2.834	2.416	1.939	1.438	0.939	#NV	5.145	4.476	3.802	3.125	2.447	1.765	1.077	#NV
	-5	10.292	8.895	7.544	6.196	4.847	3.491	#NV	#NV	3.263	2.932	2.549	2.145	1.723	1.277	#NV	#NV	4.925	4.277	3.631	2.983	2.334	1.683	#NV	#NV
	-10	8.962	7.779	6.593	5.412	4.185	3.057	#NV	#NV	2.95	2.614	2.268	1.903	1.6	1.105	#NV	#NV	4.663	4.047	3.432	2.817	2.229	1.587	#NV	#NV
	-15	7.772	6.75	5.718	4.687	3.66	2.632	#NV	#NV	2.616	2.315	2	1.674	1.328	0.962	#NV	#NV	4.371	3.79	3.212	2.635	2.058	1.479	#NV	#NV
	-20	6.78	5.88	4.97	4.059	3.159	2.368	#NV	#NV	2.344	2.051	1.764	1.467	1.148	0.661	#NV	#NV	4.087	3.537	2.991	2.447	1.905	1.357	#NV	#NV
	-22	6.493	5.615	4.739	3.894	3.02	2.269	#NV	#NV	2.238	1.968	1.694	1.24	0.982	0.545	#NV	#NV	3.99	3.452	2.918	2.317	1.806	1.248	#NV	#NV
50	16	17.117	14.447	12.079	9.837	7.66	5.529	3.411	1.164	4.492	4.226	3.858	3.377	2.799	2.109	1.314	0.466	6.023	5.196	4.428	3.642	2.847	2.043	1.234	0.426
	15	16.725	14.114	11.773	9.574	7.451	5.403	3.321	1.153	4.4	4.229	3.874	3.393	2.808	2.092	1.308	0.438	5.966	5.201	4.428	3.645	2.849	2.045	1.237	0.428
	10	14.697	12.542	10.508	8.536	6.64	4.794	2.913	#NV	4.314	4.045	3.68	3.226	2.66	1.996	1.265	#NV	5.893	5.146	4.385	3.61	2.829	2.037	1.237	#NV
	5	12.855	11.049	9.275	7.549	5.885	4.235	2.585	#NV	4.137	3.802	3.406	2.952	2.401	1.799	1.133	#NV	5.737	4.998	4.248	3.496	2.738	1.974	1.203	#NV
	0	11.256	9.686	8.138	6.648	5.198	3.736	#NV	#NV	3.867	3.515	3.127	2.665	2.15	1.601	#NV	#NV	5.519	4.799	4.076	3.35	2.622	1.891	#NV	#NV
	-5	9.77	8.463	7.136	5.816	4.547	3.266	1.972	#NV	3.547	3.195	2.807	2.394	1.916	1.418	0.873	#NV	5.247	4.562	3.872	3.18	2.487	1.793	1.09	#NV
	-10	8.529	7.344	6.205	5.067	3.965	2.856	#NV	#NV	3.21	2.887	2.509	2.117	1.688	1.162	#NV	#NV	4.949	4.295	3.641	2.988	2.337	1.65	#NV	#NV
	-15	7.36	6.347	5.354	4.396	3.409	2.493	#NV	#NV	2.873	2.561	2.227	1.851	1.477	0.89	#NV	#NV	4.62	4.005	3.393	2.782	2.17	1.481	#NV	#NV
	-20	6.371	5.511	4.645	3.803	2.941	2.177	#NV	#NV	2.566	2.285	1.944	1.505	1.198	0.589	#NV	#NV	4.294	3.719	3.141	2.507	1.949	1.282	#NV	#NV
	-22	6.065	5.262	4.431	3.588	2.766	2.064	#NV	#NV	2.476	2.167	1.869	1.371	1.092	0.46	#NV	#NV	4.186	3.621	3.061	2.393	1.857	1.194	#NV	#NV
55	16	16.431	13.973	11.595	9.311	7.132	5.05	2.98	#NV	5.154	4.648	4.303	3.835	3.272	2.571	1.719	#NV	6.757	5.748	4.878	4.019	3.153	2.273	1.374	#NV
	15	16.02	13.65	11.33	9.087	6.952	4.937	3.006	#NV	5.099	4.556	4.244	3.802	3.243	2.518	1.682	#NV	6.708	5.691	4.858	4.004	3.142	2.261	1.376	#NV
	10	14.061	11.978	9.932	8.013	6.148	4.393	#NV	#NV	4.814	4.385	4.034	3.55	2.978	2.273	#NV	#NV	6.453	5.557	4.73	3.893	3.05	2.197	#NV	#NV
	5	12.271	10.454	8.716	7.018	5.414	3.836	#NV	#NV	4.509	4.16	3.756	3.264	2.706	2.076	#NV	#NV	6.166	5.364	4.558	3.748	2.933	2.113	#NV	#NV
	0	10.659	9.108	7.601	6.151	4.752	3.356	#NV	#NV	4.224	3.866	3.452	2.979	2.435	1.861	#NV	#NV	5.897	5.122	4.35	3.572	2.793	2.013	#NV	#NV
	-5	9.168	7.915	6.579	5.348	4.133	2.896	#NV	#NV	3.924	3.519	3.141	2.688	2.189	1.681	#NV	#NV	5.581	4.845	4.11	3.373	2.636	1.897	#NV	#NV
	-10	7.944	6.814	5.699	4.639	3.574	2.466	#NV	#NV	3.568	3.199	2.821	2.394	1.94	1.517	#NV	#NV	5.237	4.54	3.847	3.155	2.464	1.763	#NV	#NV
	-15	6.781	5.835	4.871	3.955	3.088	2.072	#NV	#NV	3.22	2.869	2.517	2.125	1.688	1.369	#NV	#NV	4.865	4.215	3.568	2.92	2.263	1.613	#NV	#NV
	-20	5.782	4.966	4.22	3.419	2.662	1.711	#NV	#NV	2.901	2.589	2.227	1.813	1.442	1.24	#NV	#NV	4.409	3.892	3.297	2.643	2.043	1.445	#NV	#NV
	-22	5.534	4.738	3.986	3.22	2.508	1.576	#NV	#NV	2.768	2.468	2.128	1.69	1.344	1.193	#NV	#NV	4.376	3.785	3.195	2.528	1.949	1.374	#NV	#NV
57	16	16.063	13.708	11.356	9.078	6.894	4.832	#NV	#NV	5.142	4.76	4.429	3.931	3.44	2.721	#NV	#NV	6.836	5.901	5.033	4.138	3.257	2.345	#NV	#NV
	15	15.661	13.315	11.049	8.851	6.731	4.708	#NV	#NV	5.102	4.752	4.372	3.949	3.391	2.676	#NV	#NV	6.796	5.875	5.008	4.134	3.241	2.332	#NV	#NV
	10	13.725	11.7	9.661	7.749	5.916	4.169	#NV	#NV	4.884	4.516	4.151	3.7	3.12	2.457	#NV	#NV	6.562	5.714	4.882	4.008	3.136	2.257	#NV	#NV
	5	12.011	10.17	8.439	6.759	5.198	3.765	#NV	#NV	4.647	4.328	3.913	3.416	2.845	2.248	#NV	#NV	6.333	5.513	4.682	3.846	3.009	2.165	#NV	#NV
	0	10.392	8.82	7.354	5.918	4.499	3.496	#NV	#NV	4.366	4.04	3.603	3.117	2.617	2.043	#NV	#NV	6.046	5.255	4.458	3.658	2.86	2.057	#NV	#NV
	-5	8.908	7.633	6.353	5.146	3.867	3.362	#NV	#NV	4.11	3.695	3.28	2.816	2.384	1.86	#NV	#NV	5.719	4.959	4.204	3.448	2.695	1.932	#NV	#NV
	-10	7.663	6.52	5.441	4.428	3.292	3.363	#NV	#NV	3.729	3.377	2.985	2.588	2.174	1.681	#NV	#NV	5.351	4.64	3.929	3.224	2.505	1.78	#NV	#NV
	-15	6.473	5.565	4.648	3.721	2.771	3.499	#NV	#NV	3.411	3.04	2.658	2.318	1.978	1.512	#NV	#NV	4.967	4.298	3.633	2.977	2.296	1.632	#NV	#NV
	-20	5.549	4.736	4.001	3.211	2.305	3.77	#NV	#NV	3.037	2.734	2.287	2.024	1.798	1.353	#NV	#NV	4.577	3.959	3.286	2.692	2.065	1.457	#NV	#NV
	-22	5.183	4.459	3.768	3.015	2.134	3.916	#NV	#NV	2.875	2.548	2.138	1.911	1.731	1.292	#NV	#NV	4.387	3.777	3.141	2.573	1.967	1.382	#NV	#NV

E.4 Cooling - Reference System

		dot_Q_cond [kW]								P_el [kW]							
		N_rot [Hz]								N_rot [Hz]							
T_water [°C]	T_ambient [°C]	150	130	110	90	70	50	30	10	150	130	110	90	70	50	30	10
6	20	15.801	13.858	11.864	9.82	7.726	5.583	#NV	#NV	3.933	3.262	2.639	2.065	1.54	1.067	#NV	#NV
	22	15.563	13.652	11.691	9.68	7.618	5.506	#NV	#NV	4.167	3.465	2.812	2.207	1.652	1.147	#NV	#NV
	25	15.2	13.341	11.429	9.467	7.453	5.389	#NV	#NV	4.513	3.768	3.07	2.419	1.818	1.266	#NV	#NV
	30	14.581	12.809	10.983	9.104	7.173	5.19	#NV	#NV	5.086	4.267	3.495	2.77	2.093	1.464	#NV	#NV
	35	13.959	12.264	10.522	8.73	6.884	4.984	#NV	#NV	5.633	4.754	3.913	3.114	2.362	1.658	#NV	#NV
	40	13.319	11.712	10.053	8.342	6.585	4.772	#NV	#NV	6.166	5.221	4.316	3.453	2.628	1.85	#NV	#NV
	43	12.92	11.37	9.765	8.108	6.399	4.641	#NV	#NV	6.482	5.498	4.553	3.65	2.787	1.964	#NV	#NV
	45	12.648	11.136	9.569	7.948	6.275	4.551	#NV	#NV	6.691	5.681	4.71	3.779	2.89	2.039	#NV	#NV
8	20	16.76	14.709	12.601	10.437	8.217	5.941	#NV	#NV	3.943	3.253	2.617	2.028	1.507	1.036	#NV	#NV
	22	16.506	14.49	12.417	10.288	8.101	5.859	#NV	#NV	4.188	3.467	2.799	2.181	1.625	1.121	#NV	#NV
	25	16.119	14.157	12.138	10.06	7.926	5.734	#NV	#NV	4.552	3.785	3.07	2.407	1.799	1.246	#NV	#NV
	30	15.458	13.59	11.661	9.674	7.627	5.523	#NV	#NV	5.153	4.309	3.516	2.775	2.088	1.454	#NV	#NV
	35	14.794	13.008	11.17	9.275	7.319	5.304	3.228	#NV	5.726	4.82	3.955	3.137	2.371	1.658	0.998	#NV
	40	14.11	12.419	10.669	8.861	7	5.077	3.093	#NV	6.284	5.309	4.378	3.493	2.65	1.859	1.12	#NV
	43	13.685	12.054	10.363	8.612	6.803	4.938	#NV	#NV	6.615	5.599	4.626	3.699	2.817	1.979	#NV	#NV
	45	13.393	11.804	10.153	8.442	6.67	4.844	#NV	#NV	6.833	5.79	4.791	3.835	2.925	2.058	#NV	#NV
12	20	18.802	16.524	14.177	11.758	9.27	6.712	#NV	#NV	3.939	3.212	2.549	1.951	1.42	0.957	#NV	#NV
	22	18.512	16.276	13.968	11.589	9.139	6.619	#NV	#NV	4.208	3.447	2.749	2.117	1.55	1.051	#NV	#NV
	25	18.072	15.898	13.651	11.331	8.94	6.477	#NV	#NV	4.608	3.796	3.047	2.362	1.742	1.189	#NV	#NV
	30	17.32	15.253	13.11	10.893	8.602	6.237	3.799	#NV	5.267	4.371	3.538	2.767	2.06	1.418	0.844	#NV
	35	16.564	14.59	12.551	10.44	8.253	5.99	3.651	#NV	5.895	4.933	4.02	3.164	2.372	1.643	0.98	#NV
	40	15.786	13.922	11.982	9.97	7.891	5.734	#NV	#NV	6.505	5.468	4.485	3.556	2.679	1.865	#NV	#NV
	43	15.301	13.506	11.634	9.687	7.667	5.575	#NV	#NV	6.866	5.785	4.757	3.782	2.862	1.997	#NV	#NV
	45	14.969	13.222	11.396	9.494	7.516	5.467	#NV	#NV	7.105	5.995	4.936	3.932	2.981	2.084	#NV	#NV
16	20	21.013	18.498	15.894	13.203	10.424	7.559	4.606	#NV	3.9	3.134	2.445	1.834	1.303	0.854	0.489	#NV
	22	20.685	18.216	15.658	13.011	10.276	7.453	4.542	#NV	4.195	3.392	2.665	2.015	1.445	0.957	0.553	#NV
	25	20.185	17.787	15.298	12.72	10.053	7.294	4.446	#NV	4.632	3.774	2.991	2.286	1.656	1.109	0.645	#NV
	30	19.331	17.055	14.685	12.223	9.669	7.022	4.284	#NV	5.353	4.404	3.529	2.728	2.005	1.361	0.798	#NV
	35	18.471	16.301	14.052	11.71	9.273	6.743	#NV	#NV	6.039	5.019	4.057	3.165	2.348	1.608	#NV	#NV
	40	17.587	15.543	13.406	11.178	8.865	6.453	3.945	#NV	6.704	5.603	4.566	3.594	2.685	1.852	1.096	#NV
	43	17.035	15.071	13.011	10.856	8.611	6.274	#NV	#NV	7.097	5.949	4.863	3.842	2.886	1.997	#NV	#NV
	45	16.657	14.748	12.741	10.637	8.439	6.152	#NV	#NV	7.357	6.177	5.059	4.005	3.017	2.093	#NV	#NV
18	20	22.152	19.545	16.808	13.974	11.042	8.014	4.888	#NV	3.868	3.081	2.379	1.761	1.232	0.791	0.444	#NV
	22	21.835	19.245	16.557	13.77	10.884	7.901	#NV	#NV	4.175	3.351	2.608	1.951	1.381	0.9	#NV	#NV
	25	21.302	18.789	16.175	13.46	10.645	7.731	4.717	#NV	4.632	3.75	2.95	2.233	1.602	1.059	0.608	#NV
	30	20.393	18.01	15.523	12.931	10.238	7.443	#NV	#NV	5.385	4.409	3.512	2.7	1.967	1.323	#NV	#NV
	35	19.476	17.206	14.848	12.387	9.819	7.146	#NV	#NV	6.101	5.052	4.064	3.154	2.326	1.582	#NV	#NV
	40	18.534	16.399	14.16	11.82	9.384	6.838	4.185	#NV	6.794	5.661	4.597	3.603	2.679	1.837	1.081	#NV
	43	17.946	15.896	13.74	11.477	9.114	6.648	4.072	#NV	7.204	6.021	4.907	3.863	2.889	1.989	1.173	#NV
	45	17.542	15.552	13.452	11.245	8.931	6.518	#NV	#NV	7.474	6.259	5.111	4.033	3.027	2.09	#NV	#NV

E.5 Cooling - Novel System using RT64 PCM

		dot_Q_cond [kW]								dot_Q_RPW [kW]								P_el [kW]							
		N_rot [Hz]								N_rot [Hz]								N_rot [Hz]							
T_water [°C]	T_ambient [°C]	150	130	110	90	70	50	30	10	150	130	110	90	70	50	30	10	150	130	110	90	70	50	30	10
6	20	15.847	13.886	11.878	9.826	7.728	5.583	3.389	#NV	1.326	0.944	0.618	0.349	0.139	0.007	0.002	#NV	3.885	3.234	2.624	2.058	1.538	1.067	0.645	#NV
	22	15.626	13.691	11.712	9.69	7.622	5.507	3.343	#NV	1.666	1.245	0.875	0.562	0.311	0.127	0.074	#NV	4.106	3.428	2.791	2.197	1.648	1.146	0.694	#NV
	25	15.285	13.385	11.461	9.483	7.461	5.392	3.274	#NV	2.155	1.694	1.254	0.886	0.576	0.318	0.187	#NV	4.434	3.716	3.039	2.403	1.81	1.264	0.765	#NV
	30	14.708	12.892	11.034	9.133	7.187	5.195	3.155	#NV	3.011	2.45	1.917	1.437	1.018	0.642	0.377	#NV	4.973	4.191	3.447	2.743	2.079	1.459	0.884	#NV
	35	14.12	12.379	10.597	8.773	6.906	4.993	3.034	#NV	3.898	3.246	2.585	2.006	1.472	0.976	0.592	#NV	5.499	4.655	3.847	3.075	2.342	1.65	1	#NV
	40	13.516	11.85	10.147	8.403	6.615	4.786	2.909	#NV	4.79	4.026	3.309	2.593	1.941	1.336	0.802	#NV	6.015	5.11	4.237	3.401	2.6	1.837	1.115	#NV
	43	13.148	11.528	9.871	8.176	6.438	4.658	2.833	#NV	5.345	4.547	3.742	2.963	2.228	1.533	0.936	#NV	6.32	5.377	4.469	3.594	2.754	1.949	1.182	#NV
	45	12.892	11.311	9.682	8.021	6.317	4.572	2.781	#NV	5.691	4.88	4.021	3.208	2.418	1.691	1.026	#NV	6.521	5.555	4.622	3.722	2.855	2.022	1.227	#NV
8	20	16.81	14.727	12.614	10.441	8.214	5.938	3.606	#NV	1.23	0.855	0.53	0.237	0.053	0.01	0.01	#NV	3.895	3.229	2.604	2.03	1.506	1.037	0.617	#NV
	22	16.571	14.523	12.438	10.297	8.103	5.859	3.558	#NV	1.574	1.156	0.78	0.466	0.225	0.039	0.01	#NV	4.126	3.432	2.779	2.176	1.621	1.12	0.669	#NV
	25	16.21	14.211	12.17	10.077	7.933	5.736	3.485	#NV	2.11	1.617	1.189	0.809	0.491	0.252	0.079	#NV	4.468	3.733	3.038	2.391	1.792	1.244	0.746	#NV
	30	15.587	13.68	11.717	9.704	7.642	5.528	3.36	#NV	3.008	2.411	1.883	1.383	0.951	0.584	0.325	#NV	5.031	4.228	3.466	2.747	2.074	1.448	0.873	#NV
	35	14.969	13.133	11.251	9.322	7.343	5.314	3.231	#NV	3.919	3.216	2.591	1.988	1.429	0.959	0.564	#NV	5.58	4.713	3.884	3.095	2.35	1.649	0.996	#NV
	40	14.325	12.573	10.774	8.928	7.035	5.092	3.098	#NV	4.851	4.085	3.312	2.592	1.924	1.319	0.796	#NV	6.138	5.186	4.293	3.437	2.62	1.846	1.117	#NV
	43	13.93	12.228	10.481	8.686	6.846	4.956	3.016	#NV	5.431	4.593	3.795	2.976	2.233	1.542	0.932	#NV	6.435	5.467	4.534	3.639	2.781	1.963	1.187	#NV
	45	13.657	11.996	10.282	8.522	6.717	4.864	2.961	#NV	5.776	4.946	4.108	3.248	2.441	1.685	1.021	#NV	6.646	5.651	4.691	3.772	2.887	2.041	1.294	#NV
12	20	18.852	16.549	14.185	11.758	9.27	6.712	4.082	#NV	1.022	0.612	0.26	0.005	0.001	-0.001	0.01	#NV	3.892	3.189	2.541	1.951	1.42	0.957	0.564	#NV
	22	18.583	16.314	13.986	11.595	9.139	6.619	4.027	#NV	1.403	0.95	0.563	0.241	0.008	0.001	-0.001	#NV	4.144	3.411	2.732	2.111	1.55	1.051	0.621	#NV
	25	18.175	15.96	13.684	11.347	8.946	6.478	3.943	#NV	1.975	1.466	1.011	0.624	0.312	0.083	0.063	#NV	4.517	3.74	3.016	2.347	1.737	1.188	0.705	#NV
	30	17.482	15.359	13.173	10.926	8.617	6.243	3.8	#NV	2.957	2.341	1.772	1.263	0.824	0.473	0.213	#NV	5.128	4.28	3.482	2.736	2.046	1.413	0.843	#NV
	35	16.772	14.742	12.649	10.496	8.28	6	3.653	#NV	3.972	3.226	2.567	1.927	1.354	0.86	0.418	#NV	5.723	4.808	3.937	3.117	2.348	1.633	0.978	#NV
	40	16.034	14.107	12.111	10.052	7.932	5.749	3.503	#NV	4.935	4.168	3.374	2.61	1.891	1.228	0.677	#NV	6.307	5.322	4.383	3.49	2.645	1.85	1.111	#NV
	43	15.579	13.715	11.778	9.779	7.718	5.597	3.411	#NV	5.548	4.712	3.862	3.045	2.227	1.514	0.858	#NV	6.65	5.627	4.647	3.71	2.821	1.979	1.189	#NV
	45	15.269	13.449	11.553	9.594	7.573	5.492	3.349	#NV	6.005	5.06	4.184	3.326	2.464	1.682	0.99	#NV	6.872	5.829	4.821	3.856	2.937	2.064	1.241	#NV
16	20	21.061	18.515	15.894	13.203	10.424	7.559	4.582	#NV	0.805	0.355	0.004	0	-0.001	-0.002	0.01	#NV	3.858	3.119	2.445	1.834	1.303	0.854	0.491	#NV
	22	20.758	18.251	15.669	13.011	10.276	7.453	4.524	#NV	1.211	0.727	0.309	0.004	0.001	-0.001	0.01	#NV	4.131	3.36	2.654	2.015	1.445	0.957	0.553	#NV
	25	20.301	17.852	15.33	12.732	10.053	7.296	4.436	#NV	1.851	1.287	0.805	0.403	0.081	0.12	0.01	#NV	4.534	3.717	2.962	2.273	1.655	1.108	0.645	#NV
	30	19.517	17.176	14.757	12.259	9.683	7.027	4.282	#NV	2.89	2.232	1.635	1.114	0.665	0.319	0.061	#NV	5.196	4.304	3.469	2.697	1.992	1.357	0.796	#NV
	35	18.713	16.48	14.166	11.774	9.304	6.754	4.12	1.398	4.018	3.194	2.492	1.846	1.245	0.737	0.37	0.106	5.837	4.876	3.964	3.112	2.322	1.598	0.945	0.37
	40	17.842	15.761	13.559	11.275	8.913	6.473	3.951	#NV	5.049	4.217	3.375	2.586	1.847	1.203	0.663	#NV	6.464	5.432	4.448	3.518	2.646	1.836	1.091	#NV
	43	17.314	15.313	13.186	10.968	8.678	6.3	3.846	#NV	5.707	4.803	3.931	3.06	2.384	1.478	0.831	#NV	6.831	5.761	4.733	3.758	2.835	1.977	1.178	#NV
	45	16.972	15.008	12.93	10.76	8.52	6.182	3.774	1.283	6.101	5.225	4.28	3.383	2.743	1.664	0.94	0.347	7.078	5.975	4.921	3.915	2.958	2.07	1.236	0.468
18	20	22.105	19.527	16.808	13.974	11.042	8.014	4.887	#NV	0.723	0.218	0.001	0	-0.002	-0.003	-0.007	#NV	3.828	3.071	2.379	1.761	1.232	0.791	0.444	#NV
	22	21.909	19.278	16.564	13.77	10.884	7.901	4.839	#NV	1.134	0.608	0.17	0.001	0	-0.002	0.01	#NV	4.132	3.322	2.602	1.951	1.381	0.9	0.511	#NV
	25	21.422	18.855	16.205	13.469	10.645	7.731	4.717	#NV	1.752	1.187	0.692	0.276	0.002	0	-0.002	#NV	4.532	3.694	2.923	2.225	1.602	1.059	0.608	#NV
	30	20.584	18.139	15.596	12.968	10.252	7.446	4.545	#NV	2.849	2.18	1.569	1.035	0.572	0.232	0.02	#NV	5.239	4.303	3.451	2.667	1.955	1.32	0.769	#NV
	35	19.719	17.401	14.971	12.454	9.85	7.157	4.37	#NV	4.024	3.191	2.449	1.782	1.188	0.685	0.31	#NV	5.883	4.897	3.967	3.099	2.3	1.573	0.924	#NV
	40	18.798	16.63	14.327	11.925	9.432	6.856	4.19	#NV	5.074	4.228	3.362	2.559	1.74	1.085	0.617	#NV	6.535	5.476	4.47	3.522	2.64	1.822	1.076	#NV
	43	18.226	16.151	13.929	11.6	9.181	6.675	4.081	1.387	5.739	4.8	3.91	3.059	2.205	1.449	0.89	0.284	6.915	5.819	4.767	3.772	2.838	1.968	1.165	0.443
	45	17.818	15.824	13.658	11.379	9.008	6.55	4.008	#NV	6.147	5.25	4.301	3.393	2.483	1.646	1.092	#NV	7.17	6.041	4.962	3.936	2.97	2.065	1.224	#NV

E.6 Cooling - Novel System using RT54 PCM

		dot_Q_cond [kW]									dot_Q_RPW [kW]									P_el [kW]							
		N_rot [Hz]									N_rot [Hz]									N_rot [Hz]							
T_water [°C]	T_ambient [°C]	150	130	110	90	70	50	30	10		150	130	110	90	70	50	30	10		150	130	110	90	70	50	30	10	
6	20	15.872	13.902	11.89	9.833	7.732	5.584	3.387	#NV		1.877	1.469	1.09	0.748	0.468	0.249	0.084	#NV		3.864	3.217	2.613	2.051	1.534	1.064	0.644	#NV
	22	15.647	13.708	11.724	9.697	7.626	5.509	3.342	#NV		2.173	1.736	1.331	0.96	0.635	0.357	0.161	#NV		4.087	3.412	2.78	2.18	1.644	1.144	0.691	#NV
	25	15.31	13.414	11.473	9.491	7.465	5.393	3.274	#NV		2.669	2.187	1.717	1.281	0.888	0.551	0.276	#NV		4.414	3.701	3.028	2.396	1.836	1.262	0.764	#NV
	30	14.746	12.918	11.049	9.141	7.193	5.197	3.157	#NV		3.473	2.918	2.368	1.834	1.315	0.869	0.475	#NV		4.956	4.176	3.435	2.735	2.074	1.457	0.882	#NV
	35	14.176	12.426	10.619	8.788	6.914	4.998	3.036	#NV		4.279	3.664	3.013	2.389	1.774	1.201	0.681	#NV		5.488	4.643	3.833	3.064	2.335	1.646	0.999	#NV
	40	13.601	11.923	10.184	8.426	6.63	4.793	2.911	#NV		5.111	4.438	3.692	2.985	2.251	1.554	0.888	#NV		6.011	5.099	4.222	3.385	2.59	1.831	1.113	#NV
	43	13.227	11.637	9.909	8.21	6.455	4.667	2.835	#NV		5.491	4.915	4.113	3.357	2.55	1.773	1.01	#NV		6.324	5.373	4.452	3.577	2.741	1.942	1.18	#NV
	45	12.975	11.374	9.76	8.062	6.337	4.583	2.783	#NV		5.851	5.118	4.425	3.6	2.771	1.922	1.109	#NV		6.527	5.55	4.607	3.701	2.84	2.014	1.225	#NV
8	20	16.833	14.755	12.628	10.448	8.222	5.943	3.608	#NV		1.812	1.394	1.021	0.671	0.391	0.177	0.068	#NV		3.871	3.208	2.591	2.022	1.502	1.054	0.671	#NV
	22	16.592	14.548	12.451	10.305	8.109	5.862	3.559	#NV		2.136	1.692	1.279	0.89	0.569	0.307	0.136	#NV		4.103	3.412	2.766	2.167	1.617	1.118	0.672	#NV
	25	16.231	14.233	12.184	10.086	7.938	5.739	3.486	#NV		2.611	2.142	1.672	1.234	0.836	0.499	0.243	#NV		4.447	3.714	3.025	2.383	1.787	1.241	0.748	#NV
	30	15.614	13.704	11.733	9.714	7.648	5.53	3.361	#NV		3.474	2.933	2.345	1.802	1.32	0.839	0.436	#NV		5.01	4.21	3.452	2.738	2.068	1.446	0.872	#NV
	35	14.994	13.163	11.275	9.339	7.353	5.318	3.232	#NV		4.306	3.671	3.033	2.401	1.782	1.189	0.647	#NV		5.562	4.697	3.868	3.082	2.341	1.644	0.994	#NV
	40	14.353	12.635	10.818	8.956	7.05	5.1	3.1	#NV		5.076	4.468	3.743	3.023	2.267	1.554	0.876	#NV		6.108	5.174	4.276	3.419	2.609	1.839	1.114	#NV
	43	13.972	12.307	10.527	8.722	6.864	4.966	3.019	#NV		5.565	4.971	4.168	3.405	2.589	1.788	1.022	#NV		6.432	5.456	4.517	3.62	2.767	1.955	1.185	#NV
	45	13.7	12.047	10.347	8.56	6.738	4.875	2.964	#NV		5.888	5.194	4.475	3.65	2.806	1.953	1.123	#NV		6.646	5.643	4.677	3.752	2.871	2.031	1.232	#NV
12	20	18.879	16.574	14.203	11.77	9.274	6.712	4.086	#NV		1.675	1.242	0.843	0.496	0.215	0.018	0.053	#NV		3.861	3.165	2.523	1.94	1.417	0.957	0.569	#NV
	22	18.595	16.339	14.004	11.607	9.146	6.62	4.029	#NV		2.03	1.558	1.129	0.736	0.413	0.167	0.108	#NV		4.133	3.387	2.715	2.1	1.543	1.049	0.625	#NV
	25	18.193	15.983	13.703	11.359	8.953	6.482	3.945	#NV		2.546	2.033	1.56	1.105	0.71	0.389	0.202	#NV		4.488	3.717	2.998	2.336	1.73	1.185	0.707	#NV
	30	17.441	15.377	13.192	10.94	8.625	6.246	3.801	#NV		3.451	2.873	2.289	1.743	1.22	0.765	0.386	#NV		5.097	4.257	3.465	2.724	2.039	1.41	0.842	#NV
	35	16.748	14.758	12.671	10.515	8.292	6.007	3.655	#NV		4.231	3.631	3.042	2.388	1.743	1.151	0.605	#NV		5.704	4.789	3.919	3.101	2.337	1.628	0.975	#NV
	40	15.962	14.114	12.138	10.08	7.952	5.759	3.506	#NV		5.147	4.436	3.788	3.044	2.295	1.567	0.86	#NV		6.28	5.309	4.363	3.47	2.63	1.843	1.107	#NV
	43	15.529	13.719	11.81	9.812	7.741	5.609	3.415	#NV		5.679	4.912	4.26	3.459	2.635	1.821	1.029	#NV		6.629	5.615	4.626	3.689	2.803	1.969	1.185	#NV
	45	15.225	13.45	11.587	9.634	7.599	5.507	3.354	#NV		5.962	5.318	4.552	3.748	2.887	1.995	1.149	#NV		6.864	5.811	4.801	3.833	2.917	2.052	1.237	#NV
16	20	21.09	18.549	15.919	13.207	10.422	7.556	4.606	#NV		1.53	1.067	0.649	0.288	0.014	0.01	0.003	#NV		3.818	3.087	2.422	1.826	1.303	0.856	0.489	#NV
	22	20.755	18.281	15.695	13.027	10.281	7.454	4.543	#NV		1.91	1.417	0.959	0.552	0.227	0.005	0.041	#NV		4.092	3.329	2.631	2	1.441	0.957	0.552	#NV
	25	20.243	17.873	15.355	12.749	10.063	7.297	4.448	#NV		2.477	1.925	1.421	0.96	0.556	0.244	0.125	#NV		4.496	3.688	2.94	2.258	1.645	1.106	0.644	#NV
	30	19.449	17.184	14.774	12.277	9.697	7.032	4.286	#NV		3.337	2.762	2.205	1.647	1.117	0.663	0.303	#NV		5.165	4.277	3.447	2.682	1.981	1.352	0.796	#NV
	35	18.535	16.466	14.169	11.796	9.321	6.762	4.122	#NV		4.26	3.62	3.003	2.355	1.701	1.09	0.539	#NV		5.804	4.851	3.943	3.092	2.308	1.591	0.944	#NV
	40	17.632	15.69	13.57	11.3	8.936	6.485	3.954	#NV		5.133	4.458	3.743	3.041	2.303	1.543	0.826	#NV		6.428	5.41	4.43	3.497	2.628	1.825	1.089	#NV
	43	17.069	15.258	13.173	10.995	8.699	6.316	3.852	#NV		5.655	4.944	4.293	3.487	2.67	1.837	1.031	#NV		6.794	5.745	4.709	3.735	2.817	1.963	1.173	#NV
	45	16.687	14.913	12.924	10.786	8.539	6.2	3.782	#NV		6.001	5.351	4.568	3.795	2.931	2.029	1.158	#NV		7.033	5.952	4.901	3.891	2.942	2.055	1.229	#NV
18	20	22.304	19.597	16.831	13.979	11.042	8.014	4.884	#NV		1.428	0.972	0.545	0.171	-0.001	-0.002	0.01	#NV		3.787	3.035	2.358	1.756	1.232	0.791	0.446	#NV
	22	21.916	19.313	16.594	13.784	10.887	7.901	4.819	#NV		1.834	1.326	0.865	0.453	0.12	-0.001	-0.002	#NV		4.07	3.287	2.575	1.938	1.378	0.9	0.511	#NV
	25	21.384	18.87	16.234	13.489	10.656	7.734	4.717	#NV		2.412	1.858	1.347	0.876	0.468	0.162	0	#NV		4.491	3.661	2.897	2.207	1.592	1.057	0.608	#NV
	30	20.404	18.115	15.614	12.989	10.266	7.452	4.548	1.543		3.355	2.731	2.16	1.585	1.062	0.603	0.239	0.048		5.177	4.273	3.427	2.649	1.944	1.315	0.767	0.308
	35	19.487	17.319	14.96	12.479	9.867	7.165	4.374	1.485		4.224	3.61	2.994	2.305	1.647	0.997	0.489	0.165		5.85	4.868	3.942	3.078	2.285	1.566	0.921	0.36
	40	18.544	16.519	14.306	11.949	9.461	6.874	4.196	#NV		5.043	4.478	3.768	3.04	2.296	1.533	0.832	#NV		6.506	5.45	4.448	3.499	2.618	1.809	1.072	#NV
	43	17.983	15.976	13.886	11.622	9.211	6.694	4.086	#NV		5.506	5.096	4.289	3.487	2.676	1.842	1.015	#NV		6.893	5.781	4.741	3.748	2.815	1.953	1.162	#NV
	45	17.609	15.668	13.647	11.403	9.039	6.576	4.012	1.363		5.803	5.323	4.534	3.764	2.924	2.111	1.152	0.384		7.148	6.016	4.947	3.913	2.946	2.047	1.221	0.463

E.7 Cooling - Reference System with reduced Fan Speed

		dot_Q_cond [kW]								P_el [kW]							
		N_rot [Hz]								N_rot [Hz]							
T_water [°C]	T_ambient [°C]	150	130	110	90	70	50	30	10	150	130	110	90	70	50	30	10
6	20	14.537	12.899	11.182	9.367	7.454	5.444	3.339	#NV	5.032	4.09	3.213	2.423	1.723	1.116	0.603	#NV
	22	14.298	12.694	11.004	9.223	7.343	5.366	3.293	#NV	5.245	4.278	3.381	2.563	1.833	1.195	0.651	#NV
	25	13.934	12.382	10.735	9.004	7.175	5.248	3.222	#NV	5.562	4.557	3.629	2.77	1.996	1.313	0.723	#NV
	30	13.309	11.849	10.29	8.634	6.889	5.046	3.103	#NV	6.082	5.015	4.022	3.107	2.264	1.507	0.841	#NV
	35	12.658	11.296	9.829	8.262	6.597	4.838	2.979	#NV	6.591	5.464	4.409	3.429	2.526	1.699	0.958	#NV
	40	11.992	10.716	9.349	7.876	6.3	4.624	2.851	#NV	7.076	5.904	4.789	3.746	2.777	1.886	1.073	#NV
	43	11.581	10.362	9.048	7.635	6.116	4.494	2.773	#NV	7.356	6.157	5.013	3.933	2.926	1.995	1.141	#NV
	45	11.298	10.123	8.842	7.47	5.99	4.405	2.72	#NV	7.54	6.321	5.161	4.057	3.024	2.067	1.187	#NV
8	20	15.341	13.631	11.835	9.927	7.91	5.785	3.553	#NV	5.162	4.177	3.262	2.442	1.721	1.101	0.586	#NV
	22	15.085	13.413	11.644	9.774	7.792	5.702	3.503	#NV	5.385	4.373	3.438	2.588	1.835	1.184	0.637	#NV
	25	14.695	13.08	11.357	9.54	7.614	5.576	3.428	#NV	5.716	4.665	3.697	2.805	2.007	1.308	0.713	#NV
	30	14.026	12.51	10.882	9.145	7.308	5.361	3.301	#NV	6.258	5.143	4.109	3.158	2.288	1.512	0.836	#NV
	35	13.328	11.917	10.39	8.748	6.996	5.139	3.173	#NV	6.789	5.612	4.513	3.495	2.562	1.713	0.956	#NV
	40	12.62	11.296	9.875	8.335	6.679	4.91	3.044	#NV	7.29	6.071	4.91	3.827	2.826	1.91	1.074	#NV
	43	12.178	10.922	9.554	8.078	6.483	4.772	2.966	#NV	7.58	6.331	5.144	4.022	2.981	2.024	1.142	#NV
	45	11.881	10.665	9.334	7.902	6.348	4.677	2.914	#NV	7.775	6.502	5.297	4.152	3.084	2.099	1.188	#NV
12	20	17.02	15.172	13.214	11.118	8.884	6.515	4.011	#NV	5.426	4.347	3.351	2.467	1.702	1.058	0.542	#NV
	22	16.728	14.923	12.996	10.943	8.75	6.421	3.956	#NV	5.668	4.561	3.544	2.627	1.828	1.15	0.598	#NV
	25	16.282	14.543	12.669	10.677	8.547	6.278	3.872	#NV	6.028	4.878	3.826	2.865	2.016	1.286	0.681	#NV
	30	15.515	13.892	12.128	10.227	8.2	6.034	3.727	#NV	6.617	5.399	4.276	3.252	2.325	1.51	0.818	#NV
	35	14.719	13.214	11.567	9.775	7.844	5.782	3.578	#NV	7.188	5.908	4.716	3.62	2.626	1.731	0.953	#NV
	40	13.912	12.51	10.978	9.305	7.485	5.523	3.424	#NV	7.721	6.4	5.148	3.982	2.914	1.946	1.086	#NV
	43	13.401	12.081	10.609	9.011	7.261	5.365	3.328	#NV	8.034	6.68	5.402	4.196	3.084	2.073	1.161	#NV
	45	13.063	11.784	10.366	8.809	7.108	5.257	3.264	#NV	8.239	6.863	5.563	4.337	3.197	2.156	1.217	#NV
16	20	18.791	16.811	14.691	12.402	9.941	7.312	4.515	#NV	5.695	4.513	3.429	2.477	1.664	0.998	0.484	#NV
	22	18.457	16.527	14.444	12.203	9.79	7.205	4.452	#NV	5.957	4.745	3.64	2.652	1.802	1.098	0.545	#NV
	25	17.947	16.094	14.072	11.901	9.559	7.043	4.356	#NV	6.346	5.089	3.947	2.912	2.008	1.248	0.637	#NV
	30	17.069	15.351	13.456	11.389	9.165	6.767	4.193	#NV	6.981	5.653	4.435	3.334	2.346	1.493	0.787	#NV
	35	16.171	14.575	12.816	10.876	8.761	6.483	4.025	#NV	7.584	6.204	4.913	3.735	2.676	1.736	0.936	#NV
	40	15.241	13.779	12.144	10.341	8.353	6.187	3.851	#NV	8.156	6.726	5.381	4.128	2.99	1.974	1.082	#NV
	43	14.671	13.286	11.729	10.006	8.099	6.009	3.745	#NV	8.489	7.026	5.651	4.36	3.175	2.11	1.169	#NV
	45	14.285	12.944	11.451	9.775	7.925	5.887	3.673	#NV	8.705	7.223	5.824	4.513	3.298	2.2	1.226	#NV
18	20	19.708	17.666	15.467	13.08	10.503	7.737	4.785	#NV	5.83	4.594	3.465	2.475	1.638	0.96	0.449	#NV
	22	19.352	17.363	15.203	12.869	10.341	7.624	4.718	#NV	6.103	4.836	3.684	2.658	1.782	1.065	0.514	#NV
	25	18.807	16.901	14.807	12.552	10.096	7.452	4.616	#NV	6.506	5.194	4.004	2.928	1.997	1.221	0.609	#NV
	30	17.867	16.108	14.151	12.001	9.677	7.158	4.443	#NV	7.165	5.78	4.512	3.37	2.351	1.479	0.767	#NV
	35	16.913	15.277	13.467	11.454	9.245	6.855	4.264	#NV	7.784	6.351	5.009	3.788	2.695	1.732	0.922	#NV
	40	15.914	14.432	12.748	10.883	8.811	6.54	4.079	#NV	8.374	6.888	5.495	4.197	3.023	1.981	1.075	#NV
	43	15.305	13.902	12.31	10.525	8.541	6.351	3.965	1.374	8.715	7.198	5.772	4.438	3.216	2.124	1.166	0.361
	45	14.892	13.534	12.011	10.279	8.355	6.221	3.888	#NV	8.936	7.401	5.951	4.597	3.344	2.218	1.226	#NV

E.8 Cooling - Novel System with reduced Fan Speed using RT64 PCM

		dot_Q_cond [kW] N_rot [Hz]								dot_Q_RPW [kW] N_rot [Hz]								P_el [kW] N_rot [Hz]							
T_water [°C]	T_ambient [°C]	150	130	110	90	70	50	30	10	150	130	110	90	70	50	30	10	150	130	110	90	70	50	30	10
6	20	14.784	13.065	11.274	9.411	7.471	5.448	3.339	#NV	2.897	2.194	1.547	0.994	0.558	0.228	0.023	#NV	4.811	3.937	3.126	2.381	1.707	1.111	0.603	#NV
	22	14.569	12.875	11.113	9.272	7.366	5.373	3.294	#NV	3.216	2.466	1.795	1.206	0.727	0.354	0.104	#NV	5.008	4.114	3.28	2.511	1.811	1.188	0.65	#NV
	25	14.243	12.589	10.868	9.075	7.206	5.259	3.225	#NV	3.702	2.901	2.166	1.527	0.964	0.553	0.24	#NV	5.299	4.375	3.509	2.703	1.966	1.302	0.721	#NV
	30	13.696	12.108	10.455	8.733	6.938	5.065	3.107	1.08	4.521	3.64	2.818	2.061	1.414	0.873	0.461	0.136	5.774	4.799	3.88	3.019	2.22	1.49	0.837	0.27
	35	13.133	11.616	10.033	8.383	6.663	4.866	2.987	#NV	5.324	4.391	3.48	2.613	1.862	1.199	0.673	#NV	6.239	5.214	4.242	3.327	2.468	1.674	0.951	#NV
	40	12.559	11.112	9.6	8.026	6.379	4.662	2.864	#NV	6.19	5.171	4.155	3.212	2.303	1.544	0.888	#NV	6.687	5.615	4.596	3.626	2.712	1.854	1.063	#NV
	43	12.215	10.804	9.337	7.806	6.206	4.536	2.788	#NV	6.707	5.64	4.56	3.547	2.588	1.736	1.019	#NV	6.954	5.852	4.804	3.803	2.854	1.96	1.128	#NV
	45	11.971	10.602	9.163	7.66	6.091	4.453	2.737	#NV	7.044	5.967	4.878	3.796	2.795	1.89	1.105	#NV	7.127	6.007	4.935	3.916	2.946	2.029	1.173	#NV
8	20	15.617	13.816	11.931	9.974	7.927	5.788	3.552	#NV	2.964	2.219	1.551	0.967	0.501	0.164	0.01	#NV	4.921	4.011	3.168	2.397	1.704	1.097	0.586	#NV
	22	15.391	13.616	11.765	9.833	7.816	5.708	3.504	#NV	3.307	2.522	1.803	1.187	0.68	0.3	0.049	#NV	5.124	4.193	3.328	2.532	1.813	1.178	0.636	#NV
	25	15.05	13.313	11.505	9.618	7.642	5.587	3.431	1.172	3.847	2.97	2.203	1.519	0.942	0.494	0.193	0.026	5.421	4.464	3.565	2.733	1.975	1.297	0.71	0.223
	30	14.46	12.802	11.067	9.255	7.362	5.381	3.306	#NV	4.646	3.727	2.868	2.085	1.406	0.843	0.429	#NV	5.919	4.906	3.952	3.062	2.24	1.494	0.832	#NV
	35	13.871	12.284	10.617	8.884	7.069	5.169	3.178	1.087	5.524	4.536	3.559	2.667	1.866	1.193	0.659	0.213	6.396	5.333	4.329	3.383	2.5	1.686	0.952	0.307
	40	13.268	11.751	10.161	8.504	6.768	4.952	3.046	#NV	6.41	5.342	4.274	3.279	2.35	1.55	0.883	#NV	6.862	5.75	4.695	3.694	2.753	1.875	1.069	#NV
	43	12.882	11.433	9.88	8.274	6.585	4.819	2.966	#NV	6.902	5.881	4.708	3.665	2.648	1.763	1.014	#NV	7.137	5.989	4.91	3.876	2.902	1.986	1.138	#NV
	45	12.65	11.197	9.702	8.118	6.464	4.729	2.911	#NV	7.309	6.125	5.033	3.908	2.869	1.908	1.102	#NV	7.315	6.158	5.048	3.995	2.997	2.058	1.184	#NV
12	20	17.366	15.399	13.335	11.17	8.899	6.515	4.011	#NV	3.106	2.291	1.537	0.896	0.384	0.023	0	#NV	5.139	4.151	3.243	2.419	1.687	1.058	0.542	#NV
	22	17.114	15.174	13.142	11.011	8.774	6.425	3.955	#NV	3.495	2.603	1.818	1.134	0.58	0.175	0.002	#NV	5.353	4.349	3.416	2.566	1.805	1.146	0.598	#NV
	25	16.727	14.836	12.852	10.77	8.584	6.288	3.872	#NV	4.05	3.106	2.255	1.506	0.874	0.399	0.082	#NV	5.674	4.638	3.671	2.783	1.982	1.276	0.68	#NV
	30	16.064	14.262	12.359	10.363	8.263	6.056	3.731	#NV	4.924	3.927	2.978	2.138	1.378	0.772	0.337	#NV	6.203	5.112	4.089	3.138	2.27	1.491	0.814	#NV
	35	15.392	13.682	11.861	9.947	7.934	5.817	3.586	#NV	5.841	4.804	3.754	2.789	1.894	1.155	0.594	#NV	6.712	5.567	4.492	3.484	2.552	1.701	0.945	#NV
	40	14.698	13.092	11.345	9.521	7.597	5.573	3.438	1.18	6.744	5.702	4.512	3.449	2.432	1.558	0.849	0.28	7.207	6.007	4.886	3.82	2.826	1.907	1.075	0.343
	43	14.274	12.735	11.034	9.262	7.392	5.424	3.348	#NV	7.277	6.256	4.989	3.855	2.759	1.798	1.066	#NV	7.498	6.264	5.116	4.017	2.988	2.029	1.151	#NV
	45	13.989	12.495	10.824	9.087	7.253	5.323	3.287	#NV	7.634	6.632	5.308	4.132	2.981	1.961	1.209	#NV	7.689	6.431	5.267	4.147	3.094	2.109	1.201	#NV
16	20	19.223	17.09	14.835	12.459	9.954	7.312	4.535	#NV	3.281	2.365	1.531	0.814	0.248	0.001	0.002	#NV	5.352	4.281	3.307	2.426	1.653	0.998	0.484	#NV
	22	18.936	16.839	14.621	12.281	9.813	7.206	4.453	#NV	3.673	2.713	1.843	1.08	0.467	0.024	0.028	#NV	5.583	4.494	3.492	2.584	1.781	1.097	0.545	#NV
	25	18.497	16.459	14.295	12.011	9.6	7.052	4.358	#NV	4.249	3.243	2.304	1.482	0.794	0.279	0.105	#NV	5.923	4.804	3.766	2.818	1.972	1.24	0.636	#NV
	30	17.749	15.816	13.747	11.556	9.24	6.781	4.184	#NV	5.223	4.136	3.112	2.167	1.35	0.687	0.238	#NV	6.475	5.307	4.211	3.2	2.284	1.473	0.784	#NV
	35	16.978	15.156	13.186	11.091	8.871	6.523	4.034	1.388	6.185	5.035	3.916	2.876	1.914	1.121	0.511	0.129	7.009	5.795	4.644	3.572	2.588	1.702	0.928	0.286
	40	16.192	14.471	12.608	10.614	8.494	6.248	3.866	1.332	7.164	5.954	4.74	3.6	2.514	1.563	0.81	0.251	7.522	6.262	5.065	3.933	2.884	1.925	1.069	0.335
	43	15.709	14.053	12.255	10.323	8.263	6.08	3.764	#NV	7.703	6.472	5.251	4.048	2.879	1.832	0.98	#NV	7.836	6.544	5.309	4.143	3.057	2.057	1.152	#NV
	45	15.386	13.768	12.017	10.122	8.108	5.967	3.694	1.274	8.107	6.825	5.605	4.329	3.126	2.022	1.076	0.363	8.035	6.728	5.468	4.283	3.17	2.142	1.207	0.383
18	20	20.194	17.977	15.624	13.14	10.512	7.737	4.785	#NV	3.408	2.449	1.522	0.72	0.17	0	-0.003	#NV	5.452	4.343	3.334	2.424	1.63	0.96	0.449	#NV
	22	19.886	17.709	15.398	12.951	10.363	7.624	4.718	#NV	3.803	2.767	1.854	1.048	0.404	0.002	-0.002	#NV	5.689	4.565	3.525	2.587	1.763	1.065	0.514	#NV
	25	19.416	17.307	15.054	12.666	10.138	7.459	4.616	#NV	4.352	3.314	2.336	1.469	0.751	0.212	0.001	#NV	6.048	4.884	3.808	2.83	1.961	1.215	0.609	#NV
	30	18.616	16.624	14.475	12.185	9.757	7.182	4.446	#NV	5.366	4.234	3.179	2.19	1.323	0.648	0.185	#NV	6.609	5.402	4.267	3.225	2.285	1.458	0.764	#NV
	35	17.801	15.922	13.879	11.693	9.368	6.898	4.273	1.473	6.337	5.14	3.998	2.915	1.925	1.09	0.476	0.1	7.161	5.907	4.716	3.611	2.6	1.696	0.915	0.277
	40	16.965	15.203	13.268	11.19	8.969	6.608	4.095	#NV	7.346	6.178	4.86	3.679	2.543	1.563	0.773	#NV	7.685	6.375	5.148	3.983	2.908	1.929	1.062	#NV
	43	16.456	14.756	12.894	10.881	8.726	6.43	3.987	1.377	7.955	6.672	5.393	4.138	2.934	1.852	0.96	0.303	7.99	6.667	5.398	4.201	3.086	2.065	1.149	0.359
	45	16.112	14.442	12.635	10.673	8.561	6.311	3.914	1.353	8.364	7.053	5.719	4.456	3.2	2.047	1.088	0.354	8.189	6.844	5.566	4.343	3.203	2.154	1.205	0.38

E.9 Cooling - Novel System with reduced Fan Speed using RT54 PCM

		dot_Q_cond [kW] N_rot [Hz]								dot_Q_RPW [kW] N_rot [Hz]								P_el [kW] N_rot [Hz]							
T_water [°C]	T_ambient [°C]	150	130	110	90	70	50	30	10	150	130	110	90	70	50	30	10	150	130	110	90	70	50	30	10
6	20	14.834	13.103	11.301	9.428	7.48	5.453	3.34	#NV	3.306	2.631	1.982	1.377	0.866	0.457	0.178	#NV	4.775	3.905	3.101	2.364	1.697	1.107	0.602	#NV
	22	14.626	12.915	11.142	9.295	7.376	5.377	3.295	#NV	3.644	2.895	2.231	1.593	1.031	0.577	0.249	#NV	4.972	4.083	3.254	2.493	1.801	1.184	0.649	#NV
	25	14.307	12.64	10.9	9.095	7.217	5.263	3.226	#NV	4.067	3.324	2.6	1.899	1.284	0.759	0.36	#NV	5.273	4.346	3.482	2.686	1.956	1.298	0.719	#NV
	30	13.751	12.159	10.498	8.76	6.953	5.071	3.11	#NV	4.765	4.008	3.212	2.433	1.715	1.077	0.552	#NV	5.756	4.773	3.852	2.996	2.206	1.484	0.835	#NV
	35	13.249	11.705	10.099	8.419	6.684	4.875	2.99	#NV	5.558	4.734	3.855	2.999	2.161	1.407	0.761	#NV	6.236	5.195	4.215	3.298	2.45	1.665	0.948	#NV
	40	12.649	11.241	9.695	8.076	6.41	4.675	2.867	#NV	6.249	5.453	4.534	3.57	2.638	1.754	0.954	#NV	6.705	5.613	4.57	3.596	2.688	1.843	1.06	#NV
	43	12.383	10.925	9.426	7.861	6.24	4.552	2.792	#NV	6.801	5.835	4.902	3.935	2.946	1.983	1.097	#NV	6.985	5.853	4.78	3.769	2.828	1.947	1.125	#NV
	45	12.114	10.702	9.248	7.713	6.127	4.469	2.741	#NV	7.02	6.084	5.162	4.149	3.154	2.133	1.191	#NV	7.172	6.02	4.915	3.886	2.92	2.016	1.169	#NV
8	20	15.67	13.86	11.967	9.995	7.938	5.794	3.554	#NV	3.394	2.68	2.002	1.372	0.836	0.417	0.131	#NV	4.879	3.974	3.139	2.378	1.693	1.092	0.585	#NV
	22	15.443	13.659	11.796	9.854	7.827	5.714	3.506	#NV	3.714	2.945	2.246	1.593	1.01	0.544	0.205	#NV	5.085	4.159	3.3	2.532	1.802	1.173	0.635	#NV
	25	15.099	13.364	11.541	9.641	7.662	5.592	3.432	#NV	4.159	3.414	2.638	1.923	1.273	0.739	0.319	#NV	5.393	4.43	3.536	2.713	1.962	1.292	0.709	#NV
	30	14.517	12.861	11.119	9.287	7.379	5.388	3.307	#NV	4.859	4.1	3.286	2.486	1.73	1.07	0.522	#NV	5.899	4.878	3.921	3.035	2.224	1.487	0.83	#NV
	35	13.947	12.36	10.683	8.925	7.094	5.181	3.18	#NV	5.655	4.837	3.935	3.062	2.211	1.419	0.742	#NV	6.389	5.313	4.299	3.352	2.478	1.676	0.949	#NV
	40	13.324	11.857	10.248	8.566	6.801	4.968	3.05	#NV	6.396	5.589	4.638	3.675	2.703	1.789	0.968	#NV	6.87	5.737	4.667	3.662	2.727	1.861	1.066	#NV
	43	12.946	11.504	9.964	8.328	6.623	4.837	2.971	#NV	6.875	5.903	5.007	4.013	3.018	2.02	1.114	#NV	7.157	6.002	4.885	3.843	2.873	1.971	1.134	#NV
	45	#NV	11.278	9.814	8.18	6.5	4.749	2.917	#NV	#NV	6.214	5.35	4.264	3.231	2.19	1.221	#NV	#NV	6.166	5.029	3.965	2.969	2.042	1.179	#NV
12	20	17.408	15.448	13.375	11.198	8.915	6.523	4.01	#NV	3.506	2.751	2.032	1.347	0.767	0.324	0.064	#NV	5.087	4.109	3.207	2.394	1.672	1.05	0.542	#NV
	22	17.142	15.223	13.183	11.04	8.79	6.433	3.956	#NV	3.893	3.072	2.3	1.595	0.962	0.467	0.144	#NV	5.301	4.304	3.38	2.539	1.79	1.138	0.597	#NV
	25	16.75	14.883	12.895	10.802	8.602	6.296	3.874	#NV	4.291	3.519	2.71	1.957	1.254	0.684	0.268	#NV	5.638	4.597	3.637	2.755	1.966	1.269	0.678	#NV
	30	16.078	14.303	12.412	10.403	8.288	6.066	3.734	#NV	5.05	4.199	3.419	2.571	1.759	1.053	0.49	#NV	6.176	5.08	4.05	3.105	2.348	1.481	0.811	#NV
	35	#NV	13.722	11.916	9.993	7.967	5.833	3.591	#NV	#NV	4.982	4.108	3.169	2.281	1.438	0.731	#NV	#NV	5.543	4.456	3.45	2.525	1.688	0.942	#NV
	40	#NV	13.104	11.41	9.576	7.639	5.594	3.444	#NV	#NV	5.693	4.797	3.803	2.828	1.849	0.985	#NV	#NV	6.005	4.854	3.784	2.794	1.89	1.069	#NV
	43	#NV	12.735	11.115	9.322	7.436	5.447	3.354	#NV	#NV	6.135	5.303	4.205	3.144	2.106	1.151	#NV	#NV	6.274	5.082	3.981	2.954	2.008	1.144	#NV
	45	#NV	12.484	10.867	9.147	7.303	5.348	3.293	1.129	#NV	6.427	5.447	4.448	3.383	2.286	1.263	0.424	#NV	6.453	5.25	4.112	3.058	2.087	1.194	0.387
16	20	19.243	17.137	14.887	12.497	9.975	7.318	4.512	#NV	3.617	2.871	2.057	1.328	0.687	0.212	0.01	#NV	5.295	4.228	3.262	2.393	1.633	0.992	0.484	#NV
	22	#NV	16.839	14.673	12.319	9.835	7.217	4.451	#NV	#NV	3.271	2.356	1.586	0.901	0.371	0.046	#NV	#NV	4.418	3.447	2.551	1.761	1.087	0.544	#NV
	25	18.499	16.475	14.347	12.054	9.623	7.063	4.359	#NV	4.492	3.676	2.802	1.978	1.222	0.612	0.186	#NV	5.873	4.746	3.721	2.783	1.95	1.23	0.634	#NV
	30	#NV	15.629	13.792	11.605	9.273	6.806	4.201	#NV	#NV	4.357	3.524	2.633	1.776	1.02	0.443	#NV	#NV	5.272	4.168	3.161	2.256	1.46	0.78	#NV
	35	#NV	15.151	13.219	11.143	8.913	6.544	4.041	#NV	#NV	5.151	4.294	3.284	2.343	1.443	0.707	#NV	#NV	5.766	4.597	3.532	2.555	1.685	0.923	#NV
	40	#NV	14.485	12.64	10.671	8.543	6.277	3.876	#NV	#NV	5.86	4.931	3.985	2.931	1.909	0.99	#NV	#NV	6.263	5.034	3.89	2.847	1.903	1.062	#NV
	43	#NV	14.08	12.283	10.382	8.316	6.113	3.775	#NV	#NV	6.293	5.347	4.41	3.287	2.196	1.171	#NV	#NV	6.553	5.285	4.099	3.019	2.032	1.144	#NV
	45	#NV	13.808	12.042	10.178	8.164	6.001	3.706	1.275	#NV	6.58	5.61	4.6	3.535	2.378	1.299	0.413	#NV	6.744	5.451	4.248	3.132	2.117	1.197	0.382
18	20	#NV	18.036	15.684	13.183	10.538	7.742	4.785	#NV	#NV	2.866	2.085	1.314	0.643	0.149	-0.002	#NV	#NV	4.293	3.283	2.386	1.606	0.955	0.449	#NV
	22	19.899	17.752	15.452	12.996	10.389	7.634	4.718	#NV	4.067	3.183	2.373	1.582	0.866	0.317	0	#NV	5.64	4.509	3.477	2.55	1.74	1.055	0.514	#NV
	25	#NV	17.337	15.108	12.715	10.168	7.472	4.618	#NV	#NV	3.663	2.839	1.986	1.201	0.57	0.141	#NV	#NV	4.832	3.76	2.79	1.936	1.203	0.607	#NV
	30	#NV	16.675	14.501	12.236	9.795	7.2	4.451	1.532	#NV	4.492	3.591	2.643	1.782	1	0.411	0.073	#NV	5.368	4.219	3.185	2.253	1.443	0.76	0.224
	35	#NV	16.049	13.911	11.746	9.412	6.923	4.283	1.474	#NV	5.352	4.283	3.319	2.364	1.457	0.689	0.184	#NV	5.9	4.677	3.569	2.565	1.676	0.908	0.276
	40	#NV	15.46	13.273	11.238	9.022	6.639	4.106	1.415	#NV	6.244	5.004	4.03	2.969	1.918	0.99	0.293	#NV	6.429	5.12	3.941	2.868	1.905	1.053	0.328
	43	#NV	15.124	12.894	10.93	8.78	6.466	3.999	1.378	#NV	6.794	5.411	4.483	3.327	2.232	1.178	0.349	#NV	6.745	5.382	4.155	3.047	2.037	1.139	0.359
	45	#NV	14.908	12.636	10.722	8.619	6.35	3.927	#NV	#NV	7.168	5.682	4.709	3.608	2.446	1.316	#NV	#NV	6.953	5.555	4.302	3.162	2.125	1.195	#NV

E.10 DHW - Reference System with 60°C DHW Temperature

		dot_Q_cond [kW] N_rot [%]								P_el [kW] N_rot [%]							
T_water [°C]	T_ambient [°C]	150	130	110	90	70	50	30	10	150	130	110	90	70	50	30	10
60	-22	8.233	7.116	5.739	4.891	3.788	2.693	1.652	0.545	4.425	3.837	3.135	2.662	2.077	1.491	0.917	0.329
	-20	8.626	7.466	6.297	5.133	3.974	2.825	1.731	0.572	4.54	3.942	3.34	2.737	2.135	1.534	0.939	0.336
	-15	9.958	8.646	7.32	5.994	4.664	3.317	2.021	0.67	4.893	4.262	3.624	2.983	2.336	1.68	1.022	0.364
	-10	11.474	9.969	8.462	6.954	5.421	3.88	2.316	0.787	5.236	4.569	3.897	3.218	2.527	1.826	1.111	0.401
	-5	13.121	11.408	9.692	7.971	6.243	4.485	2.693	0.909	5.547	4.849	4.144	3.429	2.701	1.959	1.197	0.425
	0	14.896	12.962	11.023	9.075	7.117	5.141	3.11	1.05	5.817	5.093	4.36	3.615	2.855	2.078	1.275	0.45
	5	16.796	14.629	12.453	10.266	8.062	5.836	3.553	1.204	6.036	5.295	4.542	3.774	2.988	2.179	1.343	0.473
	10	18.825	16.405	13.982	11.542	9.08	6.585	4.034	1.362	6.198	5.448	4.683	3.899	3.093	2.261	1.398	0.492
	15	21.012	18.287	15.605	12.901	10.168	7.39	4.544	1.54	6.287	5.547	4.778	3.987	3.17	2.323	1.439	0.509
	20	22.958	20.001	17.119	14.199	11.231	8.197	5.06	1.735	6.258	5.525	4.771	3.992	3.185	2.344	1.455	0.517
	25	24.938	21.809	18.683	15.514	12.288	8.984	5.562	#NV	6.192	5.472	4.725	3.953	3.154	2.318	1.438	#NV
	30	27.026	23.689	20.312	16.888	13.397	9.864	6.098	#NV	6.068	5.363	4.631	3.873	3.086	2.244	1.381	#NV
	35	29.223	25.634	22.001	18.313	14.551	10.784	6.686	#NV	5.886	5.199	4.489	3.747	2.979	2.18	1.339	#NV
	38	30.796	27.019	23.166	19.332	15.374	11.355	7.041	#NV	5.797	5.132	4.423	3.716	2.963	2.129	1.291	#NV
	40	31.751	27.871	23.897	19.96	15.883	11.708	7.264	#NV	5.702	5.052	4.35	3.659	2.919	2.047	1.257	#NV

E.11 DHW - Reference System with 50°C DHW Temperature

		dot_Q_cond [kW]								P_el [kW]							
		N_rot [%]								N_rot [%]							
T_water [°C]	T_ambient [°C]	150	130	110	90	70	50	30	10	150	130	110	90	70	50	30	10
50	-22	8.663	7.514	6.364	5.208	4.042	2.879	1.757	0.585	4.055	3.521	2.989	2.453	1.916	1.377	0.845	0.306
	-20	9.065	7.864	6.662	5.458	4.255	3.019	1.844	0.619	4.15	3.606	3.062	2.516	1.958	1.414	0.869	0.31
	-15	10.354	9.009	7.66	6.306	4.926	3.533	2.137	0.717	4.426	3.855	3.284	2.709	2.126	1.535	0.936	0.338
	-10	11.884	10.349	8.807	7.257	5.695	4.101	2.469	0.842	4.699	4.1	3.498	2.89	2.276	1.65	1.008	0.373
	-5	13.54	11.799	10.051	8.291	6.516	4.717	2.862	0.978	4.933	4.314	3.687	3.052	2.407	1.751	1.075	0.402
	0	15.317	13.359	11.39	9.408	7.405	5.372	3.281	1.12	5.121	4.488	3.844	3.187	2.519	1.836	1.132	0.408
	5	17.165	15.016	12.825	10.607	8.362	6.08	3.737	1.282	5.242	4.612	3.962	3.293	2.608	1.904	1.177	0.424
	10	19.026	16.586	14.166	11.744	9.283	6.768	4.173	1.453	5.258	4.628	3.984	3.321	2.636	1.929	1.195	0.433
	15	21.004	18.308	15.599	12.947	10.249	7.487	4.63	1.617	5.226	4.605	3.968	3.311	2.628	1.922	1.189	0.425
	20	23.015	20.058	17.103	14.213	11.268	8.249	5.117	1.779	5.136	4.529	3.905	3.257	2.584	1.888	1.164	0.412
	25	25.036	21.814	18.678	15.54	12.341	9.055	5.635	1.974	4.994	4.405	3.794	3.161	2.506	1.824	1.12	0.393
	30	27.047	23.66	20.319	16.927	13.465	9.902	6.208	2.183	4.805	4.231	3.635	3.022	2.39	1.73	1.044	0.365
	35	29.453	25.618	22.023	18.37	14.638	10.791	6.788	2.412	4.561	4.001	3.428	2.84	2.235	1.606	0.965	0.323
	38	30.847	26.869	23.094	19.272	15.363	11.329	7.149	2.552	4.382	3.852	3.305	2.741	2.156	1.548	0.909	0.296
	40	31.792	27.688	23.809	19.877	15.854	11.698	7.397	2.65	4.252	3.735	3.203	2.653	2.084	1.491	0.848	0.274

E.12 DHW - Novel System using RT64 PCM

		dot_Q_cond [kW]								dot_Q_RPW [kW]								P_el [kW]							
		N_rot [%]								N_rot [%]								N_rot [%]							
T_water [°C]	T_ambient [°C]	150	130	110	90	70	50	30	10	150	130	110	90	70	50	30	10	150	130	110	90	70	50	30	10
60	-22	5.691	4.876	4.041	3.298	2.517	#NV	#NV	#NV	2.563	2.26	1.785	1.375	1.113	#NV	#NV	#NV	4.41	3.826	3.149	2.522	1.97	#NV	#NV	#NV
	-20	5.981	5.131	4.283	3.508	2.682	#NV	#NV	#NV	2.668	2.356	2.031	1.524	1.23	#NV	#NV	#NV	4.524	3.929	3.33	2.653	2.074	#NV	#NV	#NV
	-15	6.966	5.993	5.022	4.064	3.121	#NV	#NV	#NV	3.013	2.672	2.315	1.944	1.554	#NV	#NV	#NV	4.874	4.245	3.611	2.973	2.33	#NV	#NV	#NV
	-10	8.104	6.974	5.857	4.755	3.651	#NV	#NV	#NV	3.391	3.015	2.623	2.214	1.788	#NV	#NV	#NV	5.215	4.55	3.88	3.205	2.528	#NV	#NV	#NV
	-5	9.361	8.054	6.767	5.496	4.242	#NV	#NV	#NV	3.784	3.375	2.944	2.492	2.014	#NV	#NV	#NV	5.521	4.827	4.125	3.413	2.691	#NV	#NV	#NV
	0	10.733	9.238	7.762	6.308	4.873	3.455	#NV	#NV	4.188	3.746	3.28	2.784	2.259	1.695	#NV	#NV	5.785	5.067	4.339	3.597	2.842	2.07	#NV	#NV
	5	12.203	10.525	8.847	7.194	5.562	3.949	2.348	#NV	4.606	4.128	3.626	3.09	2.516	1.897	1.213	#NV	5.967	5.264	4.518	3.754	2.972	2.169	1.338	#NV
	10	13.834	11.912	10.022	8.153	6.311	4.487	2.681	#NV	5.027	4.518	3.981	3.407	2.785	2.11	1.361	#NV	6.153	5.411	4.654	3.877	3.075	2.249	1.392	#NV
	15	15.552	13.391	11.284	9.189	7.12	5.07	3.035	#NV	5.455	4.913	4.344	3.731	3.065	2.334	1.517	#NV	6.22	5.499	4.744	3.961	3.15	2.309	1.433	#NV
	20	17.484	14.961	12.586	10.239	7.923	5.65	3.393	#NV	5.482	5.04	4.534	3.963	3.31	2.548	1.669	#NV	6.19	5.47	4.727	3.959	3.16	2.324	1.446	#NV
	25	19.599	16.863	14.211	11.585	8.986	6.421	3.863	#NV	5.349	4.947	4.475	3.933	3.307	2.568	1.702	#NV	6.119	5.41	4.676	3.916	3.127	2.298	1.428	#NV
	30	21.719	18.636	15.693	12.803	9.927	#NV	#NV	#NV	5.769	5.368	4.849	4.241	3.597	#NV	#NV	#NV	6.081	5.393	4.654	3.887	3.115	#NV	#NV	#NV
	35	24.022	20.597	17.342	14.16	10.982	#NV	#NV	#NV	5.903	5.547	5.03	4.406	3.776	#NV	#NV	#NV	5.945	5.281	4.554	3.795	3.05	#NV	#NV	#NV
	38	25.468	21.827	18.376	15.012	11.644	#NV	#NV	#NV	5.968	5.644	5.129	4.495	3.878	#NV	#NV	#NV	5.838	5.192	4.473	3.722	2.997	#NV	#NV	#NV
	40	26.458	22.669	19.084	15.595	12.097	#NV	5.645	1.948	6.005	5.703	5.191	4.55	3.944	#NV	1.626	0.624	5.755	5.124	4.411	3.665	2.955	#NV	1.242	0.427

E.13 DHW - Novel System using RT54 PCM

		dot_Q_cond [kW]								dot_Q_RPW [kW]								P_el [kW]							
		N_rot [%]								N_rot [%]								N_rot [%]							
T_water [°C]	T_ambient [°C]	150	130	110	90	70	50	30	10	150	130	110	90	70	50	30	10	150	130	110	90	70	50	30	10
50	-22	6.146	5.298	4.459	3.785	2.95	#NV	#NV	#NV	2.53	2.227	1.914	1.169	0.91	#NV	#NV	#NV	4.039	3.509	2.979	2.321	1.803	#NV	#NV	#NV
	-20	6.444	5.555	4.742	3.959	3.082	#NV	#NV	#NV	2.635	2.32	1.939	1.366	1.072	#NV	#NV	#NV	4.134	3.593	3.05	2.434	1.896	#NV	#NV	#NV
	-15	7.404	6.401	5.404	4.415	3.423	#NV	#NV	#NV	2.963	2.62	2.265	1.898	1.51	#NV	#NV	#NV	4.405	3.838	3.271	2.699	2.118	#NV	#NV	#NV
	-10	8.557	7.4	6.25	5.108	3.974	#NV	#NV	#NV	3.342	2.962	2.567	2.157	1.727	#NV	#NV	#NV	4.672	4.079	3.482	2.878	2.267	#NV	#NV	#NV
	-5	9.817	8.492	7.176	5.868	4.567	3.273	#NV	#NV	3.738	3.321	2.886	2.432	1.956	1.45	#NV	#NV	4.903	4.288	3.667	3.037	2.397	1.743	#NV	#NV
	0	11.183	9.678	8.182	6.696	5.216	3.742	2.233	#NV	4.148	3.695	3.221	2.722	2.197	1.636	1.053	#NV	5.088	4.458	3.819	3.169	2.507	1.827	1.126	#NV
	5	12.599	10.93	9.266	7.592	5.92	4.251	2.584	#NV	4.552	4.074	3.567	3.026	2.451	1.835	1.158	#NV	5.197	4.572	3.932	3.271	2.593	1.894	1.171	#NV
	10	14.414	12.395	10.448	8.549	6.664	4.785	2.905	#NV	4.61	4.19	3.715	3.193	2.618	1.983	1.269	#NV	5.211	4.59	3.948	3.291	2.615	1.916	1.186	#NV
	15	16.47	14.162	11.892	9.748	7.615	5.484	3.344	#NV	4.532	4.146	3.704	3.198	2.634	2.004	1.287	#NV	5.174	4.561	3.932	3.278	2.604	1.907	1.18	#NV
	20	18.602	16.014	13.46	11.05	8.652	6.252	3.829	#NV	4.413	4.045	3.641	3.161	2.616	1.999	1.29	#NV	5.087	4.48	3.866	3.222	2.558	1.871	1.154	#NV
	25	20.839	17.922	15.152	12.457	9.778	7.09	4.364	1.381	4.199	3.894	3.524	3.082	2.563	1.966	1.272	0.595	4.93	4.352	3.751	3.125	2.476	1.805	1.108	0.387
	30	23.284	19.984	16.839	13.894	10.915	#NV	#NV	#NV	4.096	3.852	3.531	2.991	2.514	#NV	#NV	#NV	4.755	4.203	3.631	2.99	2.368	#NV	#NV	#NV
	35	25.907	22.209	18.712	15.478	12.177	#NV	#NV	#NV	3.804	3.639	3.381	2.803	2.383	#NV	#NV	#NV	4.501	3.985	3.447	2.808	2.217	#NV	#NV	#NV
	38	27.563	23.612	19.893	16.479	12.976	#NV	#NV	2.068	3.591	3.479	3.264	2.66	2.28	#NV	#NV	0.486	4.322	3.829	3.314	2.678	2.111	#NV	#NV	0.289
	40	28.702	24.576	20.704	17.169	13.526	#NV	#NV	2.19	3.432	3.358	3.175	2.552	2.202	#NV	#NV	0.463	4.191	3.715	3.218	2.583	2.032	#NV	#NV	0.268

F Paper submitted to the 25th IIR International Congress of Refrigeration 2019

Manuscript ID: 645
DOI: 10.18462/iir.icr.2019.645

Integration of a compact two fluid PCM heat exchanger into the hot superheated section of an air source heat pump cycle for optimized DHW generation

Johann EMHOFER[(a)], Tilman BARZ[(a)], Klemens MARX[(a)], Felix HOCHWALLNER[(a)], Luisa F. CABEZA[(b)], Gabriel ZSEMBINSZKI[(b)], Andreas STREHLOW[(c)], Birgo NITSCH[(c)], Michael WEISS[(d)]

[(a)] AIT Austrian Institute of Technology, Center for Energy, 1210 Wien, Austria, johann.emhofer@ait.ac.at
[(b)] GREiA Research Group, INSPIRES Research Centre, Universitat de Lleida, 25001 Lleida, Spain, lcabeza@diei.udl.cat
[(c)] AKG Verwaltungsgesellschaft mbH, 34369 Hofgeismar, Germany, andreas.strehlow@akg-gruppe.de
[(d)] OCHSNER Wärmepumpen GmbH, 4020 Linz, Austria, michael.weiss@ochsner.com

ABSTRACT

This contribution presents a concept for the direct integration of a refrigerant/water Heat Exchanger (HEX) with a Phase Change Material (PCM) in the hot superheated section of an R32 - air source compression Heat Pump (HP) cycle, for optimized Domestic Hot Water (DHW) generation in multi-family houses. The concept takes advantage of the PCMs high thermal storage capacity integrated into a high performance compact enhanced plate-and-fin aluminium HEX. On the refrigerant side, it works as a de-superheater for DHW generation during heating and cooling operation whereas the process water is connected to decentralized DHW storages located in single apartments of a low energy building. We present results from simulations at a system level for typical operating conditions and corresponding seasonal and annual performances. Compared to conventional systems, the results indicate savings up to 11% of electric energy over the year for DHW generation in average climate.

Keywords: domestic hot water, energy efficiency, heat pump, heating, hot gas, phase change material.

1. INTRODUCTION

Today's commercially available air source HPs work highly efficient and make a valuable contribution to reach climatic goals as the reduction of CO_2 in our atmosphere. To further increase the efficiency of HPs many different concepts using latent heat thermal energy storage technologies were proposed recently. The aim is to decrease the size of buffer tanks and to avoid the oversizing of HPs reducing thermal peak loads by shifting heating and cooling demands in time (Pardiñas *et al.*, 2017), to optimize integration of solar thermal collectors (Kapsalis *et al.*, 2016), to enhance the storage density of DHW storages (Zou *et al.*, 2017) or to enhanced the defrosting performance of air source HPs (Song *et al.*, 2018). Recent studies showed further that a wide spectrum of PCMs are available to be used in such storages at different temperature levels (Cabeza *et al.*, 2011).

This contribution employs latent heat thermal energy storage technology to increase the efficiency of air source HP systems in multi-family houses for DHW generation. The key idea is to optimally use the available exergy of the refrigerant during operation all over the year. This means that thermal energy at a high temperature level in the superheated section of the HP cycle is stored in a PCM to be used later for high temperature DHW generation rather than being used at intermediate temperatures for heating or even being wasted in the case of cooling operation. The optimal assignment of high temperature heat during conventional operation is realized by the direct integration of a refrigerant (R)/water (W) heat exchanger (HEX) with phase (P) change material – in short: RPW-HEX . The compact RPW-HEX is integrated in the hot refrigerant flow exiting the

compressor of a compression HP on the primary side and in the process water flow on the secondary side. From the secondary side of the RPW-HEX, the process water delivers the thermal energy to decentralized DHW storages located in the individual apartments of a multi-family house. The RPW-HEX also manages flexible DHW demands and by this minimizes the operation of the air source HP in the highly non-efficient direct DHW operating mode. Furthermore, it adds the necessary flexibility by decoupling the high temperature high power energy streams (for DHW generation) and the low temperature and low power energy stream (for heating). To guarantee high heat transfer coefficients between the hot gaseous refrigerant and the PCM, between the PCM and the process water and between the refrigerant and the process water, with a minimum of refrigerant mass, a plate and fin aluminium heat exchanger design is used. The present study answers the question, how much of the heat can be stored in the RPW-HEX and therefore delivered to the decentralized DHW storages in a typical application. Furthermore, possible savings in electric energy are quantified and compared to a reference system without the RPW-HEX. For doing so, simulation studies at selected operating points were carried out. Annual efficiencies for the proposed system and the reference system without RPW-HEX were calculated by summing up steady states over one year on an hourly basis.

2. CASE STUDY AND OPERATION MODES

The case study considers an application with three apartments located in average climate conditions in Europe and an air source HP. The main purpose is heating in winter and DHW generation all over the year. Through switching into reverse mode, cooling during summer is also possible.

The proposed system distinguishes between six operating modes (a-f) whilst a conventional system distinguishes between mainly three operating modes, namely heating, cooling and DHW generation which have similar efficiencies as (d,e,f) in the proposed system,

(a) heating operation and charging the RPW-HEX ($0 < SoC\uparrow \leq 1$)
(b) cooling operation and charging the RPW-HEX ($0 < SoC\uparrow \leq 1$)
(c) energy efficient DHW generation by discharging the RPW-HEX ($0 \leq SoC\downarrow \leq 1$)
(d) conventional (inefficient) direct DHW generation ($SoC = 0$)
(e) heating operation when the RPW-HEX is fully charged ($SoC = 1$)
(f) cooling operation when the RPW-HEX is fully charged ($SoC = 1$)

where SoC refers to the state of charge of the RPW-HEX (Barz *et al.*,2018). Figure 1 (a)-(d) show the operation modes (a)-(d) in a system sketch, where the conventional operation modes (e), (f) are omitted for the sake of brevity. The HP is connected to the apartments with two hydraulic lines and the switching between charging the decentralized DHW storages and heating/cooling takes place in the apartments. During heating mode (a), most of the sensible energy in the superheated hot gas charges the RPW-HEX (R). The amount of transferred heat depends on the hot gas temperature, the refrigerant mass flow, the phase transition temperature of the (solid/liquid) PCM, and the overall heat transfer coefficients of the RPW-HEX. Hot gas temperature and refrigerant mass flow result from the operating point whereas the switching temperature range of the PCM and the heat transfer capabilities of the RPW-HEX are design inherent (design parameters). For the proposed concept, R32 as a refrigerant was used and Rubitherm PCM RT64HC as PCM with a phase change temperature of 64℃ and a narrow phase transition temperature range was selected (Rubitherm, 2019). R32 has a rather high hot gas temperature when compared to other refrigerants. To limit the compressor discharge temperature at low temperatues, liquid refrigerant from the condenser exit is injected into the compressor (which is able to handle a small amount of liquid refrigerant) entrance by means of a liquid injection valve (B). In doing so, the hot gas temperature can be limited to ≈115℃. Furthermore, an additional HEX (F) is introduced to ensure that the refrigerant is in the liquid phase at the expansion valve (X) entry. Via the condenser (C), the heat is delivered to the apartments by the heating distribution system (H). In cooling mode (b), the four-way valve (W) switches to reverse mode and the evaporator (E) acts as a heat sink, whereas the condenser (C) cools the building via the heating and cooling network (H). Because the four-way valve (W) is located after the RPW-HEX, the PCM is also charged by the hot gas during cooling operation. Note that contrary to heating mode, where it would also be possible to use the energy stored in the PCM for heating (of course with a low exergy efficiency), the energy stored in the RPW-HEX during cooling is usually not used in a

conventional system. Once, the RPW-HEX is fully charged (SoC =1) by mode (a) or (b), the HP system switches to DHW generation mode (c). Contrary to direct DHW-generation mode (d), the condensing temperature, and therefore the COP, remains at the values for heating mode in (c). Therefore, the process water from the return line of the decentralized DHW storages (S) is pre-heated by the condenser at a beneficial COP. Subsequently the process water is boosted to the DHW set-point temperature ($\vartheta_w \approx 62$ °C) by discharging the RPW-HEX (R). During this operation mode, additionally the hot gas will transfer its sensible energy via the RPW-HEX (R) to the process water. Once the RPW-HEX is discharged, the HP switches back to heating or cooling mode, respectively. In the case that the thermal energy for DHW generation cannot be provided entirely by operating mode (c), e.g. during spring, the HP has to switch to the direct DHW generation mode (d). In this mode, similar to a conventional system, DHW has to be generated by increasing the condensing

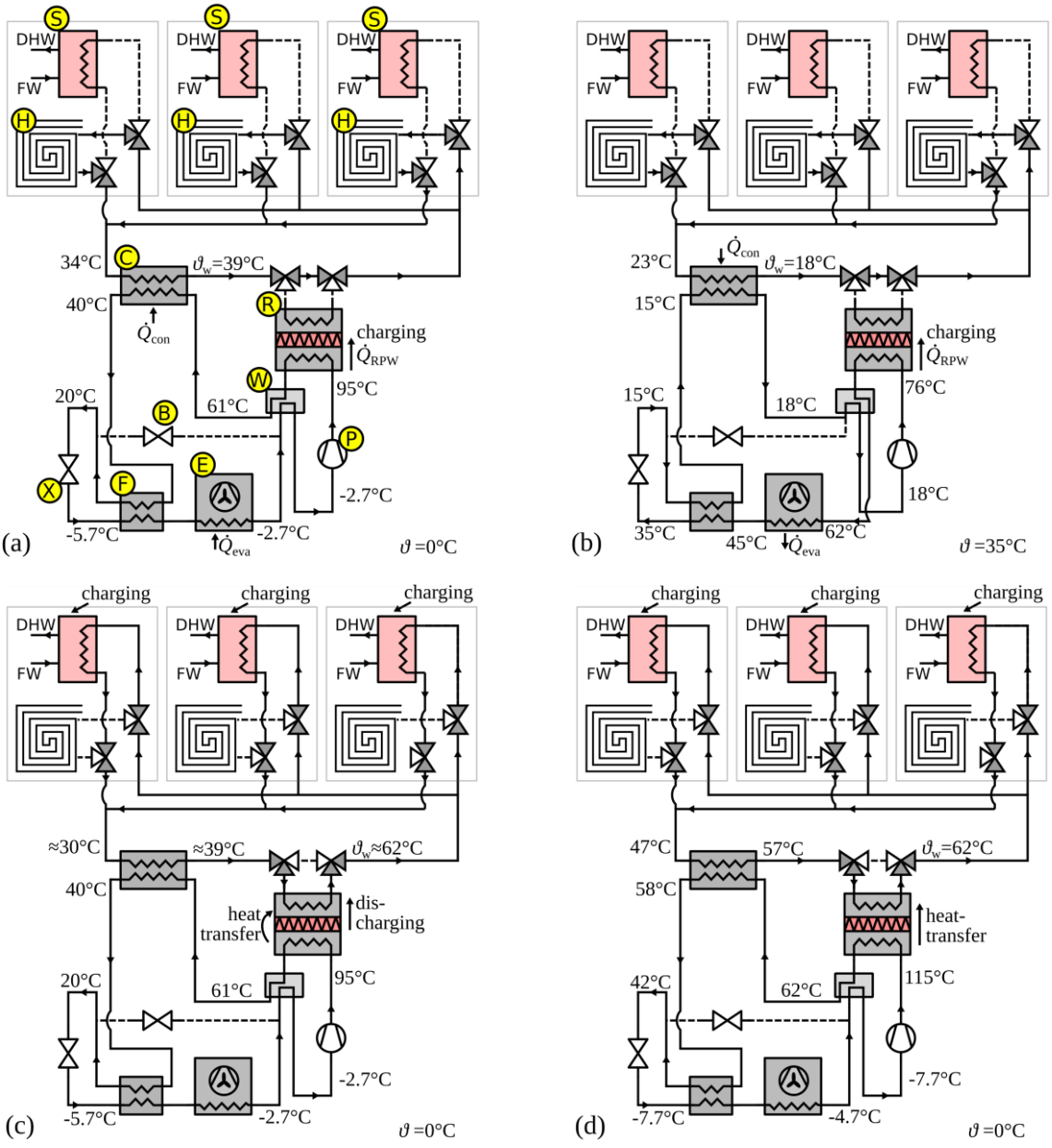

Figure 1: Concept of the proposed system for a scenario with three apartments during: (a) heating operation, (b) cooling operation, (c) energy efficient DHW generation by discharging the RPW-HEX and (d) direct DHW. (S) Decentralized sensible DHW storage, (H) low- or intermediate temperature heating system, (C) condenser, (R) RPW-HEX, (W) four way valve, (B) bypass expansion valve, (X) regular expansion valve, (F) fluid phase heat exchanger, (E) evaporator and fan, (P) compressor. The temperatures indicated in (a),(b) and (d) were taken from steady-states at an SoC of 20% and 50% for heating and cooling, respectively, whereas they were taken shortly after switching from mode (a) to (c) in (c). The ambient temperature (ϑ) was 0°C in (a,c and d) and 35°C in (b).

temperature to values suitable for DHW. The RPW-HEX acts in this case solely as HEX and transfers the sensible energy of the hot gas directly to process water. In operating mode (e) and (f) the RPW-HEX is fully charged and the modes are comparable to conventional heating and cooling modes.

3. METHODOLOGY

3.1 Simulation models

Simulation studies were carried out for both, the novel system and the reference system without RPW-HEX. The following performance indicators were computed to calculate the annual efficiencies: Coefficient of Performance related to the hot side of the HP for heating and cooling: COP_h, Coefficient of Performance related to the hot side of the HP for DHW: COP_{DHW} and RPW-HEX utilization factor: ε_{RPW}. The simulations were carried out in the Dymola/Modelica modelling environment using ThermoCycle library components (Quoilin *et al.*, 2014). Additionally, models for the RPW-HEX, the outdoor unit and the four way valve were developed in.house (Emhofer *et al.*, 2018, Frazzica *et al.*, 2018). Thermodynamic properties were taken from the CoolProp library (Bell *et al.*, 2014). The performance indicators were derived from the dynamic simulation when the system is in steady-state or when the SoC reached 20% or 50% for heating and cooling, respectively. Defrosting operation was neglected, and electric power consumption for COP calculations solely reflects the consumption of the compressor and the fan of the outdoor unit. All HP geometry/component design parameters, efficiencies and heat transfer coefficients were taken from design sheets or calculated from well-established equations and were later experimentally validated with measurements of the prototype air source HP used in the H2020 project HYBUILD (HYBUILD, 2017) without RPW-HEX.

3.2 Annual Energy Efficiency Calculations

A quasi-static approach to estimate the annual energy demand of the systems was adopted. Performance parameters at different ambient temperature levels were considered for heating, cooling and DHW generation mode (a), (b) and (d) on an hourly basis over one year or 8760 hours. Please note, that pre-heating of the process water with the condenser in operation mode (c) is not considered in the following because this process is highly dynamic and can't be handled with this quasi-static approach. Hence, the entire energy for energy efficient DHW generation is always taken from the RPW-HEX. The assumed scenario is defined by ambient temperatures (ϑ) from Strasbourg in an hourly resolution (Meteonorm, 2016). Furthermore, the feed water temperature to the heating distribution system (ϑ_w) was taken from the model described in the EN14825 (2016), see Eq. (1), using the intermediate heating and cooling ceiling scenario:

$$\vartheta_w(\vartheta) = \begin{cases} -0.577 \times \vartheta + 39.1\,°\mathrm{C}, & \vartheta \leq 2°\mathrm{C} \\ -1 \times \vartheta + 40\,°\mathrm{C}, & 2°\mathrm{C} \leq \vartheta \leq \vartheta_{on,h} = 16°\mathrm{C} \\ 18\,°\mathrm{C}, & \vartheta \geq \vartheta_{on,c} = 20°\mathrm{C} \end{cases} \qquad \text{Eq. (1)}$$

Note that heating starts below $\vartheta_{on,h}$ = 16 °C and cooling starts above $\vartheta_{on,c}$ = 20 °C, respectively. Because the condenser is connected to the heating and cooling distribution system (c.f. Fig. 1 (a,b)), $\dot{Q}_{con}$ is used to describe the heating and cooling demand of the building which needs to be covered by the HP at all times. The design point of the HP is defined by a heating demand of $\dot{Q}_{con} = 2$ kW per apartment at ϑ=$\vartheta_{design,h}$=-10°C, typical for a low energy building. As the main purpose of the system is heating, the design cooling load ($\dot{Q}_{con}(\vartheta_{design,c})$) is calculated from the definitions from heating by considering solely heat conduction between the apartment and the ambient air while neglecting solar radiation. This approach will underestimate the cooling demand but was used to be able to work without a detailed building model. The design cooling load is given in Eq. (2):

$$\dot{Q}_{con}(\vartheta_{design,c}) = \mathrm{UA}\,(20°\mathrm{C} - \vartheta_{design,c}) = \frac{\dot{Q}_{con}(\vartheta_{design,h})}{\vartheta_{on,h} - \vartheta_{design,h}}\,(\vartheta_{on,c} - \vartheta_{design,c}) \qquad \text{Eq. (2)}$$

where $\vartheta_{design,c}$=35 °C. With Eq. (2) one finds a cooling load of 1.15 kW per apartment at 35 °C. The part load behaviour $\dot{Q}_{con}(\vartheta)$ is obtained assuming a linear dependence between $\vartheta_{on,h}$ and $\vartheta_{design,h}$, and between $\vartheta_{on,c}$ and $\vartheta_{design,c}$, respectively (EN14825, 2016), as shown in Eq. (3):

$$\dot{Q}_{con}(\vartheta) = \begin{cases} \frac{\vartheta - \vartheta_{on,h}}{\vartheta_{\text{design,h}} - \vartheta_{on,h}} \times \dot{Q}_{con}(\vartheta_{design,h}), & \text{heating}, \vartheta \leq 16°\text{C} \\ \frac{\vartheta - \vartheta_{on,c}}{\vartheta_{\text{design,c}} - \vartheta_{on,c}} \times \dot{Q}_{con}(\vartheta_{design,c}), & \text{cooling}, \vartheta \geq 20°\text{C} \end{cases} \quad \text{Eq. (3)}$$

The amount of heat transferred to the RPW-HEX $\dot{Q}_{RPW}$, is calculated using a utilization factor ε_{RPW} which relates to the total thermal energy transferred at the hot side $\dot{Q}_{hot}(\vartheta)$ and furthermore, to the heat transferred at the condenser $\dot{Q}_{con}(\vartheta)$ only, as shown in Eq. (4):

$$\dot{Q}_{RPW}(\vartheta) = \varepsilon_{RPW}(\vartheta)\, \dot{Q}_{hot}(\vartheta) = \varepsilon_{RPW}(\vartheta) \times \begin{cases} \dot{Q}_{con}(\vartheta)\, \frac{1}{1 - \varepsilon_{RPW}(\vartheta)}, & \text{heating} \\ \dot{Q}_{con}(\vartheta)\, \frac{COP_h(\vartheta)}{COP_h(\vartheta) - 1}, & \text{cooling} \end{cases} \quad \text{Eq. (4)}$$

where the heat transferred on the hot and cold side of the heat pump are given by Eq.(5) and Eq.(6):

$$\dot{Q}_{hot}(\vartheta) = COP_h(\vartheta)\, W(\vartheta) = \begin{cases} \dot{Q}_{con} + \dot{Q}_{RPW}, & \text{heating, DHW generation} \\ \dot{Q}_{eva} + \dot{Q}_{RPW}, & \text{cooling} \end{cases} \quad \text{Eq. (5)}$$

$$\dot{Q}_{cold}(\vartheta) = (COP_h(\vartheta) - 1)\, W(\vartheta) = \begin{cases} \dot{Q}_{eva}, & \text{heating , DHW generation} \\ \dot{Q}_{con}, & \text{cooling} \end{cases} \quad \text{Eq. (6)}$$

Note that ε_{RPW} in Eq. (4) strongly depends on the temperature conditions. In the reference system ε_{RPW} is zero and therefore, the entire thermal energy on the hot side (Eq. (5)) is transferred to the condenser during heating or to the evaporator during cooling, respectively.

Furthermore a daily DHW consumption of Q^d_{DHW} =5.845 kWh per apartment is assumed, which is comparable to a medium water consumption as defined in the EN16147 (2017). The load profile is also taken from the standard, and it is assumed that the energy stored in the RPW-HEX can always be delivered to the decentralized water storages without thermal losses in space and time.

The annual energy efficiency ratios (EER) for heating and cooling are calculated by means of Eq. (7) and Eq. (8), similarly to the basic definitions for the $SCOP_h$ and $SCOP_c$ in the EN14825 (2016):

$$EER_{heating} = \frac{Q^y_{\text{heating}}}{W^y_{\text{heating}}} = \frac{\sum_{j=1}^{8760} Q_{con}(\vartheta_j)}{\sum_{j=1}^{8760} \left(\frac{Q_{con}(\vartheta_j)}{COP_h(\vartheta_j)} \right)} \quad \text{Eq. (7)}$$

$$EER_{cooling} = \frac{Q^y_{\text{cooling}}}{W^y_{\text{cooling}}} = \frac{\sum_{j=1}^{8760} Q_{\text{con}}(\vartheta_j)}{\sum_{j=1}^{8760} \left(\frac{Q_{\text{con}}(\vartheta_j)}{COP_h(\vartheta_j) - 1} \right)} \quad \text{Eq. (8)}$$

where the superscript y indicates the annual demand and W ist the electric energy demand of the compressor and the fan. In the reference as well as in the proposed HP system in direct heating mode (d), the COP for DHW generation COP_{DHW} will be significantly lower than the COP for heating due to the higher temperature difference between evaporator and condenser. The electric energy consumption at a certain ambient temperature ϑ_j at a certain hour of the year h_j is given in Eq. (9):

$$W_{\text{DHW}}(\vartheta_j, h_j) = \frac{Q_{DHW}(h_j)}{COP_{DHW}(\vartheta_j)} \quad \text{Eq. (9)}$$

With the aid of the RPW-HEX, a certain amount of thermal energy can be generated with a better with COP_h instead of COP_{DHW} leading to a reduction of the electric energy demand. The situation is

different in cooling mode. In the reference system, the total energy transferred on the hot side dissipates in the evaporator and is lost. Therefore, DHW is not only generated with a better COP with the RPW-HEX, but for free, as waste heat is utilized. The reduction of electric energy demand compared to direct DHW generation is therefore given in Eq. (10):

$$\Delta \mathrm{W}_{\mathrm{DHW,RPW}}(\vartheta_j, h_j) = \begin{cases} Q_{RPW}(\vartheta_j)\left(\frac{1}{COP_{DHW}(\vartheta_j)} - \frac{1}{COP_h(\vartheta_j)}\right), & \text{heating} \\ \frac{Q_{RPW}(\vartheta_j)}{COP_{DHW}(\vartheta_j)} & \text{cooling} \end{cases} \qquad \text{Eq. (10)}$$

where $\dot{Q}_{RPW}$ follows from Eq. (4) for heating and cooling. With Eq. (9) and Eq. (10), the anual efficiency for DHW generation reads:

$$EER_{DHW} = \frac{Q^y_{\mathrm{DHW}}}{W^y_{\mathrm{DHW}}} = \frac{\sum_{j=1}^{8760} Q_{\mathrm{DHW}}(\mathrm{h_j})}{\sum_{\mathrm{j=0}}^{8760}\left(W_{\mathrm{DHW}}(\vartheta_j, h_j) - \Delta W_{\mathrm{DHW,RPW}}(\vartheta_j, h_j)\right)} \qquad \text{Eq. (11)}$$

4. RESULTS AND DISCUSSION

4.1 Performance indicators obtained from simulation studies

Figure 2 shows results of the performance indicators obtained from the simulations for different constant ambient temperatures. For annual calculations missing values between the depicted points were calculated by linear interpolation. As expected the COPs significantly decrease for low (heating) and high (cooling) ambient temperatures due to the high temperature lift between evaporator and condenser. The COPs of both system are almost equal although the sensible heat of the hot gas can be used for heating in the reference heating case and doesn't need to be cooled by the outdoor air in the cooling case for the novel system. Heating, cooling and direct DHW behaviour in Fig. 2(a) corresponds to operating modes (a),(b) and (d) for the novel system. Note that if the RPW-HEX can be charged, DHW can be generated with operating mode (c) with the better COPs "heating and RPW-DHW" and "cooling and RPW-DHW", respectively, instead of "direct DHW" generation. The RPW-HEX is able to store energy for ambient temperatures below 10 °C and above 30 °C (Fig. 2(b)). Between 10 °C and 30 °C, the hot gas temperature is too low ($\lesssim 64$ °C). Below ≈ -5 °C, the liquid injection valve starts to work and therefore, the hot gas temperature is limited to ≈ 115 °C. The storable energy from superheated refrigerant then only depends on the mass flow of the refrigerant.

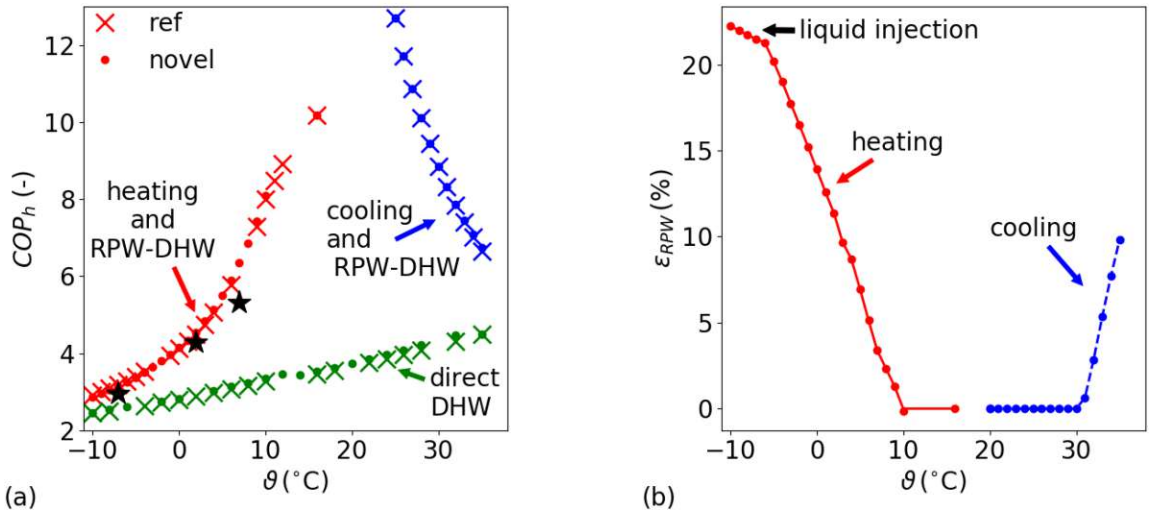

Figure 2: Performance indicators of the HP system in relation to the ambient temperature. The black stars in (a) denote the values from the measurements of the prototype HP without RPW-HEX.

4.2 Annual energy efficiency

The resulting annual heating and cooling demands are Q^{y}_{heating}=12 847 kWh and Q^{y}_{cooling}=1 093 kWh, respectively. Furthermore, the annual heating demand for DHW is Q^{y}_{DHW} = 6 400 kWh. Figure 3 shows how much thermal energy can be provided by the RPW-HEX for DHW generation on a daily basis. During winter times in 17 days the RPW-HEX can deliver more than necessary to cover the DHW consumption. Hence, the surplus thermal energy might be shifted to the decentralized DHW storages. Due to the relatively low hot gas temperature in summer times, and the low amount of hot days (only 30 hours with temperatures above 30 °C) the RPW-HEX will not contribute significantly to the DHW generation given the climatic scenario selected here.

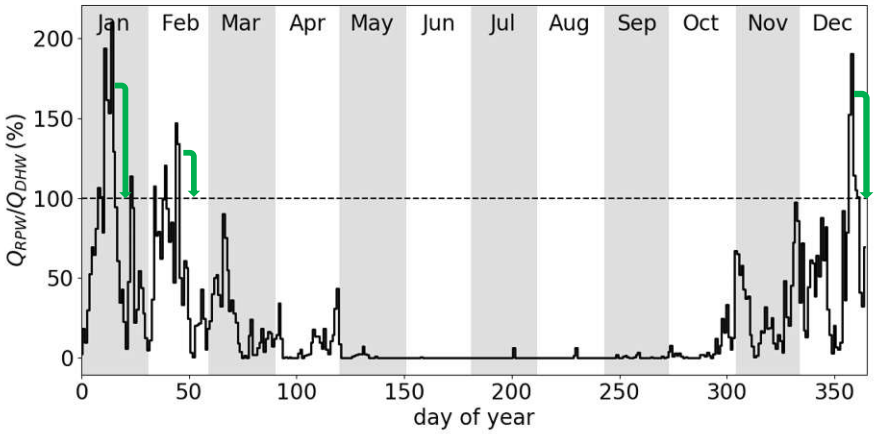

Figure 3: Coverage ratio of energy for DHW provided by the RPW-HEX. Note that, for the calculated annual performance indicators, it is assumed that surplus energy gained from the RPW-HEX can be stored for usage during the days to come (green arrows).

Table 1 summarizes the annual performance indicators and the electric energy consumption of the reference and the novel system. The annual performance for heating EER_h and cooling EER_c are almost equal whereas, the annual performance for DHW is about 11 % higher for the novel system compared to the reference system. To sum up, the novel concept saves 200 kWh electricity per year which results in 4.3 % lower annual total electric energy consumption.

Table 1: Calculated annual energy efficiencies

	Q^{y}_{RPW}(kWh)	W_{sum}(kWh)	W_h(kWh)	W_c(kWh)	W_{DHW}(kWh)	EER_h	EER_c	EER_{DH}
Reference	0	4654	2586	105	1963	4.97	10.4	3.26
Novel	1389	4456	2583	105	1768	4.97	10.4	3.62

5. CONCLUSIONS AND OUTLOOK

Technical details and economic benefits are presented for a novel heat pump system, with a Refrigerant/PCM/Water Heat EXchanger (RPW-HEX) directly integrated in the hot gas section of an air source HP, for energy efficient DHW generation. Annual calculations indicate for average climatic conditions, intermediate heating temperatures and medium DHW consumptions, estimated savings of about 4.3 % of electric energy when compared to conventional air source HP systems. These energy savings result from a 11 % better performance for DHW generation with the novel system. The case study considers three apartments located in a low energy building, each with a heat demand of 2 kW per apartment at -10 °C and a DHW demand of 5.825 kWh per day. The absolute savings amount in this case is 200 kWh of electric energy with the proposed system per year. Next steps will include the assessment of the annual performances for other climatic conditions, heating demands, building conditions and PCM materials, as the yearly performance strongly depend on these constraints. Furthermore, experiments with the experimental air source HP and the RPW-HEX will be carried out in the months to come.

ACKNOWLEDGEMENTS

The authors thank C. Köfinger, M. Lauermann, W. Pink and A. Zottl for critical discussion.This project has received funding from the European Union's Horizon 2020 research and innovation programme under grant agreement No 768824 (HYBUILD). GREiA is certified agent TECNIO in the category of technology developers from the Government of Catalonia. The authors would like to thank the Catalan Government for the quality accreditation given to their research group (2017 SGR 1537).

REFERENCES

Barz, T., Seliger, D., Marx, K., Sommer, A., Walter, S. F., Bock, H. G., Körkel, S., 2018, State and state of charge estimation for a latent heat storage, Control Engineering Practice, *72*, 151-166.

Bell, I. H., Wronski, J., Quoilin, S., Lemort, V., 2014, Pure and Pseudo-pure Fluid Thermophysical Property Evaluation and the Open-Source Thermophysical Property Library CoolProp, Industrial & Engineering Chemistry Research, 53 (6), 2498--2508.

Cabeza, L.F., Castell, A., Barreneche, C., de Gracia, A., Fernández, A.I., 2011, Materials used as PCM in thermal energy storage in buildings: A review, Renew Sust Energ Rev, 15, 1675–1695.

Emhofer, J., Barz, T., Palomba, V., Frazzica, A., Sergi, F., Varvagiannis, S., Karellas, S., Oró, E., Zsembinszki, G., Cabeza, L.F., Deliverable D3.1 of the HYBUILD-Project: Modular flow sheet simulation of the hybrid (sub-)system, 2018. [Online]. Available: http://www.hybuild.eu/publications/deliverables/

EN 16 147: Heat pumps with electrically driven compressors - Testing, performance rating and requirements for marking of domestic hot water units, EN 16 147, 2017-01

EN 14 825: Air conditioners, liquid chilling packages and heat pumps, with electrically driven compressors, for space heating and cooling — Testing and rating at part load conditions and calculation of seasonal performance, EN 14 825, 2016-03

Frazzica, A., Palomba, V., Sergi, F., Ferraro, M., Cabeza. L.F., Zsembinszki, G., Oró E., Karellas, S., Varvagiannis, S., Emhofer, J., Barz, T, 2018, Dynamic Modelling of a Hybrid Solar Thermal/electric Energy Storage System for Application in Residential Buildings. Proceedings of the 12th International Conference on Solar Energy for Buildings and Industry, Raperswil, Switzerland.

HYBUILD, Innovative compact hybrid storage systems for low energy buildings, 2017, http://www.hybuild.eu/, acessed Jan. 22, 2019.

Kapsalis, V., Karamanis, D., 2016, Solar thermal energy storage and heat pumps with phase change materials,Applied Thermal Engineering, 99, 1212-1224.

Meteonorm, Irradiation data for every place on Earth, 2016. [Online] Available: http://www.meteonorm.com/en/

Pardiñas, A.A., Alonso, M.J., Diz, R., Kvalsvik, K.H., Fernández-Seara, J., 2017, State-of-the-art for the use of phase-change materials in tanks coupled with heat pumps, Energy and Buildings, 140,28-41.

Quoilin, S., Desideri, A., Wronski, J., Bell, I., Lemort, V., 2014. ThermoCycle: A Modelica library for the simulation of thermodynamic systems, in: Proc. of the 10th Int. Modelica Conference. Lund, Sweden.

Song, M., Deng, S., Dang, C., Mao, N., Wang, Z., 2018, Review on improvement for air source heat pump units during frosting and defrosting, Applied Energy 211, 1150-1170.

Pardiñas, A.A., Alonso, M.J., Diz, R., Kvalsvik, K.H., Fernández-Seara, J., 2017, State-of-the-art for the use of phase-change materials in tanks coupled with heat pumps, Energy and Buildings, 140,28-41.

Rubitherm, Rubitherm GmbH, 2019, https://www.rubitherm.eu/en/ acessed Jan. 30, 2019

Zou, D., Ma, X., Liu, X., Zheng, P., Cai, B., Huang, J., Guo, J., Liu, M., 2017, Experimental research of an air-source heat pump water heater using water-PCM for heat storage, Applied Energy, 206, 784-792,

NOMENCLATURE

COP	Coefficient of Performance (-)	UA	Thermal conductance (kW/K)
EER	Energy Efficiency Ratio (-)	W	Electric energy (kWh)
EER	Energy Efficiency Ratio (-)	ε_{RPW}	Utilization factor of the RPW-HEX (-)
Q	Thermal energy (kWh)	ϑ	Temperature (°C)